Improving tropical forest aboveground biomass estimations : insights from canopy trees structure and spatial organization

Pierre Ploton

N°: 2017AGPT0005

Doctorat AgroParisTech

T H È S E

pour obtenir le grade de docteur délivré par

L'Institut des Sciences et Industries du Vivant et de l'Environnement

(AgroParisTech)

Spécialité : Ecologie et Biodiversité

présentée et soutenue publiquement par

Pierre PLOTON

le 27 Mars 2017

Improving tropical forest aboveground biomass estimations: insights from canopy trees structure and spatial organization

Directeur de thèse : **Dr. Raphaël PELISSIER**
Co-encadrement de la thèse : **Prof. Dr. Uta BERGER**

Jury

M. Lilian BLANC, Chercheur (HDR), CIRAD	Rapporteur
M. Laurent SAINT-ANDRE, Directeur de Recherche, INRA	Rapporteur
M. Hans-Gerd MAAS, Professeur, Technische Universität Dresden	Rapporteur
M. Pierre COUTERON, Directeur de Recherche, IRD	Président
Mme Uta BERGER, Professeur, Technische Universität Dresden	Co-directeur de thèse
M. Raphaël PELISSIER, Directeur de Recherche, IRD	Directeur de thèse

AgroParisTech - IRD
Unité Mixte de Recherche AMAP
TA A-51 / PS1 Bd de la Lironde, 34398 Montpellier cedex 5, FRANCE

ACKNOWLEDGEMENTS

This doctoral thesis was realized thanks to the support of the 2013-2016 Forest, Nature and Society (FONASO) grant, funded by the European Commission's Erasmus Mundus Joint Doctorate programme (EMJD). Part of the thesis was funded by the CoForTips project as part of the ERA-Net BiodivERsA 2011-2012 European joint call (ANR-12-EBID-0002). I am also grateful for the multiple travelling funds I received from the UMR AMAP of the French Institut de Recherche pour le Développement (IRD).

I have benefited from the support, advices and help of numerous people during the 3 (and a half…) years of this PhD project. First and foremost, I would like to thank Dr. Raphaël Pélissier, who's been supervising my work since my first steps in the world of forest research, about 7 years ago at the French Institute of Pondicherry. I'm deeply indebted to you for the opportunity you gave me to work on such fascinating subjects during the past years. For your incredible patience while reading long and sometimes crazy "results syntheses" I've been sending you, for helping me to see broader implications rather than details in my analyses, for your positive attitude toward our findings, thank you. I am also very grateful to Prof. Uta Berger, who kindly provided support and guidance during this project, and made this Joint Doctoral Programme a very positive experience for me.

I must also warmly thank Dr. Nicolas Barbier for the considerable amount of time we spent, at the office or in the field, brainstorming about our common research interests. Beyond invaluable scientific guidance, total availability for my questions and concerns, deep involvement in the different projects we undertook, you've simply been of great company, and I'm thankful for the tons of fun we had in the field.

This list is far from being exhaustive, but I should also mention my deep gratitude to Dr. Pierre Couteron, Dr. Christophe Proisy and Dr. Maxime Réjou-Méchain for the fruitful discussions we had, notably on FOTO texture and biomass allometric models. I am also very grateful to Dr. Gilles Le Moguedec for his availability and good will to help me resolve statistical issues I've been having throughout this project.

Last but not least, this PhD project largely beneficiated from the field work several colleagues and I carried out in Cameroon. I owe a great deal of thanks to Prof. Bonaventure Sonké, who warmly welcomed me in his research team and created a pleasant and efficient working environment. I'd also like to thank Dr. Vincent Droissart with whom, just like with Nicolas, I spent a formidable time in the field. My thoughts also go to the Cameroonian students and friends I've been collecting field data with, notably S.T. Momo, M. Libalah, N.G. Kamdem, H. Taedoumg, G. Kamdem Meikeu and D. Zebaze.

TABLE OF CONTENTS

LIST OF FIGURES

LIST OF TABLES

1 GENERAL INTRODUCTION

This chapter provides an overview of the general research topics addressed in the course of my doctoral study. Specifically, I give a concise justification of the impetus for scientific research on tropical forest carbon and stress the crucial role of remote-sensing in this dynamic. The focus is then put on two important aspects of the remote sensing-based carbon mapping chain that I present in separate sections: (1) the actual remote sensing of forest carbon and (2) field estimations of forest carbon, which constitute the 'ground truth' of the mapping chain. Each section leads to broad methodological orientations that have been taken in this thesis and identifies key problems. In the end, I present the research objectives, the pantropical scope of this work and the organization of the thesis chapters.

1.1 Context and challenges

1.1.1 Tropical forests and climate change

International concerns about climate change have fostered research on the global carbon cycle, as carbon dioxide (CO_2) is the largest contributor to anthropogenically enhanced greenhouse effect (Houghton, 2007). Together with the soil, terrestrial vegetation composes the "terrestrial ecosystems carbon reservoir" (Houghton et al., 2009) and interacts with the carbon cycle by fixing atmospheric CO_2 (photosynthesis) and sequestrating it in plant's material. Plants carbon is quantified through biomass (as dry weight is c. 50 % carbon), often distinguishing live biomass (above and below ground) from dead material. Among terrestrial biomes, the focus is usually put on forest ecosystems which store the vast majority of biomass stocks (c. 70-90 %) (Houghton et al., 2009), and within forest biomes, tropical forests are the largest ones in surface with about c. 1949 Mha (i.e. c. 50 % of total forested lands) and store approximately c. 55 % of the global forest carbon, against c. 32 % in boreal and c. 14 % in temperate forests (Pan et al., 2011). Perhaps more important to the global carbon cycle than forest carbon stocks themselves is how these stocks change in time. Forests are dynamical ecosystems presenting continuous change in forest age structure and community composition. A broadly accepted pattern of forest biomass dynamics in undisturbed systems is a fast increase early in forest succession ('forest aggradation' phase) followed by a gradual decrease of biomass growth rate with forest age (e.g. Ryan et al., 1997). Associated changes in stand structure properties, such as tree dimensions and spatial organization, can partly be observed from above the forest, for instance from a satellite sensor, and can be used to monitor forest biomass (as we will see in section 1.1.3.2). Growing (or re-growing) forests thus behave as carbon sinks, trapping atmospheric CO_2 at different rates. On the other hand, forest carbon can be released back into the atmosphere through combustion and decomposition of forest biomass. Change in land use (i.e. deforestation) and forest degradation (e.g. logging) are the principal drivers of forest-related carbon emissions, transforming forested lands from carbon sinks into carbon sources. The tropical forest biome is the most threatened by deforestation and degradations (e.g. Pan et al., 2011). Over the 1990 - 2007 period, Pan and colleagues (2011) estimated that gross carbon emissions from tropical deforestation represented as much as c. 40 % of carbon emissions from fossil fuel combustion. This massive carbon release was however largely offset by a massive carbon uptake in this biome (representing c. 70 % of world's forests sink), yielding a net carbon emission commonly reported around c. 12 % of total anthropogenic emissions for the first decade of the century (Houghton, 2012; Van der Werf et al., 2009), i.e. the second largest source of CO_2 emissions after fossil fuel combustion. Reducing CO_2 emissions from tropical deforestation and forest degradation is considered a cost-effective way to mitigate the rise of atmospheric CO_2 concentration (Gullison et al.,

2007) and in turn global climate change. Based on this observation, the REDD ("Reducing Emissions from Deforestation and forest Degradation") program was launched in Bali under the United Nations Framework Convention on Climate Change (UNFCCC, 2007), with at its core the idea that developed countries would compensate developing countries for avoided forest carbon emissions. Payments would, however, be conditional to a verified monitoring of avoided carbon emissions. Beside sociopolitical challenges that REDD poses, it also constitutes a formidable scientific challenge, as its success partly lies on our ability to accurately monitor forest carbon variation in space and time.

1.1.2 REDD monitoring frame of tropical forest biomass: basics and challenges

The methodological approach for monitoring forest carbon emissions as defined in the IPCC Good Practice Guidelines (e.g. Eggleston et al., 2006) is fairly simple in its design. It consists in combining estimations of *forest area change* (i.e. activity data) with coefficients which quantify the *carbon stock change* per unit area (i.e. emission factors).

Estimating forests area at one point in time and its dynamics during a time period (i.e. *forest area change*, driven by deforestation or forest regrowth) can be achieved with remote-sensing (RS) or census data (i.e. from national forest inventories or global Forest Resources Assessments, e.g. FAO, 2010). Remote-sensing presents interesting characteristics for *forest area change* monitoring: it allows repeated, wall-to-wall coverage of the Earth surface and provides spatially explicit products, allowing one to accurately locate spots of deforestation and forest regrowth. Since forest inventories in tropical countries may be out of date, non-representative or even entirely lacking (Houghton, 2005), RS is thought as providing more reliable, consistent and accurate estimates of forests area and *forests area change* (Houghton, 2012). Technically, the forest detection (thus its gains and losses in time-series data) is nowadays reliably achieved with medium resolution (10 – 30 m) optical images. A typical example of sensor that can be used to perform national-scale *forest area change* monitoring is Landsat (TM and ETM+), which offers more than three decades of free, open-access archives (De Sy et al., 2012; Morton, 2016). Important efforts are being made to facilitate the access and analysis of NASA-sponsored imagery (including Landsat) and derived products (e.g. NDVI, forest gain/loss) through web-based platforms such as the Google Earth Engine (GEE) or Global Forest Watch (GFW). For instance, GWF has published every year (for the past 10 years) a 30 m global map of tree cover loss (annually) and gain (from year 2000), which undoubtedly represents a major step toward operational and transparent frame for *forest area change* reporting.

Attributing a carbon stock to a given forested area (or carbon density), let alone a *carbon density change* (that is, the amount of carbon before and after a time period that may or may not include a disturbance such as deforestation), is much more challenging and represents more than half of the uncertainty on large scale forest carbon emissions estimates (Houghton, 2005). The difficulty stems from the multiple spatial scales at which forest carbon or biomass density varies. At a scale < 1 ha, biomass density varies with the position of the largest canopy trees and mortality (creating canopy gaps). At the level of a forest stand (homogeneous in age and species composition) (e.g. 1-10 ha), biomass density varies with time as a result of disturbances and recovery. At the landscape level (e.g. > 100 ha), stands mosaics present spatial variations in biomass density resulting from differences in species composition and time since last disturbances (Houghton et al., 2009). Besides biomass density variations that can be attributed to intrinsic dynamics of forest ecosystems, environmental (e.g., soil type, topography) and bioclimatic (e.g. temperature, precipitation, length of dry season) drivers also influence forest biomass and vary in space at different scales, adding complexity to the accurate

estimation of biomass density for a given area. From a practical point of view, methods used to estimate biomass density can broadly be categorized into non-spatial and spatial methods. Non-spatial methods are based on a predefined classification of forest types ("land cover map") and consist in attributing to each type an average biomass density derived from forest inventory data or from the literature. This is the simplest approach that the IPCC declined in its guidelines in two different tiers of quality: Tier 1 when broad continental forest types are used (i.e. default forest strata and associated biomass densities) and Tier 2 when country-specific data are used (i.e. refined forest strata and biomass densities derived from national forest inventories). With such methods, the question of representativity of average biomass density estimates is indeed central and constitutes an obvious source of error in carbon stock and carbon stock change estimations, especially in the tropics given the paucity of forest inventories (e.g. Mattsson et al., 2016). Spatial methods produce biomass density maps based on a relationship between *in situ* biomass estimations and bioclimatic and environmental data, RS data, or both. When spatially explicit models are sufficiently accurate and precise (which is commonly interpreted as "when estimation uncertainty is no more than 20 % of the mean", Zolkos et al., 2013), this approach would correspond to the highest quality tier of the IPCC (Tier 3). Biomass density maps can be used to improve the representativity of average biomass density estimates used in non-spatial methods (e.g. Langner et al., 2014) or replace them altogether. Indeed, using biomass densities that are co-located with areas undergoing changes (e.g. deforestation) should yield more accurate estimates of emissions (Houghton, 2012).

The REDD methodological framework requires monitoring forest carbon stock changes at large spatial scale (regional, national) to limit the so-called leakage phenomenon, whereby deforestation and degradations would simply be displaced from a protected area to elsewhere. At such a large scale, the carbon estimation methods presented above lead to very different results. In 2001, Houghton et al. showed that seven estimates of total forest biomass over the Brazilian Amazon from different methods varied by a factor greater than two and did not agree on where the highest and lowest biomass densities where found. At the global scale, forest biomass estimates from the same year presented approximately the same variation factor (Houghton, 2012). Over the past decade, the two firsts maps depicting the variation of forest biomass at medium resolution (500 and 1000 m) over the entire tropics have been published (Baccini et al., 2012; Saatchi et al., 2011). The authors essentially used forest inventories to calibrate GLAS data (i.e. satellite-LiDAR) available under the form of isolated footprints across the tropics, and extrapolated the information on low-resolution RS (MODIS, notably), environmental and climatic data, so to obtain continuous predictions of forests AGB. If the two maps present some extent of agreement when predictions are aggregated at very large spatial scale (i.e. regional-, national-level), biomass variation patterns within countries do not converge, especially in areas where forest biomass is high or where field inventories are scarce (Mitchard et al., 2013). This suggests that the sensitivity of models' predictors to forest AGB variation is extremely weak. To date, uncertainties on large scale estimates of forest CO_2 emissions remain high, of the order of c. 50 % (IPCC, 2014). Reducing those uncertainties is critically important for the implementation of climate policies such as REDD (Mitchard et al., 2014; Ometto et al., 2014). Remote sensing could be a key tool for this purpose, but RS methods capable of detecting local variations of tropical forest AGB, and that over large spatial scales, need to be developed. In the next section, I give a brief presentation of the forest biomass mapping chain from RS data. Given the diversity of RS data types, associated methodological approaches and the various uncertainty sources along the biomass mapping chain, the

following presentation is by no mean exhaustive but rather provides a broad, somewhat caricatural picture, allowing the reader to apprehend the contribution of this thesis.

1.1.3 Remote sensing-based modelling of tropical forest biomass

1.1.3.1 General workflow

The estimation of forest biomass is most often restricted to the aboveground component (hereafter denoted AGB) which represents more than c. 70 % of total forest biomass (Houghton et al., 2009) and is easier to characterize, notably from remote sensing. An important remark is that no RS technology is capable of directly measuring forest AGB (e.g. Woodhouse et al., 2012). Instead, indirect relationships are established between RS indices that vary with forest AGB and estimations of AGB in forest sample plots (the 'ground truth') (Figure 1-1). Errors in biomass maps can therefore be decomposed into (1) errors stemming from field plots AGB estimation (hindering models calibration, propagating throughout carbon mapping chains, etc.) and (2) errors stemming from RS indices (e.g. insufficient predictive ability), notably. For the sake of clarity, I conserve this dichotomy in the rest of this introductory chapter (i.e. field *vs* RS estimations of AGB, Figure 1-1B).

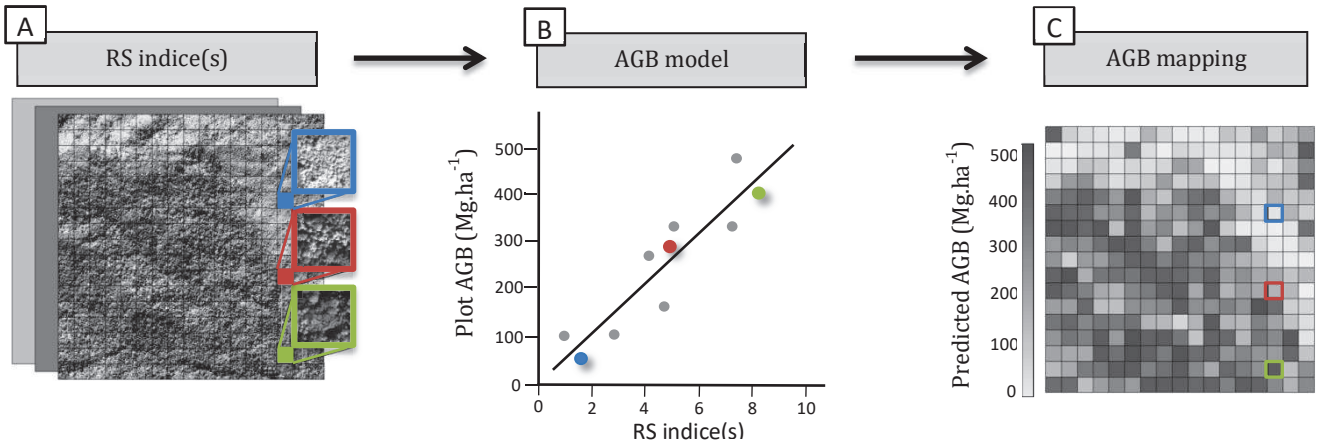

Figure 1-1. General workflow of remote sensing-based AGB mapping methods. Regardless of the remote sensing data type, remote sensing indice(s) are extracted over forest sample plots (A) and used a predictor(s) of *in situ* AGB estimations (B). Once calibrated, the model can be used to predict forest AGB over the entire study area (C).

1.1.3.2 Estimating forest sample plots AGB from remote sensing data

The advent of metric and submetric resolution RS data types

A major difficulty when it comes to mapping forest biomass in the tropics is due to the loss of sensitivity of traditional RS sensors at high AGB values. Decades of research have indeed shown that satellite-borne passive optical signals with coarse to medium resolution (e.g. MODIS, Landsat), but also active (radar) signals (e.g. L-band SAR), fail to characterize the entire range of forest structural attributes in spatially complex, high-biomass tropical forests. Signal saturation is typically observed around 100-200 $Mg.ha^{-1}$ (Foody, 2003; Huete et al., 2002; Imhoff, 1995; Mougin et al., 1999), when tropical forests AGB frequently exceeds 400 $Mg.ha^{-1}$ (Slik et al., 2013). Therefore, despite very attractive features, in particular the possibility to acquire continuous RS data coverage over extensive area extents at low cost (allowing producing biomass maps at the pantropical scale, as in Baccini et al. (2012) and Saatchi et al. (2011)), such signals cannot be expected to accurately capture AGB variations on the better half

of the tropical forest AGB gradient. The development of reliable, non-saturating AGB mapping methods in the tropical context remains an active field of research.

Since the early 2000s, Light Detection And Ranging (LiDAR) technology has become increasingly popular in this regard. Aircraft-based LiDAR systems provide information on forest structure with a ground resolution of 5 m to 50 cm (or less), depending on system characteristics. Importantly, LiDAR is an active signal that penetrates forest canopy down to the ground surface, generating a detailed description of forest three-dimensional (3D) structure. From this extremely rich data type (which often allows identifying individual trees and large branches with the naked eye), a common approach is to aggregate the information into one or several forest height indices that can be related to plot level AGB estimates (e.g. Asner et al., 2011; Véga et al., 2015). A growing body of literature suggests that aerial LiDAR indices allow detecting the full gradient of tropical forest AGB (no saturation) with a relatively high precision (10-20 % error, Zolkos et al., 2013). However, airborne data acquisition campaigns are costly and sometimes unfeasible in certain tropical countries for logistical and political reasons, hampering the use of aerial LiDAR for routine, large scale monitoring of forest AGB.

Another type of RS data that could prove useful in the carbon monitoring context and yet has largely been under-exploited is satellite-borne Very High Spatial Resolution (VHSR, with pixel size ≤ 1 m²) optical images. Much like LiDAR (although in two dimensions), the spatial resolution of these optical images allows one to visually identify individual (canopy) trees in the image. In contrast with LiDAR however, the optical signal is passive, therefore forests AGB retrieval cannot be based on forest height proxies. Instead, the two-dimensional information on canopy structure may be exploited using an analysis of canopy texture properties. The Fourier Texture Ordination (FOTO) method for instance (which rationale and previous case studies are presented in chapter 4) have shown promising results for the retrieval of classical stand structure parameters (e.g. basal area, mean tree diameter) and AGB in high-biomass tropical forests (Couteron et al., 2005; Proisy et al., 2007). Biophysical mechanisms governing relationships between canopy texture features and forest structure are, however, not fully understood. This is an important knowledge gap as it prevents to move from local applications (i.e. statistical relationships established on a single forest type, over a few hundred km²) to larger scales (i.e. several forest types, over several thousands km²).

The prospects of coupling 3D plant models and radiative transfer models

Deepening our understanding of how forest 3D structure controls canopy texture properties, how texture-based indices translate back into standard stand structure parameters (including AGB) and how those relations vary across forest ecosystems and spatial scales is made difficult by the absence of a sufficiently large dataset featuring both field inventories and VHSR data. Besides, sun-sensor geometry (e.g. sun elevation angle) at the time of satellite image acquisition influences canopy texture properties (e.g. by modifying the amount and spatial distribution of shadows on the canopy) (Barbier et al., 2011), any empirical approach of the problem must therefore account for this phenomenon by disentangling instrumental perturbation from the effect of forest stand structure on canopy texture. On a small set of VHSR images, this issue is typically bypassed by inter-calibrating texture-based indices when images partly overlap (as in Bastin et al., 2014) or analyzing images acquired in similar acquisition angles, but restricting image acquisition angles to relatively narrow range of values is an important constraint for image providers and can hardly be envisaged, in practice, for large images sets. A potential workaround is to use a simulation approach (Figure 1-2) coupling (i) a 3D forest simulation

model, based on information commonly available in forest inventories and a few allometry rules and (ii) a radiative transfer model (e.g. Discrete Anistropic Radiative Transfer (DART) model, Gastellu-Etchegorry et al., 2015), allowing to generate virtual canopy scenes with controlled sun-sensor geometry. This approach already permitted quantifying the impact of the sun-sensor geometry on canopy texture (Barbier et al., 2011). In the scope of this thesis, we highlighted the potential of simulated experiments to explore and tune texture-based RS indices for AGB carbon retrieval.

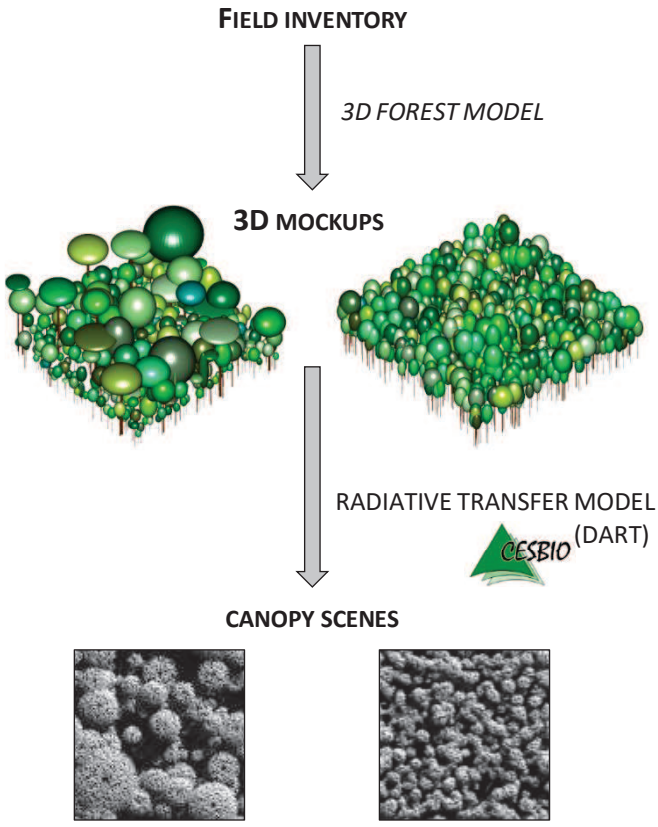

Figure 1-2. Schematic illustration of virtual canopy scenes simulation procedure. Field inventory data are used in a forest model to generate 3D mockups of the sample plots. A radiative transfer model simulates a satellite view of the mockups, for instance a VHSR 1-m IKONOS panchromatic channel.

1.1.3.2 Estimating forest sample plots AGB from inventory data

An uncertain "ground truth"

The gold-standard method for estimating the AGB of a forest plot consists in harvesting and weighting all trees in the plot. This method is, however, labor intensive, costly and destructive. It follows that in practice, an indirect approach is preferred whereby the AGB of individual trees is estimated using a mathematical model based on one or several biometric parameters that can be easily measured in large field inventories. An important step in this process is to select an appropriate AGB model. Over the years, countless models contrasting in their form (linear, power, exponential), biometric predictors (including polynomial and interaction terms), target species and sites have been published (Sileshi, 2014). The selection of a particular AGB model has an important impact on field plot AGB estimation (Molto et al., 2013; Picard et al., 2014; van Breugel et al., 2011). For example, Picard and colleagues

(2015) obtained AGB estimations varying by a factor of nearly two when comparing seven seemingly appropriate AGB models on a 9-ha forest plot of Democratic Republic of Congo. Disagreements of AGB models on levels and variation pattern of AGB across forest plots naturally limits the accuracy with which RS methods can predict spatial variations of AGB (Ahmed et al., 2013; Mitchard et al., 2013).

The pantropical biomass model

Following the seminal study of Brown (1997), J. Chave made important contributions toward standardizing the way we estimate trees AGB across the tropics by developing a pantropical approach (Chave et al., 2014, 2005). This approach has major premises that are worth being mentioned. First, pantropical AGB models are mixed-species models. Because tree species diversity in tropical forests is generally comprised between 100 and 300 species per ha (De Oliveira and Mori, 1999; Turner, 2001), developing species-specific equations as it is done in temperate forests (e.g. Brown and Schroeder, 1999) is currently unrealistic. Second, the geographical span of models validity englobes the entire tropics. This feature is particularly attractive because in most instances, as in the study of Picard and colleagues (2015), one does not have *a priori* knowledge on the relevance of a particular AGB model. Provided that AGB predictions from a pantropical model do not present systematic bias pattern at the local level (e.g. associated to specific stand species composition or environmental characteristics), using a single AGB model for all plots in large scale RS studies would provide a more consistent and transparent synthesis of spatial AGB variations derived from field data. Making accurate predictions of tree AGB regardless of species and geographic locations requires accounting for biometric predictors that reflect inter- tree AGB variation with sufficient generality and yet capture systematic trends on how tree AGB varies with tree size along ontogeny, across species and in space. Among the models proposed by Chave et al. (2014), the most powerful one (hereafter referred to as the pantropical AGB model) combines trunk diameter at breast height (D in cm), tree height (H in m) and wood specific gravity (ρ in $g.cm^{-3}$) in a compound variable related to AGB (in kg) through a power law of parameters α and β (eq. 1).

$$AGB = \alpha * (D^2 * H * \rho)^{\beta} \quad \text{(eq. 1)}$$

Equation 1 was calibrated on a destructive dataset containing more than 4000 trees from 58 sampling sites distributed across the pantropical belt. Chave and colleagues conducted a nested analysis of variance on model residuals (i.e. sampling site within forest type). The forest type factor (i.e. dry, moist, wet) accounted for less than 1 % of residuals variability, indicating that the AGB - $D^2 * H * \rho$ relationship holds well across broad environmental conditions. Sampling sites accounted for only c. 20 % of residuals variability, and adjusting equation 1 on data subsets from each site led to an average uncertainty on tree level predictions only slightly lower than with the pantropical model (i.e. c. 47 % vs c. 56 %, respectively) (Chave et al., 2014). These results provide a strong support for a pantropical approach of tree AGB modelling.

The pantropical model error on individual tree AGB prediction is huge (about 50 %), but this error levels-off when randomly accumulating trees, because positive and negative individual errors compensate (Chave et al., 2004; Picard et al., 2014). Assuming 50 % random prediction error on each tree, the prediction error on the AGB of a typical 1 ha forest plot should range between 5 and 10 % of the mean (Chave et al., 2014). High individual error stems from important AGB variations between trees of similar DBH, H and ρ (Molto et al., 2013) and could be reduced by including additional predictors in the model (e.g. crown diameter, Goodman et al., 2014), notably to increase the precision

of AGB predictions on plots of small size (e.g. < 1 ha). A more important issue is that the pantropical model systematically underestimates the AGB of large trees (c. 30 Mg) by c. 20 %. Given the importance of large trees for forest AGB stock (Bastin et al., 2015; Slik et al., 2013) and stock change (Stephenson et al., 2014), understanding the origin and consequences of this bias is of utmost concern.

Allometric theory of tree branching networks

Tree AGB models lie on the concept of 'allometry'. The term allometry was coined by Huxley and Teissier (1936) ''*to denote growth of a part* [of an organism] *at a different rate from that of* [the organism] *body as a whole*''. The simplest and most widespread type of tree AGB allometric model is a simple, bivariate relationship based on *D*. In such a model, the growth of whole tree AGB ("*the body*") is assessed through the growth of *D* ("*the part*"). Because growth data often fit particularly well to a straight line when plotted in logarithmic units (Stevens, 2009), the dominating mathematical function used to model allometries is a power function (as in equation 1). Perhaps the most important feature of the power model form in the context of allometry, and in our case AGB allometry, is that it implies a constant scaling (β) of AGB and *D* (or $D^2 * H * \rho$ in the pantropical model) across the whole ontogenic development of the organism.

On the one hand, scale-invariance (or self-similarity) properties has been documented for many animals and plants traits (e.g. West et al., 1997) and is thought to reflect universal principles governing biological systems (e.g. Marquet, 2005). Several allometric theories, such as the Metabolic Theory of Ecology (MTE, West et al., 1999, 1997), derive universal scaling laws (i.e. simple power model allometries) between plants dimensions from lower-level assumptions on plants branching structure, and thus support simple power-law allometries.

On the other hand, this scale-invariance hypothesis in the relative growth of organisms' parts (or between a part and the body as a whole) has been intensely criticized (e.g. Nijhout and German, 2012). Some consider that the power model form is fundamentally empirical and lacks biological foundations. For example, Nijhout and German (2012) pointed out that an implicit assumption in the power model form is that all body parts begin and end their growth at the same time during ontogeny. In the case of trees, it is commonly accepted that the growth in H slows down and eventually stops long before the growth in *D*. Empirically, several tree dimensions such as tree height or tree crown diameter show a constant scaling (β) with *D* only on a finite *D* range (Antin et al., 2013; Blanchard et al., 2016), leading Picard et al. (2015) to stress that since "*many non-power models can bring nearly constant scaling across a wide range of scale, simple allometry may be confused with complex allometry*" ("complex allometry" in this statement refers to a model with multiple predictors that does not necessarily take the form of a power function). Whether relationships between tree AGB and *D* or $D^2 * H * \rho$ conform to power function remains a pending question.

1.2 Research objectives

The general objective of this thesis is to use information on the structure and spatial organization of canopy trees to improve our ability to model forest AGB from field and RS data.

Our analyses are restricted to two approaches that were deemed promising: the pantropical approach for the estimation of AGB at the tree and plot level (i.e. from field data) and the canopy texture approach for the detection and extrapolation of field-derived AGB estimations via RS data.

A first part of this work seeks to increase our understanding of the pantropical model error and propose ways to mitigate this error. In particular, the compound predictor variable of the pantropical model ($D^2 * H * \rho$) does not allow capturing between-tree variations in relative crown dimensions, while crown allometries varies between species, along tree ontogeny and environmental gradients (e.g. Banin et al., 2012; Cannell, 1984; Poorter et al., 2006). We thus:

(**i**) Assess the contribution of crown mass variation to the pantropical model error, either at the tree level or when propagated to the plot level;

(**ii**) Propose a new operational strategy to explicitly take crown mass variation into account in pantropical AGB models.

We further used the predictions of the MTE on branch scaling properties as a point-of-entry to investigate the relevance of the power model form in AGB allometries. Specifically, we:

(**iii**) Test whether large trees branching structure conform to the predictions of the MTE.

A second part of the thesis focuses on assessing and improving the potential of a canopy texture-based RS method (FOTO) to retrieve tropical forest AGB. Here, a major objective was to:

(**iv**) Stabilize the texture-structure relationship across contrasted forest types from different regions of the world.

1.3 A pantropical approach

This thesis is based on two types of field data: (i) destructive measurements at the tree level and (ii) forest inventories at plot level. In this section, I briefly explain where the data I assembled came from and what the datasets are composed of.

1.3.1 Study areas and datasets

Central Africa

Core datasets of this work (at both tree- and plot-level) come from about five years of field data collection campaigns in central Africa (Cameroon, Gabon, Democratic Republic of Congo) carried out by the Institut de Recherche pour le Développement (IRD) in collaboration with the Ecole Normale Supérieure of Yaoundé I (LaBosystE, ENS, Université de Yaoundé I), the Missouri Botanical Garden (MBG) and the Université Libre de Kisangani (UniKis). During the two years preceding my thesis and during the thesis itself, I participated to the establishment of nearly 80 1-ha forest inventory plots, the bulk of which being located in south-eastern Cameroon (c. 50 %, left panel in Figure 1-3). Forests in this region have been described as a transitional type between evergreen and deciduous forests (Letouzey, 1985) and expand across the borders of neighboring countries. From a structural point of view, these forests can be described as forests mosaics that notably include patches of mixed, closed-canopy, semi-deciduous stands, open-canopy *Marantaceae* stands and monodominant *Gilbertiodendron dewevrei* stands. The diversity of stands structural profiles, from which contrasted canopy textures emerge (illustrated in Figure 1-3), justifies our interest in this region. Forests of south-eastern Cameroon are also particularly rich in tall trees and stock relatively high biomass densities

(Fayolle et al., 2016), and several logging companies are established in the region. Through a collaboration with the Alpicam company, we assembled a large destructive dataset on trees dimensions and AGB (77 trees).

Additional study areas

In the scope of this thesis, I investigate broad biophysical relationships, be it at the tree level in biomass allometry models or at the stand levels in canopy texture-based AGB models. In order to increase the robustness of the results, I compiled additional data from the literature, collaborating institutions or peer researchers (right panel on Figure 1-3).

The sets of 1 ha forest inventories from IRD and collaborators field work in central Africa were complemented with 28 1-ha plots from a forest-savanna mosaic in Republic Democratic of Congo (from Bastin et al., 2014), a 50 ha plots located in the Atlantic evergreen forests of western Cameroon (from Chuyong et al., 2004), 15 and 22 1-ha plots in evergreen and semi-deciduous forests of the Western Ghats of India (from Ploton et al., 2011 and Pargal et al., submitted) and 16 plots covering 85 ha of evergreen forests at Paracou, French Guiana (from Vincent et al., 2012). In total, texture analyses were based on 279 ha of forest inventory distributed on 3 continents.

To the 77 trees destructively sampled in south-eastern Cameroon, I added 132 trees from a semi-deciduous forest of the same region (from Fayolle et al., 2013), 99 trees sampled in a semi-deciduous forest of Gabon (from Ngomanda et al., 2014), 29 trees sampled in an evergreen forest of Ghana (from Henry et al., 2010), 285 trees sampled in a dry-to-wet forest types gradient in Madagascar (from Vieilledent et al., 2012) and 51 trees sampled in an evergreen forest of Peru (from Goodman et al., 2014). The total destructive dataset (n=673) thus comprises trees from 6 sites distributed in five tropical countries (right panel in Figure 1-3).

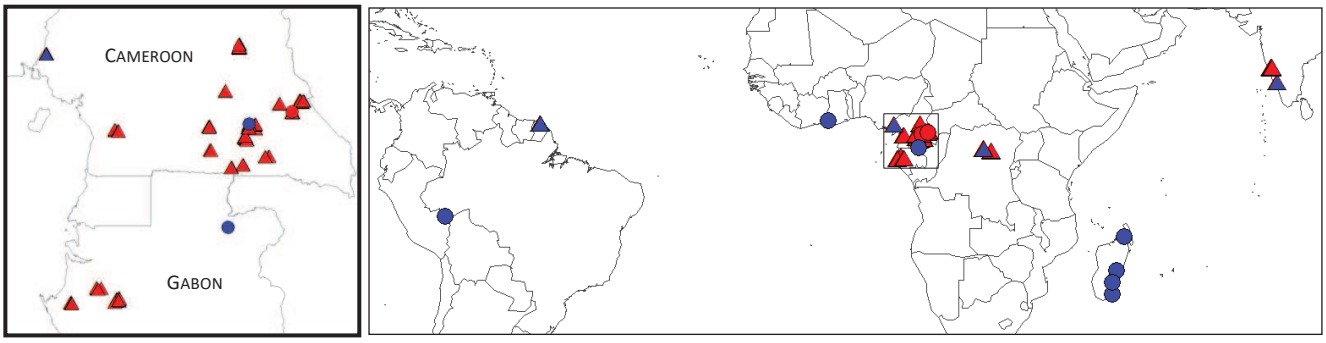

Figure 1-3. Distribution of datasets across the tropics. Dots and triangles represent tree-level destructive datasets and field plot inventories, respectively. Red color indicates that data have been collected by IRD. Blue color indicates that data were compiled from literature, collaborating institutions or shared by the peer researchers.

Figure 1-4. VHSR satellite image (GeoEye sensor) covering a typical forest mosaic from semi-deciduous forests of south-eastern Cameroon. Patches of *Gilbertiodendron dewevrei* (black square), mixed closed-canopy stands (red square) and open-canopy *Marantaceae* stands closely co-occur.

1.3.2 Sampling strategy and data description

Tree-level destructive data

Large trees exhibits the largest AGB variability at a given D and H while being insufficiently represented in biomass destructive datasets (Chave et al., 2005), probably because of the disproportionate amount of work that the biomass estimation of a large tropical canopy tree represents. To fill this gap, we exclusively targeted very large canopy trees in our field work protocol. This unique dataset, which was incorporated in the latest pantropical database (Chave et al. 2014), contains 17 out of the 30 world's heaviest sampled tropical trees. For a typical tree, we measured the trunk diameter D, the tree height H and two perpendicular crown diameters before the tree was felled. After felling, tree biomass was estimated by combining direct measurements, indirect measurements and allometries. Direct measurements (i.e. weightings) were made on branches of varying sizes, to build an allometry relating branch diameter to biomass. We estimated the volume of the largest tree components (i.e. trunk and branches with diameter > 20 cm) by measuring diameters and lengths of approximately 2-m and 1-m long subsections along the trunk and branches, respectively. Biomass values were obtained by multiplying volumes by wood density estimates, derived from wood samples. The biomass of branches with D ≤ 20 cm was obtained with species-specific biomass allometries. A detailed description of the field protocol is provided in the supplementary material of chapter 2. An important feature of this dataset is that it contains a description of the crown geometry (from diameter and length measurements) and topology (from the identification of branching points), allowing to reconstruct the tree branching network (up to a branch diameter of c. 20 cm) in 3D and explore allometries and scaling properties at the branch level.

Destructive data compiled from other studies were obtained by direct biomass measurement, I refer the reader to the publications associated to each dataset for more details. Importantly, I only considered datasets providing enough information to distinguish trunk from crown biomass (rather than ones providing a single total tree biomass estimate).

Plot level data

Apart for plots at Paracou (85 ha) and Korup (50 ha), the sampling strategy at all sites was designed to optimize canopy texture analyses from VHSR optical images. In essence, 1 ha plots were distributed over a few hundred square kilometers (the typical footprint of a VHSR image) so to capture local diversity of forest stand types and ages. Measurement protocols deployed in central Africa, India and French Guiana were similar and consisted in describing the structure and composition of forest stands for all trees with $D \geq 10$ cm. In addition to tree diameter at breast height (D), the description of stands structure included measurements of total tree height (H), trunk height (Ht) and crown diameter (Cd) on a subset of trees per plot (typically c. 50), to document local trees allometries. The identification of tree species allows retrieving species-level wood density estimates (ρ) from global databases (e.g. Zanne et al., 2009) and compute plots AGB with the reference pantropical biomass model (Chave et al., 2014).

1.4 Thesis outline

The thesis is structured into six chapters. The current chapter briefly depicts the scientific context and motivations of my doctoral study. It also includes the thesis research objectives, a description of the datasets and the thesis structure. A last section lists the publications I authored or co-authored on research topics related to the thesis subject.

In **Chapter 2**, I investigate how variations in tree form, with a particular focus on crown dimensions, influence the predictions (and error) of the pantropical biomass model. The analyses are based on the largest destructive dataset available to date that features information on tropical tree crown mass. After pinpointing the source of bias in the pantropical model, I propose an alternative model functional form. An original method for propagating tree biomass estimation error at the plot level is developed and highlights an interaction between forest structure and biomass model error, a source of uncertainty largely overlooked. This study was partly published in the journal *Biogeosciences*.

In **Chapter 3**, I further explore the structural properties of large trees crowns that could explain the deviation between large trees biomass and the mathematical power form of the pantropical biomass model. An empirical assessment of MTE's theoretical branch allometry is provided. A manuscript is in preparation from these results for the journal *Trees – Structure and Function*.

Chapter 4 presents the FOTO method, i.e. a remote sensing approach to retrieve forest structure and biomass gradients from canopy texture features. I give a concise description of how the method works and the basic rationale behind it. Further, I provide a synthetic overview of the results obtained in separate empirical FOTO case studies on diverse forest ecosystems and from various remote sensing data types. This synthesis highlights methodological limits hindering the development of FOTO as a broad-scale, operational forest biomass monitoring method. This chapter was partly published in a book entitled *Treetops at Risk* (Springer).

Chapter 5 builds upon the synthesis in chapter 4. A simulation procedure is used, which includes the representation of forest sample plots as three-dimensional mockups and the generation of virtual mockup canopy scenes. Simulated canopy scenes allow testing how the relation between texture features and stand biomass varies across forest types in a single, unified analysis frame (as opposed to previous empirical studies). The major limits identified in chapter 4 are addressed by complementing

FOTO texture with additional descriptors of forest stand structure, notably derived from lacunarity analysis. A 'generalized' biomass prediction model based on a combination of texture metrics is proposed, opening new perspectives for biomass retrieval from canopy texture at large scale. Part of these results was submitted for publication in *Remote Sensing of Environment*.

Finally, **Chapter 6** presents the overall thesis discussion, focusing on the main contributions, limits and perspectives of this work.

1.5 List of (co-)publications

Estimation of biomass in forest sample plots

- **Ploton, P.**, Barbier, N., Takoudjou Momo, S., Réjou-Méchain, M., Boyemba Bosela, F., Chuyong, G., Dauby, G., Droissart, V., Fayolle, A., Goodman, R.C., Henry, M., Kamdem, N.G., Mukirania, J.K., Kenfack, D., Libalah, M., Ngomanda, A., Rossi, V., Sonké, B., Texier, N., Thomas, D., Zebaze, D., Couteron, P., Berger, U., Pélissier, R., 2016. Closing a gap in tropical forest biomass estimation: taking crown mass variation into account in pantropical allometries. Biogeosciences 13, 1571–1585. doi:10.5194/bg-13-1571-2016
- **Ploton, P.**, Barbier, N., Couteron, P., Momo, S.T., Griffon, S., Sonké, B., Uta, B., Pélissier, R. Assessing Da Vinci's rule on large tropical tree crowns of contrasted architectures : evidence for area-increasing branching. **In preparation** for *Trees – Structure and Function.*
- Picard, N., Rutishauser, E., **Ploton, P.**, Ngomanda, A., Henry, M., 2015. Should tree biomass allometry be restricted to power models? For. Ecol. Manag. 353, 156–163. doi:10.1016/j.foreco.2015.05.035
- Chave, J., Réjou-Méchain, M., Búrquez, A., Chidumayo, E., Colgan, M.S., Delitti, W.B.C., Duque, A., Eid, T., Fearnside, P.M., Goodman, R.C., Henry, M., Martínez-Yrízar, A., Mugasha, W.A., Muller-Landau, H.C., Mencuccini, M., Nelson, B.W., Ngomanda, A., Nogueira, E.M., Ortiz-Malavassi, E., Pélissier, R., **Ploton, P.**, Ryan, C.M., Saldarriaga, J.G., Vieilledent, G., 2014. Improved allometric models to estimate the aboveground biomass of tropical trees. Glob. Change Biol. 20, 3177–3190. doi:10.1111/gcb.12629

Rational behind texture-based remote sensing methods

- Bastin, J.-F., Barbier, N., Réjou-Méchain, M., Fayolle, A., Gourlet-Fleury, S., Maniatis, D., de Haulleville, T., Baya, F., Beeckman, H., Beina, D., Couteron, P., Chuyong, G., Dauby, G., Doucet, J.-L., Droissart, V., Dufrêne, M., Ewango, C., Gillet, J.F., Gonmadje, C.H., Hart, T., Kavali, T., Kenfack, D., Libalah, M., Malhi, Y., Makana, J.-R., Pélissier, R., **Ploton, P.**, Serckx, A., Sonké, B., Stevart, T., Thomas, D.W., De Cannière, C., Bogaert, J., 2015c. Seeing Central African forests through their largest trees. Sci. Rep. 5, 13156. doi:10.1038/srep13156
- Blanchard, E., Birnbaum, P., Ibanez, T., Boutreux, T., Antin, C., **Ploton, P.**, Vincent, G., Pouteau, R., Vandrot, H., Hequet, V., 2016. Contrasted allometries between stem diameter, crown area, and tree height in five tropical biogeographic areas. Trees 1–16.
- Jucker, T., Caspersen, J., Chave, J., Antin, C., Barbier, N., Bongers, F., Dalponte, M., van Ewijk, K.Y., Forrester, D.I., Haeni, M., Higgins, S.I., Holdaway, R.J., Iida, Y., Lorimer, C., Marshall, P.L., Momo, S., Moncrieff, G.R., **Ploton, P.**, Poorter, L., Rahman, K.A., Schlund, M., Sonké, B., Sterck, F.J., Trugman, A.T., Usoltsev, V.A., Vanderwel, M.C., Waldner, P., Wedeux, B.M.M., Wirth, C., Wöll, H., Woods, M., Xiang, W., Zimmermann, N.E., Coomes, D.A., 2016. Allometric equations for integrating remote sensing imagery into forest monitoring programmes. Glob. Change Biol. doi:10.1111/gcb.13388

Estimation of biomass from canopy texture features

- **Ploton, P.**, Pélissier, R., Barbier, N., Proisy, C., Ramesh, B.R., Couteron, P., 2013. Canopy texture analysis for large-scale assessments of tropical forest stand structure and biomass, in: Treetops at Risk. Springer, pp. 237–245.
- **Ploton, P.**, Barbier, N., Couteron, P., Ayyappan, N., Antin, C.M., Bastin, J.-F., Chuyong, G., Dauby, G., Droissart, V., Gastellu-Etchegorry, J.-P., Kamdem, N.G., Kenfack, D., Libalah, M., Momo, S., Pargal, S., Proisy, C., Sonké, B., Texier, N., Thomas, D., Zebaze, D., Verley, P., Vincent, G., Berger, U., Pélissier, R. Combining canopy texture metrics from optical data to retrieve tropical forest aboveground biomass in complex forest mosaics. **Submitted to** *Remote Sensing of Environment.*
- **Ploton, P.**, Pélissier, R., Proisy, C., Flavenot, T., Barbier, N., Rai, S.N., Couteron, P., 2012. Assessing aboveground tropical forest biomass using Google Earth canopy images. Ecol. Appl. 22, 993–1003. doi:10.1890/11-1606.1
- Couteron, P., Barbier, N., Deblauwe, V., Pélissier, R., **Ploton, P.**, 2015. Texture Analysis of Very High Spatial Resolution Optical Images as a Way to Monitor Vegetation and Forest Biomass in the Tropics. Multi-Scale For. Biomass Assess. Monit. Hindu Kush Himal. Reg. Geospatial Perspect. 157.

1.6 References

Ahmed, R., Siqueira, P., Hensley, S., Bergen, K., 2013. Uncertainty of Forest Biomass Estimates in North Temperate Forests Due to Allometry: Implications for Remote Sensing. Remote Sens. 5, 3007–3036. doi:10.3390/rs5063007

Antin, C., Pélissier, R., Vincent, G., Couteron, P., 2013. Crown allometries are less responsive than stem allometry to tree size and habitat variations in an Indian monsoon forest. Trees 27, 1485–1495. doi:10.1007/s00468-013-0896-7

Asner, G.P., Mascaro, J., Muller-Landau, H.C., Vieilledent, G., Vaudry, R., Rasamoelina, M., Hall, J.S., Breugel, M. van, 2011. A universal airborne LiDAR approach for tropical forest carbon mapping. Oecologia 168, 1147–1160. doi:10.1007/s00442-011-2165-z

Baccini, A., Goetz, S.J., Walker, W.S., Laporte, N.T., Sun, M., Sulla-Menashe, D., Hackler, J., Beck, P.S.A., Dubayah, R., Friedl, M.A., 2012. Estimated carbon dioxide emissions from tropical deforestation improved by carbon-density maps. Nat. Clim. Change 2, 182–185.

Banin, L., Feldpausch, T.R., Phillips, O.L., Baker, T.R., Lloyd, J., Affum-Baffoe, K., Arets, E.J.M.M., Berry, N.J., Bradford, M., Brienen, R.J.W., Davies, S., Drescher, M., Higuchi, N., Hilbert, D.W., Hladik, A., Iida, Y., Salim, K.A., Kassim, A.R., King, D.A., Lopez-Gonzalez, G., Metcalfe, D., Nilus, R., Peh, K.S.-H., Reitsma, J.M., Sonké, B., Taedoumg, H., Tan, S., White, L., Wöll, H., Lewis, S.L., 2012. What controls tropical forest architecture? Testing environmental, structural and floristic drivers. Glob. Ecol. Biogeogr. 21, 1179–1190. doi:10.1111/j.1466-8238.2012.00778.x

Barbier, N., Proisy, C., Véga, C., Sabatier, D., Couteron, P., 2011. Bidirectional texture function of high resolution optical images of tropical forest: An approach using LiDAR hillshade simulations. Remote Sens. Environ. 115, 167–179.

Bastin, J.-F., Barbier, N., Couteron, P., Adams, B., Shapiro, A., Bogaert, J., De Cannière, C., 2014. Aboveground biomass mapping of African forest mosaics using canopy texture analysis: toward a regional approach. Ecol. Appl. 24, 1984–2001.

Bastin, J.-F., Barbier, N., Réjou-Méchain, M., Fayolle, A., Gourlet-Fleury, S., Maniatis, D., de Haulleville, T., Baya, F., Beeckman, H., Beina, D., 2015. Seeing Central African forests through their largest trees. Sci. Rep. 5. doi:doi:10.1038/srep13156

Blanchard, E., Birnbaum, P., Ibanez, T., Boutreux, T., Antin, C., Ploton, P., Vincent, G., Pouteau, R., Vandrot, H., Hequet, V., 2016. Contrasted allometries between stem diameter, crown area, and tree height in five tropical biogeographic areas. Trees 1–16.

Brown, S., 1997. Estimating biomass and biomass change of tropical forests: a primer, UN FAO Forestry Paper 134. Food and Agriculture Organization, Rome.

Brown, S.L., Schroeder, P.E., 1999. Spatial patterns of aboveground production and mortality of woody biomass for eastern US forests. Ecol. Appl. 9, 968–980.

Cannell, M.G.R., 1984. Woody biomass of forest stands. For. Ecol. Manag. 8, 299–312. doi:10.1016/0378-1127(84)90062-8

Chave, J., Andalo, C., Brown, S., Cairns, M.A., Chambers, J.Q., Eamus, D., Fölster, H., Fromard, F., Higuchi, N., Kira, T., Lescure, J.-P., Nelson, B.W., Ogawa, H., Puig, H., Riéra, B., Yamakura, T., 2005. Tree allometry and improved estimation of carbon stocks and balance in tropical forests. Oecologia 145, 87–99. doi:10.1007/s00442-005-0100-x

Chave, J., Condit, R., Aguilar, S., Hernandez, A., Lao, S., Perez, R., 2004. Error propagation and scaling for tropical forest biomass estimates. Philos. Trans. R. Soc. Lond. B. Biol. Sci. 359, 409–420. doi:10.1098/rstb.2003.1425

Chave, J., Réjou-Méchain, M., Búrquez, A., Chidumayo, E., Colgan, M.S., Delitti, W.B.C., Duque, A., Eid, T., Fearnside, P.M., Goodman, R.C., Henry, M., Martínez-Yrízar, A., Mugasha, W.A., Muller-Landau, H.C., Mencuccini, M., Nelson, B.W., Ngomanda, A., Nogueira, E.M., Ortiz-Malavassi, E., Pélissier, R., Ploton, P., Ryan, C.M., Saldarriaga, J.G., Vieilledent, G., 2014. Improved

allometric models to estimate the aboveground biomass of tropical trees. Glob. Change Biol. 20, 3177–3190. doi:10.1111/gcb.12629
Chuyong, G.B., Condit, R., Kenfack, D., Losos, E.C., Moses, S.N., Songwe, N.C., Thomas, D.W., 2004. Korup forest dynamics plot, Cameroon. Trop. For. Divers. Dynamism 506–516.
Couteron, P., Pelissier, R., Nicolini, E.A., Paget, D., 2005. Predicting tropical forest stand structure parameters from Fourier transform of very high-resolution remotely sensed canopy images. J. Appl. Ecol. 42, 1121–1128.
De Oliveira, A.A., Mori, S.A., 1999. A central Amazonian terra firme forest. I. High tree species richness on poor soils. Biodivers. Conserv. 8, 1219–1244.
De Sy, V., Herold, M., Achard, F., Asner, G.P., Held, A., Kellndorfer, J., Verbesselt, J., 2012. Synergies of multiple remote sensing data sources for REDD+ monitoring. Curr. Opin. Environ. Sustain. 4, 696–706.
Eggleston, H.S., Buendia, L., Miwa, K., Ngara, T., Tanabe, K., 2006. 2006 IPCC guidelines for national greenhouse gas inventories. Agriculture, Forestry and Other Land Use. Inst. Glob. Environ. Strateg. IGES Behalf Intergov. Panel Clim. Change IPCC Hayama Jpn. 4.
FAO, 2010. Global Forest Resources Assessment 2010 (FAO Forestry Paper No. 163). Food and Agriculture Organization of the United Nations, Rome.
Fayolle, A., Doucet, J.-L., Gillet, J.-F., Bourland, N., Lejeune, P., 2013. Tree allometry in Central Africa: Testing the validity of pantropical multi-species allometric equations for estimating biomass and carbon stocks. For. Ecol. Manag. 305, 29–37. doi:10.1016/j.foreco.2013.05.036
Fayolle, A., Loubota Panzou, G.J., Drouet, T., Swaine, M.D., Bauwens, S., Vleminckx, J., Biwole, A., Lejeune, P., Doucet, J.-L., 2016. Taller trees, denser stands and greater biomass in semi-deciduous than in evergreen lowland central African forests. For. Ecol. Manag. 374, 42–50. doi:10.1016/j.foreco.2016.04.033
Foody, G.M., 2003. Remote sensing of tropical forest environments: towards the monitoring of environmental resources for sustainable development. Int. J. Remote Sens. 24, 4035–4046.
Gastellu-Etchegorry, J.-P., Yin, T., Lauret, N., Cajgfinger, T., Gregoire, T., Grau, E., Feret, J.-B., Lopes, M., Guilleux, J., Dedieu, G., 2015. Discrete Anisotropic Radiative Transfer (DART 5) for modeling airborne and satellite spectroradiometer and LIDAR acquisitions of natural and urban landscapes. Remote Sens. 7, 1667–1701.
Goodman, R.C., Phillips, O.L., Baker, T.R., 2014. The importance of crown dimensions to improve tropical tree biomass estimates. Ecol. Appl. 24, 680–698.
Gullison, R.E., Frumhoff, P.C., Canadell, J.G., Field, C.B., Nepstad, D.C., Hayhoe, K., Avissar, R., Curran, L.M., Friedlingstein, P., Jones, C.D., Nobre, C., 2007. Tropical Forests and Climate Policy. Science 316, 985–986. doi:10.1126/science.1136163
Henry, M., Besnard, A., Asante, W.A., Eshun, J., Adu-Bredu, S., Valentini, R., Bernoux, M., Saint-André, L., 2010. Wood density, phytomass variations within and among trees, and allometric equations in a tropical rainforest of Africa. For. Ecol. Manag. 260, 1375–1388. doi:10.1016/j.foreco.2010.07.040
Houghton, R.A., 2012. Carbon emissions and the drivers of deforestation and forest degradation in the tropics. Curr. Opin. Environ. Sustain. 4, 597–603.
Houghton, R.A., 2007. Balancing the Global Carbon Budget. Annu Rev Earth Planet Sci 35, 313–347.
Houghton, R.A., 2005. Aboveground forest biomass and the global carbon balance. Glob. Change Biol. 11, 945–958.
Houghton, R.A., Hall, F., Goetz, S.J., 2009. Importance of biomass in the global carbon cycle. J. Geophys. Res. Biogeosciences 114.
Houghton, R.A., Lawrence, K.T., Hackler, J.L., Brown, S., 2001. The spatial distribution of forest biomass in the Brazilian Amazon: a comparison of estimates. Glob. Change Biol. 7, 731–746.
Huete, A., Didan, K., Miura, T., Rodriguez, E.P., Gao, X., Ferreira, L.G., 2002. Overview of the radiometric and biophysical performance of the MODIS vegetation indices. Remote Sens. Environ. 83, 195–213.

Huxley, J.S., Teissier, G., 1936. Terminology of Relative Growth. Nature 137, 780–781. doi:10.1038/137780b0

Imhoff, M.L., 1995. Radar backscatter and biomass saturation: ramifications for global biomass inventory. Geosci. Remote Sens. IEEE Trans. On 33, 511–518.

IPCC, 2014. Summary for policymakers, in: Climate Change 2014: Mitigation of Climate Change. Contribution of Working Group III to the Fifth Assessment Report of the Intergovernmental Panel on Climate Change. Cambridge University Press, Cambridge, United Kingdom and New York, NY, USA, pp. 1–30.

Langner, A., Achard, F., Grassi, G., 2014. Can recent pan-tropical biomass maps be used to derive alternative Tier 1 values for reporting REDD+ activities under UNFCCC? Environ. Res. Lett. 9, 124008. doi:10.1088/1748-9326/9/12/124008

Letouzey, R., 1985. Carte phytogéographique du Cameroun. Institut de la recherche agronomique.

Marquet, P.A., 2005. Scaling and power-laws in ecological systems. J. Exp. Biol. 208, 1749–1769. doi:10.1242/jeb.01588

Mattsson, E., Ostwald, M., Wallin, G., Nissanka, S.P., 2016. Heterogeneity and assessment uncertainties in forest characteristics and biomass carbon stocks: Important considerations for climate mitigation policies. Land Use Policy 59, 84–94. doi:10.1016/j.landusepol.2016.08.026

Mitchard, E.T., Feldpausch, T.R., Brienen, R.J., Lopez-Gonzalez, G., Monteagudo, A., Baker, T.R., Lewis, S.L., Lloyd, J., Quesada, C.A., Gloor, M., 2014. Markedly divergent estimates of Amazon forest carbon density from ground plots and satellites. Glob. Ecol. Biogeogr. 23, 935–946.

Mitchard, E.T., Saatchi, S.S., Baccini, A., Asner, G.P., Goetz, S.J., Harris, N.L., Brown, S., 2013. Uncertainty in the spatial distribution of tropical forest biomass: a comparison of pan-tropical maps. Carbon Balance Manag. 8, 10. doi:10.1186/1750-0680-8-10

Molto, Q., Rossi, V., Blanc, L., 2013. Error propagation in biomass estimation in tropical forests. Methods Ecol. Evol. 4, 175–183. doi:10.1111/j.2041-210x.2012.00266.x

Morton, D.C., 2016. Forest carbon fluxes: A satellite perspective. Nat. Clim. Change 6, 346–348. doi:10.1038/nclimate2978

Mougin, E., Proisy, C., Marty, G., Fromard, F., Puig, H., Betoulle, J.L., Rudant, J.-P., 1999. Multifrequency and multipolarization radar backscattering from mangrove forests. Geosci. Remote Sens. IEEE Trans. On 37, 94–102.

Ngomanda, A., Engone Obiang, N.L., Lebamba, J., Moundounga Mavouroulou, Q., Gomat, H., Mankou, G.S., Loumeto, J., Midoko Iponga, D., Kossi Ditsouga, F., Zinga Koumba, R., Botsika Bobé, K.H., Mikala Okouyi, C., Nyangadouma, R., Lépengué, N., Mbatchi, B., Picard, N., 2014. Site-specific versus pantropical allometric equations: Which option to estimate the biomass of a moist central African forest? For. Ecol. Manag. 312, 1–9. doi:10.1016/j.foreco.2013.10.029

Nijhout, H.F., German, R.Z., 2012. Developmental Causes of Allometry: New Models and Implications for Phenotypic Plasticity and Evolution. Integr. Comp. Biol. 52, 43–52. doi:10.1093/icb/ics068

Ometto, J.P., Aguiar, A.P., Assis, T., Soler, L., Valle, P., Tejada, G., Lapola, D.M., Meir, P., 2014. Amazon forest biomass density maps: tackling the uncertainty in carbon emission estimates. Clim. Change 124, 545–560.

Pan, Y., Birdsey, R.A., Fang, J., Houghton, R., Kauppi, P.E., Kurz, W.A., Phillips, O.L., Shvidenko, A., Lewis, S.L., Canadell, J.G., 2011. A large and persistent carbon sink in the world's forests. Science 333, 988–993.

Pargal, S., Fararoda, R., Rajashekar, G., Balachandran, N., Réjou-Méchain, M., Barbier, N., Jha, C.S., Pélissier, R., Dadhwal, V.K., Couteron, P., n.d. Characterizing aboveground biomass – canopy texture relationships in a landscape of forest mosaic in the Western Ghats of India using very high resolution Cartosat Imagery. Remote Sens.

Picard, N., Bosela, F.B., Rossi, V., 2014. Reducing the error in biomass estimates strongly depends on model selection. Ann. For. Sci. 72, 811–923. doi:10.1007/s13595-014-0434-9

Picard, N., Rutishauser, E., Ploton, P., Ngomanda, A., Henry, M., 2015. Should tree biomass allometry be restricted to power models? For. Ecol. Manag. 353, 156–163. doi:10.1016/j.foreco.2015.05.035

Ploton, P., Pélissier, R., Proisy, C., Flavenot, T., Barbier, N., Rai, S.N., Couteron, P., 2012. Assessing aboveground tropical forest biomass using Google Earth canopy images. Ecol. Appl. 22, 993–1003. doi:10.1890/11-1606.1

Poorter, L., Bongers, L., Bongers, F., 2006. Architecture of 54 moist-forest tree species: traits, trade-offs, and functional groups. Ecology 87, 1289–1301. doi:10.1890/0012-9658(2006)87[1289:AOMTST]2.0.CO;2

Proisy, C., Couteron, P., Fromard, F., 2007. Predicting and mapping mangrove biomass from canopy grain analysis using Fourier-based textural ordination of IKONOS images. Remote Sens. Environ. 109, 379–392.

Ryan, M.G., Binkley, D., Fownes, J.H., 1997. Age-related decline in forest productivity: pattern and process. Adv. Ecol. Res. 27, 213–262.

Saatchi, S.S., Harris, N.L., Brown, S., Lefsky, M., Mitchard, E.T., Salas, W., Zutta, B.R., Buermann, W., Lewis, S.L., Hagen, S., 2011. Benchmark map of forest carbon stocks in tropical regions across three continents. Proc. Natl. Acad. Sci. 108, 9899–9904.

Sileshi, G.W., 2014. A critical review of forest biomass estimation models, common mistakes and corrective measures. For. Ecol. Manag. 329, 237–254. doi:10.1016/j.foreco.2014.06.026

Slik, J.W., Paoli, G., McGuire, K., Amaral, I., Barroso, J., Bastian, M., Blanc, L., Bongers, F., Boundja, P., Clark, C., 2013. Large trees drive forest aboveground biomass variation in moist lowland forests across the tropics. Glob. Ecol. Biogeogr. 22, 1261–1271.

Stephenson, N.L., Das, A.J., Condit, R., Russo, S.E., Baker, P.J., Beckman, N.G., Coomes, D.A., Lines, E.R., Morris, W.K., Rüger, N., Álvarez, E., Blundo, C., Bunyavejchewin, S., Chuyong, G., Davies, S.J., Duque, Á., Ewango, C.N., Flores, O., Franklin, J.F., Grau, H.R., Hao, Z., Harmon, M.E., Hubbell, S.P., Kenfack, D., Lin, Y., Makana, J.-R., Malizia, A., Malizia, L.R., Pabst, R.J., Pongpattananurak, N., Su, S.-H., Sun, I.-F., Tan, S., Thomas, D., van Mantgem, P.J., Wang, X., Wiser, S.K., Zavala, M.A., 2014. Rate of tree carbon accumulation increases continuously with tree size. Nature advance online publication. doi:10.1038/nature12914

Stevens, C.F., 2009. Darwin and Huxley revisited: the origin of allometry. J. Biol. 8, 1.

Turner, I.M., 2001. The ecology of trees in the tropical rain forest. Cambridge University Press.

UNFCCC, 2007. Reducing Emissions From Deforestation in Developing Countries: Approaches to Stimulate Action.

van Breugel, M., Ransijn, J., Craven, D., Bongers, F., Hall, J.S., 2011. Estimating carbon stock in secondary forests: Decisions and uncertainties associated with allometric biomass models. For. Ecol. Manag. 262, 1648–1657. doi:10.1016/j.foreco.2011.07.018

Van der Werf, G.R., Morton, D.C., DeFries, R.S., Olivier, J.G., Kasibhatla, P.S., Jackson, R.B., Collatz, G.J., Randerson, J.T., 2009. CO2 emissions from forest loss. Nat. Geosci. 2, 737–738.

Véga, C., Vepakomma, U., Morel, J., Bader, J.-L., Rajashekar, G., Jha, C.S., Ferêt, J., Proisy, C., Pélissier, R., Dadhwal, V.K., 2015. Aboveground-Biomass Estimation of a Complex Tropical Forest in India Using Lidar. Remote Sens. 7, 10607–10625.

Vieilledent, G., Vaudry, R., Andriamanohisoa, S.F., Rakotonarivo, O.S., Randrianasolo, H.Z., Razafindrabe, H.N., Rakotoarivony, C.B., Ebeling, J., Rasamoelina, M., 2012. A universal approach to estimate biomass and carbon stock in tropical forests using generic allometric models. Ecol. Appl. 22, 572–583.

Vincent, G., Sabatier, D., Blanc, L., Chave, J., Weissenbacher, E., Pélissier, R., Fonty, E., Molino, J.-F., Couteron, P., 2012. Accuracy of small footprint airborne LiDAR in its predictions of tropical moist forest stand structure. Remote Sens. Environ. 125, 23–33.

West, G.B., Brown, J.H., Enquist, B.J., 1999. A general model for the structure and allometry of plant vascular systems. Nature 400, 664–667. doi:10.1038/23251

West, G.B., Brown, J.H., Enquist, B.J., 1997. A general model for the origin of allometric scaling laws in biology. Science 276, 122–126.

Woodhouse, I.H., Mitchard, E.T.A., Brolly, M., Maniatis, D., Ryan, C.M., 2012. Radar backscatter is not a “direct measure” of forest biomass. Nat. Clim. Change 2, 556–557. doi:10.1038/nclimate1601

Zanne, A.E., Lopez-Gonzalez, G., Coomes, D.A., Ilic, J., Jansen, S., Lewis, S.L., Miller, R.B., Swenson, N.G., Wiemann, M.C., Chave, J., 2009. Global wood density database.

Zolkos, S.G., Goetz, S.J., Dubayah, R., 2013. A meta-analysis of terrestrial aboveground biomass estimation using lidar remote sensing. Remote Sens. Environ. 128, 289–298.

2 CLOSING A GAP IN TROPICAL FOREST BIOMASS ESTIMATION: ACCOUNTING FOR CROWN MASS VARIATION IN PANTROPICAL ALLOMETRIES

P. Ploton[1,2], N. Barbier[1], S. Momo[1,3], M. Réjou-Méchain[1,4,5], F. Boyemba Bosela[6], G. Chuyong[7], G. Dauby[8,9], V. Droissart[1,10], A. Fayolle[11], R.C. Goodman[12], M. Henry[13], N.G. Kamdem[3], J. Katembo Mukirania[6], D. Kenfack[14], M Libalah[3], A. Ngomanda[15], V. Rossi[4,16], B. Sonké[3], N. Texier[1,3], D. Thomas[17], D. Zebaze[3], P. Couteron[1], U. Berger[18] and R. Pélissier[1]

[1]Institut de Recherche pour le Développement, UMR-AMAP, Montpellier, France
[2]Institut des sciences et industries du vivant et de l'environnement, Montpellier, France
[3]Laboratoire de Botanique systématique et d'Ecologie, Département des Sciences Biologiques, Ecole Normale Supérieure, Université de Yaoundé I, Yaoundé, Cameroon
[4]Centre de coopération internationale en recherche agronomique pour le développement, Montpellier, France
[5]French Institute of Pondicherry, Puducherry, India
[6]University of Kisangani, Kisangani, Democratic Republic of Congo
[7]Department of Botany and Plant Physiology, University of Buea, Buea, Cameroon
[8]Institut de Recherche pour le Développement, UMR-DIADE, Montpellier, France
[9]Evolutionary Biology and Ecology, Faculté des Sciences, Université Libre de Bruxelles, Brussels, Belgium
[10]Herbarium et Bibliothèque de Botanique africaine, Université Libre de Bruxelles, Brussels, Belgium
[11]Research axis on Forest Resource Management of the Biosystem engineering (BIOSE), Gembloux, Belgium
[12]Yale School of Forestry and Environmental Studies, New Haven, USA
[13]Food and Agricultural Organisation of the United Nations, UN-REDD Programme, Rome, Italy
[14]Center for Tropical Forest Science, Harvard University, Cambridge, USA
[15]Institut de Recherche en Ecologie Tropicale, Libreville, Gabon
[16]Université de Yaoundé I, UMMISCO, Yaoundé, Cameroon
[17]Department of Botany and Plant Pathology, Oregon State University, Corvallis, USA
[18]Technische Universität Dresden, Faculty of Environmental Sciences, Institute of Forest Growth and Forest Computer Sciences, Tharandt, Germany

Abstract

Accurately monitoring tropical forest carbon stocks is an outstanding challenge. Allometric models that consider tree diameter, height and wood density as predictors are currently used in most tropical forest carbon studies. In particular, a pantropical biomass model has been widely used for approximately a decade, and its most recent version will certainly constitute a reference in the coming years. However, this reference model shows a systematic bias for the largest trees. Because large trees are key drivers of forest carbon stocks and dynamics, understanding the origin and the consequences of this bias is of utmost concern. In this study, we compiled a unique tree mass dataset on 673 trees measured in five tropical countries (101 trees > 100 cm in diameter) and an original dataset of 130 forest plots (1 ha) from central Africa to quantify the error of biomass allometric models at the individual and plot levels when explicitly accounting or not accounting for crown mass variations. We first showed that the proportion of crown to total tree aboveground biomass is highly variable among trees, ranging from 3 to 88 %. This proportion was constant on average for trees < 10 Mg (mean of 34

%) but, above this threshold, increased sharply with tree mass and exceeded 50 % on average for trees ≥ 45 Mg. This increase coincided with a progressive deviation between the pantropical biomass model estimations and actual tree mass. Accounting for a crown mass proxy in a newly developed model consistently removed the bias observed for large trees (> 1 Mg) and reduced the range of plot-level error from -23–16 % to 0–10 %. The disproportionally higher allocation of large trees to crown mass may thus explain the bias observed recently in the reference pantropical model. This bias leads to far-from-negligible, but often overlooked, systematic errors at the plot level and may be easily corrected by accounting for a crown mass proxy for the largest trees in a stand, thus suggesting that the accuracy of forest carbon estimates can be significantly improved at a minimal cost.

2.1 Introduction

Monitoring forest carbon variation in space and time is both a sociopolitical challenge for climate change mitigation and a scientific challenge, especially in tropical forests, which play a major role in the world carbon balance (Hansen et al., 2013; Harris et al., 2012; Saatchi et al., 2011). Significant milestones have been reached in the last decade thanks to the development of broad-scale remote sensing approaches (Baccini et al., 2012; Malhi et al., 2006; Mitchard et al., 2013; Saatchi et al., 2011). However, local forest biomass estimations are still the bedrock of most (if not all) of these approaches for the calibration and validation of remote sensing models. As a consequence, uncertainties and errors in local biomass estimations may propagate dramatically to broad-scale forest carbon stock assessment (Avitabile et al., 2011; Pelletier et al., 2011; Réjou-Méchain et al., 2014). Aboveground biomass (AGB) is the major pool of biomass in tropical forests (Eggleston et al., 2006). The AGB of a tree (or TAGB) is generally predicted by empirically derived allometric equations that use measurements of the size of an individual tree as predictors of its mass (Clark and Kellner, 2012). Among these predictors, diameter at breast height (D) and total tree height (H) are often used to capture volume variations between trees, whereas wood density (ρ) is used to convert volume to dry mass (Brown et al., 1989). The most currently used allometric equations for tropical forests (Chave et al., 2005, 2014) have the following form: $TAGB = \alpha * \left(D^2 H \rho\right)^{\beta}$, where diameter, height and wood density are combined into a single compound variable related to dry mass through a power law of parameters α and β. This model form, referred to hereafter as our reference allometric model form, performs well when $\beta = 1$ or close to 1 (Chave et al., 2005, 2014), meaning that trees can roughly be viewed as a standard geometric solid for which the parameter α determines the shape (or form factor) of the geometric approximation. However, the uncertainty associated with this model is still very high, with an average error of 50 % at the tree level, illustrating the high natural variability of mass between trees with similar D, H and ρ values. More importantly, this reference allometric model shows a systematic underestimation of TAGB of approximately 20 % in average for the heaviest trees (> 30 Mg) (Fig. 2 in Chave et al. 2014), which may contribute strongly to uncertainty in biomass estimates at the plot level. It is often argued that, by definition, the least-squares regression model implies that tree-level errors are globally centered on 0, thus limiting the plot-level prediction error to approximately 5-10 % for a standard 1-ha forest plot (Chave et al., 2014; Moundounga Mavouroulou et al., 2014). However, systematic errors associated with large trees are expected to disproportionally propagate to plot-level predictions because of their prominent contribution to plot AGB (Bastin et al., 2015; Clark and Clark, 1996; Sist et al., 2014; Slik et al., 2013; Stephenson et al., 2014). Thus, identifying the origin

of systematic errors in such biomass allometric models is a prerequisite for improving local biomass estimations and thus limiting the risk of uncontrolled error propagation to broad-scale extrapolations.

As foresters have known for decades, it is reasonable to approximate stem volume using a geometric shape. Such an approximation, however, is questionable for assessing the total tree volume, including the crown. Because β is generally close to 1 in the reference allometric model, the relative proportion of crown to total tree mass (or crown mass ratio) directly affects the adjustment of the tree form factor α (e.g., Cannell 1984). Moreover, the crown mass ratio is known to vary greatly between species, reflecting different strategies of carbon allocation. For instance, Cannell (1984) observed that coniferous species have a lower proportion of crown mass (10-20 %) than tropical broadleaved species (over 35 %), whereas temperate softwood species were found to have a lower and less variable crown mass ratio (20-30 %) than temperate hardwood species (20-70 %; Freedman et al., 1982; Jenkins et al., 2003). In the tropics, distinct crown size allometries have been documented among species functional groups (Poorter et.al. 2003; Poorter, Bongers, et Bongers 2006; Van Gelder, Poorter, et Sterck 2006). For instance, at comparable stem diameters, pioneer species tend to be taller and to have shorter and narrower crowns than understory species (Poorter et al., 2006). These differences reflect strategies of energy investment (tree height *vs*. crown development) that are likely to result in different crown mass ratios among trees with similar $\mathrm{D}^2 * \mathrm{H} * \rho$ values. Indeed, Goodman et al. (2014) obtained a substantially improved biomass allometric model when crown diameter was incorporated into the equation to account for individual variation in crown size.

Destructive data on tropical trees featuring information on both crown mass and classical biometric measurements (*D*, *H*, ρ) are scarce and theoretical work on crown properties largely remains to be validated with field data. In most empirical studies published to date, crown mass models use trunk diameter as a single predictor (e.g., Nogueira et al. 2008; Chambers et al. 2001). Such models often provide good results ($R^2 \geq 0.9$), which reflect the strong biophysical constraints exerted by the diameter of the first pipe (the trunk) on the volume of the branching network (Shinozaki et al., 1964). However, theoretical results suggest that several crown metrics would scale with crown mass. For instance, Mäkelä et Valentine (2006) modified the allometric scaling theory (Enquist, 2002; West et al., 1999) by incorporating self-pruning processes into the crown. The authors showed that crown mass is expected to be a power function of the total length of the branching network, which they approximated by crown depth (i.e., total tree height minus trunk height). The construction of the crown and its structural properties have also largely been studied in the light of the mechanical stresses faced by trees (such as gravity and wind; e.g., McMahon et Kronauer 1976; Eloy 2011). Within this theoretical frame, crown mass can also be expressed as a power function of crown diameter (King and Loucks, 1978).

In the present study, we used a unique tree mass dataset containing crown mass information on 673 trees from five tropical countries and a network of forest plots covering 130 ha in central Africa to (i) quantify the variation in crown mass ratio in tropical trees; (ii) assess the contribution of crown mass variation to the reference pantropical model error, either at the tree level or when propagated at the plot level; and (iii) propose a new operational strategy to explicitly account for crown mass variation in biomass allometric equations. We hypothesize that the variation in crown mass ratio in tropical trees is a major source of error in current biomass allometric models and that accounting for this variation would significantly reduce uncertainty associated with plot-level biomass predictions.

2.2 Materials and Methods

2.2.1 Biomass data

We compiled tree *AGB* data from published and unpublished sources providing information on crown mass for 673 tropical trees belonging to 132 genera (144 identified species), with a wide tree size range (i.e., diameter at breast height, *D*: 10-212 cm) and aboveground tree masses of up to 76 Mg. An unpublished dataset for 77 large trees (with $D \geq 67$ cm) was obtained from the fieldwork of PP, NB and SM in semi-deciduous forests of Eastern Cameroon (site characteristics and field protocol in Supplement S1.1 and S1.2.1). The remaining datasets were gathered from relevant published studies: 29 trees from Ghana (Henry et al., 2010), 285 trees from Madagascar (Vieilledent et al., 2011), and 51 trees from Peru (Goodman et al., 2014, 2013, Fayolle *et al.*, 2013, and Ngomanda *et al.*, 2014). The whole dataset is available from the Dryad Data Repository (http://dx.doi.org/10.5061/dryad.f2b52), with details about the protocol used to integrate data from published studies presented in the Supplementary Information (2.8.2.2). For the purpose of some analyses, we extracted from this crown mass database (hereafter referred to as $Data_{CM1}$) a subset of 541 trees for which total tree height was available ($Data_{CM2}$; all but Fayolle *et al.* 2013) and another subset of 119 trees for which crown diameter was also available ($Data_{CD}$; all but Vieilledent *et.al.* 2011, Fayolle *et.al.* 2013, Ngomanda *et.al.* 2014 and 38 trees from our unpublished dataset). Finally, we used as a reference the data from Chave et al. (2014) on the total mass (but not crown mass) of 4,004 destructively sampled trees of many different species from all around the tropical world ($Data_{REF}$).

2.2.2 Forest inventory data

We used a set of 81 large forest plots (> 1 ha), covering a total area of 130 ha, to propagate *TAGB* estimation errors to plot-level predictions. The forest inventory data contained the taxonomic identification of all trees with a diameter at breast height (*D*) ≥ 10 cm, as well as total tree height measurements (*H*) for a subset of trees, from which we established plot-level *H vs*. *D* relationships to predict the tree height of the remaining trees. Details about the inventory protocol along with statistical procedures used to compute plot *AGB* (or *PAGB*) from field measurements are provided in the Supplementary Information (2.8.3). Among these plots, 80 were from a network of 1 ha plots established in humid evergreen to semi-deciduous forests belonging to 13 sites in Cameroon, Gabon and the Democratic Republic of Congo (unpublished data[1]). In addition, we included a 50 ha permanent plot from Korup National Park, in the evergreen Atlantic forest of western Cameroon (Chuyong et al., 2004), which we subdivided into 1 ha subplots. Overall, the inventory data encompassed a high diversity of stand structural profiles ranging from open-canopy *Marantaceae* forests to old-growth monodominant *Gilbertiodendron dewevrei* stands and including mixed *terra firme* forests with various levels of degradation.

2.2.3 Allometric model fitting

We fitted the pantropical allometric model of Chave et al. (2014) to log-transformed data using ordinary least-squares regression:

$$\ln(TAGB) = \alpha + \beta * \ln(D^2 * H * \rho) + \varepsilon \qquad \text{(eq. 1)}$$

[1]metadata available at http://vmamapgn-test.mpl.ird.fr:8080/geonetwork/srv/eng/search#|7dd46c7d-db2f-4bb0-920a-8afe4832f1b3

with *TAGB* (in kg) representing the aboveground tree mass, *D* (in cm) the tree stem diameter, *H* (in m) the total tree height, ρ (in g.cm^{-3}) the wood density and ε the error term, which is assumed to follow a normal distribution N ~ (0, RSE²), where RSE is the residual standard error of the model. This model, denoted m_0, was considered as the reference model.

To assess the sensitivity of m_0 to crown mass variations, we built a model (m_1) that restricted the volume approximation to the trunk compartment and included actual crown mass as an additional covariate:

$$\ln(\mathrm{TAGB}) = \alpha + \beta^* \ln(\mathrm{D}^2{*}\mathrm{Ht}{*}\rho) + \gamma^* \ln(\mathrm{Cm}) + \varepsilon \quad \text{(eq. 2)}$$

with *Cm* representing the crown mass (in kg) and *Ht* the trunk height (i.e., height to the first living branch, in m). Note that model m_1 cannot be operationally implemented (which would require destructive measurements of crowns) but quantifies the maximal improvement that can be made through the inclusion of crown mass proxies in a biomass allometric model.

2.2.4 Development of crown mass proxies

We further developed crown mass proxies to be incorporated in place of the real crown mass (*Cm*) in the allometric model m_1. From preliminary tests of various model forms (see Appendix A), we selected a crown mass sub-model based on a volume approximation similar to that made for the trunk component (sm_1):

$$\ln(\mathrm{Cm}) = \mathrm{a} + \mathrm{b}^* \ln(\mathrm{D}^2{*}\mathrm{Hc}{*}\rho) + \varepsilon \quad \text{(eq. 3)}$$

where D is the trunk diameter at breast height (in cm) and *Hc* the crown depth (that is *H* – *Ht*, in m), available in our dataset Data_{CM2} (n=541).

In this sub-model, tree crowns of short stature but large width are assigned a small *Hc*, thus a small mass, whereas the volume they occupy is more horizontal than vertical. We thus tested in sub-model sm_2 (eq. 4) whether using the mean crown size (eq. 5), which accounts for whether *Hc* and *Cd* (the crown diameter in m available in our dataset Data_{CD} (n=119)) reduces the error associated with sm_1:

$$\ln(\mathrm{Cm}) = \mathrm{a} + \mathrm{b}^* \ln(\mathrm{D}^2{*}\mathrm{Cs}{*}\rho) + \varepsilon \quad \text{(eq. 4)}$$

$$Cs = \frac{(Hc+Cd)}{2} \quad \text{(eq. 5)}$$

Finally, Sillett et al. (2010) showed that for large, old trees, a temporal increment of *D* and *H* poorly reflects the high rate of mass accumulation within crowns. We thus hypothesized that the relationship between Cm and $D^2 * Hc * \rho$ (or $D^2 * Cs * \rho$) depends on tree size and fitted a quadratic (second-order) polynomial model to account for this phenomenon (Niklas, 1995), if any:

$$\ln(\mathrm{Cm}) = \mathrm{a} + \mathrm{b}^* \ln(\mathrm{D}^2{*}\mathrm{Hc}{*}\rho) + \mathrm{c}^* \ln(\mathrm{D}^2{*}\mathrm{Hc}{*}\rho)^2 + \varepsilon \quad \text{(eq. 6)}$$

$$\ln(\mathrm{Cm}) = \mathrm{a} + \mathrm{b}^* \ln(\mathrm{D}^2{*}\mathrm{Cs}{*}\rho) + \mathrm{c}^* \ln(\mathrm{D}^2{*}\mathrm{Cs}{*}\rho)^2 + \varepsilon \quad \text{(eq. 7)}$$

where eqs. 6 and 7 are referred to as sub-models 3 and 4, respectively.

2.2.5 Model error evaluation

2.2.5.1 Tree-level

From biomass allometric equations, we estimated crown mass (denoted Cm_{est}) or total tree aboveground mass (denoted $TAGB_{est}$) including (Baskerville, 1972) bias correction during back-transformation from the logarithmic scale to the original mass unit (i.e., kg). In addition to classical criteria of model fit assessment (adjusted R^2, Residual Standard Error, *Akaike Information Criterion),* we quantified model uncertainty based on the distribution of individual relative residuals (in %), which is defined as follows:

$$s_i = \left(\frac{Y_{est,i} - Y_{obs,i}}{Y_{obs,i}}\right) * 100 \qquad \text{(eq. 8)}$$

where $Y_{obs,i}$ and $Y_{est,i}$ are the crown or tree biomass values in the calibration dataset (i.e., measured in the field) and those allometrically estimated for tree *i*, respectively. We reported the median of $|s_i|$ values, hereafter referred to as "*S*", as an indicator of model precision. For a tree biomass allometric model to be unbiased, we expect s_i to be locally centered on zero for any given small range of the tree mass gradient. We thus investigated the distribution of s_i values with respect to tree mass using local regression (loess method; Cleveland, Grosse & Shyu 1992).

2.2.5.2 Plot level

Allometric models are mostly used to make plot-level *AGB* predictions from non-destructive forest inventory data. Such plot-level predictions are obtained by simply summing individual predictions over all trees in a plot ($PAGB_{pred} = \sum_i TAGB_{pred}$). Prediction errors at the tree level are thus expected to yield an error at the plot level, which may depend on the actual tree mass distribution in the sample plot when the model is locally biased. To account for this effect, we developed a simulation procedure, implemented in two steps, that propagated $TAGB_{pred}$ errors to $PAGB_{pred}$. The first step consists in attributing to each tree *i* in a given plot a value of $TAGB_{sim}$ corresponding to the actual *AGB* of a similar felled tree selected in $Data_{REF}$ based on its nearest neighbor in the space of the centered-reduced variables *D*, *H* and ρ (here taken as species average from Dryad Global Wood Density Database, Chave et al., 2009; Zanne et al., 2009). In a second step, the simulation propagates individual errors of a given allometric model using the local distribution of s_i values as predicted by the loess regression: For each $TAGB_{sim}$, we drew a s_{sim} value from a local normal distribution fitted with the loess parameters (i.e., local mean and standard deviation) predicted for that particular $TAGB_{sim}$. Thus, we generated for each 1-ha plot a realistic $PAGB_{sim}$ (i.e., based on observed felled trees) with repeated realizations of a plot-level prediction error (in %) computed for *n* trees as follows:

$$\mathrm{S_{plot}} = \frac{\sum_{i=1}^{n}(\mathrm{s_{sim}(i)} * \mathrm{TAGB_{sim}(i)})}{\sum_{i=1}^{n}\mathrm{TAGB_{sim}(i)}}. \qquad \text{(eq. 9)}$$

For each of the simulated plots, we provided the mean and standard deviation of 1000 realizations of the plot-level prediction error.

All analyses were performed with R statistical software 2.15.2 (R Core Team, 2015), using packages lmodel2 (Legendre, 2011), segmented (Muggeo, 2003), FNN (Beygelzimer et al., 2013) and msir (Scrucca, 2011).

2.3 Results

2.3.1 Contribution of crown to tree mass

Our crown mass database ($Data_{CM1}$; 673 trees, including 128 trees > 10 Mg) revealed a huge variation in the contribution of crown to total tree mass, ranging from 2.5 to 87.5 % of total aboveground biomass, with a mean of 35.6 % (± 16.2 %). Despite this variation, a linear regression (model II) revealed a significant increase in the crown mass ratio with tree mass of approximately 3.7 % per 10 Mg (Figure 2-1 A). A similar trend was observed at every site, except for the Ghana dataset (Henry et al. 2010), for which the largest sampled tree (72 Mg) had a rather low crown mass ratio (46 %). Overall, this trend appeared to have been driven by the largest trees in the database (Figure 2-1 B). Indeed, the crown mass ratio appeared to be nearly constant for trees ≤ 10 Mg with an average of 34.0 % (± 16.9 %), and then to increase progressively with tree mass, exceeding 50 % on average for trees ≥ 45 Mg.

2.3.2 Crown mass sub-models

All crown mass sub-models provided good fits to our data ($R^2 \geq 0.9$, see Table 2-1). However, when information on crown diameter was available ($Data_{CD}$), models that included mean crown size in the compound variable (i.e., *Cs*, a combination of crown depth and diameter, in sm_2 and sm_4) gave lower AICs and errors (RSE and S) than models that included the simpler crown depth metric (i.e., *Hc* in sm_1 and sm_3). The quadratic model form provided a better fit than the linear model form (e.g., sm_3 vs. sm_1 fitted on $Data_{CM2}$), which can be explained by the non-linear increase in crown mass with either of the two proxy variables ($D^2 * Hc * \rho$ or $D^2 * Cs * \rho$). The slope of the relationship between crown mass and, for example, $D^2 * Hc * \rho$ presented a breaking point at approximately 7.5 Mg (Davies' test $P < 0.001$) that was not captured by sub-model sm_1 (Figure 2-2 A, full line), leading to a substantial bias in back-transformed crown mass estimations (approximately 50 % of observed crown mass for $Cm_{obs} \geq$ 10 Mg, Figure 2-2 B). The quadratic sub-model sm_3 provided fairly unbiased crown mass estimations (Figure 2-2 C). Because the first-order term was never significant in the quadratic sub-models, we retained only the second-order term as a crown mass proxy in the biomass allometric models (i.e., $(D^2 * Hc * \rho)^2$for model m_2 or $(D^2 * Cs * \rho)^2$or model m_3).

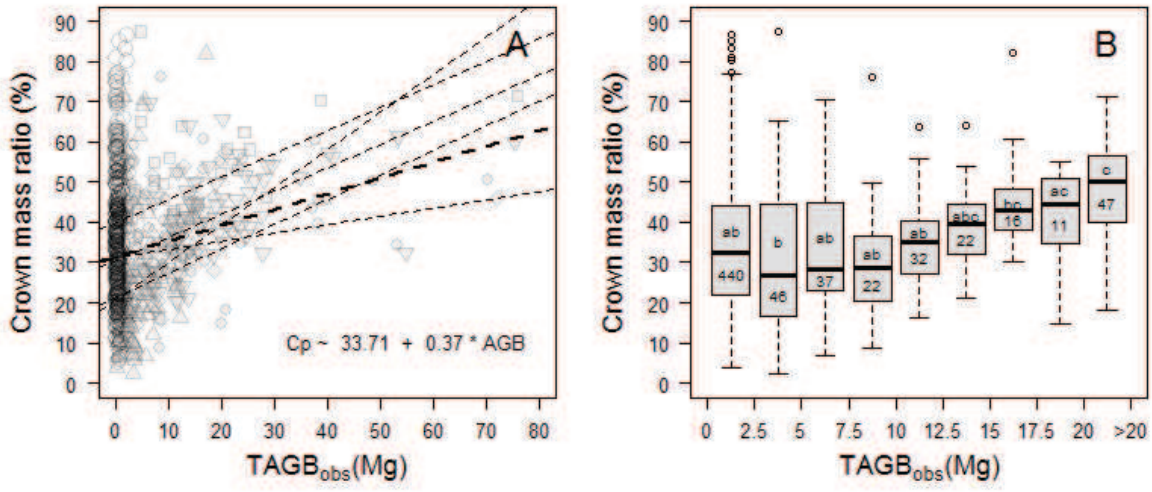

Figure 2-1. (A) Distribution of crown mass ratio (in %) along the range of tree mass (*TAGB$_{obs}$*, in Mg) for 673 trees. Dashed lines represent the fit of robust regressions (model II linear regression fitted using ordinary least square) performed on the full crown mass dataset (thick line; one-tailed permutation test on slope: p-value < 0.001) and on each separate source (thin lines), with symbols indicating the source: empty circles from Vieilledent et.al. (2011; regression line not represented since the largest tree is 3.7 Mg only); solid circles from Fayolle et.al. (2013); squares from Goodman et al. (2013, 2014); diamonds from Henry et.al. (2010); head-up triangles from Ngomanda et.al. (2014); and head-down triangles from the un-published data set from Cameroon. (B) Boxplot representing the variation in crown mass ratio (in %) across tree mass bins of equal width (2.5 Mg). The last bin contains all trees ≥ 20 Mg. The number of individuals per bin and the results of non-parametric pairwise comparisons are represented below and above the median lines, respectively.

Table 2-1. Crown mas sub-models. Model variables are Cm (crown mass, Mg), D (diameter at breast height, cm), Hc (crown depth, m), Cs (average of Hc and crown diameter, m) and ρ (wood density, g.cm-3). The general form of the models is ln(Y) ~a+ b* ln(X) + c*ln(X)². Model coefficient estimates are provided along with the associated standard error denoted SEi, with i as the coefficient. Coefficients' probability value (pv) is not reported when pv ≤ 10-4 and otherwise coded as follows: pv ≤ 10-3 : '**', pv ≤ 10-2 : '*', pv ≤ 0.05 : '.' and pv ≥ 0.05 : 'ns'. Models' performance parameters are R^2 (adjusted R square), RSE (residual standard error), S (median of unsigned relative individual errors, in %), AIC (Akaike Information Criterion), dF (degree of freedom).

model	Dataset	Model input			Model parameters						Model performance				
		Y	X	X²	a	b	c	SE_a	SE_b	SE_c	R^2	RSE	*S*	AIC	dF
sm_1	$Data_{CM2}$ (n=541)	*Cm*	$D^2Hc\,\rho$	-	-2.6345	0.9368		0.1145	0.0125		0.91	0.615	36.0	1012.6	539
sm_3			$D^2Hc\,\rho$	$(D^2Hc\,\rho)^2$	0.9017.	0.1143^{ns}	0.0452	0.5049	0.1153	0.0063	0.92	0.588	35.2	965.2	538
			-	$(D^2Hc\,\rho)^2$	1.3990		0.0514	0.0605		0.0007	0.92	0.588	35.5	964.2	539
sm_1	$Data_{CD}$ (n=119)	*Cm*	$D^2Hc\,\rho$	-	-2.9115	0.9843		0.3139	0.0289		0.91	0.516	31.8	184.1	117
sm_2			$D^2Cs\,\rho$	-	-3.0716	0.9958		0.2514	0.0231		0.94	0.414	21.8	131.9	117
sm_3			$D^2Hc\,\rho$	$(D^2Hc\,\rho)^2$	-0.2682^{ns}	0.4272^{ns}	0.0283.	1.4077	0.2908	0.0147	0.91	0.510	29.7	182.3	116
			-	$(D^2Hc\,\rho)^2$	1.7830		0.0498	0.1774		0.0015	0.91	0.512	32.2	182.5	117
sm_4			$D^2Cs\,\rho$	$(D^2Cs\,\rho)^2$	-0.5265^{ns}	0.4617.	0.0270*	1.1443	0.2356	0.0119	0.94	0.407	128.7	25.9	116
			-	$(D^2Cs\,\rho)^2$	1.6994		0.0502	0.1421		0.0012	0.94	0.412	130.5	25.8	117

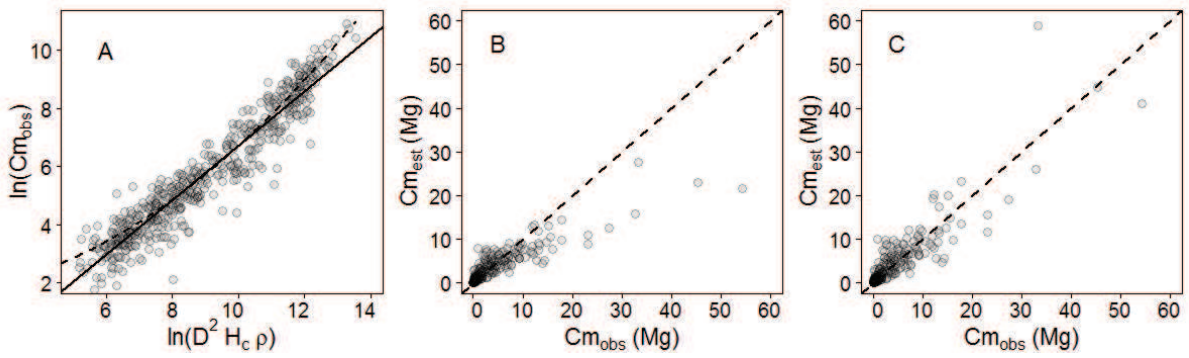

Figure 2-2. (A) Observed crown mass versus the compound variable $D^2Hc\rho$ (in log scale), displaying a slightly concave relationship. The crown mass sub-model 1 does not capture this effect (model fit represented with a full line in caption A), resulting in biased model predictions (caption B), whereas sub-model 3 does not present this error pattern (model fit represented as a dashed line in caption A, observed crown mass against model predictions in caption C). Models were fitted on $Data_{CM2}$.

2.3.3 Accounting for crown mass in biomass allometric models

The reference model (m_0) proposed by Chave et al. (2014) presented, when fitted to $DATA_{REF}$, a bias that was a function of tree mass, with a systematic *AGB* over-estimation for trees < approximately 10 Mg and an under-estimation for larger trees, reaching approximately 25 % for trees greater than 30 Mg (Figure 2-3 A). This bias pattern reflected a breaking point in the relationship between $D^2 * H * \rho$ and $TAGB_{obs}$ (Davies' test P < 0.001) located at approximately 10 Mg (Figure 2-3 B). Accounting for actual crown mass (*Cm*) in the biomass allometric model (i.e., model m_1) corrected for a similar bias pattern observed when m_0 was fitted to $DATA_{CM2}$ (Figure 2-4 A). This result shows that variation in crown mass among trees is a major source of bias in the reference biomass allometric model, m_0.

Using our simulation procedure, we propagated individual prediction errors of m_0 and m_1 to the 130 1-ha field plots from central Africa (Figure 2-4 B). This process revealed that the reference pantropical model (m_0) led to an average plot-level relative prediction error (S_{plot}) ranging from -23 % to +16 % (mean = +6.8 %) on $PAGB_{pred}$, which dropped to +1 to +4 % (mean = +2.6 %) when the model accounted for crown mass (m_1).

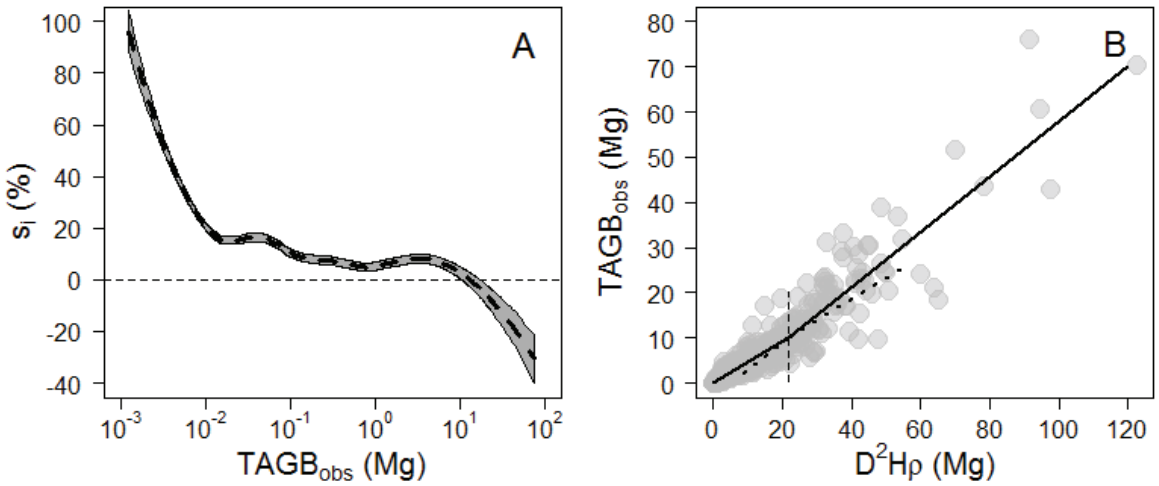

Figure 2-3. (A) Relative individual residuals (si in %) of the reference pantropical model of Chave et.al. (2014) against the tree AGB gradient. The thick dashed line represents the fit of a local regression (loess function, span = 0.5) bounded by standard errors. (B) Observed tree AGB ($TAGB_{obs}$) versus the compound variable $D^2 * H * \rho$ with *D* and *H* being the tree stem diameter and height, respectively, and ρ the wood density. A segmented regression revealed a significant break point (thin vertical dashed line) at approximately 10 Mg of $TAGB_{obs}$ (Davies test p-value < 2.2e-16).

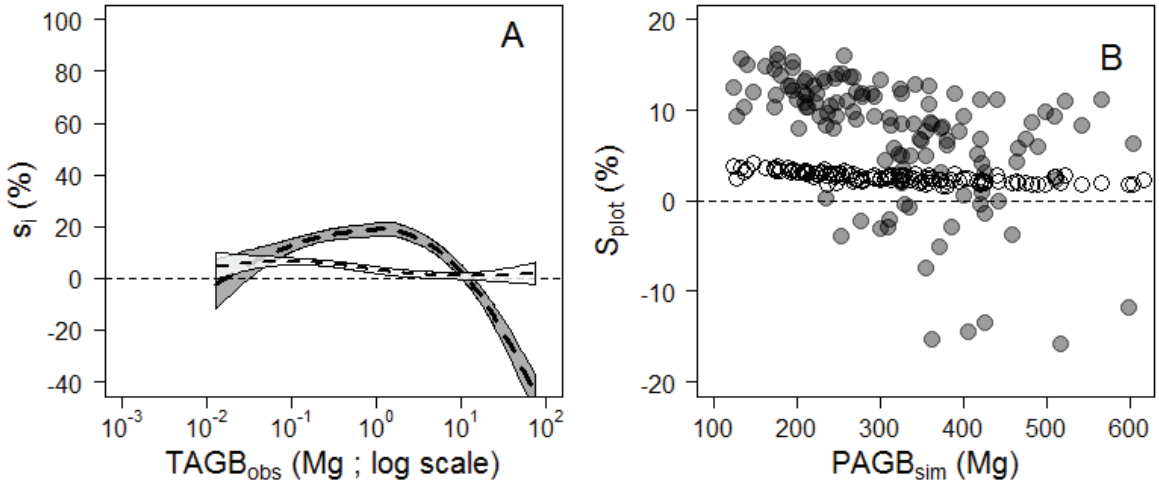

Figure 2-4. (A) Relative residuals (s_i, in %) of the reference pantropical model m_0 (grey background) and our model m_1 including crown mass (white background). Thick dashed lines represent fits of local regressions (loess function, span = 1) bounded by standard errors. (B) Propagation of individual estimation errors of m_0 (solid grey circles) and m_1 (empty circles) to the plot level.

Because in practice crown mass cannot be routinely measured in the field, we tested the potential of crown mass proxies to improve biomass allometric models. Model m_2, which used a compound variable integrating crown depth i.e., $(D^2 * Hc * \rho)^2$ as a proxy of crown mass outperformed m_0 (Table 2-2). Although the gain in precision (RSE and S) over m_0 was rather low, the model provided the striking advantage of being free of significant local bias on large trees (> 1 Mg; Figure 2-5 A). At the plot level,

this model provided a much higher precision (0 to 10 % on $PAGB_{pred}$) and a lower bias (average error of 5 %) than the reference pantropical model m_0 (Figure 2-5 B). Using a compound variable integrating crown size i.e., $(D^2 * Cs * \rho)^2$ as a crown mass proxy (model m_3), thus requiring both crown depth and diameter measurements, significantly improved model precision (m_3 *vs*. m_2, Table 2-2) while preserving the relatively unbiased distribution of relative residuals (results not shown).

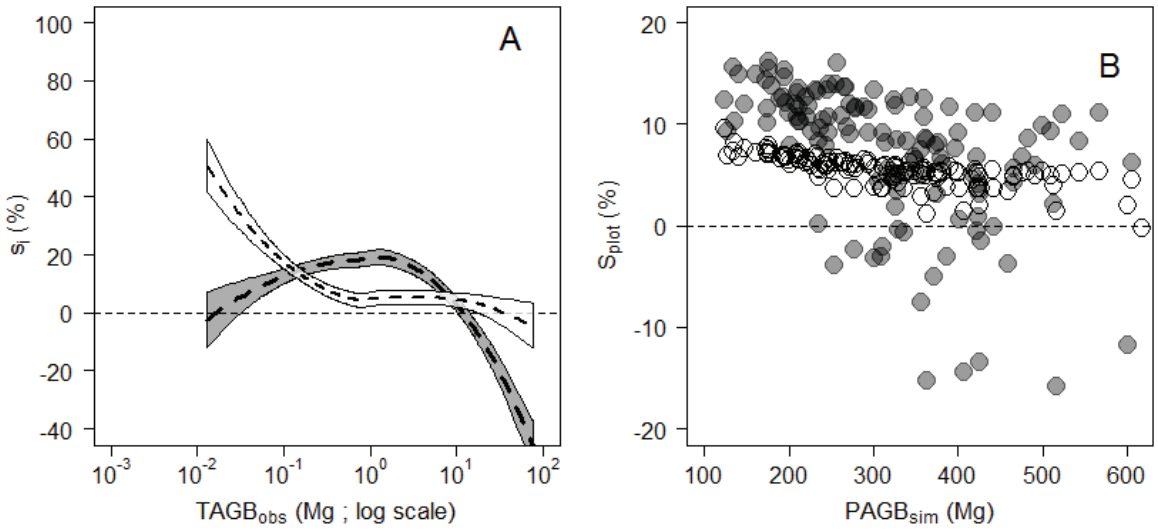

Figure 2-5. (A) Relative individual residuals (s_i, in %) obtained with the reference pantropical model m_0 (grey background) and with our model including a crown mass proxy, m_2 (white background). Thick dashed lines represent fits of local regressions (loess function, span = 1) bounded by standard errors. (B) Propagation of individual residual errors of m_0 (solid grey circles) and m_2 (empty circles) to the plot level.

Table 2-2. Models used to estimate tree *AGB*. Model parameters are D (diameter at breast height, cm), H (total height, m), Ht (trunk height, m), Hc (crown depth, m), Cm (crown mass, Mg), Cs (average of Hc and crown diameter, m) and ρ (wood density, g.cm^{-3}). The general form of the models is ln(Y) ~a+ b* ln(X_1) + c*ln(X_2). Model coefficient estimates are provided along with the associated standard error denoted SE_i, with i as the coefficient. Coefficients' probability value (pv) is not reported when pv ≤ 10^{-4} and otherwise coded as follows: pv ≤ 10^{-3} : '**', pv ≤ 10^{-2} : '*', pv ≤ 0.05 : '.' and pv ≥ 0.05 : 'ns'. Models' performance parameters are R^2 (adjusted R square), RSE (residual standard error), *S* (median of unsigned relative individual errors, in %), AIC (Akaike Information Criterion), dF (degree of freedom).

model	Dataset	Model input			Model parameters						Model performance				
		Y	X_1	X_2	a	b	c	SE_a	SE_b	SE_c	R^2	RSE	*S*	AIC	dF
m_0	$Data_{REF}$ (n=4004)	*AGB*	$D^2*H*\rho$		-2.7628	0.9759		0.0211	0.0026		0.97	0.358	22.1	3130.7	4002
m_0	$Data_{CM2}$ (n=541)	*AGB*	$D^2*H*\rho$		-2.5860	0.9603		0.0659	0.0066		0.98	0.314	18.9	284.8	539
m_1			$D^2*Ht*\rho$	*Cm*	-0.5619	0.5049	0.4816	0.0469	0.0098	0.0096	0.99	0.199	9.8	-205.7	538
m_2			$D^2*Ht*\rho$	$(D^2*Hc*\rho)^2$	0.3757	0.4451	0.0281	0.0974	0.0186	0.0010	0.98	0.298	17.8	231.5	538
m_0	$Data_{CD}$ (n=119)	*AGB*	$D^2*H*\rho$		-3.1105	1.0119		0.1866	0.0160		0.97	0.268	15.0	28.1	117
m_1			$D^2*Ht*\rho$	*Cm*	-0.5851	0.4784	0.5172	0.1117	0.0203	0.0185	0.99	0.142	7.0	-121.2	116
m_2			$D^2*Ht*\rho$	$(D^2*Hc*\rho)^2$	-0.2853^{ns}	0.5804	0.0216	0.2499	0.0397	0.0019	0.97	0.272	14.5	32.5	116
m_3			$D^2*Ht*\rho$	$(D^2*Cs*\rho)^2$	0.5800*	0.4263	0.0283	0.2662	0.0444	0.0021	0.98	0.246	12.3	9.3	116

2.4 Discussion

Using a dataset of 673 individuals including most of the largest trees that have been destructively sampled to date, we discovered tremendous variation in the crown mass ratio among tropical trees, ranging from 3 to 88 %, with an average of 36 %. This variation was not independent of tree size, as indicated by a marked increase in the crown mass ratio with tree mass for trees ≥ 10 Mg. This threshold echoed a breaking point in the relationship between total tree mass and the compound predictor variable used in the reference allometric model of Chave et al. (2014). When the compound variable is limited to trunk mass prediction, and a crown mass predictor is added to the model, the bias towards large trees is significantly reduced. As a consequence, error propagation to plot-level *AGB* estimations is largely reduced. In the following section, we discuss the significance and implication of these results from both an ecological and a practical point of view with respect to resource allocation to the tree compartments and to carbon storage in forest aboveground biomass.

2.4.1 Crown mass ratio and the reference biomass model error

We observed an overall systematic increase in the crown mass ratio with tree mass. This ontogenetic trend has already been reported for some tropical canopy species (O'Brien et al., 1995) and likely reflects changes in the pattern of resource allocation underlying crown edification in most forest canopy trees (Barthélémy and Caraglio, 2007; Hasenauer and Monserud, 1996; Holdaway, 1986; Moorby and Wareing, 1963; Perry, 1985). The overall increase in the carbon accumulation rate with tree size is a well-established trend (Stephenson et al., 2014), but the relative contribution of the trunk and the crown to that pattern has rarely been investigated, particularly on large trees for which branch growth monitoring involves a tremendous amount of work. Sillett et al. (2010) collected a unique dataset in this regard, with detailed growth measurements on very old (up to 1850 years) and large (up to 648 cm *D*) individuals of *Eucalyptus regnans* and *Sequoia sempervirens* species. For these two species, the contribution of crown to *AGB* growth increased linearly with tree size and thus the crown mass ratio. We observed the same tendency in our data for trees ≥ 10 Mg (typically with $D > 100$ cm). This result thus suggests that biomass allometric relationships may differ among small and large trees, thus explaining the systematic underestimation of *AGB* for large trees observed by Chave et al. (2014). The latter authors suggested that this model underestimation was due to a potential "majestic tree" sampling bias, in which scientists would have more systematically sampled trees with well-formed boles and healthy crowns. We agree that such an effect cannot be completely ruled out, and it is probably all the more significant that trees ≥ 10 Mg represent only 3 % of the reference dataset of Chave et al. ($Data_{REF}$). Collecting more field data on the largest tree size classes should therefore constitute a priority if we are to improve multi-specific, broad-scale allometric models, and the recent development of non-destructive *AGB* estimation methods based on terrestrial LiDAR data should help in this regard (e.g., Calder et al., 2014). However, regardless of whether the non-linear increase in crown mass ratio with tree mass held to a sampling artifact, we have shown that it was the source of systematic error in the reference model that used a unique geometric approximation with an average form factor for all trees. This finding agrees with the results of Goodman *et al.* (2014) in Peru, who found significant improvements in biomass estimates of large trees when biomass models included tree crown radius, thus partially accounting for crown ratio variations. Identifying predictable patterns of crown mass ratio variation, as performed for crown size allometries specific to some functional groups (Poorter *et.al.* 2003; Poorter, Bongers, et Bongers 2006; Van Gelder, Poorter, et Sterck 2006), therefore appears to be a potential way to improve allometric models performance.

2.4.2 Model error propagation depends on targeted plot structure

The reference pantropical model provided by Chave *et al.* (2014) presents a bias pattern that is a function of tree size (i.e., average over-estimation of small tree *AGB* and average underestimation of large tree *AGB*). Propagation of individual errors to the plot level therefore depends on tree size distribution in the sample plot, with over- or under-estimations depending on the relative importance of small or large trees in the stand (e.g., young secondary forests *vs.* old-growth forests; see Appendix B for more information on the interaction between model error, plot structure and plot size). This effect is not consistent with the general assumption that individual errors should compensate at the plot level. Although the dependence of error propagation on tree size distribution has already been raised (Marra et al., 2015; Mascaro et al., 2011), it is generally omitted from error propagation procedures (e.g., Picard, Bosela, et Rossi 2014; Moundounga Mavouroulou et al. 2014; Chen, Vaglio Laurin, et Valentini 2015). At a larger scale, such as the landscape or regional scale, plot-level errors may average out if the study area is a mosaic of forests with varying tree size distributions. However, if plot estimations are used to calibrate remote sensing products, individual plot errors may propagate as a systematic bias in the final extrapolation (Réjou-Méchain et al. 2014).

2.4.3 Accounting for crown mass variation in allometric models

We propose a modeling strategy that decomposes total tree mass into trunk and crown masses. A direct benefit of addressing these two components separately is that it should reduce the error in trunk mass estimation because the trunk form factor is less variable across species than the whole-tree form factor (Cannell, 1984). We modeled tree crown using a geometric solid whose basal diameter and height were the trunk diameter and crown depth, respectively. Crown volume was thus considered the volume occupied by branches if they were squeezed onto the main stem ("as if a ring were passed up the stem"; Cannell 1984). Using a simple linear model to relate crown mass to the geometric approximation (sm_1, sm_2) led to an under-estimation bias that gradually increased with crown mass (Figure 2-2 B). A similar pattern was observed on all crown mass models based on trunk diameter (Appendix A) and reflected a significant change in the relationship between the two variables with crown size. Consistently, a second-order polynomial model better captured such a non-linear increase in crown mass with trunk diameter-based proxies and thus provided unbiased crown mass estimates (Figure 2-2 C). Our results agree with those of Sillett et al. (2010), who showed that ground-based measurements such as trunk diameter do not properly render the high rate of mass accumulation in large trees, notably in tree crowns, and may also explain why the dynamics of forest biomass are inferred differently from top-down (e.g., airborne LiDAR) or bottom-up views (e.g., field measurement; Réjou-Méchain et al., 2015).

From a practical point of view, our tree biomass model m_2, which requires only extra information on trunk height (if total height is already measured) provides a better fit than the reference pantropical model and removes estimation bias on large trees. In scientific forest inventories, total tree height is often measured on a sub-sample of trees, including most of the largest trees in each plot, to calibrate local allometries between *H* and *D*. We believe that measuring trunk height on those trees does not represent a cumbersome amount of additional effort because trunk height is much more easily measured than total tree height. We thus recommend using model m_2 —at least for the largest trees, i.e., those with $D \geq 100$ cm — and encourage future studies to assess its performance from independent datasets.

2.5 Appendix A: Crown mass sub-models

2.5.1 Method

Several tree metrics are expected to scale with crown mass, particularly crown height (Mäkelä and Valentine, 2006), crown diameter (King and Loucks, 1978) or trunk diameter (e.g., Nogueira et al. 2008; Chambers et al. 2001). In this study, we tested whether any of these variables (i.e., trunk diameter, crown height and crown diameter) prevailed over the others in explaining crown mass variations. Power functions were fitted in log-transformed form using ordinary least-squares regression techniques (models $sm_{1\text{-}X}$):

$$\ln(Cm) \sim a + b*\ln(X) + \varepsilon \quad \text{(eq. A1)}$$

where *Cm* is the crown mass (in Mg); *X* is the structural variable of interest, namely *D* for trunk diameter at breast height (in cm), *Hc* for crown depth (in m), or *Cd* for crown diameter (in m); a and b are the model coefficients and is ε the error term assumed to follow a normal distribution.

We also assessed the predictive power of the three structural variables on crown mass while controlling for variations in wood density (ρ, in $g.cm^{-3}$), leading to models $sm_{2\text{-}X}$:

$$\ln(Cm) \sim a + b*\ln(X) + c*\ln(\rho) + \varepsilon \quad \text{(eq. A2)}$$

where c is the model coefficient of ρ.

Similarly to the cylindrical approximation of a tree trunk, we further established a compound variable for tree crown based on *D* and *Hc*, leading to model sm_3:

$$\ln(Cm) \sim a + b*\ln(D^2 Hc\ \rho) + \varepsilon \quad \text{(eq. A3)}$$

where crown height is a proxy for the length of the branching network. Results obtained using sm_3 are presented in the manuscript as well as in this appendix for comparison with those obtained using $sm_{1\text{-}x}$ and $sm_{2\text{-}x}$.

2.5.2 Results & Discussion

Among the three structural variables tested as proxies for crown mass, trunk diameter provided the best results. Model 1-D presented a high R^2 (0.88), but its precision was low, with an *S* (i.e., the median of unsigned s_i values) of 43 % (Table 2-3). Moreover, model error increased appreciably with crown mass (Figure 2-6 A). For instance, model estimations for an observed crown mass of approximately 20 Mg ranged between 5 and 55 Mg. Nevertheless, $sm_{1\text{-}D}$ outperformed $sm_{1\text{-}Hc}$ ($Data_{CM2}$, AIC of 1182 *vs.* 1603, respectively) and was slightly better than $sm_{1\text{-}Cd}$ ($Data_{CD}$, AIC of 257 *vs.* 263, respectively), suggesting that the width of the first branching network pipe is a stronger constraint on branches' mass than the external dimensions of the network (i.e., *Hc*, *Cd*).

The model based on crown depth ($sm_{1\text{-}Hc}$) was subjected to a large error (*S* of c. 80 %; Table 2-3) and clearly saturated for a crown mass ≥ 10 Mg (Figure 2-6 B). Because crown depth does not account for branch angle, it does not properly render the length of the branching network. The saturation threshold observed on large crowns supports the observations of Sillett et al. (2010): Tree height, from which crown depth directly derives, levels off in large/adult trees, but mass accumulation—notably within the crowns—continues far beyond this point. It follows that crown depth alone does not allow for the detection of the highest mass levels in large/old tree crowns.

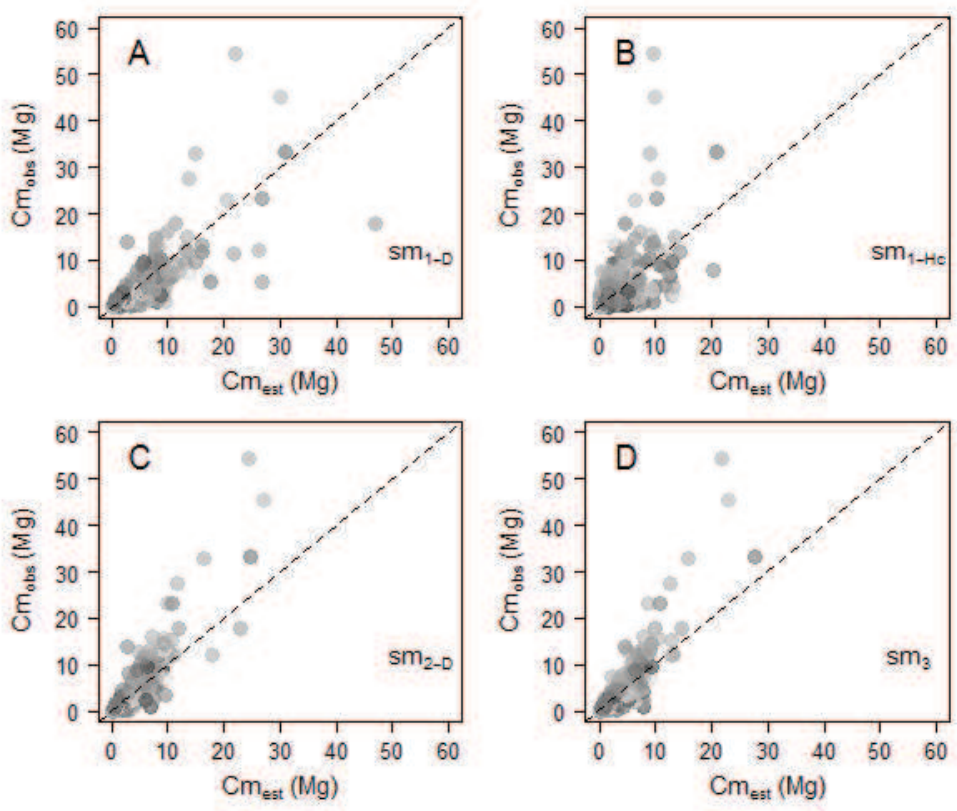

Figure 2-6. Observed against estimated crown mass (in Mg) for models 1-D (caption A), 1-Hc (caption B), 2-D (caption C), 3 (caption D). Models were calibrated on $Data_{CM2}$. Tree wood density was standardized to range between 0 and 1 and represented as a grayscale (with black the lowest values and white the highest values).

Table 2-3. Sub-models used to estimate crown *AGB*. Model parameters are *D* (diameter at breast height, cm), *Hc* (crown depth, m), *Cm* (crown mass, Mg), *Cd* (crown diameter, in m), *Cs* (average of *Hc* and *Cd*, m) and ρ (wood density, g.cm^{-3}). The general form of the models is ln(*Y*) ~ a + b*ln(*X*) + c*ln(*Y*). Model coefficients' estimates are provided along with the associated standard error denoted SE_i, with i as the coefficient. Coefficients' probability value (pv) is not reported when pv ≤ 10^{-4} and otherwise coded as follows: pv ≤ 10^{-3} : '**', pv ≤ 10^{-2} : '*', pv ≤ 0.05 : '.' and pv ≥ 0.05 : 'ns'. Models' performance parameters are R^2 (adjusted R square), RSE (residual standard error), *S* (median of unsigned relative individual errors, in %), AIC (Akaike Information Criterion), dF (degree of freedom).

model	Dataset	Model input			Model parameters						Model performance				
		Y	X_1	X_2	a	b	C	SE_a	SE_b	SE_c	R^2	RSE	S	AIC	dF
1-D	$Data_{CM2}$ (n=541)	*Cm* ~	*D*		-3.6163	2,5786		0.1514	0.0409		0.88	0.719	42.8	1181.6	539
1-Hc			*Hc*		-0.1711^{ns}	2.6387		0.1574	0.0673		0.74	1.060	82.2	1602.8	539
2-D			*D*	ρ	-3.0876	2.6048	1.1202	0.1462	0.0372	0.1048	0.90	0.653	36.7	1079.4	538
2-Hc			*Hc*	ρ	-0.3952*	2.6574	-0.3274$^{.}$	0.1959	0.0679	0.1712	0.74	1.058	80.6	1601.1	538
3			$D^2Hc\ \rho$		-2.6345	0.9368		0.1145	0.0125		0.91	0.615	36.0	1012.6	539
1-D	$Data_{CD}$ (n=119)	*Cm* ~	*D*		-3.4603	2.5684		0.4692	0.1075		0.83	0.702	39.8	257.4	117
1-Hc			*Hc*		1.3923*	2.2907		0.5392	0.1938		0.54	1.149	77.4	374.7	117
1-Cd			*Cd*		-0.1181^{ns}	2.8298		0.3403	0.1218		0.82	0.718	52.7	262.8	117
2-D			*D*	ρ	-2.7296	2.6293	1.5243	0.3528	0.0793	0.1523	0.91	0.516	30.5	185.3	116
2-Hc			*Hc*	ρ	1.1181^{ns}	2.3356	-0.2326^{ns}	0.6869	0.2063	0.3596	0.54	1.152	82.9	376.3	116
2-Cd			*Cd*	ρ	0.4677^{ns}	2.7954	0.7538	0.3585	0.1158	0.2009	0.84	0.681	44.5	251.2	116

The model based on crown diameter presented a weaker fit than $sm_{1\text{-}D}$, with a higher AIC ($Data_{CD}$, 263 *vs.* 257) and an individual relative error approximately 10 % higher (*S* of approximately 50 % and 40 %, respectively; Table 2-3). However, crown diameter appeared more informative regarding the mass of the largest crowns than trunk diameter (Figure 2-7 A-B). In fact, the individual relative error of $sm_{1\text{-}Cd}$ on crowns ≥ 10 Mg was only 26 %, versus 47 % for $sm_{1\text{-}D}$.

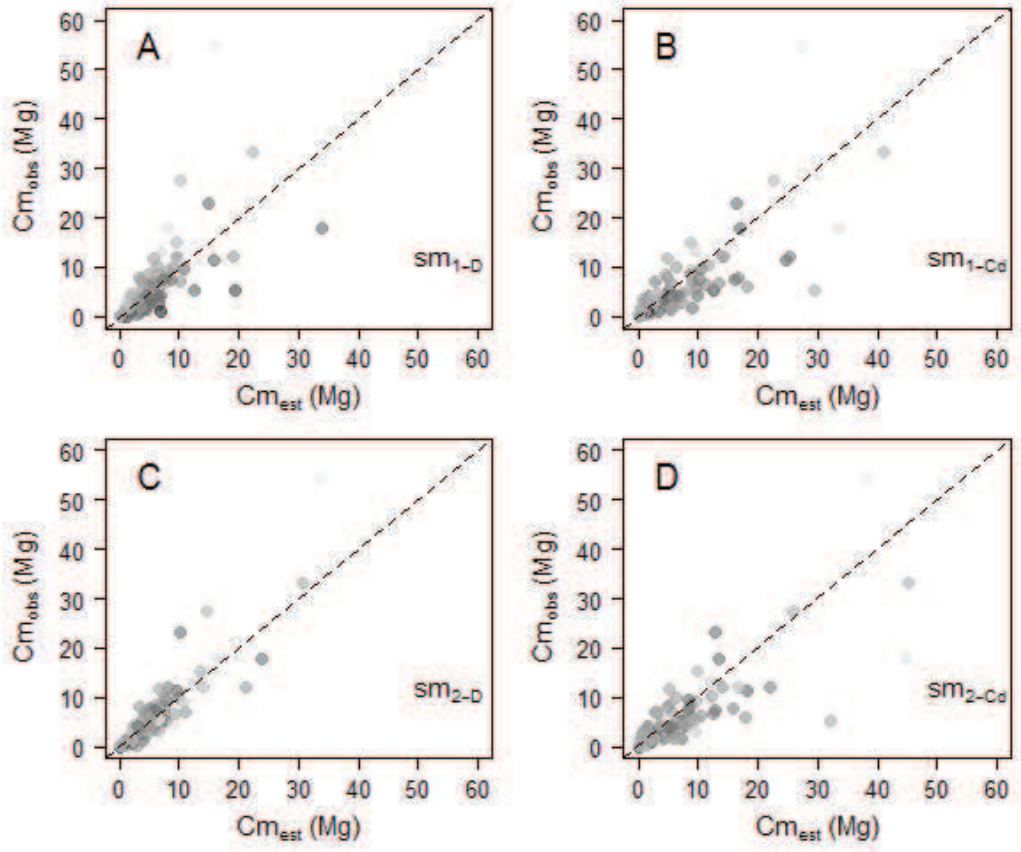

Figure 2-7. Observed versus estimated crown mass (in Mg) for models 1-D (caption A), 1-Cd (caption B), 2-D (caption C), 2-Cd (caption D). Models were calibrated on $Data_{CD}$. Tree wood density was standardized to range between 0 and 1 and is represented as a grayscale (with black the lowest values and white the highest values).

Accounting for variations in wood density improved the model based on trunk diameter. As shown in Figure 2-6, using a color code for wood density highlighted a predictable error pattern in model estimations: Trunk diameter tends to over- or under-estimate the crown mass of trees with high or low wood density, respectively. This pattern is corrected for in $sm_{2\text{-}D}$, which presents a lower AIC than $sm_{1\text{-}D}$ (i.e., 1079) and an individual relative error approximately 15 % lower (i.e., 37 %; Table 2-3). Interestingly, whereas $sm_{2\text{-}D}$ appeared to be more accurate than $sm_{1\text{-}D}$ in its estimations of large crown mass (Figure 2-6 C), it also presented an under-estimation bias that gradually increased with crown mass. Including ρ in the model based on *Cd* improved the model fit (AIC of 251 *vs*. 262 for $sm_{2\text{-}Cd}$ and $sm_{1\text{-}Cd}$, respectively) and decreased the individual relative error by approximately 15 %. Similarly to $sm_{1\text{-}Cd}$, $sm_{2\text{-}Cd}$ was outperformed by its counterpart based on *D* (AIC of 185). Moreover, the gain in precision in $sm_{2\text{-}Cd}$ was localized on small crowns, whereas estimations on large crowns were fairly

equivalent (Figure 2-7 C-D). Model 2-D was more precise on crowns ≥ 10 Mg, with an individual relative error of 23 % versus 32 % for $sm_{2\text{-}Cd}$.

The strongest crown mass predictor, *D*, was used as the basis of a geometric solid approximating crown volume ($D^2 * Hc$) and, in turn, mass ($D^2 * Hc * \rho$ in model sm_3). With one less parameter than $sm_{2\text{-}D}$, sm_3 presented a lower AIC than the former model (i.e., 1012), but the two models provided a fairly similar fit to the observations (RSE of 0.65 vs. 0.61 and S of 37 % vs. 36 % for $sm_{2\text{-}D}$ and sm_3, respectively). This result indicates that when *D* and *ρ* are known, information on crown depth is of minor importance for predicting crown mass. However, this conclusion applies to our dataset only because *Hc* might be more informative regarding crown mass variations when considering sites/species with more highly contrasting *D-H* or *D-Hc* relationships.

Similarly to $sm_{2\text{-}D}$, sm_3 presented an under-estimation bias that increased gradually with crown mass (illustrated in Figure 2-6 D).

2.6 Appendix B: Plot-level error propagation

We used the error propagation procedure described in the Methods section of the manuscript to estimate the mean plot-level *AGB* prediction error that could be expected from m_0 calibrated on $DATA_{REF}$ (i.e., the pantropical model proposed in Chave et al. 2014). Model error was propagated on 130 1-ha sample plots of tropical forest in central Africa, a network of 80 1-ha plots (field inventory protocol in Supplement Information S1.3) to which we added 50 1-ha plots from Korup 50-ha permanent plot (Chuyong et al., 2004). We further sub-sampled Korup 50-ha permanent plot in sub-plots of varying sizes (from 25 ha to 0.1 ha) to evaluate the effect of plot size on plot-level *AGB* prediction error.

From the simulated $PAGB_{sim}$ for the 130 1-ha plots, we estimated that the reference pantropical model, m_0, propagated to $PAGB_{pred}$ a mean prediction error (over 1000 realizations of S_{plot}) that ranged between -15 % and +7.7 % (Figure 2-8 A), mostly caused by trees with mass ≥ 20 Mg (Figure 2-8 B). This trend was particularly evident in the undisturbed evergreen stands of Korup (triangles in Figure 2-8 A-B), where patches of *Lecomtedoxa klaineana* (Pierre ex Engl) individuals largely drove the *PAGB* predictions (R^2= 0.87, model II OLS method). This species generates high-statured individuals of high wood density, which frequently exceed 20 Mg and result in underestimates of plot-level biomass. Interestingly, some high-biomass plots could still be over-estimated when $PAGB_{pred}$ was concentrated in trees weighting less than 20 Mg.

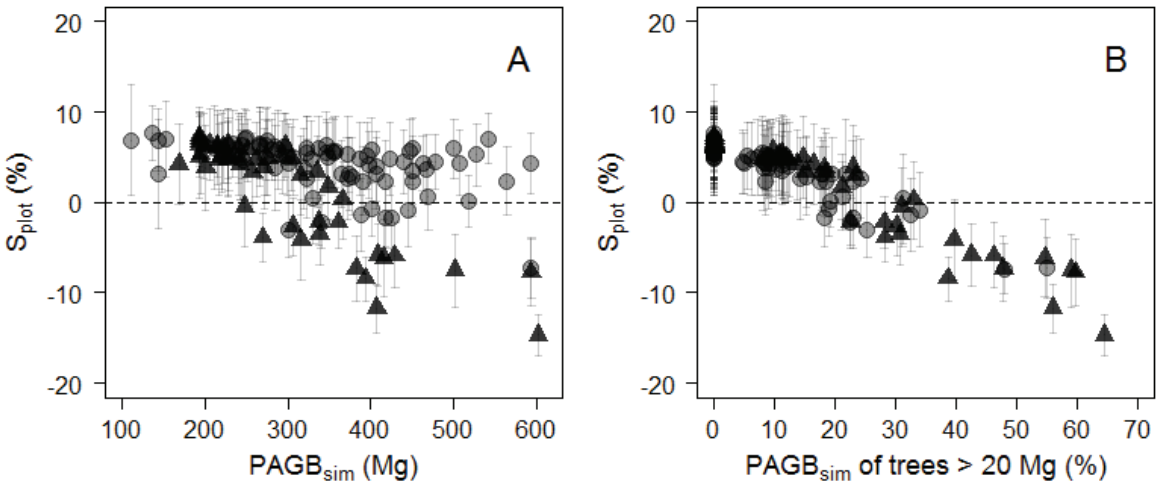

Figure 2-8. Plot-level propagation of individual-level model error. (A) Mean relative error (S_{plot}, in %) and standard deviation of 1000 random error sampling against simulated plot AGB and (B) against the fraction (%) of simulated plot AGB accounted for by trees > 20 Mg. Plots from Korup permanent plot are represented by triangles.

As a consequence of m_0 bias concentration in large trees, plot-level prediction errors for the 50 ha in Korup tended to stabilize near 0 for subplots ≥ 5 ha only. Below this threshold (i.e., for subplots ≤ 1 ha), the median error is positive but negative outliers are more frequent (Figure 2-9). Indeed, on the one hand, small plots are less likely to encompass large trees and have a positive prediction error of up to approximately +7.5 %. On the other hand, a single large tree can strongly affect $PAGB_{pred}$, occasionally leading to a large underestimation of small plots *AGB* that can exceed -15 % for a 0.25-ha and -20 % for a 0.1-ha subplot.

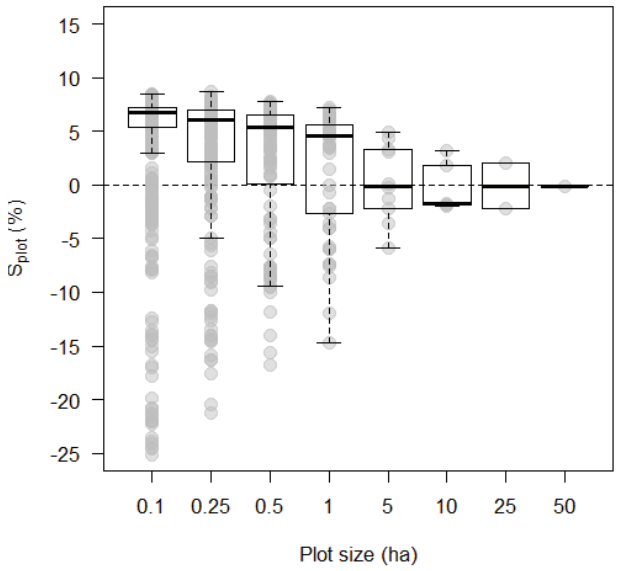

Figure 2-9. Plot-level relative error (S_{plot}, in %) as a function of plot size (in ha) in Korup permanent plot. Individual plot values are represented by grey dots.

Author contributions. Conceived and designed the experiments: PP, NB and RP. Collected data (unpublished destructive data and field inventories): SM, BS, NGK, ML, DZ, NT, FBB, JKM, GD, VD. Shared data: GC, DK, DT, AF, AN, MH, RCG. Analyzed the data: PP. Analysis feedback: RP, NB, VR, MRM, UB. Wrote the paper: PP, RP and MRM. Writing feedback: NB, AF, VR, PC, MH, RCG.

Acknowledgments. Destructive data from Cameroon were collected with the financial support from the IRD project PPR FTH-AC 'Changements globaux, biodiversité et santé en zone forestière d'Afrique Centrale' and the support and involvement of Alpicam Company. A portion of the plot data were collected with the support of the CoForTips project as part of the ERA-Net BiodivERsA 2011-2012 European joint call (ANR-12-EBID-0002). PP was supported by an Erasmus Mundus PhD grant from the 2013-2016 Forest, Nature and Society (FONASO) doctoral program.

Data Accessibility.

Destructive sampling data set available at http://dx.doi.org/10.5061/dryad.f2b52.

2.7 References

Avitabile, V., Herold, M., Henry, M. and Schmullius, C.: Mapping biomass with remote sensing: a comparison of methods for the case study of Uganda, Carbon Balance Manag., 6(7), 1–14, 2011.

Baccini, A., Goetz, S. J., Walker, W. S., Laporte, N. T., Sun, M., Sulla-Menashe, D., Hackler, J., Beck, P. S. A., Dubayah, R. and Friedl, M. A.: Estimated carbon dioxide emissions from tropical deforestation improved by carbon-density maps, Nat. Clim. Change, 2(3), 182–185, 2012.

Barthélémy, D. and Caraglio, Y.: Plant Architecture: A Dynamic, Multilevel and Comprehensive Approach to Plant Form, Structure and Ontogeny, Ann. Bot., 99(3), 375–407, doi:10.1093/aob/mcl260, 2007.

Baskerville, G. L.: Use of Logarithmic Regression in the Estimation of Plant Biomass, Can. J. For. Res., 2(1), 49–53, doi:10.1139/x72-009, 1972.

Bastin, J.-F., Barbier, N., Réjou-Méchain, M., Fayolle, A., Gourlet-Fleury, S., Maniatis, D., de Haulleville, T., Baya, F., Beeckman, H. and Beina, D.: Seeing Central African forests through their largest trees, Sci. Rep., 5, 2015.

Beygelzimer, A., Kakadet, S., Langford, J., Arya, S., Mount, D. and Li, S.: FNN: fast nearest neighbor search algorithms and applications. R package version 1.1., 2013.

Brown, S., Gillespie, A. J. and Lugo, A. E.: Biomass estimation methods for tropical forests with applications to forest inventory data, For. Sci., 35(4), 881–902, 1989.

Cannell, M. G. R.: Woody biomass of forest stands, For. Ecol. Manag., 8(3–4), 299–312, doi:10.1016/0378-1127(84)90062-8, 1984.

Chambers, J. Q., dos Santos, J., Ribeiro, R. J. and Higuchi, N.: Tree damage, allometric relationships, and above-ground net primary production in central Amazon forest, For. Ecol. Manag., 152(1), 73–84, 2001.

Chave, J., Andalo, C., Brown, S., Cairns, M. A., Chambers, J. Q., Eamus, D., Fölster, H., Fromard, F., Higuchi, N., Kira, T., Lescure, J.-P., Nelson, B. W., Ogawa, H., Puig, H., Riéra, B. and Yamakura, T.: Tree allometry and improved estimation of carbon stocks and balance in tropical forests, Oecologia, 145(1), 87–99, doi:10.1007/s00442-005-0100-x, 2005.

Chave, J., Coomes, D., Jansen, S., Lewis, S. L., Swenson, N. G. and Zanne, A. E.: Towards a worldwide wood economics spectrum, Ecol. Lett., 12(4), 351–366, doi:10.1111/j.1461-0248.2009.01285.x, 2009.

Chave, J., Réjou-Méchain, M., Búrquez, A., Chidumayo, E., Colgan, M. S., Delitti, W. B. C., Duque, A., Eid, T., Fearnside, P. M., Goodman, R. C., Henry, M., Martínez-Yrízar, A., Mugasha, W. A., Muller-Landau, H. C., Mencuccini, M., Nelson, B. W., Ngomanda, A., Nogueira, E. M., Ortiz-Malavassi, E., Pélissier, R., Ploton, P., Ryan, C. M., Saldarriaga, J. G. and Vieilledent, G.: Improved allometric models to estimate the aboveground biomass of tropical trees, Glob. Change Biol., 20(10), 3177–3190, doi:10.1111/gcb.12629, 2014.

Chen, Q., Vaglio Laurin, G. and Valentini, R.: Uncertainty of remotely sensed aboveground biomass over an African tropical forest: Propagating errors from trees to plots to pixels, Remote Sens. Environ., 160, 134–143, doi:10.1016/j.rse.2015.01.009, 2015.

Chuyong, G. B., Condit, R., Kenfack, D., Losos, E. C., Moses, S. N., Songwe, N. C. and Thomas, D. W.: Korup forest dynamics plot, Cameroon, Trop. For. Divers. Dynamism, 506–516, 2004.

Clark, D. B. and Clark, D. A.: Abundance, growth and mortality of very large trees in neotropical lowland rain forest, For. Ecol. Manag., 80(1–3), 235–244, doi:10.1016/0378-1127(95)03607-5, 1996.

Clark, D. B. and Kellner, J. R.: Tropical forest biomass estimation and the fallacy of misplaced concreteness, J. Veg. Sci., 23(6), 1191–1196, doi:10.1111/j.1654-1103.2012.01471.x, 2012.

Cleveland, W. S., Grosse, E. and Shyu, W. M.: Local regression models, Stat. Models S, 309–376, 1992.

Eggleston, H. S., Buendia, L., Miwa, K., Ngara, T. and Tanabe, K.: IPCC guidelines for national greenhouse gas inventories, Inst. Glob. Environ. Strateg. Hayama Jpn., 2006.

Eloy, C.: Leonardo's rule, self-similarity and wind-induced stresses in trees, Phys. Rev. Lett., 107(25), doi:10.1103/PhysRevLett.107.258101, 2011.

Enquist, B. J.: Universal scaling in tree and vascular plant allometry: toward a general quantitative theory linking plant form and function from cells to ecosystems, Tree Physiol., 22(15-16), 1045–1064, doi:10.1093/treephys/22.15-16.1045, 2002.

Fayolle, A., Doucet, J.-L., Gillet, J.-F., Bourland, N. and Lejeune, P.: Tree allometry in Central Africa: Testing the validity of pantropical multi-species allometric equations for estimating biomass and carbon stocks, For. Ecol. Manag., 305, 29–37, doi:10.1016/j.foreco.2013.05.036, 2013.

Freedman, B., Duinker, P. N., Barclay, H., Morash, R. and Prager, U.: Forest biomass and nutrient studies in central Nova Scotia., Inf. Rep. Marit. For. Res. Cent. Can., (M-X-134), 126 pp., 1982.

Goodman, R. C., Phillips, O. L. and Baker, T. R.: Data from: The importance of crown dimensions to improve tropical tree biomass estimates, [online] Available from: http://dx.doi.org/10.5061/dryad.p281 g (Accessed 17 May 2015), 2013.

Goodman, R. C., Phillips, O. L. and Baker, T. R.: The importance of crown dimensions to improve tropical tree biomass estimates, Ecol. Appl., 24(4), 680–698, 2014.

Hansen, M. C., Potapov, P. V., Moore, R., Hancher, M., Turubanova, S. A., Tyukavina, A., Thau, D., Stehman, S. V., Goetz, S. J. and Loveland, T. R.: High-resolution global maps of 21st-century forest cover change, science, 342(6160), 850–853, 2013.

Harris, N. L., Brown, S., Hagen, S. C., Saatchi, S. S., Petrova, S., Salas, W., Hansen, M. C., Potapov, P. V. and Lotsch, A.: Baseline map of carbon emissions from deforestation in tropical regions, Science, 336(6088), 1573–1576, 2012.

Hasenauer, H. and Monserud, R. A.: A crown ratio model for Austrian forests, For. Ecol. Manag., 84(1–3), 49–60, doi:10.1016/0378-1127(96)03768-1, 1996.

Henry, M., Besnard, A., Asante, W. A., Eshun, J., Adu-Bredu, S., Valentini, R., Bernoux, M. and Saint-André, L.: Wood density, phytomass variations within and among trees, and allometric equations in a tropical rainforest of Africa, For. Ecol. Manag., 260(8), 1375–1388, doi:10.1016/j.foreco.2010.07.040, 2010.

Holdaway, M. R.: Modeling Tree Crown Ratio, For. Chron., 62(5), 451–455, doi:10.5558/tfc62451-5, 1986.

Jenkins, J. C., Chojnacky, D. C., Heath, L. S. and Birdsey, R. A.: National-Scale Biomass Estimators for United States Tree Species, For. Sci., 49(1), 12–35, 2003.

King, D. and Loucks, O. L.: The theory of tree bole and branch form, Radiat. Environ. Biophys., 15(2), 141–165, doi:10.1007/BF01323263, 1978.

Legendre, P.: lmodel2: Model II Regression. R package version 1.7-0, See Httpcran R-Proj. Orgwebpackageslmodel2, 2011.

Mäkelä, A. and Harry T.: Crown ratio influences allometric scaling of trees, Ecology, 87(12), 2967–2972, doi:10.1890/0012-9658(2006)87[2967:CRIASI]2.0.CO;2, 2006.

Malhi, Y., Wood, D., Baker, T. R., Wright, J., Phillips, O. L., Cochrane, T., Meir, P., Chave, J., Almeida, S. and Arroyo, L.: The regional variation of aboveground live biomass in old-growth Amazonian forests, Glob. Change Biol., 12(7), 1107–1138, 2006.

Marra, D. M., Higuchi, N., Trumbore, S. E., Ribeiro, G., Santos, J. dos, Carneiro, V. M. C., Lima, A. J. N., Chambers, J. Q., Negrón-Juárez, R. I. and Holzwarth, F.: Predicting biomass of hyperdiverse and structurally complex Central Amazon forests–a virtual approach using extensive field data, Biogeosciences Discuss., 12, 15537–15581, 2015.

Mascaro, J., Litton, C. M., Hughes, R. F., Uowolo, A. and Schnitzer, S. A.: Minimizing Bias in Biomass Allometry: Model Selection and Log-Transformation of Data, Biotropica, 43(6), 649–653, doi:10.1111/j.1744-7429.2011.00798.x, 2011.

McMahon, T. A. and Kronauer, R. E.: Tree structures: deducing the principle of mechanical design, J. Theor. Biol., 59(2), 443–466, 1976.

Mitchard, E. T., Saatchi, S. S., Baccini, A., Asner, G. P., Goetz, S. J., Harris, N. L. and Brown, S.: Uncertainty in the spatial distribution of tropical forest biomass: a comparison of pan-tropical maps, Carbon Balance Manag., 8(1), 10, doi:10.1186/1750-0680-8-10, 2013.

Moorby, J. and Wareing, P. F.: Ageing in Woody Plants, Ann. Bot., 27(2), 291–308, 1963.

Moundounga Mavouroulou, Q., Ngomanda, A., Engone Obiang, N. L., Lebamba, J., Gomat, H., Mankou, G. S., Loumeto, J., Midoko Iponga, D., Kossi Ditsouga, F., Zinga Koumba, R., Botsika Bobé, K. H., Lépengué, N., Mbatchi, B. and Picard, N.: How to improve allometric equations to estimate forest biomass stocks? Some hints from a central African forest, Can. J. For. Res., 44(7), 685–691, doi:10.1139/cjfr-2013-0520, 2014.

Muggeo, V. M. R.: Estimating regression models with unknown break-points, Stat. Med., 22(19), 3055–3071, doi:10.1002/sim.1545, 2003.

Ngomanda, A., Engone Obiang, N. L., Lebamba, J., Moundounga Mavouroulou, Q., Gomat, H., Mankou, G. S., Loumeto, J., Midoko Iponga, D., Kossi Ditsouga, F., Zinga Koumba, R., Botsika Bobé, K. H., Mikala Okouyi, C., Nyangadouma, R., Lépengué, N., Mbatchi, B. and Picard, N.: Site-specific versus pantropical allometric equations: Which option to estimate the biomass of a moist central African forest?, For. Ecol. Manag., 312, 1–9, doi:10.1016/j.foreco.2013.10.029, 2014.

Niklas, K. J.: Size-dependent Allometry of Tree Height, Diameter and Trunk-taper, Ann. Bot., 75(3), 217–227, doi:10.1006/anbo.1995.1015, 1995.

Nogueira, E. M., Fearnside, P. M., Nelson, B. W., Barbosa, R. I. and Keizer, E. W. H.: Estimates of forest biomass in the Brazilian Amazon: New allometric equations and adjustments to biomass from wood-volume inventories, For. Ecol. Manag., 256(11), 1853–1867, 2008.

Pelletier, J., Ramankutty, N. and Potvin, C.: Diagnosing the uncertainty and detectability of emission reductions for REDD + under current capabilities: an example for Panama, Environ. Res. Lett., 6(2), 024005, doi:10.1088/1748-9326/6/2/024005, 2011.

Perry, D. A.: The competition process in forest stands, Attrib. Trees Crop Plants, 481–506, 1985.

Picard, N., Bosela, F. B. and Rossi, V.: Reducing the error in biomass estimates strongly depends on model selection, Ann. For. Sci., 1–13, doi:10.1007/s13595-014-0434-9, 2014.

Poorter, L., Bongers, F., Sterck, F. J. and Wöll, H.: Architecture of 53 rain forest tree species differing in adult stature and shade tolerance, Ecology, 84(3), 602–608, doi:10.1890/0012-9658(2003)084[0602:AORFTS]2.0.CO;2, 2003.

Poorter, L., Bongers, L. and Bongers, F.: Architecture of 54 moist-forest tree species: traits, trade-offs, and functional groups, Ecology, 87(5), 1289–1301, doi:10.1890/0012-9658(2006)87[1289:AOMTST]2.0.CO;2, 2006.

Réjou-Méchain, M., Muller-Landau, H. C., Detto, M., Thomas, S. C., Le Toan, T., Saatchi, S. S., Barreto-Silva, J. S., Bourg, N. A., Bunyavejchewin, S., Butt, N., Brockelman, W. Y., Cao, M., Cárdenas, D., Chiang, J.-M., Chuyong, G. B., Clay, K., Condit, R., Dattaraja, H. S., Davies, S. J., Duque, A., Esufali, S., Ewango, C., Fernando, R. H. S., Fletcher, C. D., Gunatilleke, I. A. U. N., Hao, Z., Harms, K. E., Hart, T. B., Hérault, B., Howe, R. W., Hubbell, S. P., Johnson, D. J., Kenfack, D., Larson, A. J., Lin, L., Lin, Y., Lutz, J. A., Makana, J.-R., Malhi, Y., Marthews, T. R., McEwan, R. W., McMahon, S. M., McShea, W. J., Muscarella, R., Nathalang, A., Noor, N. S. M., Nytch, C. J., Oliveira, A. A., Phillips, R. P., Pongpattananurak, N., Punchi-Manage, R., Salim, R., Schurman, J., Sukumar, R., Suresh, H. S., Suwanvecho, U., Thomas, D. W., Thompson, J., Uríarte, M., Valencia, R., Vicentini, A., Wolf, A. T., Yap, S., Yuan, Z., Zartman, C. E., Zimmerman, J. K. and Chave, J.: Local spatial structure of forest biomass and its consequences for remote sensing of carbon stocks, Biogeosciences, 11(23), 6827–6840, doi:10.5194/bg-11-6827-2014, 2014.

Réjou-Méchain, M., Tymen, B., Blanc, L., Fauset, S., Feldpausch, T. R., Monteagudo, A., Phillips, O. L., Richard, H. and Chave, J.: Using repeated small-footprint LiDAR acquisitions to infer spatial and temporal variations of a high-biomass Neotropical forest, Remote Sens. Environ., 169, 93–101, 2015.

Saatchi, S. S., Harris, N. L., Brown, S., Lefsky, M., Mitchard, E. T., Salas, W., Zutta, B. R., Buermann, W., Lewis, S. L. and Hagen, S.: Benchmark map of forest carbon stocks in tropical regions across three continents, Proc. Natl. Acad. Sci., 108(24), 9899–9904, 2011.

Scrucca, L.: Model-based SIR for dimension reduction, Comput. Stat. Data Anal., 55(11), 3010–3026, 2011.

Shinozaki, K., Yoda, K., Hozumi, K. and Kira, T.: A quantitative analysis of plant form-the pipe model theory: I. Basic analyses, 日本生態学会誌, 14(3), 97–105, 1964.

Sillett, S. C., Van Pelt, R., Koch, G. W., Ambrose, A. R., Carroll, A. L., Antoine, M. E. and Mifsud, B. M.: Increasing wood production through old age in tall trees, For. Ecol. Manag., 259(5), 976–994, doi:10.1016/j.foreco.2009.12.003, 2010.

Sist, P., Mazzei, L., Blanc, L. and Rutishauser, E.: Large trees as key elements of carbon storage and dynamics after selective logging in the Eastern Amazon, For. Ecol. Manag., 318, 103–109, doi:10.1016/j.foreco.2014.01.005, 2014.

Slik, J. W., Paoli, G., McGuire, K., Amaral, I., Barroso, J., Bastian, M., Blanc, L., Bongers, F., Boundja, P. and Clark, C.: Large trees drive forest aboveground biomass variation in moist lowland forests across the tropics, Glob. Ecol. Biogeogr., 22(12), 1261–1271, 2013.

Stephenson, N. L., Das, A. J., Condit, R., Russo, S. E., Baker, P. J., Beckman, N. G., Coomes, D. A., Lines, E. R., Morris, W. K., Rüger, N., Álvarez, E., Blundo, C., Bunyavejchewin, S., Chuyong, G., Davies, S. J., Duque, Á., Ewango, C. N., Flores, O., Franklin, J. F., Grau, H. R., Hao, Z., Harmon, M. E., Hubbell, S. P., Kenfack, D., Lin, Y., Makana, J.-R., Malizia, A., Malizia, L. R., Pabst, R. J., Pongpattananurak, N., Su, S.-H., Sun, I.-F., Tan, S., Thomas, D., van Mantgem, P. J., Wang, X., Wiser, S. K. and Zavala, M. A.: Rate of tree carbon accumulation increases continuously with tree size, Nature, advance online publication, doi:10.1038/nature12914, 2014.

Van Gelder, H. A., Poorter, L. and Sterck, F. J.: Wood mechanics, allometry, and life-history variation in a tropical rain forest tree community, New Phytol., 171(2), 367–378, doi:10.1111/j.1469-8137.2006.01757.x, 2006.

Vieilledent, G., Vaudry, R., Andriamanohisoa, S. F. D., Rakotonarivo, O. S., Randrianasolo, H. Z., Razafindrabe, H. N., Rakotoarivony, C. B., Ebeling, J. and Rasamoelina, M.: A universal approach to estimate biomass and carbon stock in tropical forests using generic allometric models, Ecol. Appl., 22(2), 572–583, doi:10.1890/11-0039.1, 2012.

West, G. B., Brown, J. H. and Enquist, B. J.: A general model for the structure and allometry of plant vascular systems, Nature, 400(6745), 664–667, doi:10.1038/23251, 1999.

Zanne, A. E., Lopez-Gonzalez, G., Coomes, D. A., Ilic, J., Jansen, S., Lewis, S. L., Miller, R. B., Swenson, N. G., Wiemann, M. C. and Chave, J.: Data from: towards a worldwide wood economics spectrum. Dryad Digital Reposit., 2009.

2.8 Supplement: Field data protocols

2.8.1 Unpublished dataset: site characteristics

Field work was conducted close to the city of Mindourou-2 (4°7'N, 14°32'E) in the logging concessions of Alpicam-Grumcam Company (67 trees) and approximately 150 km southwest of this location, in community forests (10 trees) surrounding the city of Lomie (3°9' N, 13°37'E). In both locations, the vegetation type can be classified as semi-deciduous *Celtis* forest (*sensu* Fayolle et al. 2014). The average annual rainfall of the area is 1500-2000 mm with two marked dry seasons, from mid-November to mid-March (long dry season) and from June to mid-August (small dry season). The average annual temperature is approximately 24 °C. The elevation ranges between 600 and 700 m a.s.l.

2.8.2 Biomass data

2.8.2.1 Unpublished dataset

A first set of 67 trees were felled as part of the routine activities of a logging company. Tree sampling targeted large individuals of 10 abundant species. For a second set of 10 trees, we used a less destructive protocol consisting in volume measurements on standing trees by expert tree climbers.

In both felled and standing trees, the volume of the largest components of tree structure (i.e., buttresses, stumps, trunk and large branches, namely those with a sectional diameter – or *Db* for branch diameter – greater than 20 cm) was estimated following Henry et al. (2009). For the trunk, we measured the proximal and distal diameters of approximately 2-m long conical sections and applied Smalian's formula to compute the volume of each section. A similar procedure was used for large branches, with the exception that conical sections were approximately 1 m long. Buttress volumes were estimated using the dedicated formula reported by Henry et al. (2009). On felled trees, 5-cm-thick wood slices were collected at the top of stumps and trunks and in large branches. Three parallelepipeds of approximately 5 * 5 *2.5 cm were then sampled radially from each slice at the sawmill. The wood density (ρ) of each parallelepiped sample was determined from its green volume (waster displacement method) and oven-dried mass (Williamson et Wiemann 2010). Analyses of wood density variations revealed significant species, individual and vertical (i.e., stump, buttresses and trunk *vs* large branches) effects (result not shown). We therefore converted the volume of stumps, buttresses and trunks to dry mass using an individual average of ρ estimates in these components. The volumes of large branches were converted to dry mass using individual averages of ρ estimates in large branches. For standing trees, volume estimates of all components were converted to mass using individual ρ values obtained from a single pruned branch ($10 \leq Db \leq 20$ cm).

The dry mass of small branches ($Db \leq 20$ cm) was estimated using a different protocol. On each tree, the total fresh mass and the leaf fresh mass of one to three damage-free branches were weighted, and their proximal diameter measured. From the resulting database, we built a mixed-species linear model relating branch diameter to total fresh mass (in logarithmic units). For some species presenting a significant main species effect, a species-specific model was developed (results not shown). These models were used to compute the total fresh mass of small branches ($Db \leq 20$) that were not directly weighted in the field. We then established linear models relating small branch total fresh mass to leaf fresh mass with a similar procedure. The latter models were used to decompose small branch total fresh mass predictions into leaf and wood fresh masses. Approximately 200 g of leaves per sample

branch were oven-dried to determine a species-specific fresh to dry leaf mass conversion ratio. For each tree, a wood slice was collected from a sampled small branch and ρ was determined as previously described, allowing the conversion of small branch wood fresh mass to dry mass.

The total AGB of a tree (*TAGB*) was obtained by summing the dry masses of the stump, buttresses, trunk, large branches, woody parts of small branches and leaves.

In addition to basic dendrometric measurements (*D*, *H*) and full crown structure description (branch diameters, lengths and topology), two perpendicular crown diameters were measured using a Laser Ranger-finder device (TruPulse 360R, Laser Technology Inc., Centennial, Colorado) for 39 individuals.

2.8.2.2 Other datasets

We additionally compiled destructive datasets providing information on crown mass for 29 trees from Ghana (Henry *et al.* 2010), 285 trees from Madagascar (Vieilledent *et al.* 2011), 51 trees from Peru (Goodman, Phillips & Baker 2014, 2013), 132 trees from Cameroon (Fayolle *et al.* 2013), and 99 trees from Gabon (Ngomanda *et al.* 2014). In the dataset from Ghana, we used raw field data made available by the author on 32 trees to estimate the mass of tree components using the same algorithm applied to our data, thus resulting in slight differences with respect to the *TAGB* values published by Henry *et al.* (2010). Three small trees presenting anomalous relative crown mass (≥ 100%) were excluded from the analysis. In data from Madagascar, we left out trees sampled in dry forests because they may exhibit peculiar allometries. In the data from Gabon, we excluded two trees lacking information on crown depth. Finally, we excluded trees with D < 10 cm or crown mass < 5 kg because they exhibited very large variations in crown mass ratio while being of limited interest in *AGB* studies.

The resulting database features information on crown mass for 673 trees (referred to as $Data_{CM1}$ in the manuscript, available at http://dx.doi.org/10.5061/dryad.f2b52), 541 for which there is tree height information (referred to as $Data_{CM2}$ in the manuscript) and 119 for which there is crown diameter (referred to as $Data_{CD}$ in the manuscript), as described in Table 2-4.

Table 2-4. Six destructive datasets providing information on tree crown were combined into three working datasets with increasing level of information. $Data_{CM1}$ possess information on crown mass. $Data_{CM2}$ add information on trunk height. $Data_{CD}$ add information on crown diameter.

Source	Country	$Data_{CM1}$	$Data_{CM2}$	$Data_{CD}$
P. Ploton	Cameroon	77	77	39
Henry et al. (2010)	Ghana	29	29	29
Goodman et al. (2013)	Peru	51	51	51
Fayolle et al. (2013)	Cameroon	132		
Ngomanda et al. (2014)	Gabon	99	99	
Vieilledent et al. (2012)	Madagascar	285	285	
		673	541	119

2.8.3 Inventory data

In all plots, we considered all trees with a diameter at breast height (i.e., 1.3 m or above buttresses if present) ≥ 10 cm. In the 80 1-ha plots, tree height was measured with a Laser Ranger-finder device (TruPulse 360R, Laser Technology Inc., Centennial, Colorado) on approximately 50 trees per plot, homogenously distributed across diameter classes. Following Feldpausch et al. (2012), a three-parameter Weibull function was fitted at the site level to predict height of the remaining trees: $H = a(1 - \exp(-bD^c))$. We used a relationship calibrated over two 1-ha plots near Korup to predict tree heights in the 50-ha permanent plot. Trees were identified in the field by expert botanists, and herbarium specimens were collected on each species per site for cross-identification at the herbarium of Université Libre de Bruxelles (BRLU), except for Korup, where the taxonomy was confirmed at the Missouri Botanical Garden (MO). Of 48,155 measured trees, 88.4% were identified at the species level, 4.9% at the genus level, and 0.1% at the family level, and 6.4% were left unidentified. We used the Dryad Global Wood Density Database (Chave et al. 2009; Zanne et al. 2009) to attribute to each individual tree a wood density value. For species known only at the genus or family level, the average *ρ* value at that taxonomic level was used (Chave et al. 2006).

3 ASSESSING DA VINCI'S RULE ON LARGE TROPICAL TREE CROWNS OF CONTRASTED ARCHITECTURES: EVIDENCE FOR AREA-INCREASING BRANCHING

P. Ploton[1,2], N. Barbier[1,3], P. Couteron[1,3], S.T. Momo[1,3], S. Griffon[1], B. Sonké[3], U. Berger[4] and R. Pélissier[1]

[1]Institut de Recherche pour le Développement, UMR AMAP, Montpellier, France
[2]Institut des sciences et industries du vivant et de l'environnement, Montpellier, France
[3]Laboratoire de Botanique systématique et d'Ecologie, Département des Sciences Biologiques, Ecole Normale Supérieure, Université de Yaoundé I, Yaoundé, Cameroon
[4]Technische Universität Dresden, Faculty of Environmental Sciences, Institute of Forest Growth and Forest Computer Sciences, Tharandt, Germany

3.1 Introduction

Allometric scaling relationships between tree dimensions reflect biological and physical constrains that any tree must comply with to prevent malfunction (e.g., cavitation, buckling) as it grows in size. Understanding the general principles that drive tree form and functions is a fascinating and vast research topic that has been addressed from different perspectives. Given the fundamental role of water use in trees, the focus has oftentimes been put on water transport and vascular anatomy (Tyree, 1988; Zimmermann, 1978). A renowned whole-plant model somewhat related to this theme is the Pipe model (Shinozaki et al., 1964). The latter fundamentally stems from an observation made some 500 years ago by Leonardo da Vinci, which states that "*all the branches of a tree at every stage of its height when put together are equal in thickness to the trunk*". In other words, when a parent branch splits in *i* daughters, equation 1, known as area-preservation or Da Vinci's rule, should hold on average:

$$R = (\sum_2^i Area_{daughters})/Area_{parent} = 1 \qquad \text{(eq. 1)}$$

In the Pipe model, Da Vinci's rule describes tree external architecture, which is assumed to reflect tree hydraulic architecture. It is further posited that a unit of leaf area is supplied by a unit of conducting tissue area, which provides a basis to study relationships between carbon allocation, photosynthetic production and tree structural design under different conditions of stand structure or climate forcing (Berninger and Nikinmaa, 1997; Mäkelä, 1986; Nikinmaa, 1992). Another major perspective from which whole-plant allometric scaling have been studied is biomechanics. As every physical structure, trees must obey some elementary physical laws, such as sustain static (self) and dynamic (wind) loadings (Eloy, 2011; McMahon and Kronauer, 1976; Niklas, 2016). A typical example is the elastic similarity model which considers a tree as a vertical tapering column that, in order to avoid buckling under its own weight, must follow a number of scaling rules between column diameter, height and mass (Niklas, 1995).

About two decades ago, the Metabolic Theory of Ecology (MTE) proposed a modelling framework unifying hydrodynamics and biomechanics hypotheses to account for allometric scaling phenomena in

biological organisms (West et al., 1999, 1997). MTE posited that allometries arise from structure and hydrodynamics properties of the vascular network distributing resources in the organism. More specifically, the central assumption of the theory is that evolution led to the selection of near-optimal fractal-like vascular networks maximizing the scaling of resource uptake (e.g., CO2, water, and light and minimizing the required energy for cells' delivery. West and colleagues derived a "zeroth-order" model from the theory, which relies on a small set of assumptions regarding the geometry of tree branching network to predict a myriad of 'universal' scaling exponents between plant size and geometrical, physiological and anatomical plant characteristics (see West et al. 1999) and their influence on forest stands structure and dynamics (Enquist et al., 2009). While the mathematical and biological relevance of this model as well as the very existence of 'universal' scaling laws across species have been intensely debated (e.g., Kozlowski and Konarzewski, 2004; Muller-Landau et al., 2006), relatively few studies focused on testing MTE's assumptions on tree branching networks (but see Bentley et al., 2013).

The MTE model divides tree structure into external and internal components. The external structure is simplified to a hierarchical, symmetric and self-similar (i.e. fractal) branching network (Figure 3-1 A), which is convenient to derive scaling properties. Additionally, the model assumes that the external structure conforms to the mechanical principle of safety from gravitational buckling (i.e., elastic similarity hypothesis; Niklas, 1995), which induces area-preservation (i.e. da Vinci's rule), given the simplified properties of the fractal network. The internal branching structure is composed of a network of xylem conduits which number and sizes are related to the external branching structure via simple rules (Sperry et al., 2012).

Although the Da Vinci's rule is an important parameter in the two prevailing contemporary plant models (i.e. the Pipe model of Shinozaki et al., 1964 and the MTE model), actual empirical assessments of this rule are rare (Eloy, 2011) and have mostly been made on small-sized trees (Aratsu, 1998; Bentley et al., 2013; Sone et al., 2009; von Allmen et al., 2012), generally in temperate regions. Yet, we know that tree crowns undergo major structural changes along ontogeny, notably a phase of lateral expansion through reiteration known as crown metamorphosis (Hallé et al., 1978; Shukla and Ramakrishnan, 1986). Besides, empirical evidences suggest that tree crown represents an increasing proportion of tree biomass (Ploton et al., 2016) and biomass growth (Sillett et al., 2010) as trees grow in size, which could indicate a deviation from the area-preservation hypothesis, notably at branching points bearing the largest (reiterated) branches.

In the present paper, we used a unique dataset describing the branching network geometry and topology of 72 very large tropical trees from 9 different species to assess Da Vinci's rule validity. We actually tested several assumptions of the MTE model, in particular on branch length and radii scaling exponents (which together entail Da Vinci's rule in the average MTE tree) and self-similarity. Given the inherent variability in biological entities (such as between diameters and lengths of branches growing from a given node), MTE's assumptions are assumed to hold on an average branching network (Savage et al., 2008). However, systematic deviations from MTE's average tree may occur at the species-level from variation in species architecture (Hallé et al., 1978). For instance, deviations from simple fractal-like architectures can be observed on species with high apical dominance i.e., when the terminal bud inhibits the growth of lateral buds (Horn, 2000). At adult stature and in the most extreme case of dominance, the apical bud creates a large, central axis within the crown (i.e. a continuation of the trunk within the crown) bearing more or less horizontal branches, which violates MTE's assumption of

symmetric branching (see Figure 3-1). Biomechanical models suggest that variations in branching patterns (e.g., number and asymmetry of branches at a node) lead to systematic deviations from area-preservation (Minamino and Tateno, 2014). We thus explored whether the study of contrasted architectural types allowed evidencing systematic deviations of MTE's theoretical expectations in terms of branching structure.

3.2 Methods

3.2.1 Sampled trees and field protocol

We sampled 72 large tropical canopy trees from the mixed forest of southeast Cameroon, central Africa, spanning 67 to 212 cm in diameter at breast height (*DBH*), 31 to 57 m in height. These trees have been harvested as part of commercial logging activities, and their aboveground dry biomass estimated to 5.4 to 75.4 Mg (see Ploton et al. 2016). Trees were distributed in 9 species (hereafter referred to by their common names; Table 3-1) presenting highly contrasted architectures.

Table 3-1. Number of trees sampled (n_{tree}) among species, ranges of diameter at breast height (DBH, in cm) and apical dominance (from A low dominance to C highly dominant; see Figure 3-1 for illustration).

Species	Common name	n_{tree}	DBH (min-max)	Apic. dom.
Milicia excelsa (Welw.) C.C.Berg	Iroko	9	88.4 - 126	B
Entandrophragma cylindricum (Sprague) Sprague	Sapelli	9	100.5 - 178	B
Triplochiton scleroxylon K.Schum.	Ayous	22	88.4 - 212	B
Erythrophleum suaveolens (Guill. & Perr.) Brenan	Tali	7	67.5 - 112.8	B
Cylicodiscus gabunensis Harms	Okan	5	103 - 136	A
Amphimas ferrugineus Pellegr.	Lati	3	92.5 - 113	B
Terminalia superba Engl. & Diels	Frake	7	97 - 114	C
Pycnanthus angolensis (Welw.) Warb.	Ilomba	8	88.5 - 124.2	C
Mansonia altissima (A.Chev.) A.Chev.	Bete	2	67 - 86.5	B

Harvesting such large trees resulted in substantial damages to the crowns with small branches disconnected from their branching nodes and scattered around the felled tree. We thus focused on the largest intact structures within the crowns and described their topology and geometry from the trunk to nodes bearing at least one branch with a basal diameter greater than 20 cm. For each internode segment we measured the basal diameter, the distal diameter and the internode length. Internode order was set to 1 for the trunk and incremented by 1 after each branching node, which corresponds to the centrifugal labelling system used to describe the structure of an idealized tree in the MTE (Savage et al., 2008). We noted down when internodes clearly emerged from the apical bud (i.e., vertical internode above the trunk axis), which allowed us creating a second labeling scheme opposing internodes emerging from the principal axis (hereafter referred to as PA of order 1), their siblings (order 2), and internodes of order ≥ 3 (see Figure 3-1). The full database contained a total of 3730 internodes distributed on 1682 nodes (Figure 3-2).

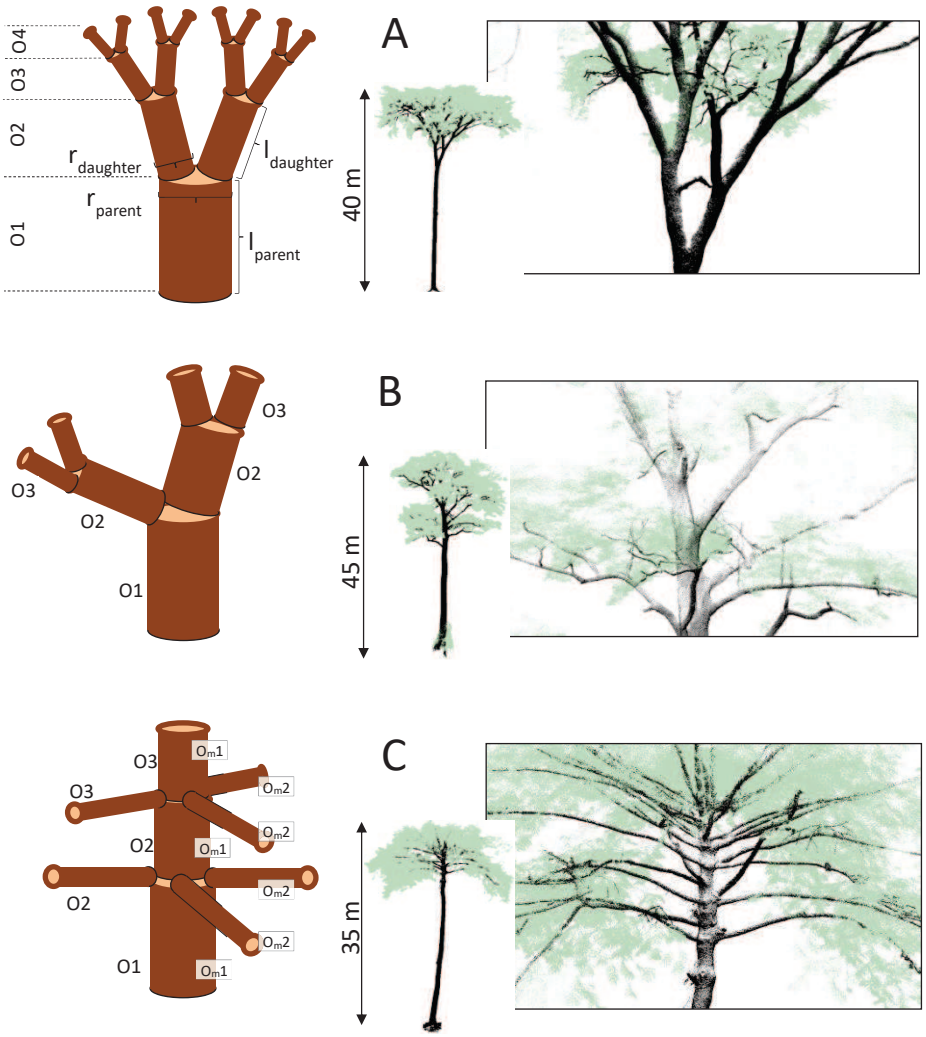

Figure 3-1. Schematic representation of different levels of asymmetry in species' architecture, from the optimal MTE tree (A) to moderately (B) and highly (C) dominant apex. O1 to O4 represent the labeling scheme of the MTE. In panel C, O_m1 to O_m2 illustrate a modified labeling scheme accounting for the presence of a principal axis in tree crown structure (see text). The right column gives illustrations of the three types of architectures based on large canopy tree species from central Africa, from top to bottom: Okan, Ayous and Ilomba (see Table 3-1 for more information on these species).

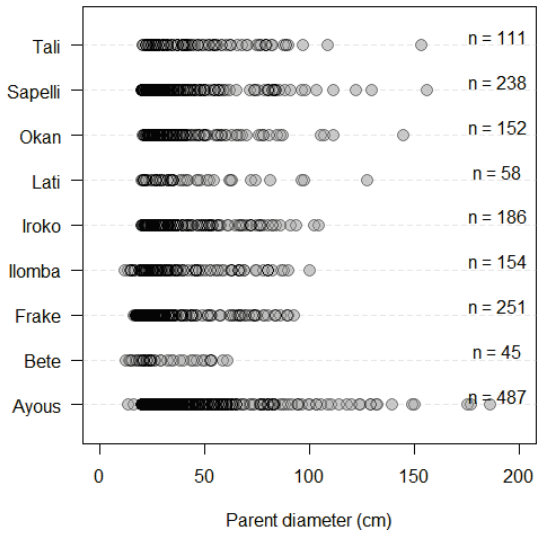

Figure 3-2. Distribution of sampled nodes along node parent diameters (in cm) in each of the 9 sampled species.

3.2.2 MTE model assumptions and predictions of branch scaling exponents

The MTE model assumes an idealized tree with a hierarchical, symmetrical and self-similar external branching network as in Figure 3-1 A (refer to Savage et al., 2008 for an exhaustive description of MTE model assumptions). The term hierarchical implies a consistent labelling scheme for branch orders (*k*) from the trunk (order 1) to leaf petioles (order *N*). Branch order *k* represents the number of branching nodes separating a given internode from the order of the trunk. The branching network is also assumed to be symmetric, implying that branches radii (r_k) and lengths (l_k) are approximately similar within a given order *k* (or that their variance is small compared to the variance across orders). Finally, the branching ratio (*n*) i.e., the number of internodes emerging from each node, is assumed to be constant across orders, leading to branches lengths and radii scaling ratios γ_k (eq. 2) and β_k (eq. 3) (West et al., 1999), respectively.

$$\gamma_k = \frac{l_{k+1}}{l_k} = n_k^{-b_k} = n^{-b_k} \quad \text{(eq. 2)}$$

$$\beta_k = \frac{r_{k+1}}{r_k} = n_k^{-a_k} = n^{-a_k} \quad \text{(eq. 3)}$$

The MTE model further evokes two secondary assumptions determining how branches radii and lengths at one order relate to those at the next order, and thus sets scaling exponents a_k and b_k in the above equations. First, the network is assumed to be space-filling (i.e., roots or leaves try to fill-in a tree-dimensional space to harvest water or light), leading to the derivation that branch scaling exponents for length is *b=1/3* (West et al., 1999, 1997), independent of branch order *k*. Second, the model adopts the elastic similarity hypothesis, which predicts $l_{TOT} \propto r^{2/3}$ (with *r* a branch basal radius and l_{TOT} the length to the tip of the most distant twig; Greenhill, 1881; McMahon and Kronauer, 1976). This last assumption, together with *b*=1/3, allows the derivation of *a* = 0.5 for the radii scaling exponent (independent of *k*) from eq. 2 and 3. With *a* and *b* independent of *k*, the network is self-similar at all scales (i.e., fractal). From eq. 3, it can also be shown that ratios of daughter branches over parent branches cross-sectional areas across orders follow eq. 4 (modified from the original demonstration of West et al. (1999) so to account for a simplification in eq. 3).

$$\frac{n*A_{k+1}}{A_k} = n * \beta_k^2 = n^{1-2a} \quad \text{(eq. 4)}$$

with A the sum of branches cross-sections at a given order. When *a* = 0.5 as expected from the above assumptions, eq. 4 reduces to unity and $n * A_{k+1} = A_k$, i.e. the branching network is area preserving and complies with Da Vinci's rule. Therefore, area preservation is not directly assumed in the MTE, but rather results from a set of lower level simplifying assumptions on the topology and geometry of the tree branching network.

We used our field data to assess area ratio (*R* from eq. 1) and branch scaling exponents at each node of the sampled branches. Contrary to theoretical MTE assumptions, real trees exhibit some variability between nodes in daughters number and symmetry, so that we estimated the branch length and radius scaling exponents a_D and b_D for each daughter (that is, a node with 3 daughters had 3 sets of scaling exponents) following eq. 5 and 6 derived from eq. 2 and 3 (Bentley et al., 2013).

$$b_D = -log\left(\frac{l_{daugther}}{l_{parent}}\right) / log(n_D) \quad \text{(eq. 5)}$$

$$a_D = -log\left(\frac{r_{daugther}}{r_{parent}}\right)/log(n_D) \quad \text{(eq. 6)}$$

with n_D the number of daughters at the node.

Since distributions of b_D and a_D may not be unimodal or symmetric (Bentley et al., 2013), we used the medians instead of the means as empirical estimates of scaling exponents at the node, branching order or species level. We further extracted 10^4 random samples from each distribution (of similar size as the original distribution) and used the 2.5 and 97.5 percentiles of resampled medians for comparison with MTE predictions (i.e., 1/3 for *b* and 1/2 for *a*). We assumed the distribution of *R* to be symmetric and used the resampled mean to obtain empirical estimates to be compared with the expected value of 1 under the area-preserving hypothesis. It is noteworthy that in the latter case, our test asymptotically converges to a *t*-test.

3.2.3 Assessing the effect of asymmetry and node morphology on species area ratio

We investigated the influence of architectural asymmetry (resulting from apical dominance) on species-level branch scaling exponents and area ratio on a subset of 3 illustrative species (Okan, Ayous and Ilomba) selected to maximize differences in the frequency of PA internodes in their respective crowns (Figure 3-3). The frequency of PA internodes correlated (r=-0.76) with the architectural asymmetry parameter (*pF*; Smith et al. 2014) while being more straightforward to compute. Species-specific scaling exponents and area ratios were pairwise-compared using two-sample Kolmogorov-Smirnov tests (including Bonferroni correction). In order to help interpreting between species differences, we also split the internode dataset into PA, PA siblings and other branch segments (i.e. with order ≥ 3) and looked at the specific distributions of b_b, a_b and *R* in each of those groups.

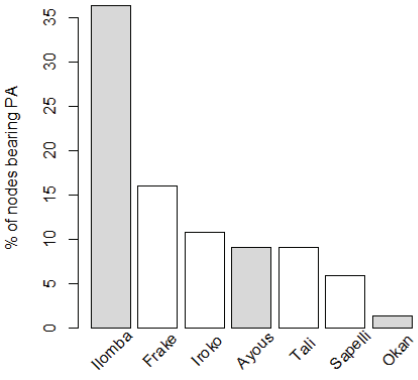

Figure 3-3. Frequency of PA internodes per species. Ilomba (35.7% : highly asymmetric), Ayous (9.4% : moderately asymmetric) and Okan (1.3%: symmetric) were selected as illustrative species in results sections 3.3 and 3.4.

Last, we tested whether other architectural parameters had a systematic influence on area ratio at node and species levels. Besides the presence of PA at a node (encoded as a presence/absence binary variable), node morphology was characterized by the number of daughters (n_D) and an index of daughters' asymmetry (*q*, eq. 7) inspired from Minamino and Tateno (2014):

$$q = \frac{\left(\max(Area_{daughters})/\left(\sum Area_{daughters}\right)\right) - {n_D}^{-1}}{((n_D - 1)/n_D)} \quad \text{(eq. 7)}$$

The *q* index ranges from 0 (perfect symmetry between n_D daughters) to 1 (one daughter is much larger than its n_D - 1 sibling(s)). We also used a simple linear model relating $\log(\sum Area_{daughters})$ to $\log(\sum Area_{parent})$ and included species and morphological parameters as covariate to detect systematic influences on area ratio.

3.3 Results

3.3.1 Does the average tree conform to branch scaling exponents and area ratio predictions?

Pooling all 9 species together, we assessed whether the average branching network complied with MTE predictions. Across the 1682 nodes, the branching ratio was close to 2 (i.e., 2.2±0.6) and did not change across branching orders (supplementary Figure 3-8 E). The distribution of length scaling exponents (b_D) was much wider than the distribution of radii scaling exponents (a_D) (Figure 3-4 A-B). Plotting daughter length (l_{k+1}) against parent length (l_k) indeed showed that branch length is much more plastic than branch diameter across orders (supplementary Figure 3-8 B-C). The median of b_D = 0.20 [0.1, 0.30] was close to, but excluded, the expected value of 1/3. The distribution of a_D presented two apparent modes and was skewed toward positive values, corresponding to small-diameter branches found on much larger parents. Similarly to the b_D distribution, the median of a_D = 0.43 [0.42, 0.45] was close to, but excluded, the expected value of 1/2.

At the node level, area ratio estimates (R) were highly variable, with a minimum and a maximum of 0.15 and 4.96, respectively. The mean of R was 1.17 [1.15, 1.18] (Figure 3-4 C), significantly higher than the expected value of 1.

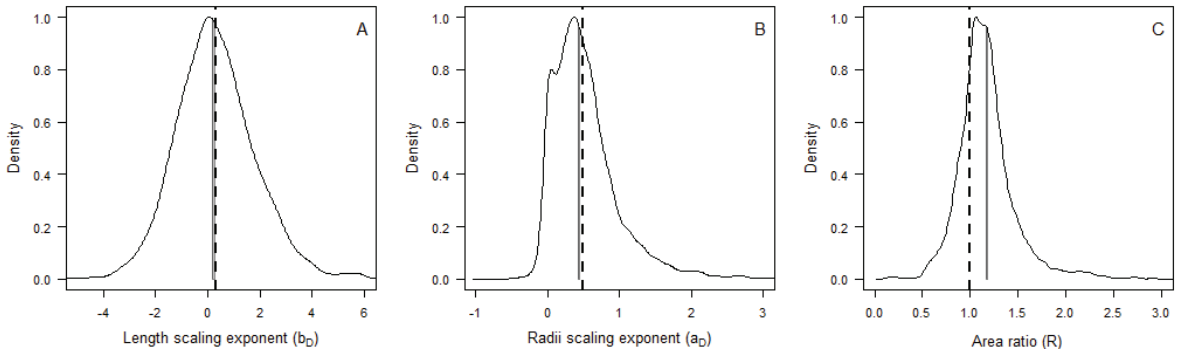

Figure 3-4. Density distributions (standardized to 1) of internodes length scaling exponents (A), radii scaling exponents (B) and nodes area ratios (C) at the inter-specific level. Dash lines represent the expected values under the Metabolic Theory of Ecology, while grey bars represent the 95% confidence interval of resampled medians (A, B) and mean (C).

3.3.2 Is the average tree self-similar?

Tree branching network is assumed to be self-similar i.e., branches scaling properties (thus area ratio) are expected to be constant across branching orders throughout the branching network. When labelling the branching orders following a centrifugal scheme (which amounts of forcing symmetry in tree crown topology), we did not observe obvious deviations in a_D, b_D or R among orders from the trends established at the interspecific-level (Figure 3-5 A-B-C). For each parameter (a_D, b_D and R), pairwise KS comparison tests across orders indicated that distributions were not significantly different, at the exception of a_D distributions for orders 2 and ≥4 (p-v < 0.05). The distribution of a_D at order 2 was indeed particularly large, indicating a greater variability in branch diameter relative to the diameter of the parent when the latter is the trunk (order 1), but the median value of the distribution did not substantially deviate from the ones of the two other distributions (i.e., order 3 and ≥4). Similarly, plotting a_D, b_D or R against parent diameter did not reveal any particular trend (Figure 3-5 D-

E-F), thus offering strong support to the assumption of self-similarity of the average hierarchical branching network on large trees.

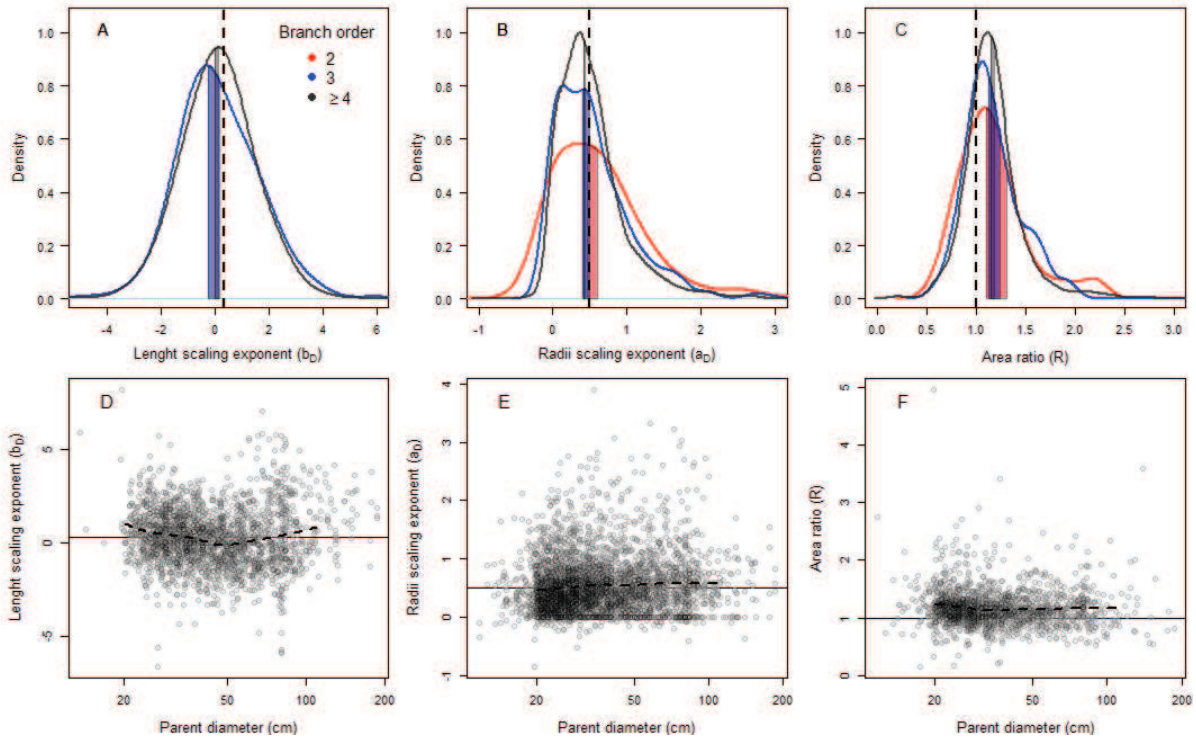

Figure 3-5. Density distributions (standardized to 1) of internodes length scaling exponents (A), radii scaling exponents (B) and nodes area ratios (C) across the first orders (i.e. 2, 3, ≥ 4) of the centrifugal labeling scheme. We excluded internodes of parent order 1 (i.e., the trunk) from analysis of length scaling exponents (in panel A). Dash black lines represent the expected values for hierarchical, symmetric, self-similar trees. Color bars represent the 2.5-97.5% interval of resampled medians per group. Branch scaling exponents and area ratios are also represented against parent diameter (D, E, F).

3.3.3 What is the effect of species asymmetry on branch scaling exponents and area ratio?

We investigated the effect of species architecture asymmetry (resulting from apical dominance) on species-level branch scaling exponents and node area ratios. The distribution of b_D exponents within species were as large as at the interspecific level (Figure 3-6 A), suggesting that the variance in daughter to parent lengths was not strongly structured per species. The distribution of b_D exponents for the highly asymmetric species (Ilomba) was significantly different from the ones of the two other species (KS tests, p-v < 0.05) and characterized by a lower median value (-0.14 [-0.40;-0.11]). This deviation reflects the architecture of asymmetric species: PA siblings tend to be much longer than their parent PA internode (Figure 3-6 B), steering species-level b_D distribution toward a lower median value when the frequency of PA increases in species crown structure. Interestingly, the median b_D for PA internodes (0.14 [0.00;0.23]) did not differ from the one of other daughters (0.18 [0.09;0.26]) (Figure 3-6 B), indicating that unlike PA siblings, lengths scaling among PA internodes conform to the daughter-parent scaling observed on nodes with more symmetric daughters.

Although all three species presented similar a_D exponents medians (i.e. overlapping confidence intervals on median estimates, Figure 3-6 C), a_D distributions of Ilomba and Ayous species were statistically different from the one of Okan species (KS tests, p-v < 0.05). These differences emerge

from the level of asymmetry in crown structure which broadens a_D distributions when small (high a_D) and large (low a_D) daughters are found on the same nodes. At nodes bearing PA (Figure 3-6 D), the asymmetry is at its maximum with the entire parent area transferred to the PA (i.e. median a_D for PA internodes of 0 [0.00;0.01]) and PA siblings having higher a_D than the expected value in case of symmetry (0.75 [0.69;0.79]).

At the species-level, Ilomba had a greater R than Ayous and Okan (KS tests, p-v < 0.05), owing to the much higher frequency of PA internodes found in the crowns of this species. At PA nodes, the mean area ratio, R, was 1.24 [1.20;1.29], higher than on nodes that did not bear PA internodes (1.16 [1.14;1.17]) (Figure 3-6 F), both distributions being statistically different (KS test, p-v < 0.05).

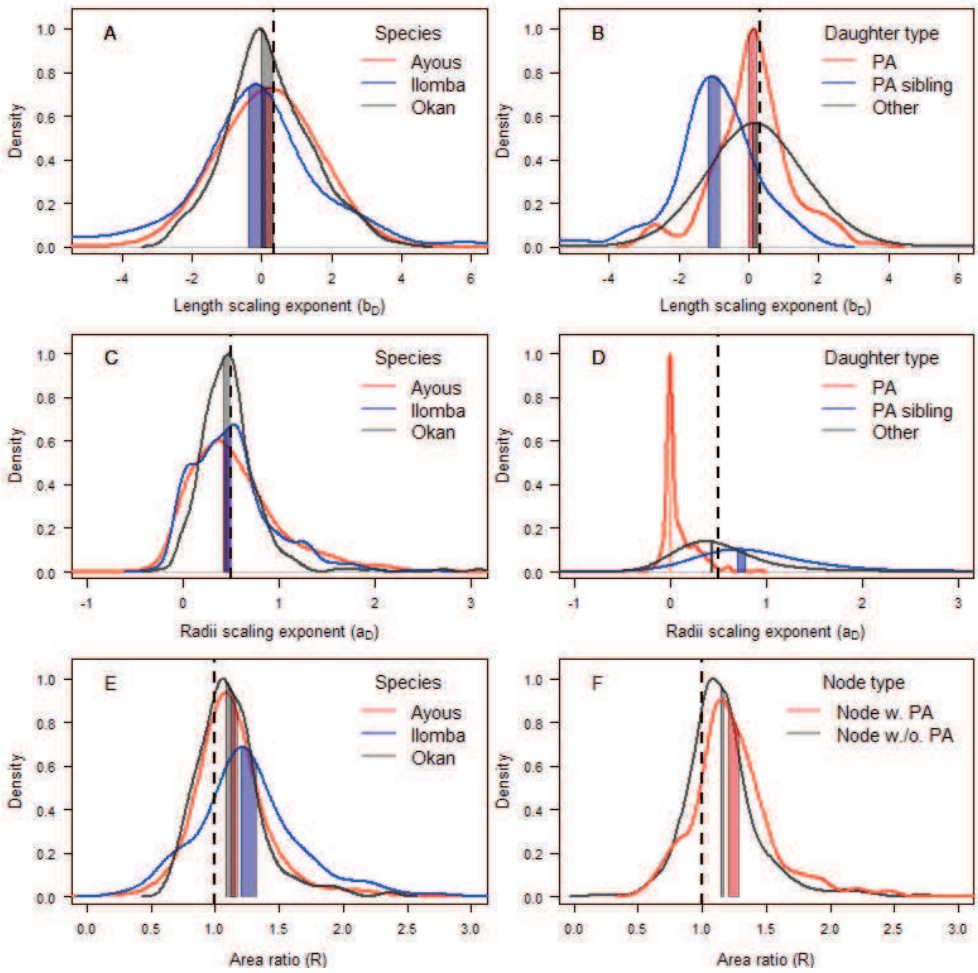

Figure 3-6. Density distributions (standardized to 1) of internode length scaling exponents (A, B), internodes radii scaling exponents (C, D) and node area ratios (E,F). In plots A, C and E, parameters are given for 3 illustrative species (i.e., Ayous, Ilomba and Okan) with contrasted frequency of PA internodes (cf. fig 3). Distributions are based on all internodes and nodes from those species, regardless of node morphology. In plots B, D and F, distributions are based on all data (inter-specific) split by node morphology i.e., internodes and nodes were grouped according to the presence of a PA, thus differentiating PA branches, their sibling(s) and branches from nodes w/o PA branch (noted "Other"). Dash black lines represent the expected values for hierarchical, symmetric, self-similar trees. Color bars represent the 2.5-97.5% interval of resampled medians per group.

3.3.4 Does node morphology induce systematic differences of area ratio at the species level?

Besides the binary variable indicating the presence or absence of PA, we used two simple descriptors of node morphology to explore systematic sources of variations on node area ratios, namely the number of daughters (n_D) and an index of daughter asymmetry (q). The number of daughters had the strongest effect on node area ratio and induced an increase of R from 1.13 [1.12; 1.15] when $n_D = 2$ to 1.39 [1.34; 1.45] for when $n_D > 2$ (Figure 3-7 A). Although the mean n_D was c. 2 across species, Ilomba had significantly more daughters (2.78±1.24) than Ayous (2.17±0.46) and Okan (2.06±0.26) (Dunn pairwise multiple comparisons test, p-values < 0.05 in both cases), and these daughters were principally located on PA nodes (supplementary Figure 3-8 F). Yet, this significant difference among species held when removing all PA nodes from the multiple comparisons test.

Node area ratios were more variable when daughters were relatively symmetric (e.g. for $q < 0.4$ in Figure 3-7 B) and converged toward 1 in situations of high asymmetry. The parameter q was indeed very highly significant as a linear predictor of log-transformed area ratio (coefficient estimate: -0.12, p-v < 0.001). It is noteworthy that introducing the binary variable of PA presence/absence in the model led to a significant main effect (parameter estimate: +0.20; p-v < 0.001) and interaction with q (coefficient for nodes bearing PA: -0.17, p-v: 0.040), indicating a faster decrease in area ratio as asymmetry increases for PA nodes (Figure 3-7 B, dark grey).

We built a log-log linear model between cumulated daughter areas and parent area and included the species factor as a covariate (incl. Ilomba, Ayous and Okan). Ayous and Ilomba were grouped into a single species category, since they were not statistically different in both slopes and intercepts. The two species groups had significantly different slopes (coefficient estimate of -0.06 for Okan, p-v: 0.036), reflecting a higher scaling of daughters area against parent area for Ilomba and Ayous (Figure 3-7 C-D). Although all three morphological parameters (i.e. N, q and the binary PA variable) only explained c. 7.6% of the variance in node area ratios, including them in the model removed the species effect.

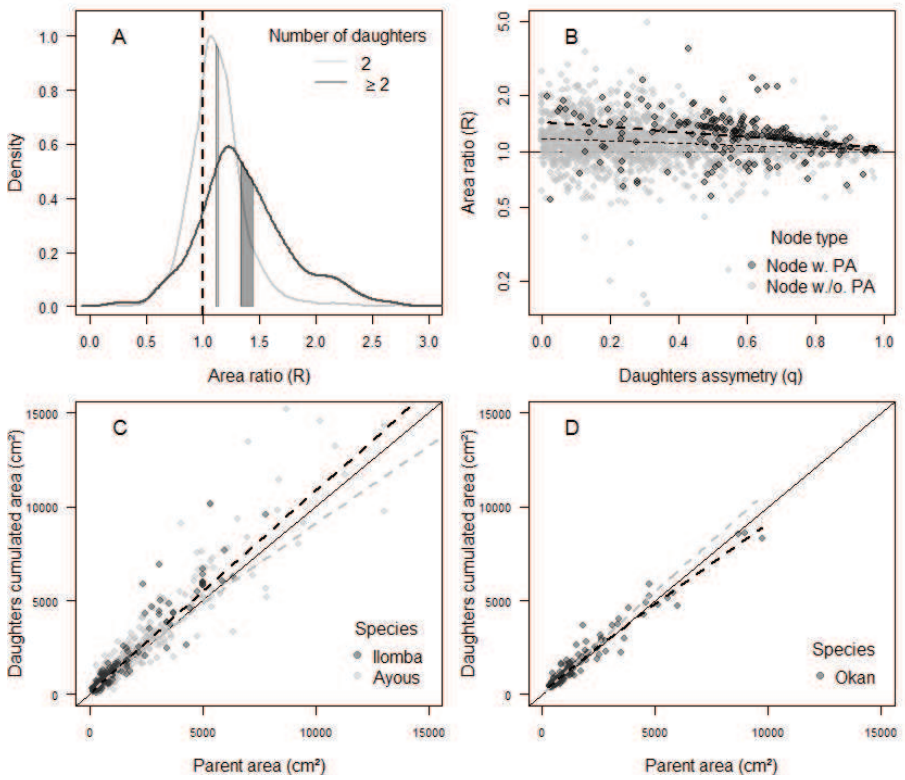

Figure 3-7. (A) Density distribution of nodes area ratio for nodes with 2 (light grey) and >2 daughters (dark grey). (B) Nodes area ratio against daughters asymmetry ('q'). Thick and thin dashed lines represent fits of linear models on nodes bearing (dark grey) or not bearing (light grey) PA branches, respectively. (C, D) Daughters cumulated area against parent area (in true unit). The upper limits of plots axes were set to 1.5 m² to ease species comparison, as branch cross-sectional areas for the Ayous species extend above c. 2.5 m². Dashed lines represent the fits of linear models on both Ayous and Ilomba (black line) and Okan (grey line). Linear models were adjusted on log-transformed data.

3.4 Discussion

We used a unique dataset describing crown geometry and topology on 72 very large tropical trees to compare empirical branching network properties to the assumptions (branch scaling exponents, self-similarity) and predictions (Da Vinci's rule) of the MTE theoretical model. Trees in our dataset showed self-similar properties, but deviations were observed from the simplified geometry of the average MTE tree. Importantly, we found an average area ratio greater than 1, thus questioning the generality of Da Vinci's rule.

3.4.1 Evidence of area increasing branching ($R > 1$)

From our direct measurements of branch diameters, we found that node area ratios were on average greater than one at the interspecific level (c. 1.15, Figure 3-4 C) and at the species level (i.e. for our three illustrative species of contrasted crown architectures, Figure 3-6 E), indicating that branching in our trees was area-increasing rather than area-preserving. Given the size of our dataset (> 1500 nodes), obtaining an average deviation from area-preservation was surprising. Indeed, Da Vinci's rule is presented as a well-established principle in theoretical modelling of plant vascular network, notably in

the MTE model (Enquist, 2002; West et al., 1999) and, as far as we know, it has never been questioned in MTE's model extensions (e.g. Smith et al., 2014; Sperry et al., 2012; von Allmen et al., 2012) and MTE-like models (e.g. Savage et al., 2010). The majority of empirical assessments of this rule have indeed reported area ratios varying around a situation of area-preservation (e.g. Bentley et al., 2013; MacFarlane et al., 2014). Yet, a survey of the literature shows that the Da Vinci's rule has not been extensively assessed (Eloy, 2011) and that in most cases, empirical studies were based on few individuals (typically less than 5) of small size (typically less than c. 15 cm D) (e.g. Bentley et al., 2013; Bertram, 1989; McMahon and Kronauer, 1976; Tredennick et al., 2013). Besides, empirical assessments are not univocal (Aratsu, 1998; Minamino and Tateno, 2014; Yamamoto and Kobayashi, 1993). Aratsu (1998) for instance, whose dataset stands out by its unusual number of large branches (> 20 cm of basal diameter), found that 9 out of 10 temperate tree species actually showed area increasing branching. The results of the present study further question the generality of Da Vinci's rule and clearly show that more research efforts should be made to assess *R* on trees of different sizes, species and regions of the world.

An important issue when sampling area ratio is the location at which branch diameter is measured, which is not defined in the Da Vinci's rule. Minamino and Tateno (2014) indeed showed that if the branching network maintains elastic similarity, branch taper should be smooth away from ramifications but change markedly before and after a branching point, leading to $R > 1$ when the distance from the point of measurement of branches diameter and the branching point is virtually null. Although we measured branch diameters at reasonable distances from branching points so to avoid the obvious swelling occurring bellow and above large branches ramification, our results ($R > 1$) could reflect this asymmetry in parent and daughters local tapers. More generally, disagreements between empirical assessments of Da Vinci's rule may come from differences in field protocols (i.e. use of distal parent diameter and basal daughters' diameter *vs* use of mid-branch diameters).

3.4.2 Sources of variation of the node area ratio

Regardless of the organization of branches in a tree, if branch scaling properties are homogeneous (i.e. regular allometry between branch diameter and length) and if the tree conforms to Da Vinci's rule, then whole-tree volume (or biomass, assuming homogeneous wood density) may be roughly approximated by the volume of a cylinder (Horn, 2000). Under the assumption of homogeneous branch scaling properties, the average area ratio thus has direct consequence on whole-tree volume and biomass scaling. Identifying systematic sources of variation of *R* associated to particular node morphologies would give us a point of departure for further analyses, such as the covariation between daughters dimensions (length, taper) and *R* in particular nodes configuration, and may provide valuable insights into how tree species could be grouped to improve allometric scaling predictions, notably on tree biomass.

Because empirical studies suggest an increase of crown mass relative to total tree mass on large tropical canopy trees (Ploton et al., 2016), an intuitive hypothesis was that *R* may increase on those trees, notably on the largest branches in tree crowns following structural changes associated to crown metamorphosis. Our data does not support this hypothesis. On the full dataset (interspecific level), *R* was higher than one on the entire range of branch size and did not show marked variation pattern on large-diameter branches (Figure 3-5 E).Species and individual-tree factors also weakly explain R variability (c. 2% and c. 7%, respectively), which illustrate the convergence of species (and trees) vascular networks to similar structural properties (from the view point of R frequency distributions) as

they share the same purposes (e.g. water transport) and constraints (hydraulic, mechanical). Most of R variability occurred at the node level, and a similar pattern of variance partitioning can be expected for branch scaling exponents (i.e. among different species and trees, most of the variability in diameter – length or diameter –mass scaling exponents is found at the branch level, Tredennick et al., 2013). We emphasize that even if two trees present similar frequency distributions of *R* (or branch scaling exponents), between-trees variation in branching pattern (architecture) may have important impact on the overall tree volume and mass, because e.g. deviation from *R* = 1 on a large or a small branch have a very different impact on whole-tree volume. Our analyses showed that node morphology (as described by n_D, *q* and the *PA* binary variable) have a systematic influence on node level *R*. The different trends that we uncovered all fall in line with the predictions of Minamino and Tateno (2014) based on mechanical calculations, suggesting that the maintenance of mechanical stability could be at the origin of our observations. It should be noted, however, that the three morphological parameters together explained less than 10% of node level *R* variation. Hereafter, we provide tentative interpretations of our findings.

First, we found that the average *R* increased substantially with the number of daughters N_D (Figure 3-7 A). Among the three species illustrating contrasting levels of apical dominance (hence architectural asymmetry), N_D was higher on average (c. 2.5-3) and more variable on the Ilomba species (highly asymmetric architecture) and appeared to converge toward n_D = 2 as the symmetry of crown architecture increased (fig S1 F). This structural trend could reflect species growth strategies. The high apical dominance is usually interpreted as a trait favoring faster height growth, a competitive advantage typically associated to pioneer species. Apical dominance also creates multi-layered crowns that are more efficient in harvesting light in bright (top-of-the-canopy) conditions. In contrast, low apical dominance (symmetric architecture) creates a mono-layered crown that minimizes self-shading, a characteristic deemed more efficient in shaded conditions (Horn, 2000, 1971). Following this trait, our three illustrative species could be ranked from pioneer-like (Ilomba) to shade tolerant-like (Okan) species (Figure 3-3 3). It is commonly acknowledge that fast growing pioneer species tend to have lighter wood (c. 0.41 $g.cm^3$ for Ilomba) than slow-growing shade tolerant species (c. 0.79 $g.cm^3$ for Okan). Hence, we hypothesize that the higher and more variable n_D observed on Ilomba than Okan could reflect a more opportunistic strategy of light harvesting, as the cost associated to growing (and shedding) daughters is lower on this species.

Second, we found that PA nodes (which compose the vertical, central axis of the crown) had a higher *R* on average (Figure 3-6 F). Conversely, *R* decreased with increasing asymmetry between daughters (parameter *q*, Figure 3-7 B). These two results may appear contradictory, because PA daughters are instinctively thought as being highly dominant over their siblings (i.e. leading to a high *q*). Figure 3-7 B shows that this is not necessarily the case: a PA daughter can have a diameter relatively close to that of its siblings (low *q*), in which case nodes reached particularly high *R* values. For those nodes (bearing a PA daughter), *R* converged faster toward 1 with increasing asymmetry (i.e. steeper decreasing slope in Figure 3-7 B). The overall variation pattern of *R* with n_D, PA and *q* may be interpreted as an ageing process. Sone et al. (2009, 2005) have shown that the sum of growth areas of daughter branches was higher than parent growth area on two *Acer* species, so that nodes that did not experience shedding had *R* > 1 and shedding was necessary to conform to Da Vinci's rule. Variability of *R* values within a crown may thus represent diverse states of modification of nodes morphology that temporarily conform to Da Vinci's rule (Minamino and Tateno, 2014). On species that present a principal axis (PA) up to the top of the crown such as Ilomba, relatively young nodes found at the crown-top bear

numerous daughters (not sampled in our field protocol) and must have *R* higher than one. As node ages, preferential allocation of carbon to the PA increases daughter's asymmetry and shedding must occur to lower *R* and maintain mechanical safety. This was particularly obvious on the upper part of Ilombas' crown (when PA diameter < 50 cm), where the increase of PA diameter (from crown top toward bottom) was associated to an increase of q (r = 0.77) and a decrease of n_D (r = -0.62). Interestingly, the importance of shedding in *R* dynamics is likely to vary with species architecture. In species with "bike wheel" architecture such as Ilomba (i.e. a vertical PA with plagiotropic, lateral branches), even the largest-diameter branches are "sun-branches" (light-gathering function) that do not evolve into structural-branches (support function) as they age, and in this sense are "expendable organs". In contrast, first-orders branches of large Ayous or Okan individuals fulfill a support function (i.e. bear the load of tree crown) and cannot be shed without profoundly altering crown structure. Figure 3-7 C indeed shows that sum of daughter cross-sectional areas over parent cross-sectional area (i.e. *R*) increases as branch size increases in the Ayous species, but this was not the case on the Okan species (Figure 3-7 D). This difference could indicate that the ratios of daughter cumulated area growths over parent area growth differ among those two species.

At the species level, we found a weak, yet significant species effect on the scaling of cumulated daughter areas to parent area (Figure 3-7 C-D), with a lower growth of cumulated daughter areas (per unit of parent area growth) when the tree crown was symmetric (i.e. Okan species). Besides differences in cumulated daughter growths over parent growth as hypothesized above, this results could also be the reflect of the abundance of node morphologies favoring higher *R* on species with asymmetric crowns (higher n_D, presence of PA) and indicates that grouping species based on crown asymmetry (or growth strategies along the sun-shade gradient) may improve whole-tree volume and biomass scaling. Further analyses are in progress on the covariation between branch morphology at a node (i.e. length, taper) and *R*, since the former may compensate for the effect of the latter on the volume (or mass) that a node bears.

3.4.3 Optimal tree of the MTE model *vs* average real trees

The MTE model posits that tree branching network is volume-filling and conforms to the elastic similarity model. These assumptions, commonly referred to as "secondary assumptions", provide theoretical values for branch length and radii scaling exponents (i.e. b=1/3 and a=1/2, respectively) that are derived analytically from the simplified, symmetric MTE tree (i.e. a branching network complying with MTE's "core" assumptions). Under this set of assumptions, the branching network is area-preserving (*R* = 1). Deviation from b = 1/3 or a = 1/2 (or both) can indicate violations of secondary assumption(s) (hence help us identify mechanisms behind $R \neq 1$), but can also result from a departure of the average branching network from the assumption of symmetry (in which case a needs not to be 1/2 to maintain *R* = 1, Bentley et al., 2013). Unlike the MTE tree, real trees are not strictly symmetric and, as far as we know, whether an average empirical branching network is symmetric is a subjective call, making interpretation of deviations from b = 1/3 and a = 1/2 difficult.

Elastic similarity (a = 1/2)

At the inter-specific level, distributions of b_D and a_D largely overlap theoretical expectations although distribution medians did not coincide with 1/3 and 1/2, respectively. The effect of asymmetry was particularly problematic for the empirical assessment of a (hence to determine whether the average tree structure may conform to elastic similarity). At a node with two daughters, a_D for the larger

daughter ranged from 0.5 (symmetry) to c. 0 ($r_{daughter} = r_{parent}$) while a_D of the smaller daughter could be higher than 3 ($r_{daughter} << r_{parent}$), yielding asymmetric a_D distributions (fig 6 C). Testing whether an asymmetric distribution conforms to a single theoretical value (with no underlying distribution) is somewhat problematic and using means instead of medians would have led to different trends. For example, while the interspecific a_D median was significantly smaller than 1/2 (i.e. 0.43 [0.42, 0.45], Figure 3-4 B), the mean was significantly higher (i.e. 0.52 [0.51, 0.54]). Distributions of a_D with similar skewness were reported in Bentley et al. (2013) for smaller trees of various species. In the latter study, the authors used credible intervals from a Bayesian statistical approach to confront empirical a_D distributions to 1/2. Credible intervals were extremely large (e.g. 0.56 [-0.08, 2.42] for Ponderosa pine trees) and rejected neither the MTE assumption (i.e. elastic similarity hypothesis) nor competing hypotheses (e.g. a = 2/3 and a = 1/3 for the stress and geometric similarity hypotheses, respectively). Directly assessing the validity of *elastic similarity* via measurements of total branch length against basal branch diameter within crown networks is likely to provide more informative results on real trees biomechanical behavior than internode-level a_D exponents, but this could not be done in this study as we did not describe crown structure beyond a branch diameter threshold of c. 20 cm (thus branches l_{TOT} were unknown).

Volume filling (b = 1/3)

Our results on branch length ratios across nodes and on length scaling exponents (b_B) are consistent with previous studies and reject the existence of an overarching volume-filling behavior of tree branching networks (Bentley et al., 2013; Duursma et al., 2010; Price et al., 2015; Tredennick et al., 2013). We found that relationships between branch segment lengths from one order to the next were extremely weak (supplementary Figure 3-8 D), leading to a wide distribution of b_B. The greater variability in length ratios over diameter ratios has been observed elsewhere (Bentley et al., 2013; Price et al., 2007) and suggests that selection primarily acts on hydrodynamics resistance (Price et al., 2007), because "*resistance depends on radius to the 4th power but only linearly on length,* [therefore] *changes in radius lead to much greater changes and penalties in energy minimisation, in turn leading to much stronger stabilising selection on radii than on lengths*" (Bentley et al., 2013). Distributions of b_B peaked at lower values than 1/3 and distribution medians differed among species (Ilomba *vs* Ayous and Okan, Figure 3-6 A), suggesting that the way tree crowns fill-in space (with leaves) is neither strictly volume filling nor, on average, similar among studied species. Following similar observations, Bentley et. al (2013) hypothesized that, as a_D and R were approximately 1/2 and 1 in their study, a modified form of volume filling may occur in their relatively young trees and b_B = 1/3 might be reached in larger trees (as hypothesized by West et al., 1999a). Our results on large trees do not support this hypothesis. Instead, we hypothesize that deviation from b = 1/3 is related to variation in crowns fractal dimension among studied species (Zeide, 1998). In a self-similar branching network, the fractal dimension (z) summarizes the distribution of foliage within the crown. Assuming that the branching network is volume filling is equivalent of assuming a constant foliage density within crown volume, so that foliage area scales with crown volume to the power (z) of 3. Yet, studies of real tree crown fractal dimensions have shown that z is not restricted to 3, but rather distributed along a continuum between 2 and 3, and varies among individual trees and species (e.g. Pretzsch and Dieler, 2012), possibly as a function of self-shading (Duursma et al., 2010).

3.4.4 Implications of the results

The systematic variations evidenced above in the relationships between branching characteristics at the node level in function of node morphology, axis type and species suggest that the assumptions of symmetry and self-similarity, which in a way are meant to be null hypotheses, are in fact rejected by biological observations. Plant axes, as they develop, add up to be eventually shed throughout plant ontogeny, are indeed known to show important differences in their function, structure and growth dynamics. The very concept of tree architectural types aims at summarizing the existing patterns of plant growth strategies (Hallé et al., 1978), and is largely based on the observed combinations in the succession of the various axis types (orthotropous, plagiotropous, monopodial, sympodial) (Barthélémy and Caraglio, 2007). As trees reiterate, possibly several times throughout their lifespan, as is the case for the large trees studied here, these successions are partly or totally reproduced. Branching order as codified by the centrifugal labeling scheme has little biological meaning in front of this reality, although this may be less apparent when pooling large datasets of species and axes types. Zeroth-order theories like the MTE model may therefore remain valid macroscopically, and explain useful overall trends, but will likely fail at explaining crucial tradeoffs in plant form and function that depend on the very organization of the plant in metamers of differentiated natures.

Identifying axes types in the field when confronted with a felled tree from a random species may prove difficult, and indeed was not properly done in this study. But plant architects have long shown that for many species, it is possible to identify simple morphological markers, such as the arrangement of leaf scars, insertion angles, etc.) allowing to retrace the whole growth history of a given trees. A new field of dendrochronological science is even developing, analogous to tree ring chronology, via the careful reconstitution of tree life through the succession of growth units and axes (Heuret et al., 2016; Morel et al., 2016).

This study is not meant to be the invalidation of –useful– universal models, but rather to remind that if we are to account for some important phenomena in real trees, such as branch mechanical stability, biomass allocation in tree crowns, variations in plant growth and resource acquisition strategies, plasticity, or bias in allometric predictions, plant architecture will need to be accounted for.

Author contributions. Conceived and designed the experiments: PP, NB and RP. Collected data: SM, BS, NB and PP. Analyzed the data: PP. Analysis feedback: RP, NB and PC. Wrote the paper: PP. Writing feedback: RP, NB, SG, UB and RP.

3.5. Reference

Aratsu, R., 1998. Leonardo was wise: trees conserve cross-sectional area despite vessel structure. J. Young Investig. 1, 1–20.

Barthélémy, D., Caraglio, Y., 2007. Plant Architecture: A Dynamic, Multilevel and Comprehensive Approach to Plant Form, Structure and Ontogeny. Ann. Bot. 99, 375–407. doi:10.1093/aob/mcl260

Bentley, L.P., Stegen, J.C., Savage, V.M., Smith, D.D., Allmen, E.I., Sperry, J.S., Reich, P.B., Enquist, B.J., 2013. An empirical assessment of tree branching networks and implications for plant allometric scaling models. Ecol. Lett. 16, 1069–1078.

Berninger, F., Nikinmaa, E., 1997. Implications of varying pipe model relationships on Scots pine growth in different climates. Funct. Ecol. 11, 146–156.

Bertram, J.A., 1989. Size-dependent differential scaling in branches: the mechanical design of trees revisited. Trees 3. doi:10.1007/BF00225358

Duursma, R.A., Mäkelä, A., Reid, D.E.B., Jokela, E.J., Porté, A.J., Roberts, S.D., 2010. Self-shading affects allometric scaling in trees: Self-shading and allometric scaling. Funct. Ecol. 24, 723–730. doi:10.1111/j.1365-2435.2010.01690.x

Eloy, C., 2011. Leonardo's rule, self-similarity and wind-induced stresses in trees. Phys. Rev. Lett. 107, 258101. doi:10.1103/PhysRevLett.107.258101

Enquist, B.J., 2002. Universal scaling in tree and vascular plant allometry: toward a general quantitative theory linking plant form and function from cells to ecosystems. Tree Physiol. 22, 1045–1064. doi:10.1093/treephys/22.15-16.1045

Enquist, B.J., West, G.B., Brown, J.H., 2009. Extensions and evaluations of a general quantitative theory of forest structure and dynamics. Proc. Natl. Acad. Sci. 106, 7046–7051. doi:10.1073/pnas.0812303106

Greenhill, A.G., 1881. Determination of the greatest height consistent with stability that a vertical pole or mast can be made, and of the greatest height to which a tree of given proportions can grow. Proc. Camb. Philos. Soc.

Hallé, F., Oldeman, R.A.A., Tomlinson, P.B., 1978. Tropical trees and forests: an architectural analysis. Springer Verl. Berl. Heidelb. doi:10.1007/978-3-642-81190-6

Heuret, P., Caraglio, Y., Sabatier, S.-A., Barthélémy, D., Nicolini, E.-A., 2016. Retrospective analysis of plant architecture: an extended definition of dendrochronology.

Horn, H.S., 2000. Twigs, trees, and the dynamics of carbon in the landscape. Scaling Biol. 199–220.

Horn, H.S., 1971. The adaptive geometry of trees. Princeton University Press.

Kozlowski, J., Konarzewski, M., 2004. Is West, Brown and Enquist's model of allometric scaling mathematically correct and biologically relevant? Funct. Ecol. 18, 283–289. doi:10.1111/j.0269-8463.2004.00830.x

MacFarlane, D.W., Kuyah, S., Mulia, R., Dietz, J., Muthuri, C., Noordwijk, M.V., 2014. Evaluating a non-destructive method for calibrating tree biomass equations derived from tree branching architecture. Trees 1–11. doi:10.1007/s00468-014-0993-2

Mäkelä, A., 1986. Implications of the pipe model theory on dry matter partitioning and height growth in trees. J. Theor. Biol. 123, 103–120. doi:10.1016/S0022-5193(86)80238-7

McMahon, T.A., Kronauer, R.E., 1976. Tree structures: deducing the principle of mechanical design. J. Theor. Biol. 59, 443–466.

Minamino, R., Tateno, M., 2014. Tree Branching: Leonardo da Vinci's Rule versus Biomechanical Models. PLoS ONE 9, e93535. doi:10.1371/journal.pone.0093535

Morel, H., Mangenet, T., Heuret, P., Nicolini, E.-A., 2016. Studying phenology of tropical forest trees using a morphological and anatomical retrospective analysis: the case of# Moronobea coccinea# Aubl.(Clusiaceae).

Muller-Landau, H.C., Condit, R.S., Chave, J., Thomas, S.C., Bohlman, S.A., Bunyavejchewin, S., Davies, S., Foster, R., Gunatilleke, S., Gunatilleke, N., Harms, K.E., Hart, T., Hubbell, S.P., Itoh, A., Kassim, A.R., LaFrankie, J.V., Lee, H.S., Losos, E., Makana, J.-R., Ohkubo, T., Sukumar, R., Sun, I.-F., Nur Supardi, M.N., Tan, S., Thompson, J., Valencia, R., Munoz, G.V., Wills, C., Yamakura, T., Chuyong, G., Dattaraja, H.S., Esufali, S., Hall, P., Hernandez, C., Kenfack, D., Kiratiprayoon, S., Suresh, H.S., Thomas, D., Vallejo, M.I., Ashton, P., 2006. Testing metabolic ecology theory for allometric scaling of tree size, growth and mortality in tropical forests. Ecol. Lett. 9, 575–588. doi:10.1111/j.1461-0248.2006.00904.x

Nikinmaa, E., 1992. Analyses of the growth of Scots pine: matching structure with function.

Niklas, K.J., 2016. Tree Biomechanics with Special Reference to Tropical Trees, in: Goldstein, G., Santiago, L.S. (Eds.), Tropical Tree Physiology, Tree Physiology. Springer International Publishing, pp. 413–435. doi:10.1007/978-3-319-27422-5_19

Niklas, K.J., 1995. Size-dependent Allometry of Tree Height, Diameter and Trunk-taper. Ann. Bot. 75, 217–227. doi:10.1006/anbo.1995.1015

Ploton, P., Barbier, N., Takoudjou Momo, S., Réjou-Méchain, M., Boyemba Bosela, F., Chuyong, G., Dauby, G., Droissart, V., Fayolle, A., Goodman, R.C., Henry, M., Kamdem, N.G., Mukirania, J.K., Kenfack, D., Libalah, M., Ngomanda, A., Rossi, V., Sonké, B., Texier, N., Thomas, D., Zebaze, D., Couteron, P., Berger, U., Pélissier, R., 2016. Closing a gap in tropical forest biomass estimation: taking crown mass variation into account in pantropical allometries. Biogeosciences 13, 1571–1585. doi:10.5194/bg-13-1571-2016

Pretzsch, H., Dieler, J., 2012. Evidence of variant intra- and interspecific scaling of tree crown structure and relevance for allometric theory. Oecologia 169, 637–649. doi:10.1007/s00442-011-2240-5

Price, C.A., Drake, P., Veneklaas, E.J., Renton, M., 2015. Flow similarity, stochastic branching, and quarter power scaling in plants. ArXiv Prepr. ArXiv150707820.

Price, C.A., Enquist, B.J., Savage, V.M., 2007. A general model for allometric covariation in botanical form and function. Proc. Natl. Acad. Sci. 104, 13204–13209. doi:10.1073/pnas.0702242104

Savage, V.M., Bentley, L.P., Enquist, B.J., Sperry, J.S., Smith, D.D., Reich, P.B., von Allmen, E.I., 2010. Hydraulic trade-offs and space filling enable better predictions of vascular structure and function in plants. Proc. Natl. Acad. Sci. 107, 22722–22727. doi:10.1073/pnas.1012194108

Savage, V.M., Deeds, E.J., Fontana, W., 2008. Sizing Up Allometric Scaling Theory. PLoS Comput. Biol. 4, e1000171. doi:10.1371/journal.pcbi.1000171

Shinozaki, K., Yoda, K., Hozumi, K., Kira, T., 1964. A quantitative analysis of plant form-the pipe model theory: I. Basic analyses. 日本生態学会誌 14, 97–105.

Shukla, R.P., Ramakrishnan, P.S., 1986. Architecture and growth strategies of tropical trees in relation to successional status. J. Ecol. 33–46.

Sillett, S.C., Van Pelt, R., Koch, G.W., Ambrose, A.R., Carroll, A.L., Antoine, M.E., Mifsud, B.M., 2010. Increasing wood production through old age in tall trees. For. Ecol. Manag. 259, 976–994. doi:10.1016/j.foreco.2009.12.003

Smith, D.D., Sperry, J.S., Enquist, B.J., Savage, V.M., McCulloh, K.A., Bentley, L.P., 2014. Deviation from symmetrically self-similar branching in trees predicts altered hydraulics, mechanics, light interception and metabolic scaling. New Phytol. 201, 217–229. doi:10.1111/nph.12487

Sone, K., Noguchi, K., Terashima, I., 2005. Dependency of branch diameter growth in young Acer trees on light availability and shoot elongation. Tree Physiol. 25, 39–48.

Sone, K., Suzuki, A.A., Miyazawa, S.-I., Noguchi, K., Terashima, I., 2009. Maintenance mechanisms of the pipe model relationship and Leonardo da Vinci's rule in the branching architecture of Acer rufinerve trees. J. Plant Res. 122, 41–52. doi:10.1007/s10265-008-0177-5

Sperry, J.S., Smith, D.D., Savage, V.M., Enquist, B.J., McCulloh, K.A., Reich, P.B., Bentley, L.P., von Allmen, E.I., 2012. A species-level model for metabolic scaling in trees I. Exploring boundaries to scaling space within and across species. Funct. Ecol. 26, 1054–1065. doi:10.1111/j.1365-2435.2012.02022.x

Tredennick, A.T., Bentley, L.P., Hanan, N.P., 2013. Allometric Convergence in Savanna Trees and Implications for the Use of Plant Scaling Models in Variable Ecosystems. PLoS ONE 8, e58241. doi:10.1371/journal.pone.0058241

Tyree, M.T., 1988. A dynamic model for water flow in a single tree: evidence that models must account for hydraulic architecture. Tree Physiol. 4, 195–217.

von Allmen, E.I., Sperry, J.S., Smith, D.D., Savage, V.M., Enquist, B.J., Reich, P.B., Bentley, L.P., 2012. A species-level model for metabolic scaling of trees II. Testing in a ring- and diffuse-porous species. Funct. Ecol. 26, 1066–1076. doi:10.1111/j.1365-2435.2012.02021.x

West, G.B., Brown, J.H., Enquist, B.J., 1999. A general model for the structure and allometry of plant vascular systems. Nature 400, 664–667.

West, G.B., Brown, J.H., Enquist, B.J., 1997. A general model for the origin of allometric scaling laws in biology. Science 276, 122–126.

Yamamoto, K., Kobayashi, S., 1993. Analysis of crown structure based on the pipe model theory. Nippon Rin Gakkai-Shi 75, 445–448.

Zeide, B., 1998. Fractal analysis of foliage distribution in loblolly pine crowns. Can. J. For. Res. 28, 106–114. doi:10.1139/cjfr-28-1-106

Zimmermann, M.H., 1978. Hydraulic architecture of some diffuse-porous trees. Can. J. Bot. 56, 2286–2295.

3.6. Supplementary figure

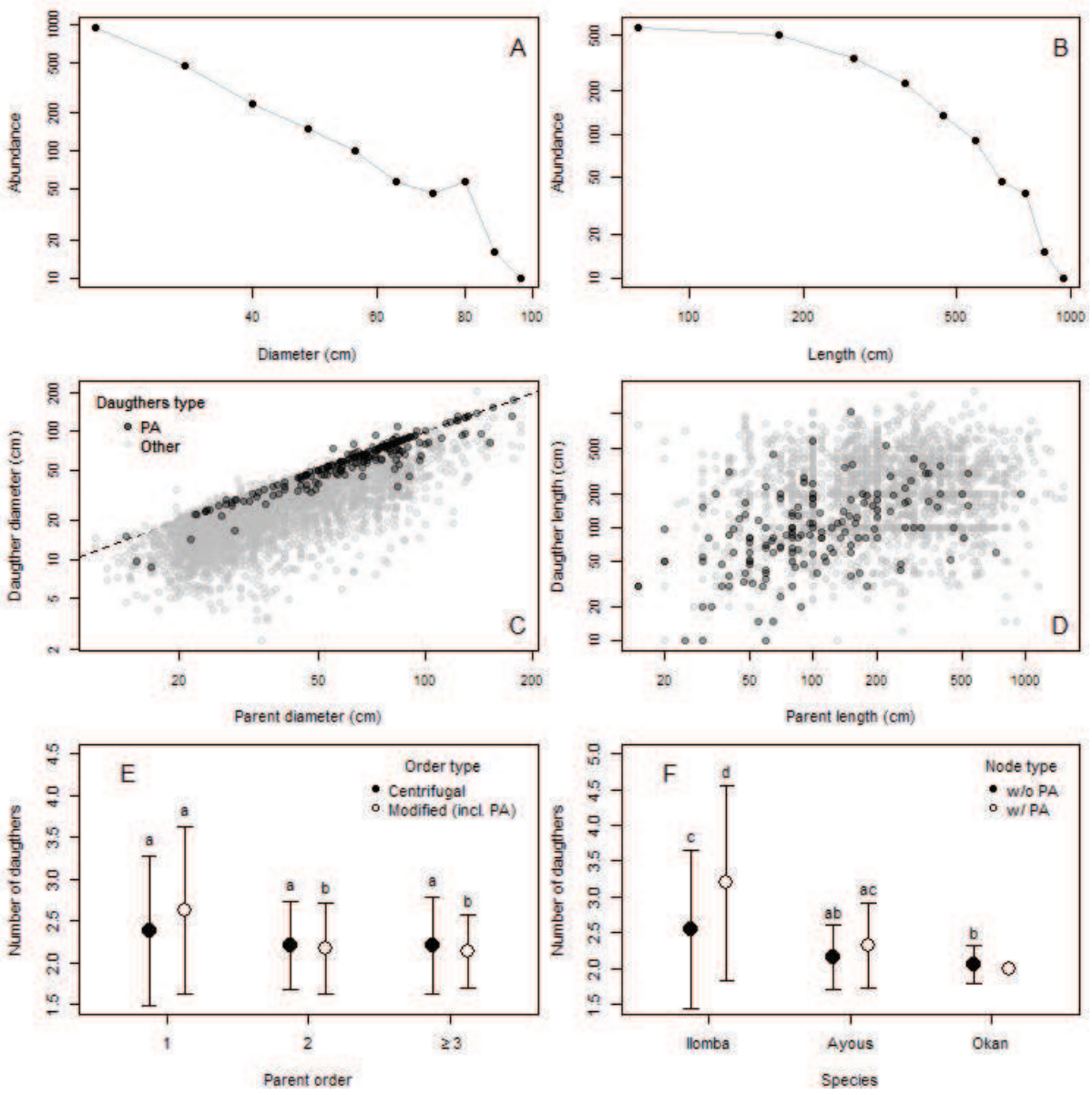

Figure 3-8. Histograms of log-transformed abundance against log-transform branch diameter (panel A) and branch length (panel B) for all nine species. Daughters dimensions (diameter, length) against parents dimensions (diameter length) are represented in panel C and D, with a color code differentiating PA daughters (solid black circles) from other daughters (solid grey circles). In panel E and F, the number of daughters (n_D) is represented against parent order and per illustrative species, respectively. In panel E, the labelling scheme used to defined parent order is either the centrifugal scheme of the MTE (solid black circles) or the modified labelling scheme distinguishing PA daughters (order 1), their siblings (order 2) and other daughters (order ≥ 3) (empty circles). In panel F, a distinction is made between nodes bearing PA daughters (solid black circles) and others nodes (empty circles). Letters represent the result of Dunn pairwise multiple comparisons tests.

4 CANOPY TEXTURE ANALYSIS FOR LARGE-SCALE ASSESSMENTS OF TROPICAL FOREST STAND STRUCTURE AND BIOMASS

P. Ploton[1,2], R. Pélissier[1,3], N. Barbier[2], C. Proisy[3], B.R. Ramesh[1] & P. Couteron[3].

[1]Ecology Department, French Institute of Pondicherry, UMIFRE 21 MAEE-CNRS, Pondicherry 605001, India
[2]IRD, UMR AMAP, University of Yaounde I, Yaounde, Cameroon
[3]IRD, UMR AMAP, F- 34000 Montpellier, France

Abstract

The structural organization of a forest canopy is an important descriptor that may provide information for vegetation mapping and management planning. We present a new approach of canopy texture analysis from diverse very-high remotely sensed optical image types, such as digitized aerial photographs, very-high resolution satellite scenes or Google Earth extractions. Based on the multivariate ordination of Fourier spectra, the FOTO method allows us to ordinate canopy images with respect to canopy grain, i.e. a combination of mean size and density of tree crowns per sampling window. Confronted to field data in different contexts across the tropics, in mangroves, evergreen to semi-evergreen lowland and mountain forests, FOTO-derived indices proved powerful for consistently retrieving certain stand structure parameters, notably aboveground biomass up to the highest levels observed. We illustrate the potential of the texture-structure model inversion for predicting stand structure parameters over vast poorly documented forest areas in India, Amazonia and central Africa. We lastly draw research perspectives to overcome current limits of the method, such as instrumental and topography-induced biases.

4.1 Introduction

The structural organization of a forest canopy is an important descriptor that may provide spatial information for vegetation mapping and management planning, such as attributes of plant species distributions, intensity of disturbances, aboveground biomass or carbon stock. A variety of airborne and satellite images have long been used to characterize forest stands from above the canopy, providing the advantage of a rapid exploration of extensive and sometimes difficultly accessible zones. Unfortunately this approach proved to be of limited applicability in wet tropical regions, notably because most optical and radar signals that deliver medium to high spatial resolution data have shown to saturate at intermediate levels of biomass ranges (ca. 150-200 $Mg.ha^{-1}$) or leaf area index values (Gibbs et al., 2007). As a consequence, while forest vs. non-forest classifications are nowadays routinely performed from such data, variations in stand structure and biomass within forests of fairly closed canopy remain almost undetectable with classical techniques and the forest treetops seen from above appear generally as a homogeneously undulating green carpet. There is however a lot of ecological evidence that rainforest structure substantially varies from place to place either naturally (as the soil, composition or forest dynamics vary) or resulting from anthropogenic degradations. Detecting, characterizing and mapping these variations over vast areas become particularly challenging within the perspective of the REDD+ agenda (Maniatis and Mollicone, 2010), which requests participating countries to periodically monitor their carbon stock variation. While promising developing instruments such as LiDAR (Light Detection and Ranging) are potentially powerful in this perspective, they remain very expensive to systematically operate for large-scale forest assessments in the tropics (but see Asner et al., 2010). We recently developed as a cost-effective alternative, a method of canopy grain texture analysis from very-high resolution air- or space-borne images, which proved efficient for retrieving and mapping stand structure parameters including abovegound biomass over vast poorly documented areas of tropical forest.

4.2 Methodological background and rationale

Given allometric relationships that exist between individual tree dimensions (such as trunk diameter, height and crown size), our approach stems from the idea that the number and size of tree crowns visible from above the canopy should inform on some other forest structural parameters. The reasoning is straightforward when considering for instance stand basal area (*G*) or aboveground biomass (AGB) in closed forest conditions since in this case the largest trees that reach the canopy can account for up to 70-80% of stand level values. However the renewed interest for allometric scaling in ecology (Enquist et al., 2009), suggests that tree dimensions and their size frequency distribution, may be relevant to infer stand properties, such as spacing relations, mortality rates or stand dynamics, from canopy characteristics. While most previous attempts were based on visual or automated delineations of individual tree crowns from very-high resolution (VHR) canopy images, we present hereafter a more holistic characterization of canopy geometrical properties through canopy grain texture analysis by two-dimensional Fourier power spectrum. The main outlines of the method that we named FOurier Textural Ordination (FOTO) are illustrated in Figure 4-1. From a digital VHR panchromatic canopy image, optionally masked for non-forested areas (clouds, water bodies, bare soils, etc.), a set of square windows with size set to include several repetitions of the largest textural pattern that compose canopy grain is first extracted (Figure 4-1 a). For closed-canopy scenes, canopy grain results from the shape, size and spatial arrangement of dominant tree crowns, so that square windows of about 1 ha proved to be a good option. A Fourier radial power spectrum (or r-spectrum) is then computed for

each window, which features how image grey levels' variance partitions into increasing spatial frequency bins (in cycles.km^{-1} i.e. the number of repetitions over 1 km) or equivalently into wavelengths (pattern sizes in m) (see Couteron, 2002 for further details). In other words, a r-spectrum represents the frequency distribution of pattern sizes in the canopy grain: while coarse canopy grain yields r-spectra significantly skewed towards small frequencies (large wavelengths), fine canopy grain yields r-spectra significantly skewed towards large frequencies (small wavelengths;Figure 4-1 b). All windows' r-spectra computed from a VHR canopy image can then be stacked into a single matrix with the canopy windows (observations) as rows and the spatial frequencies (variables) as columns (Figure 4-1 c). Such a matrix may be submitted to a standardized-PCA that systematically compares the canopy windows with respect to the relative importance of spatial frequencies in their respective spectra. The typical clockwise distribution of the spatial frequency variables in the first PCA plane straightforwardly creates a canopy texture gradient which ordinates canopy windows, from coarse- to fine-grained patterns (Figure 4-1 d). Windows' scores against the main PCA axes thus represent canopy texture indices (so-called FOTO indices), which can be related to control plots data using multivariate linear models, to calibrate and assess the indices' ability to infer stand structure parameters (Figure 4-1 e). Once calibrated, texture-structure relationships can be inverted for predicting and mapping stand structure parameters over the whole area covered by the initial VHR image (Figure 4-1 f).

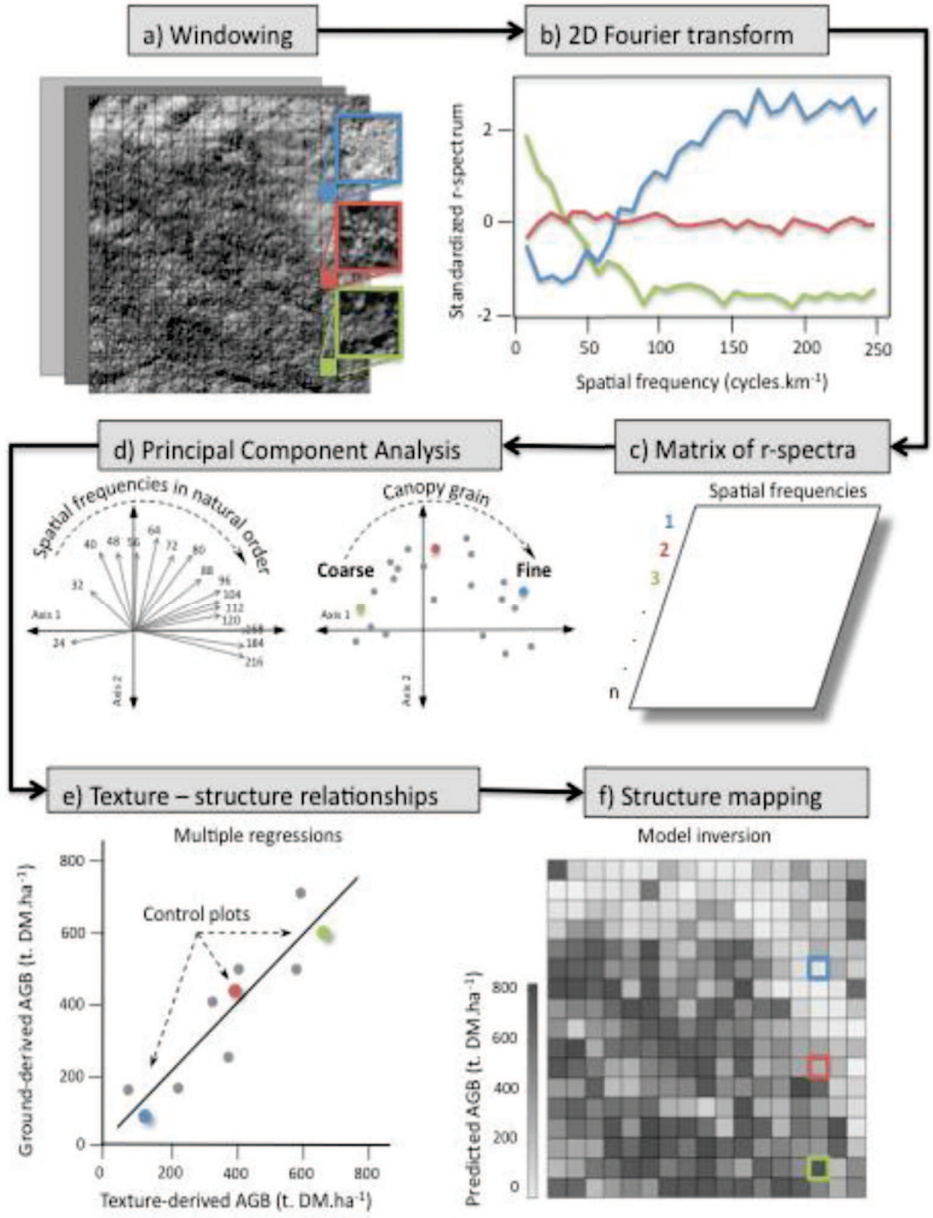

Figure 4-1. Flow of operations of the FOurier Textural Ordination (FOTO) method.

4.3 Results from some case studies

The method has been tested on a variety of tropical forest types (evergreen, semi-evergreen and mangrove forests) in various regions (Amazonia, India and central Africa) using different VHR image data (digitized aerial photographs, commercial and freely-accessible satellite images). We also used virtual closed-forest canopy scenes simulated using allometric 3D forest mock-ups and a discrete anisotropic radiative transfert model to benchmark FOTO indices against controlled stand structures (Barbier et al., 2012). Such virtual scenes were for instance used by Barbier et al. (2010) as a preliminary step to a basin-wide analysis of Amazonian *terra firme* lowland forest canopy images, to evidence a strong relationship between FOTO indices and stand mean apparent crown sizes in simulated images (R^2 = 0.96). These results illustrate the theoretical backbone underlying the allometric assumption on which the approach relies: canopy grain information as captured by FOTO indices mostly pertains to pseudo-periodic patterns of crown diameters' repetitions within the scene. Though pseudo-periodic

canopy patterns are generally noisy in real forest types as a result of interacting endogenous (stand composition and dynamics) and exogenous (e.g. topography, degradation intensity, etc.) factors, we were able to consistently discriminate observed forest scenes on the basis of their canopy grain features and to reveal in a number of situations strong correlations with structural parameters measured in ground-truth field plots (Table 4-1). In even-aged mangrove stands where most trees occupy the canopy layer, FOTO indeed yielded very good predictions on AGB (R^2 = 0.92; Proisy et al., 2007) with no apparent maximal biomass limitation. As expected, weaker though strong relationships were obtained on uneven, hyper-diverse forests displaying more complex canopy patterns such as lowland evergreen forests of French Guiana, India and Cameroon (see Table 4-1). While some structure parameters showed fairly stable relationships with canopy texture, such as the mean quadratic diameter (*Dg*) in Indian and Guianan *terra firme* forests (R^2= 0.68 and 0.71, respectively) or AGB in Indian forests and Guianan mangroves (R^2 = 0.78 and 0.92, respectively), other parameters showed contrasted relationships that reveal differences in the local variation of stand structural characteristics. For instance, the gradient of sampled forest structures in French Guiana *terra firme* plots relates to old-growth forests on contrasted soil conditions, which yields a strong correlation between canopy grain and tree density (*N*) or mean quadratic diameter (Dg), but no relationship with basal area (*G*) because the denser stands are located on poor soils that do not support many large trees (Couteron et al., 2005). Conversely, in India the area studied encompasses a gradient of forest succession stages from highly degraded secondary formations recovering from burning to old-growth undisturbed forests. In this case, FOTO clearly detected the gradual increase in density of the largest trees (N_{30}), *G* and AGB throughout forest successions, while total tree density (*N*) did not lead to a predictable relationship (Ploton et al., 2012). In a different context, in Southeastern Cameroon forests that mix mono-dominant *Gilbertiodendron dewevrei* forests, along with degraded *Maranthaceae* facies and old-growth mixed-forest patches, canopy texture mostly correlates with maximum tree diameter (D_{max}) and density of very large trees (N_{100}), while overall stand structure parameters exhibit only weak relationships with FOTO indices (see Table 4-1). On the one hand, high-biomass *G. dewevrei* stands display a very fine canopy grain, possibly because of the high evenness of tree heights and strong imbrications of their crowns. On the other hand, the varying degree of canopy closeness in *Maranthaceae* forests, which may contain very few emergent trees dominating a low understorey, results in bimodal r-spectrum dominated by both large and fine textural patterns. Interestingly, canopy texture allows the segmentation of these different forest types, therefore potentially permitting separate, type-wise inversions. The FOTO method thus not only offer good prospects for saturation-free tropical forest biomass assessments but appears also valuable to draw ecological insights into forest stand structure variation.

It has also to been noticed that our case studies were conducted from image types as different as digitized panchromatic aerial photographs (French Guiana *terra firme*), panchromatic IKONOS or GeoEye satellite data (India, Cameroon and French Guiana mangroves), or RGB true color bands average of Google Earth (GE) extractions (Amazonian *terra firme* and India), however providing consistent results as long as images are in the optical domain with a spatial resolution of metric order (i.e. VHR). This underlines a promising feature of FOTO with respect to inter-operating image data types and providing a cost-free alternative to commercial data (GE) for large-scale assessments (for instance within the REDD+ framework), or retrospective analyses from old aerial photographs in the pre-satellite period.

Study site		Data type		Forest attribute		Texture - Structure		Sources
Area	Forest type	Image	Control plot	Parameter	Range	R^2	Rrmse (%)	
French Guiana	Evergreen (terra firme)	Aerial photographs	Field plots (12 1-ha)	*N*	455 - 861	0.8	-	Couteron et al. 2005
				G	28.41 - 42.38	0.007 ns	-	
				Dg	20.6 - 34.2	0.71	-	
				H	21.1 - 30.4	0.57	-	
	Mangroves	Ikonos	Field plots (26 1-ha)	AGB	80 - 436	0.92	17.3	Proisy et al. 2007
Amazonia	*terra firme*	Google Earth	Simulations (330 2.25-ha)	*Cd*	7 – 25	0.96	-	Barbier et al. 2010
India	Evergreen	Ikonos / Google Earth	Field plots (15 1-ha)	*N*	371 - 733	0.109 ns / 0.132 ns	14.4 / 13.8	Ploton et al. 2011
				N_{30}		0.773 / 0.770	14.6 / 14.3	
				G	10.3 - 54.4	0.779 / 0.741	13.1 / 13.5	
				Dg	17.9 - 36.4	0.657 / 0.687	7.4 / 7.9	
				AGB	124.1 - 683.6	0.779 / 0.741	13.1 / 13.5	
			Simulations (10 1-ha)	Cd	7 - 25	0.96 / 0.93	1.17 / 1.64	
Cameroon	Evergreen to semi-evergreen	GeoEye	Field plots (10 1-ha)	D_{max}	89 - 144	0.93		Unpublished results
				N_{100}	0 - 10	0.64		
				N	225 - 525	0.34		
				G	13 – 43	0.38		
				Dg	22 – 33	0.30		

Table 4-1. FOTO explanatory power on several common forest stand attributes over a variety of tropical forest types. Quality of the relationships is characterized by the coefficient of determination (R^2), the associated P-value (ns: > 0.05) and the relative root mean square error Rrmse (in %). Forest attributes: *N* = density of trees more than 10 cm dbh (trees.ha-1), N_{30} = density of trees more than 30 cm dbh (trees.ha^{-1}), N_{100} = density of trees more than 100 cm dbh (trees.ha^{-1}), *Dmax* = maximum tree dbh (cm), *Dg* = quadratic mean dbh (cm), *G* = basal area (m².ha^{-1}), AGB = aboveground biomass (Mg.ha^{-1} dry matter), *Cd* = mean crown diameter (m), *H* = dominant tree height (m).

4.4 Limits and perspectives

Further case studies and simulation works are going on to validate the FOTO method in various tropical forest contexts. One of the limits of the canopy grain approach arises when canopy texture properties deviate too much from a pseudo-periodicity so that the main canopy pattern does not result from repetitions of crown diameters. Such heterogeneity may result from the presence of canopy gaps or treefalls of varying sizes, or of contrasted illumination patterns due to abrupt relief variations (e.g. two sides of a ridge line or a deep thalweg). Typically, r-spectra of windows displaying a high degree of spatial heterogeneity are skewed towards low frequencies due to the contribution of heterogeneity to the largest size patterns. It follows that such windows can be erroneously interpreted as containing large tree crowns and must be removed from the analysis so not to bias the texture-structure relationship (Ploton et al., 2012). Similarly, when shifting from pure evergreen to semi-evergreen or mixed deciduous tropical forest types, textural information may be influenced by seasonal changes in the canopy that still require to be investigated.

Though the FOTO method offers good prospects for large-scale implementation, further difficulties arise when several canopy images with different acquisition parameters have to be mosaicked. Indeed, the sun-scene-sensor geometry influences the size and proportion of tree shadows in the canopy scene, and thus modifies the textural properties as detected by Fourier r-spectrum. To ensure a consistent comparison between different canopy scenes, one must either use images with similar acquisition conditions, or correct for the influences of changing acquisition conditions on canopy textural properties. To this end, Barbier et al. (2011) introduced a Bidirectional Texture Function (BTF) that allows correcting for instrumental bias based on a partitioned standardization of the r-spectrum prior to PCA. A very similar problem arises with relief variations, which modify the proportion of sun-lighted vs. shadowed crowns. In mountainous regions, this effect has the potential to make FOTO detecting a finer grain on illuminated hillsides and coarser grain on shaded ones regardless of forest structure. A partitioned standardization of the r-spectrum according to hillshade classes may also provide a solution to correct for such a bias (Ploton, 2010).

Author contributions. Wrote the paper: PP. Writing feedback: RP, NB, CP, BRR and PC.

4.5 Reference

Asner, G.P., Powell, G.V.N., Mascaro, J., Knapp, D.E., Clark, J.K., Jacobson, J., Kennedy-Bowdoin, T., Balaji, A., Paez-Acosta, G., Victoria, E., Secada, L., Valqui, M., Hughes, R.F., 2010. High-resolution forest carbon stocks and emissions in the Amazon. Proc. Natl. Acad. Sci. 107, 16738–16742. doi:10.1073/pnas.1004875107

Barbier, N., Couteron, P., Gastelly-Etchegorry, J.-P., Proisy, C., 2012. Linking canopy images to forest structural parameters: potential of a modeling framework. Ann. For. Sci. 69, 305–311. doi:10.1007/s13595-011-0116-9

Barbier, N., Couteron, P., Proisy, C., Malhi, Y., Gastellu-Etchegorry, J.-P., 2010. The variation of apparent crown size and canopy heterogeneity across lowland Amazonian forests. Glob. Ecol. Biogeogr. 19, 72–84.

Barbier, N., Proisy, C., Véga, C., Sabatier, D., Couteron, P., 2011. Bidirectional texture function of high resolution optical images of tropical forest: An approach using LiDAR hillshade simulations. Remote Sens. Environ. 115, 167–179.

Couteron, P., 2002. Quantifying change in patterned semi-arid vegetation by Fourier analysis of digitized aerial photographs. Int. J. Remote Sens. 23, 3407–3425.

Couteron, P., Pelissier, R., Nicolini, E.A., Paget, D., 2005. Predicting tropical forest stand structure parameters from Fourier transform of very high-resolution remotely sensed canopy images. J. Appl. Ecol. 42, 1121–1128.

Enquist, B.J., West, G.B., Brown, J.H., 2009. Extensions and evaluations of a general quantitative theory of forest structure and dynamics. Proc. Natl. Acad. Sci. 106, 7046–7051. doi:10.1073/pnas.0812303106

Gibbs, H.K., Brown, S., Niles, J.O., Foley, J.A., 2007. Monitoring and estimating tropical forest carbon stocks: making REDD a reality. Environ. Res. Lett. 2, 045023.

Maniatis, D., Mollicone, D., 2010. Options for sampling and stratification for national forest inventories to implement REDD+ under the UNFCCC. Carbon Balance Manag. 5, 1.

Ploton, P., 2010. Analyzing canopy heterogeneity of the tropical forests by texture analysis of very-high resolution images-A case study in the Western Ghats of India.

Ploton, P., Pélissier, R., Proisy, C., Flavenot, T., Barbier, N., Rai, S.N., Couteron, P., 2012. Assessing aboveground tropical forest biomass using Google Earth canopy images. Ecol. Appl. 22, 993–1003. doi:10.1890/11-1606.1

Proisy, C., Couteron, P., Fromard, F., 2007. Predicting and mapping mangrove biomass from canopy grain analysis using Fourier-based textural ordination of IKONOS images. Remote Sens. Environ. 109, 379–392.

5 TOWARD A GENERAL TROPICAL FOREST BIOMASS PREDICTION MODEL FROM VERY HIGH RESOLUTION OPTICAL SATELLITE IMAGES

P. Ploton[1,2], N. Barbier[1], P. Couteron[1], C.M. Antin[1], N. Ayyappan[3], N. Balachandran[3], N. Barathan[3], J.-F. Bastin[4], G. Chuyong[5], G. Dauby[6,7], V. Droissart[1,8], J.-P. Gastellu-Etchegorry[9], N.G. Kamdem[10], D. Kenfack[11], M. Libalah[10], G.II. Mofack[10], S.T. Momo[1, 10], S. Pargal[1], P. Petronelli[12], C. Proisy[1,3], M. Réjou-Méchain[1,3], B. Sonké[10], N. Texier[1, 10], D. Thomas[13], P. Verley[1], D. Zebaze Dongmo[10], U. Berger[14] and R. Pélissier[1,3]

[1]Institut de Recherche pour le Développement, UMR-AMAP, Montpellier, France
[2]Institut des sciences et industries du vivant et de l'environnement, Montpellier, France
[3]French Institute of Pondicherry, Puducherry, India
[4]Landscape Ecology and Plant Production Systems Unit, Université Libre de Bruxelles, Brussels, Belgium
[5]Department of Botany and Plant Physiology, University of Buea, Buea, Cameroon
[6]Institut de Recherche pour le Développement, UMR-DIADE, Montpellier, France
[7]Evolutionary Biology and Ecology, Faculté des Sciences, Université Libre de Bruxelles, Brussels, Belgium
[8]Herbarium et Bibliothèque de Botanique africaine, Université Libre de Bruxelles, Brussels, Belgium
[9]Université Paul Sabatier, CESBIO, Toulouse, France
[10]Laboratoire de Botanique systématique et d'Ecologie, Département des Sciences Biologiques, Ecole Normale Supérieure, Université de Yaoundé I, Yaoundé, Cameroon
[11]Center for Tropical Forest Science — Forest Global Earth observatory, Smithsonian Tropical Research Institute, Washington, USA
[12]Centre de coopération Internationale en Recherche Agronomique pour le Développement, UMR-ECOFOG, Kourou, France
[13]Department of Biological Sciences, Washington State University, Vancouver, U.S.A.
[14]Technische Universität Dresden, Faculty of Environmental Sciences, Institute of Forest Growth and Forest Computer Sciences, Tharandt, Germany

ABSTRACT

Very high spatial resolution (VHSR) optical data have shown a good potential to provide non-saturating proxies of tropical forest aboveground biomass (AGB), notably from canopy texture features extracted with Fourier transform. However, the relationships between Fourier texture features and forest AGB varies among forest types and regions of the world, hampering the deployment of a broad scale forest carbon monitoring method based on these sole texture metrics. Our aim here was to complement Fourier texture features with additional information on forest structure to generalize the texture-based approach. We explored how canopy texture properties related to forest AGB estimation using 279 1-ha tropical forest inventory plots distributed across the tropics for which we simulated VHSR optical canopy scenes. This allowed controlling for instrumental effects and focusing on the sole canopy texture features – forest AGB relations. Globally, Fourier texture of simulated canopies significantly explained AGB variations (R^2=0.46), with an uncertainty of c. 30%. The strength of this relationship varied among sites with higher accuracy found on forests with close, fairly periodic

canopies (reflecting a self-thinning process) while heterogeneity in stand and canopy structure (reflecting gap phase dynamics) was detrimental. We found that including a gradient of canopy heterogeneity from a lacunarity analysis largely improved AGB model performances (R^2=0.76, rRMSE=20%). As texture analysis of two-dimensional images cannot retrieve large-scale variations in forest height, a bioclimatic proxy of tree slenderness further improved model goodness-of-fit at the global level (R^2=0.88) and reduced model error at the local level (reduction of site-level prediction biases). The final texture-based approach was tested on a set of 3 Pleiades images covering a complex mosaic of forest types in the Congo basin and led to uncertainty levels (RMSE = 62 $Mg.ha^{-1}$, rRMSE=21%) comparable to those obtained from airborne LiDAR-based models. The increasing availability of VHSR optical sensors (such as from constellations of small satellite platforms) raises the possibility of routine repeated imaging of the world's tropical forests and suggests that texture-based analyses could become an essential tool in international efforts to monitor carbon emissions from deforestation and forest degradations (REDD+ program).

5.1 Introduction

Concerns about the effects of increasing atmospheric carbon on climate have led to an international program aiming at reducing emissions of greenhouse gases from deforestation and forest degradations (UN-REDD+ program), notably in the tropics where the bulk of global deforestation occurs (Pan et al., 2011). REDD+ implementation fundamentally relies on our capacity to monitor forest carbon stock and dynamics at multiple spatial scales, from entire countries down to scales at which deforestation and degradation processes occur. In this context, remote sensing naturally becomes an essential tool (Baccini et al., 2012; DeFries et al., 2007; Saatchi et al., 2011). However, remote sensing of forest carbon stocks (often through forest aboveground biomass, hereafter denoted AGB) is challenging in the tropics because most satellite sensors are not sensitive to AGB variation above c. 150 $Mg.ha^{-1}$, while tropical forests AGB often exceeds 400 $Mg.ha^{-1}$ (Slik et al., 2013). This saturation is well documented for passive optical sensors of coarse to intermediate spatial resolution such as the Moderate Resolution Imaging Spectroradiometer (MODIS) or Landsat Thematic Mapper (e.g. Lu, 2006; Lu et al., 2012; Zhao et al., 2016) but also for radar signals (notably L-band SAR, Mermoz et al., 2015), and thus constitutes a crippling limit for those data types. Aircraft-based light detection and ranging (A-LiDAR) systems have become vastly popular for about a decade in tropical forest studies, as they appear to be free of saturation. Small-footprint A-LiDAR data provide a detailed description of forest three-dimensional (3D) structure from which forest AGB can be estimated with reasonable confidence (c. 15% relative error on 1-ha plots, e.g. Réjou-Méchain et al., 2015; Zolkos et al., 2013). Unfortunately this information comes at a cost rendering the wall-to-wall and regular coverage of large territories uneconomical (Erdody and Moskal, 2010; Messinger et al., 2016). A potentially interesting alternative to A-LiDAR for large-scale monitoring of tropical forests may be found in very high spatial resolution (VHSR) optical images, as they are routinely captured by a range of satellite platforms and, therefore, does not involve costly airborne data acquisition campaigns. The improvement brought by the increased spatial resolution over coarser, widely-used optical data (e.g. Landsat), lies on a fundamental change in the analysis: at metric to sub-metric resolutions, individual trees are now discernable in the image, allowing one to exploit the geometric properties of tree crowns (i.e. crown delineation algorithms, e.g. Broadbent et al., 2008; Zhou et al., 2013) or forest canopies (i.e. texture analysis, e.g.

Couteron et al., 2005) that conceptually more directly relate to stand biomass than spectral greenness indices.

Texture analysis of panchromatic VHSR canopy images (e.g. Couteron et al., 2005; Frazer et al., 2005) have shown promising results to retrieve stand and canopy forest attributes, including tropical forest AGB with no sign of saturation (e.g. Bastin et al., 2014; Ploton et al., 2012). Generally speaking, texture analysis (*sensu* Haralick, 1979) gives us a measure of the spatial arrangement of grey levels within a canopy image by directly reflecting the contrasts between sunlit and shadowed surfaces, thus providing information on the size and distribution of crowns of canopy trees and inter-crowns canopy gaps. Texture is scale-dependent, so that meaningful texture metrics have to be multi-scale by nature (e.g. Fourier r-spectra; Couteron, 2002) or measurable at multiple scales (e.g. lacunarity; Frazer et al., 2005). Those analyses are often carried out on image excerpts over scales related to local variations in crown and gap sizes (e.g. canopy window of c. 1-ha) while comparing texture features, whatever their source, over very large forest tracts (e.g. hundreds of square kilometers). A systematic comparison between canopy windows texture features can be performed through standard multivariate ordination technics (e.g. Principal Component Analysis). Principal axes thus display canopy windows along uncorrelated texture and spatial heterogeneity gradients that facilitate their separation and interpretation. Window scores on the principal axes are then used as dependent variables (texture indices) in regression analyses in order to examine the statistical relationship between canopy texture and stand structure parameters, for instance AGB, as measured from field plots data (e.g. Couteron et al., 2005; Proisy et al., 2007). The basic idea is that once calibrated such relationships can be inverted to predict and map stand structure parameters outside the sampling plots from texture analysis of VHSR panchromatic images.

To date, the FOurier Textural Ordination (or FOTO method; Couteron, 2002; Proisy et al., 2007) has been applied in a number of tropical forest case studies to derive plot-level AGB estimates from panchromatic canopy images (e.g. Ploton et al., 2012; Proisy et al., 2007; Singh et al., 2014) or LiDAR Canopy Height Models (e.g. Véga et al., 2015). Study footprint is generally a few hundreds of square kilometers covered by one or two VHSR images. At this scale, the texture gradient provides good relationships with forest stand structure parameters, with a relative error on 1-ha plot AGB estimations, generally below 20%. It has indeed been demonstrated from simulations that in closed-forest canopies, FOTO-texture indices characterize the size distribution of canopy crowns (Barbier et al., 2012), which are allometrically linked to tree size and AGB (Jucker et al., 2016; Ploton et al., 2016). It is increasingly evident, however, that the texture-structure relationship is forest type- and/or site-dependent (Bastin et al., 2014), thus limiting broad-scale applications. As a consequence, texture analysis of large mixed-forest landscapes currently requires a stratification into homogeneous texture-AGB strata as in the forest mosaics of the Congo basin (Bastin et al., 2014). It is worth mentioning that similar limitations have been encountered for LiDAR-based studies, requiring complementary information layers to allow multi-site comparisons (e.g. Asner et al., 2011; Vincent et al., 2014, 2012). Generalizing the texture-structure relationship across contrasted forest types from different regions of the world would therefore be a major step towards an operational method to monitor forest structure and AGB from VHSR optical data.

Here, our hypothesis is that canopy heterogeneity created by different environmental conditions and canopy gap dynamics may influence the texture-structure relationship derived from the FOTO method. In a VHSR canopy image, tree crowns and gaps are visible to the naked-eye from local brightness

variations, but texture patterns captured by FOTO cannot discriminate large tree crowns from canopy gaps as they both appear as aggregates of bright or dark pixels of similar size in the image. Coarse texture thus indistinctively results from closed canopies comprised of large tree crowns and from open canopies where aggregates of tree crowns alternate with canopy openings. Thus, a same texture may represent high or low AGB values, respectively. To overcome this drawback, FOTO texture can be complemented by other textural features characterizing canopy heterogeneity at multiple scales, such as lacunarity, which proved to correlate well with canopy cover and gap volume on simulated forest stands (Frazer et al., 2005).

Another constraint limiting the empirical exploration of the link between canopy texture and the underlying forest stand structure over large regions covered by several VHSR images is of instrumental nature. Forest texture indices are indeed sensitive to sensor optical properties and spatial resolution (Ploton et al., 2012; Proisy et al., 2007), but also to sun-sensor geometry (Barbier et al., 2011; Barbier and Couteron, 2015). Disentangling the effect of forest structure on canopy texture from instrumental effects thus requires having a sufficiently large set of VHSR images acquired in homogeneous sun-sensor configurations and covering an extensive field plot network. An efficient workaround is to adopt a modelling approach coupling the simulation of 3D forest stand mockups and the generation of virtual canopy images by applying a radiative transfer model onto the 3D mockups (Barbier et al., 2012). By controlling parameters of the radiative transfer model, canopy images in identical acquisition configurations can be generated for a variety of 3D stand mockups. Forest mockups built from simple tree shapes derived from field data (tree location, height, diameter and crown dimensions) allow bridging the gap between ground observations and remote sensing data (e.g. Frazer et al. 2005, Schneider et al., 2014). They ultimately help us to translate signal information into biophysical parameters. Modeling trees with simple geometrical shapes and homogeneous optical properties may appear as a coarse representation of reality, but it led to valuable insights into how the 3D arrangement of stems and leaves is linked to important processes of the forest dynamics (Stark et al., 2015; Taubert et al., 2015).

In this study, we compiled data from 279 1-ha forest inventory plots from several tropical regions on three continents to test whether a generalized canopy texture model could provide consistent estimates of AGB in structurally contrasted forest types. The analysis was based on simulated canopy scenes so to specifically address the link between canopy texture and stand structure, notably AGB. We first investigated the respective merits of the FOTO method (Couteron, 2002) and the lacunarity analysis (Frazer et al., 2005) in predicting stand AGB both locally (within sites) and globally (across sites). Second, we explored whether combining the two methods improved AGB prediction models. Third, we built a final 'generalized' model also accounting for the variation in potential canopy height related to regional bioclimatic stress on forest growth, as it has been shown to be a determining factor of pantropical variation in forest AGB (Chave et al., 2014). Finally, we tested our generalized texture-structure regression framework on three real Pleiades images acquired in comparable configurations over 49 1-ha field plots from a complex mosaic of forest types in Central Africa.

5.2 Material and Methods

5.2.1 Forest inventory data

We used a set of 279 1-ha forest sample plots in tropical Africa (157 ha), India (37 ha), and French Guiana (85 ha). Forest inventory data contained tree diameter at breast height (*D*) for all trees with *D*

≥ 10 cm, representing 142,791 trees in total. Tree taxonomic identification was available at the species level for 78% of the trees, at the genus level for 6%, at the family level for 5% and 11% of the trees were left unidentified. We used the Dryad Global Wood Density Database (Chave et al., 2009; Zanne et al., 2009) and the World Agroforestry Center's Wood Density Database (ICRAF, 2007) to attribute to each individual tree the mean wood density value of the species it belongs to. For those known only to the genus or family level, the average wood density at that taxonomic level was used (Chave et al., 2006). Unidentified individuals were attributed the average wood density of the 1-ha plot. Beside *D*, other tree dimensions were recorded on a subset of trees per plot, namely total tree height (*H*, n=23,237), trunk height defined as the height to the lowest main branch (*Ht*, n=6,502) and tree crown diameter (*Cd*, n = 4,438). The distribution of field inventory data among sampling sites is provided in supplementary Table 5-3. We established allometric models for tree *H*, *Ht* and *Cd* in order to predict the dimensions of unmeasured trees. Because calibration data for allometric models were missing for some plots, models were established at the plot-, site- and regional-levels (i.e. Africa, India and French Guiana) and the most local one was selected.

Following Feldpausch *et al.* (2012), we used a three-parameter Weibull function to predict tree *H* from *D*: $H = a(1 - \exp(-bD^c))$. Trunk height was modeled as a power function of *H*: $Ht = a * H^b$, fitted in logarithmic units and accounting for Baskerville correction (Baskerville, 1972) . The same model and transformation were applied to fit the crown diameter, *Cd*, to *D*, at the exception that a 2-segments model was used when a significant breaking point was found in the relationship (following the procedure described in Antin et al., 2013). Finally, we used the pantropical model of Chave et al. (2014), including *D*, *H* and wood density to compute tree AGB estimates.

Overall, the sample plots spanned wide gradients of tree density (139 to 848 trees.ha^{-1}), stand basal area (10.3 to 57.7 m².ha^{-1}) and dominant height (17.8 to 50.5 m) and thus captured a large array of forest age and 3D organizations.

5.2.2 Generation of 3D forest mockups

We constructed a 3D representation of the 279 1-ha sample plots using local tree allometries and tree location data (either exact coordinates or by quadrats of 20-m side). The 3D modelling process of a sample plot can be summarized as follows: (1) we built a simplified representation of each tree in the plot with the crown modelled as an ellipsoid of diameter *Cd* and depth *Hc* (i.e. *H – Ht*, in m) using field measurements if available or local allometric models otherwise; (2) if tree relative coordinates within the plot were known (i.e. for 135 of the 279 1-ha plots), we generated a single plot mockup by placing trees at their actual position; if trees position were only known at the quadrat-level (i.e. for the remaining 144 plots): (i) trees were sorted from the tallest to the smallest; (ii) tentatively located at random in their respective quadrats starting from the tallest tree downward; (iii) retained if their crown volume did not overlap crowns of already placed trees by more than 25% of tree crown volume. If the algorithm failed to place a tree after 50 iterations (in 5.3% of the cases), its crown diameter was reduced by randomly sampling a value in the distribution of the crown diameter allometric model residuals. For those 144 plots, we generated 3 mockups per plot so as to capture some variability in canopy texture emerging from the random component of the mockup generation algorithm.

5.2.3 Simulation of canopy images

We simulated very-high spatial resolution optical images of the 567 forest mockups using the Discrete Anisotropic Transfer model (DART, version 5.5.3, Gastellu-Etchegorry et al., 2015). DART is able to handle the forest mockups as a 3D array of cells (voxels) of different sizes. We used 1-m^3 voxels so to match with the metric resolution on which FOTO analyses are typically performed. Voxels contain a mixture of air and vegetation elements, either as solid facets or as turbid medium with a predefined distribution of leaf volume density. Given that optical properties have little influence on canopy texture, we used leaf and bark optical properties of an African canopy tree species (*Terminalia superba* Engl. & Diels) as input parameters for all the trees in DART. Tree trunks were represented as solid cylinders and crowns as turbid ellipsoids with a spherical distribution of leaf angles. Volume density within tree crown cells was adjusted to represent a Leaf Area Index of 5 at the plot scale (Asner and Martin, 2008), independently of plot biophysical structure. We thus assumed a limited influence of LAI on canopy texture properties but also acknowledge the difficulty of accurately measuring such integrative parameter in tropical forests (Jonckheere et al., 2004; Olivas et al., 2013). To represent a vegetated understory, we additionally attributed to the lowest 1-m layer above the ground the optical properties of a pioneer tree species (*Musanga cecropioides* R.Br. ex Tedlie) with a spherical distribution of leaf angles and leaf area density of 0.3 $m^2.m^{-3}$.

We used DART in ray tracing, reflectance mode with the sun and the atmosphere as the only radiation sources. We simulated top of atmosphere (TOA) panchromatic reflectance images (see Gastellu-Etchegorry et al., 2015 for further details) in the 0.35 µm - 1.1 µm domain that we decomposed into 75 spectral bands of 0.01 µm each. The radiative transfer calculations were conducted to represent observation and solar illumination zenith angles set to 6.3° and 40.4°, respectively, and a sun-viewing azimuth difference set to 200.5°. For each DART image pixel, the reflectance channel of any VHSR sensor can then be obtained from the summation of reflectance values provided in the 75 bands in proportion to the panchromatic sensor response level within each of the 0.01 µm bands. Computation time was about 40 minutes per image with about 12 GB of RAM on 64-bit Windows with an Intel Core i7 GHz processor.

5.2.4 Real satellite images

We used a set of three real VHSR optical images from the Pleiades sensor acquired over a network of 49 1-ha sample plots in the transition area between evergreen and semi-deciduous forests of Eastern Cameroon, in central Africa. Images were taken approximately two years after the establishment of the sample plots. Since the three images were in backward configuration (i.e. with sun behind the sensor) with relatively homogeneous elevation angles (Table 5-1), textural bias induced by image acquisition configurations is expected to be low (Barbier and Couteron, 2015). Following previous applications, texture analysis was based on panchromatic bands resampled from 0.5 m to 1 m per pixel.

Table 5-1. Date and acquisition parameters of Pleiades panchromatic satellite images over Eastern Cameroon, central Africa

Date		Sensor		Sun	
month	year	azimuth	elevation	azimuth	elevation
12	2014	227.6	64.5	145.3	57.0
12	2014	248.5	79.7	146.4	55.3
1	2015	229.6	65.7	138.3	57.3

#1 catalog ID: DS_PHR1A_201412210944201_FR1_PX_E013N03_0909_01764
#2 catalog ID: DS_PHR1A_201412210943258_FR1_PX_E013N05_0606_01395
#3 catalog ID: DS_PHR1A_201501160944349_FR1_PX_E013N03_0702_00899

5.2.5 Canopy texture analysis

We performed texture analysis of panchromatic VHSR canopy images using both FOTO (Couteron, 2002) and lacunarity (Frazer et al., 2005) analysis as they are expected to provide complementary information on stand structure attributes. FOTO method has been extensively described elsewhere (e.g. Couteron, 2002; Couteron et al., 2005) and we only give a brief outline of the procedure hereafter. The first step consists in dividing a panchromatic satellite image into square 1-ha (N = 100 m) canopy unit-windows, a size which proved suitable from previous studies to capture several repetitions of the largest tree crowns in closed forest stands. On each window, the two-dimensional Fast Fourier Transform (fft2) function is applied to transpose the spectral radiance from the spatial domain to the frequency domain, using sine-cosine functions at integer frequencies (i.e. wavenumbers, 1, 2, …, N/2) along the X and Y directions of the plane. The squared amplitude of the fft2 yields a 2D periodogram, which represents an apportionment of the variance in spectral radiance among spatial frequency bins in all possible planar directions within the window. The orientation information was here neglected by averaging the periodogram across all directions, which provided the one-dimensional so-called radial- or r-spectrum. Knowing image spatial resolution, wavenumbers can equivalently be expressed in wavelengths (λ, in m) so that a r-spectrum gives the frequency distribution of the number of times a pattern of size λ repeats itself in a unit canopy window of side N = 100 m. An issue with the method is that sampling according to harmonic Fourier frequencies (stemming from fft2) results in denser spectrum values as λ decreases, so that intermediate scales of patterns relevant for canopy characterization may be badly sampled. To overcome this we used the modified algorithm presented in Barbier and Couteron (2015), in which, after signal centering, unit-window size is doubled in each direction using zero-padding, which allows increasing intermediate λ sampling. The resulting list of λ is pruned to conserve a sampling of λ values as regular as possible, thus decreasing information redundancy at small wavelengths. Finally, a set of 26 λ values was retained from 2 up to 99 m. All r-spectra for a given satellite image were assembled into a single matrix, **F**, with the individual canopy windows as rows and Fourier spatial frequencies as columns. Canopy windows with r-spectra dominated by high Fourier frequencies (low λ) are expected to display fine grain canopy textures due to the succession of small tree crowns, while coarse grain canopy textures correspond to r-spectra dominated by low Fourier frequencies expected to reflect the repetition of large canopy trees (see e.g. Barbier et al., 2012).

Lacunarity was formally defined by Mandelbrot (1983) as the deviation of a fractal pattern from translational invariance, a concept further expanded to non-fractal patterns (Allain and Cloitre, 1991). It basically measures how patterns fill space, those having more or larger gaps having generally a higher lacunarity or gapiness. It is a scale dependent descriptor of an image texture that showed an interesting

potential in forest studies to describe spatial variation in stand structure heterogeneity, notably related to canopy openness (Frazer et al., 2005). In the present paper, we computed lacunarity following Frazer et al. (2005) to which the reader should refer for more details. Lacunarity was computed in canopy windows of size *N* = 100 m as Fourier r-spectra. On each unit-window, a moving square box of size *s* (in pixels) is glided by one pixel at a time along all rows and columns. For each box of size *s*, the mass, *M*, is computed as the sum of all pixels' spectral radiance (previously normed per unit-window), so that the probability distribution function *Q(M,s)* represents the frequency distribution of *M* divided by the number of boxes at size *s*. The lacunarity statistic is then computed as $\Delta(s) = Z_Q^{(2)}(s)/\left(Z_Q^{(1)}(s)\right)^2$, where $Z_Q^{(1)}(s)$ and $Z_Q^{(2)}(s)$ are the mean and mean of squared values of *Q(M, s)*, respectively. In our study we used 10 discrete box sizes, *s*, from 1 to 99 m, and normalized all lacunarity values by dividing them by Δ(1). We then denote as a window lacunarity spectrum the series of normalized lacunarity statistics computed at each box size for a given canopy window. All normalized lacunarity spectra for a given satellite image were assembled into a single matrix, **L**, with the unit canopy windows as rows and the box sizes as columns. The decreasing pattern of lacunarity with increasing box size reflects the rate of increase in canopy heterogeneity from the finer to the coarser scale patterns, which in the context of forest canopies is related to the degree of inter-crowns canopy openness (see Frazer et al., 2005).

5.2.6 Statistical analyses

In order to systematically compare the canopy windows from a given satellite image, both the **F** table of Fourier r-spectra, and the **L** table of lacunarity spectra were submitted independently to Principal Component Analyses (PCA) as in Couteron et al. (2005) and Frazer et al. (2005). Columns' normalization prior to PCA (normed-PCA) allows uncovering texture gradients even when the absolute variation between unit-windows is small. This led to independently synthetize the FOTO- and Lacunarity-texture gradients present in the satellite images. From the 3D forest mockups, we extracted simple parameters of stand structure and heterogeneity (listed in Table 2) in order to help the interpretation of texture gradients produced by the two PCA. We then investigated the agreement between these two analyses using a co-inertia analysis (COIA; Dolédec and Chessel, 1994, Dray et al. 2003). COIA is a simple and robust method for the simultaneous analysis of two data tables matching by observations (here, windows). Between two PCA, COIA is mathematically equivalent to the Inter-battery analysis of Tucker (1958). The method maximizes the square covariance between the projected coordinates of the unit-windows on the PCA axes of **F** and **L**. It thus simultaneously maximizes the variance in **F** and **L** separately (the two PCA) and the correlation between the two sets of principal components. The texture gradients captured by FOTO and by the lacunarity analysis can thus be projected on common orthogonal components.

We then used window scores on the PCA or COIA analysis as independent texture indices in AGB regression models. We used the Random Forest (RF) algorithm as implemented in the package "randomForest" version 4.6.12 for R statistical software (R Core Team, 2016). RF is an ensemble of learning methods for classification and regression based on decision trees (Breiman, 2001) increasingly used in remote-sensing studies, notably for carbon mapping (Baccini et al., 2012; Mascaro et al., 2014; Vieilledent et al., 2016). The aim is to overcome over-fitting problems that can occur using individual decision trees. The algorithm builds a large number of decision trees that are trained on random samples of both the training set (i.e. the observations) and the predictor variables, and outputs the average of individual trees predictions. An interesting feature of such learning machine technics is that

it allows integrating a large number of variables of potentially different statistical distributions (Marvin et al., 2016) and does not request specifying an explicit model form.

We evaluated regression model errors using the internal validation scheme of RF. At each run (*n* = 500), RF training set is by default composed of two thirds of the total number of observations, leaving one third of the data to compute an independent estimate of model error, so-called "out-of-bag" (OOB) error. A mean OOB model error over the 500 runs (±sd) is provided as pseudo R-squared (R^2), root-mean-square error (RMSE) and relative RMSE (rRMSE in %), along with the mean signed deviation (MSD), used to compare local (i.e. per site) prediction bias in global (i.e. multi-site) models (Xu et al., 2016).

Although RF have been developed to avoid overfitting (Breiman, 2001) it is not completely immune to this problem (e.g. Mascaro et al., 2014). We thus assessed predictors' importance using a built-in metric denoted IncMSE (in %), which quantifies the percent increase in the mean MSE when predictors are randomly permuted. We then applied a variable selection procedure using the VSURF package (Genuer et al., 2015), which builds several RF models with increasing number of predictors, starting with the most important ones (based on IncMSE) and retains the smallest significant model (see VSURF description for computational details).

In this paper RF models were built to evaluate the potential of canopy texture to discriminate variations in stand AGB among the full set of simulated canopy scenes. FOTO- and Lacunarity-texture indices were first evaluated separately using windows scores from the two independent PCA (leading to the F- and L-models, respectively). Both sources of texture information were then combined in a single RF model using windows coordinates on the COIA axes (FL-model). Last, we added to the predictors a bioclimatic proxy accounting for the regional variation in potential canopy height, as environmental stress on forest growth has been shown to be a determining factor of pantropical variation in forest AGB (Chave et al., 2014). This environmental stress variable E, a compound variable based on water deficit, temperature seasonality and precipitation seasonality, is available as a global gridded layer at 2.5 arc sec resolution at http://chave.ups-tlse.fr/pantropical_allometry.htm (Chave et al., 2014) and was used here as a proxy for forest potential height in a global model based on FOTO- and lacunarity-textures (called FLE-model).

5.3 Results

5.3.1 Texture analysis of virtual canopy images

We applied both the FOTO method and the lacunarity analysis on all simulated canopy windows generated from the 279 1-ha plots of tropical forest inventory. The plan 1-2 of the FOTO-PCA explained 53.5% (37% and 16.5% for axes 1 and 2, respectively) of the total textural variability among windows r-spectra (F-table) and produced a typical correlation circle with spatial patterns sorted from short to long wavelengths (or from high to low frequency wavenumbers) (Figure 5-1 A). Wavelengths (λ) of about 5 to 10 m (visually relating to small crown sizes) were found on the positive side of the first PCA axis (F-PCA1), intermediate λ (25 to 35 m) on the positive side of F-PCA2 and λ of 25 to 35 m (largest crown sizes) on the negative side of F-PCA1. The ordination gradient on the first FOTO-PCA plan thus corresponded to a fineness-coarseness canopy texture gradient, with aperiodic canopies found close to the origin and heterogeneous ones (i.e. mixing small and large crown patches) found on the lower-left part of the plan. The general decrease of canopy grain size along F-PCA1 negatively correlated with

stand maximum tree size (Pearson's $r \geq -0.67$ with DBH_m, H_m and Cd_m in Table 5-2) as well as stand basal area and canopy roughness ($r \geq -0.57$ with G and H_v10 in Table 5-2).

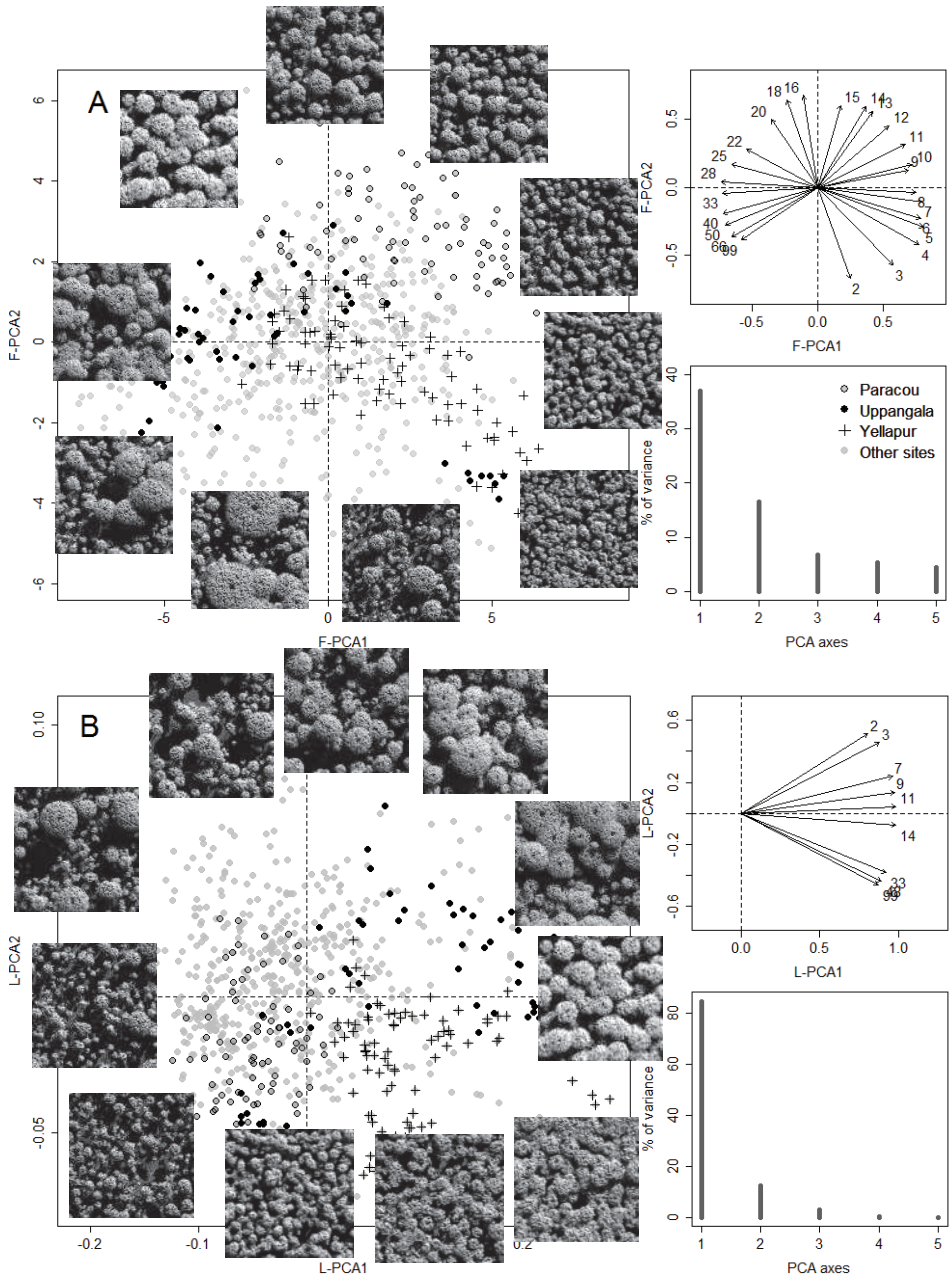

Figure 5-1. Canopy texture ordinations based on (A) the FOTO method and (B) the lacunarity analysis. In both cases, scatter plots of PCA scores along the first two principal axes are shown, with 3 example sites highlighted with particular symbols (Paracou, Uppangala and Yellapur). Correlation circles are given with wavelength, λ (A) or box size, s (B) in meter. Histograms of eigenvalues in % of total variance.

The first Lacunarity-PCA plan explained 95.7% (82.6% and 13.1% for axes 1 and 2, respectively) of the variance among normalized lacunarity spectra (L-table). The first PCA axis (L-PCA1) sorted windows according to their degree of gapiness (Figure 5-1 B) as shown by a negative correlation with stand gap fraction (r=-0.63 with GF in Table 5-2), which coincided with a positive correlation with stand basal area (r=0.59) and mean tree crown diameter (r=0.53). L-PCA1 thus sorted windows from fairly open stands (featuring frequent patches of small trees, less than 2 m in height) to fully-stocked stands having

a canopy made of larger trees. L-PCA2 captured variations in the rate of decrease in lacunarity with box size, which reflected a gradient in canopy grain and heterogeneity. Fairly homogeneous canopy (smooth canopy grain) characterized by a low rate of decrease in lacunarity with box size were found on the negative side of L-PCA2, while heterogeneous canopy were found on the positive side of L-PCA2. As a matter of fact, L-PCA2 was positively correlated with the canopy roughness index, H_v10 (r=0.7) and with maximum tree size (r=0.72 and 0.7 with H_m and DBH_m, respectively). F-PCA1 and L-PCA2 displayed a very high correlation of 0.93 (axes orientations are not informative in PCA) and fundamentally depicted the same coarseness – fineness gradient of canopy aspect. On the other hand, correlations between F-PCA2 and both Lacunarity-based PCA axes were weak, suggesting complementarity.

Table 5-2. Correlation between stand structure parameters extracted from three-dimensional mockups and canopy window scores on the texture ordination axes based on the FOTO method (F-PCA1 and F-PCA2) and the lacunarity analysis (L-PCA1 and L-PCA2). Probability value of Pearson correlation test are provided between brackets and coded following standard notation (*** P ≤ 0.01, ** P ≤ 0.01, * P ≤ 0.05, ns = non-significant).

	Stand structure parameters	F-PCA1	F-PCA2	L-PCA1	L-PCA2
GF	Gap fraction (cumulated area of pixels < 2 m in height)	0.04 (ns)	-0.18 (***)	-0.63 (***)	0.12 (**)
H_v10	Standard deviation of maximum tree height among 10 m quadrats	-0.6 (***)	-0.26 (***)	-0.27 (***)	0.7 (***)
DBH_m	Stand maximum tree DBH	-0.74 (***)	-0.21 (***)	0.17 (***)	0.7 (***)
H_m	Stand maximum tree height	-0.69 (***)	0.17 (***)	-0.1 (**)	0.72 (***)
Cd_m	Stand maximum crown diameter	-0.67 (***)	-0.3 (***)	0.17 (***)	0.64 (***)
N	Stand tree density	0.08 (*)	0.15 (***)	-0.01 (ns)	-0.07 (.)
G	Stand basal area	-0.57 (***)	0.17 (***)	0.59 (***)	0.43 (***)
DBH_{mean}	Quadratic mean of tree DBH	-0.46 (***)	0.06 (.)	0.48 (***)	0.35 (***)
CD_{mean}	Quadratic mean of tree crowns diameter	-0.19 (***)	0.16 (***)	0.53 (***)	0.09 (*)

Combining the two texture analyses in a common co-inertia analysis (Figure 5-2) revealed a slight but significant co-structure between the two PCA (*RV* = 0.24, *P* < 0.001). This indicates that while both analyses are partly redundant in describing canopy texture, they also provide complementary information. The first COIA plan captured 97.1% of the co-inertia, which was mostly one-dimensional (88.3% on COIA-1). The inertia projected on F-PCA1 was almost entirely found on COIA-1 (i.e. 96.2%, against 68.1% for L-PCA1), and 85.7% of the cumulated inertia projected on F-PCA 1 and 2 was captured on COIA-1 and 2 (against 90.3% for L-PCA1 and 2). Figure 2 illustrates that while the co-inertia analysis preserves the structure of each separate PCA, i.e. the canopy texture gradients described by the FOTO (Figure 5-2 A) and lacunarity analyses (Figure 5-2 D), some disagreements between the two methods appeared at both the site and window level. For instance, while Yellapur site was close to Paracou site in terms of FOTO-texture properties, it was more similar to Uppangala in terms of lacunarity-texture properties (Figure 5-2 C). In Paracou, canopy texture described by FOTO and lacunarity provided very similar information for all the sampled canopy windows (short arrows in Figure 5-2 F), while for Yellapur and Uppangala, some canopy windows that exhibited very different FOTO textures (i.e. found at the opposite on COIA-1) showed a convergence towards similar lacunarity-derived textures (long convergent arrows in Figure 5-2 F).

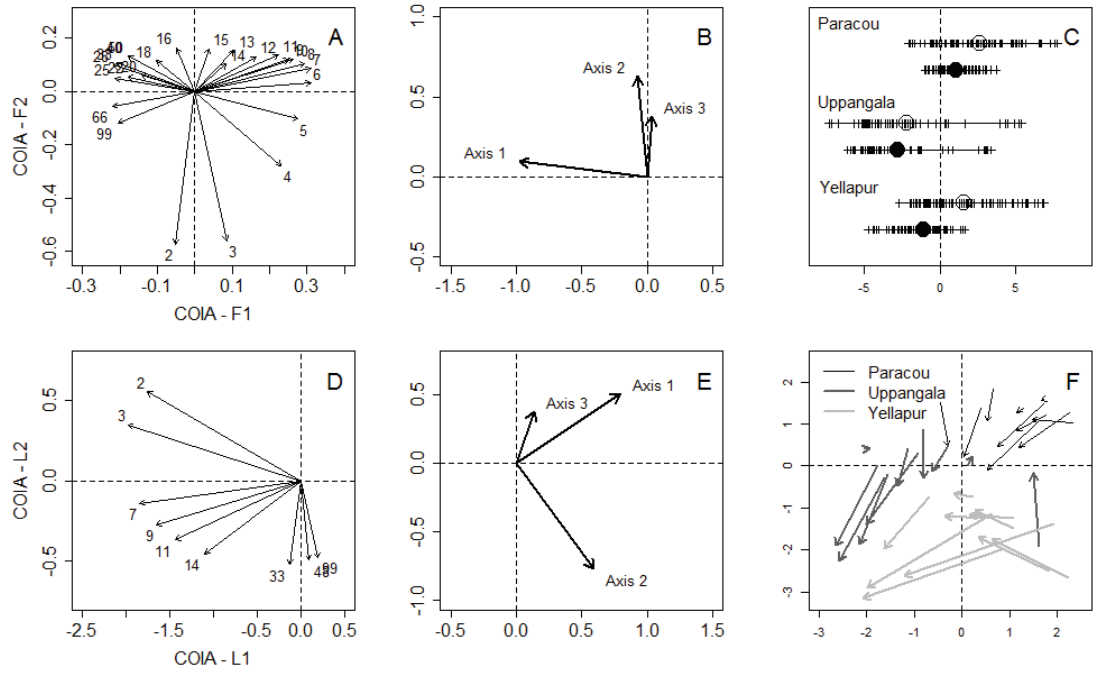

Figure 5-2. Co-inertia analysis. Position on the first co-inertia plane of the FOTO r-spectra wavelengths, λ (A) and the lacunarity box size, s (D). Components of the F-PCA (B) and the L-PCA (E) projected onto the co-inertia axes. Ordination of windows from the 3 example sites (Paracou, Uppangala and Yellapur) on COIA-1 (C) with large empty and full circles representing the average site-level score for FOTO and Lacunarity features, respectively. Normed scores of 10 randomly sampled canopy windows from the 3 example sites on the first co-inertia plane (F), with each arrow linking a canopy window position for FOTO and Lacunarity characteristics, respectively.

5.3.2 Canopy texture - AGB models

Global Random Forest prediction models of stand AGB based either on FOTO texture (F-model) and on lacunarity texture indices (L-model) derived from the virtual canopy images, led to retain the two first axes for both F and L analyses (Figure 5-3 top), but provided quite low goodness of fit (R^2 = 0.46 and 0.31, with rRMSE = 31 and 38%, respectively). In both cases model predictions showed a systematic pattern of errors with respect to the 1:1 line, which led to underestimations at high biomass levels,

reaching -32.7% (MSD) in average with the L-model for forest plots from Paracou. Conversely, a RF model based on both FOTO and lacunarity scores on the two first co-inertia axes (FL-model in Figure 5-3) largely increased the prediction power on stand AGB estimations (R^2 = 0.76 with a rRMSE = 20%). This global model also improved the local predictions at our three example sites, with a substantial reduction in MSD as compared to previous models, except for the F-model at Yellapur. It is also noteworthy that site-level MSD seemed to decrease with the range of biomass encompassed across plots in a site: while plots in Yellapur (MSD = 5.2%) and Paracou (MSD = -8%) are restricted to low and high biomass levels, respectively, in Uppangala (MSD = 2.4 %) plots have been sampled along a biomass gradient spanning from c. 150 up to > 600 Mg.ha^{-1}. This indicates that the underlying texture-AGB relationship may vary between sites as a function of samplings, but also with respect to local site characteristics. For instance, while tree density in Paracou correlated well with FOTO and lacunarity scores on COIA-1 (r = 0.75 and 0.52, respectively), it did not in Yellapur (r < 0.15). Similar observations can be made for maximum tree slenderness (i.e. Hmax/Dmax) which correlated well with scores in Uppangala (r = 0.88 and 0.82, respectively) but not so clearly in Yellapur (r = 0.38 and 0.66, respectively).

To account for this between-sites variation in the texture-structure relationship, we finally added to our global model the bioclimatic stress variable E implemented by Chave et al. (2014), with the aim to capture variations in height-diameter relationships (i.e. tree slenderness).The FLE-model which incorporates E along with FOTO and lacunarity texture indices indeed improved goodness of fit (R^2 = 0.88, with rRMSE = 14%) and reduced local prediction errors of the 3 example sites (MSD < 5%). The variable selection procedure retained only 3 predictor variables in this model, which are in order of importance: L-COIA1, E and F-COIA2 (see supplementary Table 5-4).

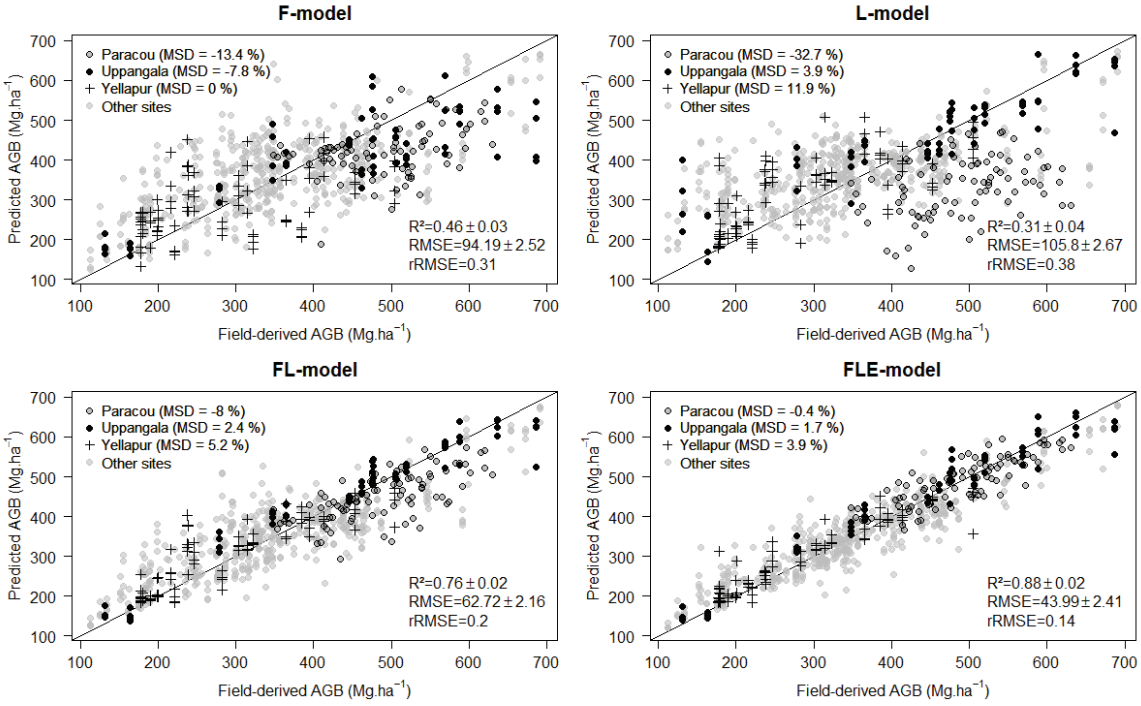

Figure 5-3. Multi-site AGB prediction models based on FOTO texture (F-model), Lacunarity texture (L-model), the two sources of texture information (FL-model) to which we also added a forest canopy height proxy E (FLE-model). Texture features were extracted from virtual canopy scenes. Goodness of fit statistics are defined in Methods section.

5.3.3 Application to real satellite images

We tested the approach developed above on a set of three real VHSR optical images. FOTO and lacunarity analysis were conducted in similar conditions than with the virtual canopy images and Random Forest AGB models were developed based on window scores on F-PCA axes (i.e. F-model), L-PCA axes (i.e. L-model) and co-inertia axes and the bioclimatic stress variable E (FLE-model). The F- and L-model did not, or weakly discriminate AGB variations (R^2 = 0.03 and R^2 = 0.18, respectively). The variable selection procedure on the FLE model (m4 in supplementary Table 5-5) retained the following variables ranked by order of importance: F-COIA2 (IncMSE: 26.2%), E (25.6%) and L-COIA2 (24.8%). The final AGB prediction model (m4* in supplementary Table 5-5) led to an R^2 = 0.59 with a rRMSE of about 21% and site level errors (MSD) below 2% (Figure 5-4).

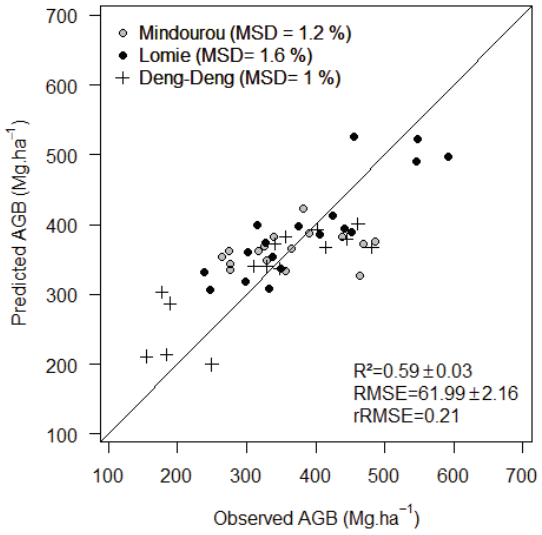

Figure 5-4. Multi-site AGB prediction model over 49 1-ha plots in central Africa, based on both FOTO-texture and Lacunarity-texture indices to which we added the bioclimatic stress variable E as a proxy of potential canopy height (FLE-model).

5.4 Discussion

Over the past decade, about two dozen studies successfully used canopy texture analysis applied on VHSR optical or LiDAR CHM data to uncover spatial gradients in forest structure and AGB, including in high-biomass tropical forests (e.g. Couteron et al., 2005; Frazer et al., 2005; Malhi and Román-Cuesta, 2008; Proisy et al., 2007). These studies were however limited to relatively small geographical areas and often retrieved structure gradients within a single, homogeneous forest type. The few attempts made in mosaics of heterogeneous forest patches (e.g. Bastin et al., 2014; Singh et al., 2014) have shown that the information carried by canopy texture depends on forest type, hindering broad-scale applications of texture-based methods. Using 279 1-ha plots distributed among different forest types across the tropics, we evaluated whether a generalized biomass prediction model based on canopy texture indices could provide consistent predictions at both local and global scales. The results presented here based on virtual canopy images show that it is worth complementing FOTO with lacunarity texture indices capturing canopy features related to canopy openness. Introducing a bioclimatic stress variable that captured regional variation in potential canopy height also substantially improved the accuracy and precision of forest AGB retrievals among forest sites. A practical application

of the method to a mosaic of real canopy images in the Congo basin showed that forest AGB inferences could be made with high precision (i.e. c. 20% of error) up to 600 $Mg.ha^{-1}$, i.e. without saturation.

5.4.1 Contrasted canopy texture - stand AGB relationships among sites

Global models based only on FOTO or lacunarity texture indices (F- and L-model, respectively) significantly explained AGB variations but presented a relatively high uncertainty (rRMSE = 30-40%), consistent with what other studies have reported for heterogeneous forest landscapes (e.g. Bastin et al. 2014). To circumvent the problem and improve AGB inferences, previous empirical studies typically used a forest type stratification step prior to the calibration of within-class texture–AGB models, suggesting that the relationship is dependent on forest type (Bastin et al., 2014; Singh et al., 2014). We indeed found that forest plots from different geographical sites were often clustered along the texture gradients, generating systematic biases, and that texture indices did not always correlate with the same stand structure parameters in different sites.

The relationship between FOTO-texture indices and forest AGB is expected to hold well for periodic canopy patterns with homogeneous grain size (Proisy et al., 2007). In this ideal case, Fourier r-spectra peak at the scale of the mean crown size of canopy trees (Barbier et al., 2010). Because crown size is allometrically related to tree AGB (Jucker et al., 2016; Ploton et al., 2016) and that the 20 biggest trees in 1-ha stands capture c. 85% of whole stands AGB variability in tropical forests (Bastin et al., 2015), FOTO texture accurately predicts forest stand AGB. This is for instance the case along the successional development pathway of mangrove tree cohorts (Proisy et al., 2007) but can also apply to mixed-forests where the coarseness-fineness canopy texture gradient reflects difference in mature tree statures (e.g. due to contrasting soil fertility, Couteron et al., 2005) or forest biomass gradients. At Paracou study site for instance, a good linear correlation (r = -0.88) exists between tree density (N) and the mean quadratic diameter (DBH_{mean}) suggesting that sample plots align along a self-thinning trajectory (see also Vincent et al., 2012). Our simulation procedure based on simple allometric relationships thus produced fully-stocked virtual canopy images often displaying a periodic aspect (see Figure 5-1) and for which a local F-model (i.e. based on FOTO texture only) provided very accurate AGB predictions (rRMSE = c. 10%, results not shown). However, when the forest enters the gap phase dynamics (Withmore, 1975), stand structure becomes heterogeneous in both the horizontal and vertical dimensions, leading to higher canopy roughness, more frequent canopy gaps alternating with clusters of large trees (e.g. Franklin et al., 2002; Guariguata and Ostertag, 2001; Spies, 1998). In Uppangala for instance, where N and DBH_{mean} did not correlate over the sampling plots (r = -0.09), simulated canopy images were highly heterogeneous (see Figure 5-1), and a local L-model (i.e. based on lacunarity texture only) produced more accurate AGB predictions (rRMSE< 10% vs. c. 20% with a local F-model, results not shown). Other studies confirmed that lacunarity is an efficient method to reveal canopy openness and heterogeneity gradients (e.g. Frazer et al., 2005; Malhi and Román-Cuesta, 2008). It is therefore easy to understand that combining both types of texture indices largely improved our multi-site prediction model (FL-model) at both the local and multi-site levels.

At the global scale however, variation in canopy height (Fayad et al., 2016; Saatchi et al., 2011) and tree slenderness (Feldpausch et al., 2012), which proved critical for accurate AGB estimations (Chave et al., 2014), cannot be directly accounted for by a 2D analysis of canopy texture, whatever the method. Along a local forest successional gradient, canopy height variations follow increment in tree size visible from above through the mean crown sizes. But, the maximal height reachable by dominant trees is known to generally reveal the growth potential of a forest in relation to soil and regional

bioclimatic constraints, in particular with regard to water stress (Chave et al., 2014). Introducing the E bioclimatic variable, which combines water deficit with temperature and precipitation seasonality (see Chave et al., 2014) improved goodness of fit of our global regression model (FLE-model) and significantly reduced local prediction errors.

On the set of real images from the Congo basin forest mosaic, the generalized texture-based model was able to detect spatial variations in AGB within a tropical forest mosaic characterized by both high AGB levels and forest types showing important variations in stand 3D structure, from closed-canopy mixed-species mature stands to open-canopy *Marantaceae* forests. We have also shown here that the multi-site FLE-model was the most robust with uncertainty of about 62 $Mg.ha^{-1}$ at 1-ha scale (RMSE) corresponding to a relative error of 21% (rRMSE). For such high-biomass forests, where the averaged sampled plots AGB exceeds 350 $Mg.ha^{-1}$ (i.e. 359±98), error levels reported here are only slightly higher than those obtained from small-footprint airborne LiDAR (Zolkos et al., 2013). This result confirms and expands the results previously obtained with a variety of satellite sensors (Quickbird, GeoEye, IKONOS, SPOT-5), aerial images and even images freely available from the Google Earth engine (Bastin et al., 2014; Meng et al., 2016; Ploton et al., 2012; Proisy et al., 2007; Singh et al., 2015, 2014) in temperate or tropical forests. This represents an important step toward using VHSR optical imagery for broad-scale assessments of forest AGB, as it eliminates the need of a preliminary forest classification (see for instance Pargal et al., *submitted*). Recent progress also opened the perspective to perform texture analysis on inter-calibrated satellite images from various sensors and/or in various configurations, provided they partly overlap (Barbier and Couteron, 2015).

5.4.2 On 3D stand mockups and virtual canopy images for model calibration

Our stand modelling approach follows previously published studies on image texture simulations, notably Barbier et al. (2012, 2010), Barbier and Couteron (2015) and Proisy et al. (2016). At the scale of 1-ha forest plots, the size distribution of large objects within the scene (individual and aggregated tree crowns) and their spatial arrangements (e.g. inter-crown gaps and associated shadows, variations in tree density and size between subplots, etc.) are crucial determinants of spatial variations of the apparent reflectance. Using a unique, simplified tree shape representation (i.e. cylindrical trunks and non-plastic, ellipsoid crowns) allows generating sufficiently realistic brightness variation patterns at those coarse scales for the interpretation of canopy texture gradients. For instance, Proisy et al. (2016) showed that this approach allows producing texture r-spectra that have similar frequency peaks than real ones over a wide range of mangrove successional stages. In the present study, a particular care was taken to develop local tree size allometries and integrate field information on the spatial positions of trees within stands, to mimic as well as possible the coarse-scale heterogeneity observed in real field plots. This proved to be efficient to add consistent texture information related to the alternation between patches of tree crowns and canopy gaps captured in high lacunarity values. However, our stand simulation procedure could still be improved by accounting for crown plasticity (like for instance in Boudon and Le Moguédec, 2007) or for between-species variations in trees inner-crown properties, either geometric (e.g. foliage clumping and porosity, leaf angle distribution) or optical (Schneider et al., 2014) that may influence grayscale variations at very small spatial scale. Considering these different aspects is a long term research effort, and will likely benefit from technological advances in LiDAR scanning and unmanned aerial vehicles (e.g. Morton and Cook, 2016). We suspect lacunarity analysis to be more sensitive than FOTO to these geometric and optical parameters, making lacunarity a more relevant complement to FOTO when analyzing simulated images than when analyzing real images.

An invaluable advantage of virtual canopy images is that they can be simulated in homogeneous acquisition configurations on the basis of field data from different sites and regions. Texture indeed quantifies pattern characteristics related to the contrasts between sunlit and shadowed surfaces and is thus highly sensitive to the sun to sensor and scene angles (Barbier et al. 2011). Even if inter-calibration procedures can help, particular configurations (e.g. backward scattering modes, near hotspot directions) are intrinsically detrimental to canopy texture analysis and fatal to large-scale applications over a mosaic of several images (Barbier and Couteron, 2015). On another hand, programming image acquisition in controlled configurations, though possible, remains difficult, sometimes costly and often very long, particularly over tropical zones where optical images frequently suffer atmospheric pollutions related to dense cloud cover or persistent nebulosity. Another pitfall of the detection of texture gradients through ordination is that the principal axes extracted from the data are highly dependent on available samples and particular image sets may not reflect the entire possible gradients of forest structure and canopy texture variations. In our example sites for instance, it clearly appears that when the texture gradient is short, as was the case in Paracou, the texture-structure relationship (as measured by R^2) was not as strong as it was in areas covering a more extended gradient (as in Uppangala). Simulated images thus allowed us to place all plots and sites along a large gradient of canopy texture in order to stabilize the PCA axes and thus to increase robustness of the texture-structure relationship, making it more universal than when fitted within sites. We therefore call for the collaborative construction of a pantropical database of 3D forest mockups, that could be incremented from plot data and local allometries in order to document all the particular situations encountered in tropical forests. These mockups could then be processed with DART in homogeneous acquisition conditions to produce arrays of canopy images of sufficient generality. The relevant simulated spectral bands could finally be assembled according to the specific characteristics of any of the VHSR sensor from which it could appear realistic to gather a very large array of real world, homogeneous images as to perform global scale canopy texture analysis. This would be a way to consolidate the reference gradients in canopy texture that emerged from our simulation results as to benchmark real observations, i.e. for canopy texture analyses performed from real canopy images. This perspective is a straightforward extension of the approach we introduced in the present paper, that would lead us towards a tentative robust operational texture-structure relationship from which accurate assessments of tropical forests AGB and carbon stocks could be produced.

Acknowledgments

Pierre Ploton was supported by an Erasmus Mundus PhD grant from the 2013–2016 Forest, Nature and Society (FONASO) doctoral program. Satellite images were acquired through the Forest project funded by the European Institute of Technology-Climate Knowledge & Innovation Community (grant N° PIN0040_2015-3.1-044_P032_01-01). Forest inventory data were collected with the support of the CoForTips project as part of the ERA-Net BiodivERsA 2011-2012 European joint call (ANR-12-EBID-0002), the IRD project PPR FTH-AC “Changements globaux, biodiversité et santé en zone forestière d’Afrique Centrale”, the IFPCAR project “Controlling for Uncertainty in Assessment of Forest Aboveground Biomass in the Western Ghats of India” (grant N° 4509-1), Eramet, the World Bank, WWF, the African Development Bank and the Center for Tropical Forest Science – Forest Global Earth Observatory (CTFS-ForestGEO) of the Smithsonian Tropical Research Institute.

Author contributions. Conceived and designed the experiments: PP, NB and RP. Collected data (field inventories): GD, VD, NGK, ML, GIIM, BS, NT, STM, DZD, NB and PP. Shared data: CMA, NA, NBal, NBar, JFB, GC, DK, SP, PPe and DT. Analyzed the data: PP. Analysis feedback: RP, NB, MRM, JPG, PV and PC. Wrote the paper: PP. Writing feedback: PC, NB, MRM, CP, UB and RP.

5.5 Reference

Allain, C., Cloitre, M., 1991. Characterizing the lacunarity of random and deterministic fractal sets. Phys. Rev. A 44, 3552.

Antin, C., Pélissier, R., Vincent, G., Couteron, P., 2013. Crown allometries are less responsive than stem allometry to tree size and habitat variations in an Indian monsoon forest. Trees 27, 1485–1495. doi:10.1007/s00468-013-0896-7

Asner, G.P., Martin, R.E., 2008. Spectral and chemical analysis of tropical forests: Scaling from leaf to canopy levels. Remote Sens. Environ. 112, 3958–3970.

Asner, G.P., Mascaro, J., Muller-Landau, H.C., Vieilledent, G., Vaudry, R., Rasamoelina, M., Hall, J.S., Breugel, M. van, 2011. A universal airborne LiDAR approach for tropical forest carbon mapping. Oecologia 168, 1147–1160. doi:10.1007/s00442-011-2165-z

Baccini, A., Goetz, S.J., Walker, W.S., Laporte, N.T., Sun, M., Sulla-Menashe, D., Hackler, J., Beck, P.S.A., Dubayah, R., Friedl, M.A., 2012. Estimated carbon dioxide emissions from tropical deforestation improved by carbon-density maps. Nat. Clim. Change 2, 182–185.

Barbier, N., Couteron, P., 2015. Attenuating the bidirectional texture variation of satellite images of tropical forest canopies. Remote Sens. Environ. 171, 245–260. doi:10.1016/j.rse.2015.10.007

Barbier, N., Couteron, P., Gastelly-Etchegorry, J.-P., Proisy, C., 2012. Linking canopy images to forest structural parameters: potential of a modeling framework. Ann. For. Sci. 69, 305–311. doi:10.1007/s13595-011-0116-9

Barbier, N., Couteron, P., Proisy, C., Malhi, Y., Gastellu-Etchegorry, J.-P., 2010. The variation of apparent crown size and canopy heterogeneity across lowland Amazonian forests. Glob. Ecol. Biogeogr. 19, 72–84.

Barbier, N., Proisy, C., Véga, C., Sabatier, D., Couteron, P., 2011. Bidirectional texture function of high resolution optical images of tropical forest: An approach using LiDAR hillshade simulations. Remote Sens. Environ. 115, 167–179.

Baskerville, G.L., 1972. Use of Logarithmic Regression in the Estimation of Plant Biomass. Can. J. For. Res. 2, 49–53. doi:10.1139/x72-009

Bastin, J.-F., Barbier, N., Couteron, P., Adams, B., Shapiro, A., Bogaert, J., De Cannière, C., 2014. Aboveground biomass mapping of African forest mosaics using canopy texture analysis: toward a regional approach. Ecol. Appl. 24, 1984–2001.

Bastin, J.-F., Barbier, N., Réjou-Méchain, M., Fayolle, A., Gourlet-Fleury, S., Maniatis, D., de Haulleville, T., Baya, F., Beeckman, H., Beina, D., 2015. Seeing Central African forests through their largest trees. Sci. Rep. 5. doi:doi:10.1038/srep13156

Boudon, F., Le Moguédec, G.L., 2007. Déformation asymétrique de houppiers pour la génération de représentations paysagères réalistes. Rev. Electron. Francoph. Inform. Graph. 1.

Breiman, L., 2001. Random forests. Mach. Learn. 45, 5–32.

Broadbent, E.N., Asner, G.P., Peña-Claros, M., Palace, M., Soriano, M., 2008. Spatial partitioning of biomass and diversity in a lowland Bolivian forest: Linking field and remote sensing measurements. For. Ecol. Manag. 255, 2602–2616. doi:10.1016/j.foreco.2008.01.044

Chave, J., Coomes, D., Jansen, S., Lewis, S.L., Swenson, N.G., Zanne, A.E., 2009. Towards a worldwide wood economics spectrum. Ecol. Lett. 12, 351–366. doi:10.1111/j.1461-0248.2009.01285.x

Chave, J., Muller-Landau, H.C., Baker, T.R., Easdale, T.A., Steege, H. ter, Webb, C.O., 2006. Regional and phylogenetic variation of wood density across 2456 neotropical tree species. Ecol. Appl. 16, 2356–2367. doi:10.1890/1051-0761(2006)016[2356:RAPVOW]2.0.CO;2

Chave, J., Réjou-Méchain, M., Búrquez, A., Chidumayo, E., Colgan, M.S., Delitti, W.B.C., Duque, A., Eid, T., Fearnside, P.M., Goodman, R.C., Henry, M., Martínez-Yrízar, A., Mugasha, W.A., Muller-Landau, H.C., Mencuccini, M., Nelson, B.W., Ngomanda, A., Nogueira, E.M., Ortiz-Malavassi, E., Pélissier, R., Ploton, P., Ryan, C.M., Saldarriaga, J.G., Vieilledent, G., 2014. Improved allometric models to estimate the aboveground biomass of tropical trees. Glob. Change Biol. 20, 3177–3190. doi:10.1111/gcb.12629

Chuyong, G.B., Condit, R., Kenfack, D., Losos, E.C., Moses, S.N., Songwe, N.C., Thomas, D.W., 2004. Korup forest dynamics plot, Cameroon. Trop. For. Divers. Dynamism 506–516.

Couteron, P., 2002. Quantifying change in patterned semi-arid vegetation by Fourier analysis of digitized aerial photographs. Int. J. Remote Sens. 23, 3407–3425.

Couteron, P., Pelissier, R., Nicolini, E.A., Paget, D., 2005. Predicting tropical forest stand structure parameters from Fourier transform of very high-resolution remotely sensed canopy images. J. Appl. Ecol. 42, 1121–1128.

DeFries, R., Achard, F., Brown, S., Herold, M., Murdiyarso, D., Schlamadinger, B., de Souza, C., 2007. Earth observations for estimating greenhouse gas emissions from deforestation in developing countries. Environ. Sci. Policy 10, 385–394.

Dolédec, S., Chessel, D., 1994. Co-inertia analysis: an alternative method for studying species–environment relationships. Freshw. Biol. 31, 277–294.

Erdody, T.L., Moskal, L.M., 2010. Fusion of LiDAR and imagery for estimating forest canopy fuels. Remote Sens. Environ. 114, 725–737.

Fayad, I., Baghdadi, N., Guitet, S., Bailly, J.-S., Hérault, B., Gond, V., El Hajj, M., Minh, D.H.T., 2016. Aboveground biomass mapping in French Guiana by combining remote sensing, forest inventories and environmental data. Int. J. Appl. Earth Obs. Geoinformation 52, 502–514.

Feldpausch, T.R., Lloyd, J., Lewis, S.L., Brienen, R.J., Gloor, M., Monteagudo Mendoza, A., Lopez-Gonzalez, G., Banin, L., Abu Salim, K., Affum-Baffoe, K., 2012. Tree height integrated into pantropical forest biomass estimates. Biogeosciences 3381–3403.

Franklin, J.F., Spies, T.A., Van Pelt, R., Carey, A.B., Thornburgh, D.A., Berg, D.R., Lindenmayer, D.B., Harmon, M.E., Keeton, W.S., Shaw, D.C., 2002. Disturbances and structural development of natural forest ecosystems with silvicultural implications, using Douglas-fir forests as an example. For. Ecol. Manag. 155, 399–423.

Frazer, G.W., Wulder, M.A., Niemann, K.O., 2005. Simulation and quantification of the fine-scale spatial pattern and heterogeneity of forest canopy structure: A lacunarity-based method designed for analysis of continuous canopy heights. For. Ecol. Manag. 214, 65–90.

Gastellu-Etchegorry, J.-P., Yin, T., Lauret, N., Cajgfinger, T., Gregoire, T., Grau, E., Feret, J.-B., Lopes, M., Guilleux, J., Dedieu, G., 2015. Discrete Anisotropic Radiative Transfer (DART 5) for modeling airborne and satellite spectroradiometer and LIDAR acquisitions of natural and urban landscapes. Remote Sens. 7, 1667–1701.

Genuer, R., Poggi, J.-M., Tuleau-Malot, C., 2015. VSURF: An R Package for Variable Selection Using Random Forests. R J. 7, 19–33.

Guariguata, M.R., Ostertag, R., 2001. Neotropical secondary forest succession: changes in structural and functional characteristics. For. Ecol. Manag. 148, 185–206.

Haralick, R.M., 1979. Statistical and structural approaches to texture. Proc. IEEE 67, 786–804.

ICRAF, 2007. Wood density database. World Agrofor. Cent. Nairobi Kenya http://db.worldagroforestry.org//wd.

Jeyakumar, S., Ayyappan, N., Muthuramkumar, S., Rajarathinam, K., in press. Impacts of selective logging on diversity, species composition and biomass of residual lowland dipterocarp forest in central Western Ghats, India. Trop. Ecol.

Jonckheere, I., Fleck, S., Nackaerts, K., Muys, B., Coppin, P., Weiss, M., Baret, F., 2004. Review of methods for in situ leaf area index determination: Part I. Theories, sensors and hemispherical photography. Agric. For. Meteorol. 121, 19–35.

Jucker, T., Caspersen, J., Chave, J., Antin, C., Barbier, N., Bongers, F., Dalponte, M., van Ewijk, K.Y., Forrester, D.I., Haeni, M., Higgins, S.I., Holdaway, R.J., Iida, Y., Lorimer, C., Marshall, P.L., Momo, S., Moncrieff, G.R., Ploton, P., Poorter, L., Rahman, K.A., Schlund, M., Sonké, B., Sterck, F.J., Trugman, A.T., Usoltsev, V.A., Vanderwel, M.C., Waldner, P., Wedeux, B.M.M., Wirth, C., Wöll, H., Woods, M., Xiang, W., Zimmermann, N.E., Coomes, D.A., 2016. Allometric equations for integrating remote sensing imagery into forest monitoring programmes. Glob. Change Biol. doi:10.1111/gcb.13388

Lu, D., 2006. The potential and challenge of remote sensing-based biomass estimation. Int. J. Remote Sens. 27, 1297–1328.

Lu, D., Chen, Q., Wang, G., Moran, E., Batistella, M., Zhang, M., Vaglio Laurin, G., Saah, D., 2012. Aboveground Forest Biomass Estimation with Landsat and LiDAR Data and Uncertainty Analysis of the Estimates. Int. J. For. Res. 2012, 1–16. doi:10.1155/2012/436537

Malhi, Y., Román-Cuesta, R.M., 2008. Analysis of lacunarity and scales of spatial homogeneity in IKONOS images of Amazonian tropical forest canopies. Remote Sens. Environ. 112, 2074–2087.

Mandelbrot, B.B., 1983. The fractal geometry of nature. Macmillan.

Marvin, D.C., Koh, L.P., Lynam, A.J., Wich, S., Davies, A.B., Krishnamurthy, R., Stokes, E., Starkey, R., Asner, G.P., 2016. Integrating technologies for scalable ecology and conservation. Glob. Ecol. Conserv. 7, 262–275. doi:10.1016/j.gecco.2016.07.002

Mascaro, J., Asner, G.P., Knapp, D.E., Kennedy-Bowdoin, T., Martin, R.E., Anderson, C., Higgins, M., Chadwick, K.D., 2014. A Tale of Two "Forests": Random Forest Machine Learning Aids Tropical Forest Carbon Mapping. PLoS ONE 9, e85993. doi:10.1371/journal.pone.0085993

Meng, S., Pang, Y., Zhang, Z., Jia, W., Li, Z., 2016. Mapping Aboveground Biomass using Texture Indices from Aerial Photos in a Temperate Forest of Northeastern China. Remote Sens. 8, 230. doi:10.3390/rs8030230

Mermoz, S., Réjou-Méchain, M., Villard, L., Le Toan, T., Rossi, V., Gourlet-Fleury, S., 2015. Decrease of L-band SAR backscatter with biomass of dense forests. Remote Sens. Environ. 159, 307–317. doi:10.1016/j.rse.2014.12.019

Messinger, M., Asner, G., Silman, M., 2016. Rapid Assessments of Amazon Forest Structure and Biomass Using Small Unmanned Aerial Systems. Remote Sens. 8, 615. doi:10.3390/rs8080615

Morton, D.C., Cook, B.D., 2016. Amazon forest structure generates diurnal and seasonal variability in light utilization. Biogeosciences 13, 2195.

Olivas, P.C., Oberbauer, S.F., Clark, D.B., Clark, D.A., Ryan, M.G., O'Brien, J.J., Ordonez, H., 2013. Comparison of direct and indirect methods for assessing leaf area index across a tropical rain forest landscape. Agric. For. Meteorol. 177, 110–116.

Pan, Y., Birdsey, R.A., Fang, J., Houghton, R., Kauppi, P.E., Kurz, W.A., Phillips, O.L., Shvidenko, A., Lewis, S.L., Canadell, J.G., 2011. A large and persistent carbon sink in the world's forests. Science 333, 988–993.

Pargal, S., Fararoda, R., Rajashekar, G., Balachandran, N., Réjou-Méchain, M., Barbier, N., Jha, C.S., Pélissier, R., Dadhwal, V.K., Couteron, P., n.d. Characterizing aboveground biomass – canopy texture relationships in a landscape of forest mosaic in the Western Ghats of India using very high resolution Cartosat Imagery. Remote Sens.

Ploton, P., Barbier, N., Takoudjou Momo, S., Réjou-Méchain, M., Boyemba Bosela, F., Chuyong, G., Dauby, G., Droissart, V., Fayolle, A., Goodman, R.C., Henry, M., Kamdem, N.G., Mukirania, J.K., Kenfack, D., Libalah, M., Ngomanda, A., Rossi, V., Sonké, B., Texier, N., Thomas, D., Zebaze, D., Couteron, P., Berger, U., Pélissier, R., 2016. Closing a gap in tropical forest biomass estimation: taking crown mass variation into account in pantropical allometries. Biogeosciences 13, 1571–1585. doi:10.5194/bg-13-1571-2016

Ploton, P., Pélissier, R., Proisy, C., Flavenot, T., Barbier, N., Rai, S.N., Couteron, P., 2012. Assessing aboveground tropical forest biomass using Google Earth canopy images. Ecol. Appl. 22, 993–1003. doi:10.1890/11-1606.1

Proisy, C., Couteron, P., Fromard, F., 2007. Predicting and mapping mangrove biomass from canopy grain analysis using Fourier-based textural ordination of IKONOS images. Remote Sens. Environ. 109, 379–392.

Proisy, C., Féret, J.-B., Lauret, N., Gastellu-Etchegorry, J.-P., 2016. Mangrove forest dynamics using very high spatial resolution optical remote sensing., in: Remote Sensing of Land Surfaces: Urban and Coastal Area. N.N. Baghdadi & M. Zribi, Paris, pp. 274–300.

R Core Team, 2016. R: A language and environment for statistical computing. R Foundation for Statistical Computing, Vienna, Austria. URL https://www.R-project.org/.

Réjou-Méchain, M., Tymen, B., Blanc, L., Fauset, S., Feldpausch, T.R., Monteagudo, A., Phillips, O.L., Richard, H., Chave, J., 2015. Using repeated small-footprint LiDAR acquisitions to infer spatial and temporal variations of a high-biomass Neotropical forest. Remote Sens. Environ. 169, 93–101.

Saatchi, S.S., Harris, N.L., Brown, S., Lefsky, M., Mitchard, E.T., Salas, W., Zutta, B.R., Buermann, W., Lewis, S.L., Hagen, S., 2011. Benchmark map of forest carbon stocks in tropical regions across three continents. Proc. Natl. Acad. Sci. 108, 9899–9904.

Schneider, F.D., Leiterer, R., Morsdorf, F., Gastellu-Etchegorry, J.-P., Lauret, N., Pfeifer, N., Schaepman, M.E., 2014. Simulating imaging spectrometer data: 3D forest modeling based on LiDAR and in situ data. Remote Sens. Environ. 152, 235–250. doi:10.1016/j.rse.2014.06.015

Singh, M., Evans, D., Friess, D.A., Tan, B.S., Nin, C.S., 2015. Mapping Above-Ground Biomass in a Tropical Forest in Cambodia Using Canopy Textures Derived from Google Earth. Remote Sens. 7, 5057–5076. doi:10.3390/rs70505057

Singh, M., Malhi, Y., Bhagwat, S., 2014. Biomass estimation of mixed forest landscape using a Fourier transform texture-based approach on very-high-resolution optical satellite imagery. Int. J. Remote Sens. 35, 3331–3349. doi:10.1080/01431161.2014.903441

Slik, J.W., Paoli, G., McGuire, K., Amaral, I., Barroso, J., Bastian, M., Blanc, L., Bongers, F., Boundja, P., Clark, C., 2013. Large trees drive forest aboveground biomass variation in moist lowland forests across the tropics. Glob. Ecol. Biogeogr. 22, 1261–1271.

Spies, T.A., 1998. Forest structure: a key to the ecosystem. Northwest Sci. 72, 34–36.

Stark, S.C., Enquist, B.J., Saleska, S.R., Leitold, V., Schietti, J., Longo, M., Alves, L.F., Camargo, P.B., Oliveira, R.C., 2015. Linking canopy leaf area and light environments with tree size distributions to explain Amazon forest demography. Ecol. Lett. n/a-n/a. doi:10.1111/ele.12440

Taubert, F., Jahn, M.W., Dobner, H.-J., Wiegand, T., Huth, A., 2015. The structure of tropical forests and sphere packings. Proc. Natl. Acad. Sci. 112, 15125–15129.

Tucker, L.R., 1958. An inter-battery method of factor analysis. Psychometrika 23, 111–136.

Véga, C., Vepakomma, U., Morel, J., Bader, J.-L., Rajashekar, G., Jha, C.S., Ferêt, J., Proisy, C., Pélissier, R., Dadhwal, V.K., 2015. Aboveground-Biomass Estimation of a Complex Tropical Forest in India Using Lidar. Remote Sens. 7, 10607–10625.

Vieilledent, G., Gardi, O., Grinand, C., Burren, C., Andriamanjato, M., Camara, C., Gardner, C.J., Glass, L., Rasolohery, A., Rakoto Ratsimba, H., Gond, V., Rakotoarijaona, J.-R., 2016. Bioclimatic envelope models predict a decrease in tropical forest carbon stocks with climate change in Madagascar. J. Ecol. 104, 703–715. doi:10.1111/1365-2745.12548

Vincent, G., Sabatier, D., Blanc, L., Chave, J., Weissenbacher, E., Pélissier, R., Fonty, E., Molino, J.-F., Couteron, P., 2012. Accuracy of small footprint airborne LiDAR in its predictions of tropical moist forest stand structure. Remote Sens. Environ. 125, 23–33.

Vincent, G., Sabatier, D., Rutishauser, E., 2014. Revisiting a universal airborne light detection and ranging approach for tropical forest carbon mapping: scaling-up from tree to stand to landscape. Oecologia 175, 439–443. doi:10.1007/s00442-014-2913-y

Withmore, T.C., 1975. Tropical rain forest of the far east. Claredon Prees Oxf. Univ. Prees Lond.

Xu, L., Saatchi, S.S., Yang, Y., Yu, Y., White, L., 2016. Performance of non-parametric algorithms for spatial mapping of tropical forest structure. Carbon Balance Manag. 11. doi:10.1186/s13021-016-0062-9

Zanne, A.E., Lopez-Gonzalez, G., Coomes, D.A., Ilic, J., Jansen, S., Lewis, S.L., Miller, R.B., Swenson, N.G., Wiemann, M.C., Chave, J., 2009. Data from: towards a worldwide wood economics spectrum. Dryad Digital Reposit.

Zhao, P., Lu, D., Wang, G., Wu, C., Huang, Y., Yu, S., 2016. Examining Spectral Reflectance Saturation in Landsat Imagery and Corresponding Solutions to Improve Forest Aboveground Biomass Estimation. Remote Sens. 8, 469. doi:10.3390/rs8060469

Zhou, J., Proisy, C., Descombes, X., Le Maire, G., Nouvellon, Y., Stape, J.-L., Viennois, G., Zerubia, J., Couteron, P., 2013. Mapping local density of young Eucalyptus plantations by individual tree detection in high spatial resolution satellite images. For. Ecol. Manag. 301, 129–141.

Zolkos, S.G., Goetz, S.J., Dubayah, R., 2013. A meta-analysis of terrestrial aboveground biomass estimation using lidar remote sensing. Remote Sens. Environ. 128, 289–298.

5.6 Appendix

Table 5-3. Distribution of forest inventory data among sampling sites. Tree dimensions collected in field plots include the diameter at breast height (*D*), tree height (*H*), trunk height (*Ht*) and crown diameter (*Cd*).

Source	Country	Site	Plot (ha)	Tree dimensions				Taxonomic identification (in %)			
				D	*H*	*Ht*	*Cd*	Species	Genus	Family	unidentified
Bastin et al. (2014)	Congo	Malebo	28	10092	10092	0	0	96,5	3,5	0	0
Unpublished (IRD-AMAP/ENS)	Cameroon	Deng-Deng	15	7847	343	342	42	62,1	17	17	3,9
Unpublished (CIRAD)	French Guyana	Paracou	85	53685	2191	1667	1740	85,3	0	0	14,7
CTFS - Chuyong et al. (2004)	Cameroon	Korup	50	24590	0	0	0	95,8	4	0,2	0
Unpublished (IRD-AMAP/ENS)	Cameroon	Djomedjo	10	4959	505	504	186	65,4	14,4	17,7	2,5
Unpublished (IRD-AMAP/ENS)	Cameroon	Lomié	8	3571	539	128	0	75,5	7,7	11,1	5,7
Unpublished (IRD-AMAP/ENS)	Cameroon	Mabounié	12	4475	592	525	113	53,4	19,2	24,4	3
Unpublished (IRD-AMAP/ENS)	Cameroon	Mindourou I	11	5163	908	559	306	61,6	16,8	15,1	6,5
Unpublished (IRD-AMAP/ENS)	Cameroon	Mindourou II	12	5598	920	667	233	56,4	26,2	11,7	5,7
Unpublished (IRD-AMAP/ENS)	Cameroon	Ngoila	6	2611	126	161	0	69,6	18,5	6,1	5,8
Unpublished (IRD-AMAP/ENS)	Cameroon	Nemeyong	5	2824	260	227	90	65,6	17,2	14,6	2,7
Ploton et al. (2012)	India	Uppangala	15	8220	1729	1722	1728	0	0	0	100[1]
Pargal et al. (submitted)	India	Yellapur	22	9156	5032	0	0	97,8	0,4	0	1,8

[1] AGB values at Uppangala were computed using the average wood density of four 1-ha plots in the area (from Jeyakumar et al., *in press*)

Table 5-4. Importance of predictors (ie. IncMSE, in %) in RF regression models calibrated on simulated canopy scenes. Model m1 is based on FOTO-texture, m2 on Lacunarity-texture, m3 on FOTO- and Lacunarity-texture, m4 all textural indices and the bioclimatic variable E. F-PCA1 and F-PCA2 represent the 2 FOTO-texture indices. L-PCA1 and L-PCA2 represent the 2 Lacunarity-texture indices.

Model	F-PCA1	F-PCA2	L-PCA1	L-PCA2	E
m1	111.99	106.32			
m2			86.71	78.58	
m3	46.19	95.04	61.17	42.68	
m4	45.17	45.82	52.40	36.67	73.43
m4*		65.77	151.83		103.88

"*" indicates that the model went through the variables selection procedure

Table 5-5. Importance of predictors (ie. IncMSE, in %) in RF regression models calibrated on real satellite images. Model m1 is based on FOTO-texture, m2 on Lacunarity-texture, m3 on FOTO- and Lacunarity-texture, m4 all textural indices and the bioclimatic variable E. F-PCA1 and F-PCA2 represent the 2 FOTO-texture indices. L-PCA1 and L-PCA2 represent the 2 Lacunarity-texture indices.

Model	F-PCA1	F-PCA2	L-PCA1	L-PCA2	E
m4	10.45	20.32	10.38	21.22	17.69
m4*		26.23		24.77	25.75

"*" indicates that the model went through the variables selection procedure

6 GENERAL DISCUSSION

In this chapter, I discuss the main findings, limits and perspectives of this thesis with respect to the general thesis objective, which was to improve AGB estimations from field data (tree- and plot-level) and RS data (landscape-level) using information on large trees structure, distribution and spatial organization.

6.1 Estimation of forest AGB from field data

Field-derived estimations of AGB in forest sample plots constitute the bed rock of all forest AGB monitoring methods (both non-spatial and spatial). Identifying the different sources of error associated to those estimations, understanding the mechanisms behind those error sources and attempting to mitigate them is of obvious relevance in the frame of the REDD program. In the current thesis, we focused on the pantropical AGB model recently published in Chave et al. (2014) (of the form $AGB = \alpha * (\rho * D^2 * H)^{\beta}$) since this model, as its predecessor (Chave et al., 2005), is being widely employed by international carbon scientists and managers. Chave et al. (2014) observed a systematic under-estimation of AGB for large trees (≥ 30 Mg) with this model, which is an important drawback since large trees compose most of stand-level AGB stocks (Bastin et al., 2015), drive spatial AGB variations (Slik et al., 2013) and dominate stand-level AGB growth (Stephenson et al., 2014). A central objective of the current work was to better understand the origin of this error, its consequences on forest stand AGB estimations, and to propose a way to mitigate this error. To that end, we assembled a large set of destructive data (i.e. measurements of trees dimensions and destructive estimates of trees AGB), in which most of the largest trees came from our own field work, and studied whether the error pattern of the pantropical model was related to variation in tree structure / morphology (i.e., with respect to crown dimensions and crown contribution to tree AGB). Current allometric theories, in particular the Metabolic Theory of Ecology (MTE), derive constant scaling exponent (β) of tree AGB with *D* and *H* (hence D^2H), at the cost of several simplifying assumptions made on the structure and topology of trees branching network. Attempting to get further insights into what might cause the systematic error on large trees in the pantropical model, we empirically assessed MTE's set of simplifying assumptions, which has not been done so far on large tropical trees and therefore constitute an original contribution of this thesis. Last, the pantropical model error was propagated at the plot-level in tropical forests of contrasted structure and composition, providing practical insights for model users. Overall, chapters 2 and 3 shed some light on the limits of the current pantropical model (and model form) and identify potential improvement avenues.

6.1.1 Driver(s) of pantropical model bias on large trees

The pantropical model form is based on simple geometric arguments: tree mass is wood density (ρ) multiplied by tree volume, and tree volume can be approximated by the volume of a simple geometric solid i.e. D^2H (Chave et al., 2005), leading to eq. 1. In equation 1, *F* is the whole-tree "form factor" (Cannel et al. 1984) which defines the taper of the geometric shape (e.g. from a cylinder to a cone). When equation 1 is adjusted to the data, we set a constant form factor to all trees. In practice, equation 2 is preferred (with $\beta \neq 1$) because it provides a better statistical fit (Chave et al., 2005).

$$AGB = F * \rho * (D^2 * H) \quad \text{(eq. 1)}$$

$$AGB = \alpha * (\rho * D^2 * H)^{\beta} \quad \text{(eq. 2)}$$

In equation 2, the relationship between tree mass and the compound predictor variable is not proportional i.e. we set a $\beta\%$ increase of tree mass per 1% increase of $\rho * D^2 * H$, which can be interpreted as a monotonic change of tree form as the tree change in mass. An important finding of this thesis (chapter 2) is that the distribution of tree mass between trunk and crown is neither constant, nor does it show a monotonic change along the tree mass gradient. This is particularly important because the crown mass ratio (i.e. the proportion of tree aboveground mass in the crown) influences the whole-tree form factor (Cannel et al. 1984). In our dataset (which includes most of the largest trees used in Chave et al. 2014), the crown mass ratio was nearly constant up to a tree mass threshold of 10 Mg, then sharply increased with tree mass. Analyses in chapter 2 demonstrated that this non-linear change in tree structure (i.e. shift in crown mass proportion after 10 Mg) is not capture by the pantropical model and is responsible for the prediction bias observed on large trees. This finding therefore leads us to a new question: **is the observed change in tree structure a systematic, biologically meaningful pattern, or is it a sampling artifact?** In the former case, improving AGB predictions accuracy on large trees would require modifying the form of the pantropical model. We investigated alternative model forms and made a proposition along this line in chapter 2. In the latter case, the prediction bias that we observe on large trees holds to a peculiarity in the structure of those (sampled) trees and would decrease or disappear when the model is applied to a larger (more representative) set of large trees.

The **hypothesis of a sampling bias** has been mentioned by Chave et al. (2014), whom rightfully argued that a "majestic tree sampling bias" may occur, where scientists would preferentially select well-conformed trees. The authors further noticed that most of the largest trees in their dataset were selected in the frame of commercial logging activities (referring to the field work of this thesis), hence those trees must have been particularly well-conformed. I would like to point out that the trees collected in this thesis follow, but do not particularly steer the bias pattern observed in the pantropical model (Figure 6-1). In our analyses, the increase of crown mass proportion among large trees was indeed observed in all sampling sites (Figure 2-1) and was not a peculiarity of our Cameroonian dataset. Confirming or ruling out the sampling bias hypothesis requires sampling more large trees (≥ 10 Mg), which remain dramatically under-represented in the pantropical destructive dataset (c. 3%). Ultimately, this would improve our knowledge of and ability to model pantropical trees biomass allometry, and should therefore be a priority of future field campaigns. In this regard, methods to extract tree volume and biomass from non-destructive terrestrial LiDAR scans are rapidly developing (e.g. Calders et al., 2015; Hackenberg et al., 2014; Raumonen et al., 2013) and may soon revolutionize tree AGB modelling strategies by considerably increasing the size and spatial representativity of tree biomass reference datasets.

In thesis chapter 2, we hypothesized that the greater proportion of crown mass in large trees could reflect an **ontogenetic pattern** associated to the process of tree crown metamorphosis. This hypothesis goes against the MTE which, at the exception of size-dependent scaling between tree diameter and length from seedling to sapling stages, predicts constant scaling exponents between tree dimensions (and biomass) along tree ontogeny (Enquist et al., 2007; Niklas and Spatz, 2004). Yet, several studies have documented changes in crown shape and allometric scaling with tree size among trees > 10 cm *D* (e.g. Antin et al., 2013; Poorter et al., 2003; Smith et al., 2014). A well-documented size-dependent change in crown allometric scaling is known as "crown liberation" (Cusset, 1980): upon

attaining the canopy, a typical tree decreases resources investment in height growth at the benefit of lateral crown expansion, which can be interpreted as a strategy to enhance light capture (hence maximize growth, Poorter et al., 2006) and/or shade and out-competed smaller neighbors (Sterck and Bongers, 2001). Although ontogenetic shifts in allometric scaling of external crown dimensions (i.e. crown diameter, depth) cannot be directly interpreted in terms of biomass, it is reasonable to think that associated changes in inner crown structure (crown "metamorphosis" or "edification" through reiteration, Hallé et al., 1978; Oldeman, 1974), changes in biomechanical constraints once the tree reaches the upper canopy (notably due to wind exposure) and increased carbon allocation to supporting tissues (Loehle, 2016) may modify whole-tree biomass scaling. None of these parameters are included in the MTE, which – for example – implicitly assumes a constant access to light throughout tree ontogeny.

Another hypothesis that has not been evocated in chapter 2 is that the crown mass ratio is dependent of species traits, notably adult stature. Variation in tree allometric relationships with adult stature have been widely documented (e.g. Antin et al., 2013; Bohlman and O'Brien, 2006; King, 1996; Sterck and Bongers, 2001; Yang et al., 2015). In the destructive dataset, the increase of crown mass ratio above 10 Mg is driven by a few canopy and emergent tree species (i.e. capable of producing individuals > 10 Mg). Destructive data recently made available on the tallest African tree species (*Entandrophragma excelsum*) confirm this trend with large *E. excelsum* individuals having high crown mass ratio (c. 80 % for the largest sampled tree, Hemp et al., 2016) and following the bias pattern of the pantropical model (star symbol in Figure 6-1). However, whether there is a non-linear, ontogenic increase of crown mass ratio among large-stature species remain unclear. On *Triplochiton scleroxylon* for instance, a canopy tree species for which enough individuals have been sampled so to look at species-specific trend in the destructive database (i.e. 22 individuals from c. 6 to c. 47 Mg), we did not find any significant breaking-point of crown mass ratio along tree mass. This could indicate that the non-linear increase of crown mass ratio with tree mass applies when all species are pooled, but pooling species may mask species-level patterns that are not necessarily non-linear. Under this hypothesis, it might be more efficient to calibrate the pantropical model per group of species (e.g. based on adult stature) rather than changing the model form.

Besides adult stature, considering species branching patterns might also be relevant to improve pantropical biomass scaling relationships. In chapter 3, we found different scaling relationships between daughter branches cross sections and parent branch cross-section (i.e. area ratio) among species exhibiting different level of apical dominance (or frequency of branch segments along a central, "principal" axis within the crown). Systematic differences in area ratio would, all else being equal, impact species biomass scaling. Apical dominance is usually associated to species growth strategy (fast growing pioneer-like vs slow-growing shade-tolerant species), as it favor faster height growth, influence the overall crown shape (multi-layered vs mono-layered, respectively) and its efficiency at gathering light in different conditions (bright vs shaded environments, respectively) (Horn, 2000, 1971). Among tree species studied in chapter 3, the pioneer to shade tolerant-like gradient that could be established from species apical dominance was well supported by species-level wood density, with a decreasing trend of wood density with increasing apical dominance (i.e. toward fast-growing, cheap-wooded species). It is therefore possible that a species classification based on growth strategies along the sun-shade gradient would capture different patterns of branch organization and associated biomass scaling relationships. Documenting tropical tree species growth strategies and structural development patterns represents a considerable amount of field work, but methodological

development on terrestrial LiDAR technology should soon allow to automatically extract and analyze detailed tree-level information from entire forest stands. It should therefore be possible to document standardized branching pattern-traits for a large number of species and build a global, operational database, much like what have been done with species wood density (Zanne et al., 2009) and multiple other plant morphological characteristics (such as TRY or Cofortraits databases, Bénédet et al., 2014; Kattge et al., 2011). In contrast, it should already be possible to attribute an adult stature group to most tropical tree species based on maximum species D or H observed in forest inventory datasets.

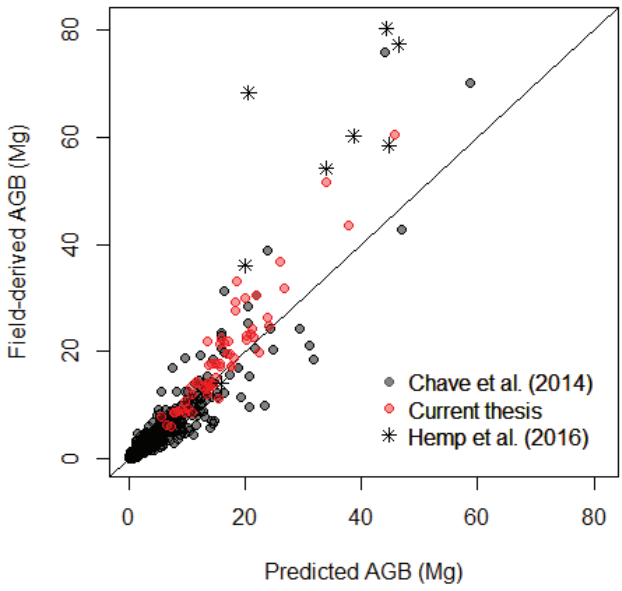

Figure 6-1. Field-derived AGB vs AGB predicted from the pantropical model of Chave et. al (2014). Circles represent the trees of Chave et al. (2014) destructive database, with the red color highlighting the trees sampled in the frame of this thesis. Stars represent *Entandrophragma excelsum* individuals sampled by Hemp et al. (2016).

6.1.2 The influence of forest structure on plot-level AGB modelling error

The interaction between forest structure and AGB model error may influence the estimation of average forest stratum carbon density. If forests in a given stratum are essentially composed of small trees and that the AGB model over-estimate the biomass of those trees (as it is the case with the pantropical model), the average carbon density assigned to the stratum may be biased upward. Inversely, a stratum of old growth, undisturbed forest dominated by large trees may be attributed a carbon density that is biased downward. We investigated this issue in chapter 2, by propagating the pantropical model bias on forest plots established in diverse forest types in the Congo basin. Across all plots (which could correspond to the broad "African tropical rainforest" stratum of the Tier 1 IPCC approach), the median bias was low, of the order of c. +5%. Using a more refined forest stratification (as recommended in the Tier 2 approach), biases on average forest strata estimates are likely to remain low for at least two reasons. First, in absence of very large trees (such as in regrowth forests, degraded forests, or mature forests with light-wooded canopy species), the upward bias limit does not depart much from c. +5% at 1 ha scale (i.e. c. +7.5%, Figure 2-8 B). Second, in forest types containing very

large trees (such as the Atlantic evergreen forests of western Cameroon), forest patches that are mostly composed of very large trees are quiet rare (only 2 out of 130 1-ha plots in our dataset underwent an under-estimation bias higher than -10%, Figure 2-8 B) and, therefore, should not have much influence on average forest stratum carbon density. Our analyses therefore suggested that the pantropical model bias should have relatively little impact on the estimation of forests carbon stock (and stock change) derived from non-spatial monitoring methods (i.e. based on average carbon density per forest strata). While non-spatial methods may provide an accurate estimation of forests carbon stock at relatively large scales (e.g. national, regional), it is likely that spatially-explicit methods will play a prominent role for forest monitoring in the near future, because of the much greater potential of such methods to lower estimations uncertainties (and that at all spatial scales). Contrary to non-spatial methods, spatially explicit carbon mapping methods (e.g. based on remote-sensing data) rely on individual plot-level AGB estimations for signal calibration and should therefore be impacted by plot-level bias. It is easily conceivable that a structure-dependent bias in calibration data would have deleterious effects on our appraisal of a remote-sensing signal ability to discriminate AGB variations (notably when the signal is directly linked to forest structure characteristics, such as crown size repetitions or forest height), and eventually lead to an underestimation of remote-sensing signal error and to a loss of prediction accuracy. On our dataset, the spread of biases at 1 ha scale was far from being negligible (i.e. -15% to +7.7%) and increase when plot sized decreased (e.g. c. -20% to +10% at 0.25 ha scale), indicating that aerial LiDAR studies (which often use field plots ≤ 0.3 ha, e.g. Asner and Mascaro, 2014) might be particularly sensitive to this issue. If the bias of the pantropical model does not emerge from a sampling artifact (as discussed in the previous section), it should be included in error propagation procedures and, given its impact of plot-level AGB estimations, efforts should be made to mitigate it, for instance from complementary field measurements as proposed in chapter 2.

6.2 The influence of forest structure on the canopy texture – AGB relationship

Part of this thesis dealt with the extrapolation of field-plot AGB via canopy texture features from very high spatial resolution optical images. In chapter 4, I presented the Fourier Transform Ordination (FOTO) method and gave a brief synthesis of empirical applications that have been made at local scale (i.e. over a few hundreds square km) on diverse forest types and regions of the world. A major pitfall of the method that emerged from chapter 4 is that the nature and strength of the information carried by FOTO texture features on forest stand structure varies across forest types and sites. In other words, the structure and spatial organization of trees in a forested area influence the relationship between the emerging canopy texture (as described by FOTO) and forest stand structure parameters. In order for canopy texture to be a useful source of information on forest carbon content at larger scale than that of local case studies, it was necessary to identify and integrate the different factors influencing the canopy texture – AGB relationship in the AGB regression model, so to stabilize model predictions (i.e. across forest types and sites).

To that end, I adopted a simulation approach in chapter 5 and investigated how (simulated) canopy texture features translated back into stand structure parameters in forests of contrasted structure and dynamics across the tropics. Given the purpose of this analysis, using simulated forests and canopy scenes was unavoidable, because acquiring real satellite images over multiple sites with a constraint on acquisition angles is costly and, in some areas, simply unfeasible due to persistent clouds cover. Despite the simplicity of trees 3D geometry in our simulations (symmetric, rounded crowns, notably),

this coarse level of realism proved sufficient to reconstruct FOTO canopy texture spectra in mangrove forests (Proisy et al., 2016) and get consistent insights into instrumental effects on canopy texture (Barbier et al., 2011; Barbier and Couteron, 2015). Among the different sampling sites that we studied here, simulated Fourier texture features did not always correlate with the same structure parameters: we often observed a good correlation with the mean tree diameter (*Dg*), but texture features correlated with tree density (*N*) at some sites and with stand basal area (*G*) at others (results not shown in chapter 5), which had consequences for AGB predictions. This instability between FOTO texture metrics and stand structure parameters is consistent with past empirical case studies (chapter 4) and confirms that the assemblage of simple lollipop-like trees is sufficient to study, at least to some extent, the performance and limits of canopy texture-based indices in different ecological contexts, even in *terra firme* forests which are more diverse and structurally complex than mangroves. The "lollipop-tree" approach however reached its limits at some sites where we observed blatant deviations between simulated texture and actual canopy texture in real satellite images. This was particularly the case of Paracou's forests, where individual trees in the highly packed canopy layer were easily discernable in simulated canopies but much less so in real images (as canopy volume was entirely filled with crowns). Using a rigid, simplified (ellipsoidal) crown representation leads to spatial distributions of plant material that are unrealistically clustered (within crowns) and enhances the contrast between shadowed and sunlit parts of tree crowns (Schneider et al., 2014), which artificially increases the performance of texture-based indices in characterizing tree size distribution. FOTO texture on real canopy images of Paracou's forest is, for instance, much less informative on AGB variations that what simulated canopy scenes suggested. Although several simplifying assumptions on tree geometry and optical properties will require further attention in our simulation process (such as leaf area density and its spatial distribution within stands and tree crowns, leaves angles, etc.), incorporating some plasticity in crown shape stood out as the most important step to improve scenes realism.

When pooling all sites together, our analyses nonetheless showed that even with simplified tree crowns shape, FOTO texture indices alone did not accurately capture forest AGB variations (Figure 5-3, F-model). In closed-canopy conditions and when apparent crowns are of fairly homogeneous sizes within unit canopy windows, FOTO texture characterizes the "mean" or "dominant" crown size, which allometrically relates to *Dg* (e.g. Blanchard et al., 2016). FOTO texture indeed correlated well with *Dg* variations in past case studies (e.g. Couteron et al., 2005; Ploton et al., 2012) as well as in most sites studied in chapter 5. Dynamics of *N*, *Dg* and *G* (which is a strong predictor of AGB) along forest development have been generalized in the well-known self-thinning theory (Reineke, 1933), which predicts a gradual decrease of *N* and a concomitant increase of *Dg* and *G* as forest ages. The parameters of self-thinning trajectories (intercept and slope) vary with tree crown and height allometric relationships (Gül et al., 2005; Sterba and Monserud, 1993) which constrain the number of "average trees" that can fit into a given area. If multi-specific canopy tree crown allometric relationships are relatively stable across tropical forest sites (Blanchard et al., 2016), total forest height and tree height allometry show important spatial variation driven by climate and soil (Banin et al., 2012; Chave et al., 2014; Feldpausch et al., 2012; Ouédraogo et al., 2016), local topography (Yang et al., 2016) and stand structure (Molto et al., 2014), notably. It is therefore not surprising that relationships between texture features and stand structure varies across sites with local forest dynamics, local allometries and

perhaps sampling intensity. At some sites, the slope of the self-thinning trajectory did not deviate much from *G* isoline (see Paracou *vs* Deng-Deng in Figure 6-2), so FOTO texture correlated well with *N* gradients but variation of *G* might be more elusive to capture (as in Couteron et al., 2005). In other sites, sample plots captured large forest aggradation gradients, even at local scale (as in Deng-Deng, Figure 6-2), with little or inconsistent *N* variation with increasing *Dg*, hence FOTO texture correlated well with *G* and AGB (as in Ploton et al., 2012). It follows that FOTO texture alone (or *Dg* itself) is not sufficient to consistently capture the dynamic of forest structure when several sites are pulled together, and complementary structural predictors must be accounted for. A very similar issue occurs with LiDAR data as LiDAR-derived forest height is only one piece of the AGB puzzle and cannot consistently depict AGB variation at large scale, unless it is associated to an additional layer of information on forest structure, notably on forest *G* (as in Asner et al., 2011). In chapter 5, we associated to FOTO texture a bioclimatic stress proxy (*E*, Chave et al., 2014) so to capture inter-site variation in tree height allometry in the AGB regression model (hence, to some extent, self-thinning lines parameters). The *E* variable largely improve model fit at the pantropical scale (i.e. on simulated scenes) but its contribution to the AGB regression model naturally decreased at the local scale of our final case study, since the control of climate on tree allometry occurs at a macro-scale. Refining the stratification of forest potential height (or site carrying capacity) and tree slenderness so to detect variations at smaller spatial scales that what can be obtained from climate-related variables is a key research perspective to improve texture-based forest AGB mapping. The recent study of Yang et al. (2016) suggested that together with climate and soil, topography heterogeneity (at 50-100 km² scale) conveys a large share of information on macro-scale variation of tropical forests dominant height. At much smaller spatial scales (over a few tens or hundreds of ha), several studies have also shown that terrain heterogeneity increases spatial variability of forest AGB (e.g. Réjou-Méchain et al., 2014; Véga et al., 2015), and spatial autocorrelation typically found in LiDAR-AGB model residuals is often though to derive from small-scale variation in trees height allometry (e.g. Réjou-Méchain et al., 2015), which possibly reflect local terrain conditions (at least to some extent). Since topography-related parameters can be computed at 30- or 90-m resolutions from a freely available data sources (i.e. SRTM, available from NASA), and that over national, regional or even global scale given current computational means, future researches should test whether including such type of covariates improves texture-based forest AGB predictions.

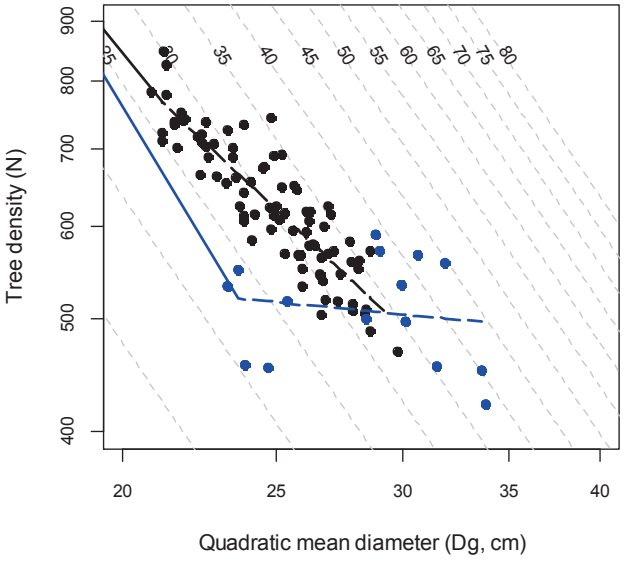

Figure 6-2. Tree density (N) against quadratic mean diameter (Dg) at two sites (black: Paracou, blue: Deng-Deng). Grey dot lines represent basal area (G) isolines.

Besides variation in canopy trees allometry, canopy openness / gaps also influence the interplay between *N*, *Dg*, *G* and AGB across forest stands (as described in the self-thinning theory when stands deviate from asymptotic density). The gap fraction (or proportion of gaps per unit area) have indeed shown to be an important parameter to account for when developing "generalized" (i.e. multi-site) forest AGB model form based on aerial LiDAR data (Bouvier et al., 2015). An important pitfall of FOTO

texture is that it cannot discriminate between tree crowns and gaps. Besides, forests canopies that are too open (such as *Maranthaceae* forests) and/or heterogeneous in vertical and horizontal structure usually display aperiodic canopy grains that are not properly characterized and discriminated by FOTO. An important finding of our simulated experiment is that lacunarity analysis of canopy texture, which have shown in our study and elsewhere to correlate with canopy openness and heterogeneity (Frazer et al., 2005; Malhi and Román-Cuesta, 2008), provides an information that is complementary to FOTO texture. Combining FOTO texture and lacunarity texture features indeed largely improved AGB model fit across sites (Figure 5-3, FL-model), but also among some sites where FOTO alone led to poor results (which was typically the case of aperiodic canopies from Yellapur, results not shown). This last result is very encouraging. In some of the forest sites considered in chapter 5, structure parameters of sample plots did not clearly represent self-thinning trajectories (as Deng-Deng in Figure 6-2) but rather suggested forest landscapes composed of complex mosaics of patches undergoing different dynamics, perhaps due to different times since last disturbance, variation in local species composition and/or local abiotic conditions. These strong, local variations in forest structural profile (and emerging canopy texture) go hand in hand with a high local variability in forest AGB, as observed in other mature tropical forests (see for instance Guitet et al., 2015; Réjou-Méchain et al., 2014). When spatial changes in canopy texture are not gradual in the landscape (contrary to mangrove forests, Proisy et al., 2007) but rather a "salt-and-paper" mosaic of small patches, chances are that canopy texture intercepted by 1 ha unit windows display some level of heterogeneity. At the Uppangala site for example, Ploton et al. (2012) reported a strong relationship between FOTO texture and AGB (R^2 of c. 0.78), but we specifically targeted the few large forest patches (≥ 4-ha) displaying homogeneous grain size in the area to establish calibration plots. This sampling strategy was motivated, at the time, by the will to mitigate the effect plots geolocation error on texture-AGB relationship. I suspect however that it hided the spurious effect of canopy heterogeneity on FOTO texture-AGB, and that the actual predictive accuracy of the published model over the (heterogeneous) local forest mosaic is substantially lower than what calibration fit metrics indicated. A similar issue occurs at several locations of south-eastern Cameroon where the high heterogeneity of forests structure and texture at small spatial scales did not enable us so far to find a significant relationship between FOTO texture features and stand AGB (pers. com. with Dr. N. Barbier), which is in line with our final case studies of chapter 5 (i.e. when FOTO texture alone was used). Although validating the added-value of the FOTO-lacunarity combination over the traditional FOTO method will require multiple empirical assessments, the case study that we performed confirmed the potential of the approach, as field plots AGB estimates were inferred with reasonable accuracy and precision. If the approach proves relevant, an obvious step to take on would be to propagate field plots AGB error into the texture-based model.

Over the past 15 years, canopy texture analysis from very high resolution (VHR) optical data have demonstrated its ability to retrieve quantitative information on forest structure and AGB at local scale, from various satellite sensors (Quickbird, GeoEye, IKONOS, SPOT-5) and aerial images (e.g. Bastin et al., 2014; Ploton et al., 2012; Singh et al., 2015, 2014). In the study undertook in chapter 5, we clarified some of the discrepancies observed between texture features and stand structure in past case studies, and showed that it should be possible to develop a sounded, steady AGB inversion frame for broad scale forest assessments. The recent launch of SPOT 6 and 7 (providing images up to 60 * 600 km in stable configuration), the rapid deployment of cubesat constellations (suggesting that near-real time VHR monitoring of Earth is not too far off, Marvin et al., 2016), the progress being made on simultaneous texture analysis of multiple images (Barbier et al., 2011; Barbier and Couteron, 2015),

indicate that texture features from VHR imagery could play a key role in the REDD monitoring program. Beyond the refinement of forest emission factors, producing fine resolution biomass maps at large scale would help us improve our understanding of topical forest biomass variation and the relative contribution of climate, soil, topography and disturbances at various scales.

6.3 Key thesis findings

The main results obtained in the present thesis are the following:

- The negative prediction bias of the pantropical tree biomass model on large trees pertains to a systematic change in tree form with tree size: the contribution of crown to total tree mass sharply increased on sampled trees ≥ 10 Mg (chapter 2) ;
- Accounting for proxies of crown dimensions (diameter, depth) allowed building an unbiased generic tree biomass model, but it did not substantially increase model precision (chapter 2).
- Species with contrasted patterns of branch organization exhibited different scaling ; relationships in crown structure (paper 3) ; this suggests that a classification based on how species fill-in the 3D crown volume – in light of species growth strategies for example – may be used to improve the precision of tree generic biomass models ;
- The bias of the pantropical tree biomass model propagates a systematic error at the plot level that varies with stand structure (from c. -15 % to c. +8 % of mean plot biomass on our network of 1-ha plots in central Africa) and increases as plot size decreases (up to c. -25 % for 0.1 subplots) (chapter 2) ; this error source (i.e. interaction between model error and stand structure) is overlooked in published error propagation procedures ;
- Canopy textural properties from very high resolution optical images can be used to extrapolate forest plot biomass estimations, but a simple simulation procedure showed that the nature and strength of texture – biomass relationship varies between forest sites, in agreement with previous empirical findings (chapter 4) ;
- Based on simulations of a large set of tropical forest plots, our analyses showed that (chapter 5) :
    - While Fourier analysis of forest canopy images do not capture canopy openness, lacunarity analysis does. Combining both types of analyses provided a more comprehensive picture of forest structure, hence improved biomass predictions ;
    - Accounting for a bioclimatic proxy of forest height, which cannot be retrieved from 2D analyses of forest canopy images, further improved biomass model predictions ;
- While the classical Fourier-based analysis failed to predict forest biomass variations on a mosaic of high-biomass forests in central Africa, our generalized biomass model gave an R^2 of c. 0.6 and a RMSE of c. 62 $Mg.ha^{-1}$ (chapter 5), suggesting that broad-scale monitoring of tropical forests biomass from very-high resolution images may not be too far off.

6.4 Reference

Antin, C., Pélissier, R., Vincent, G., Couteron, P., 2013. Crown allometries are less responsive than stem allometry to tree size and habitat variations in an Indian monsoon forest. Trees 27, 1485–1495. doi:10.1007/s00468-013-0896-7

Asner, G.P., Mascaro, J., 2014. Mapping tropical forest carbon: Calibrating plot estimates to a simple LiDAR metric. Remote Sens. Environ. 140, 614–624.

Asner, G.P., Mascaro, J., Muller-Landau, H.C., Vieilledent, G., Vaudry, R., Rasamoelina, M., Hall, J.S., Breugel, M. van, 2011. A universal airborne LiDAR approach for tropical forest carbon mapping. Oecologia 168, 1147–1160. doi:10.1007/s00442-011-2165-z

Banin, L., Feldpausch, T.R., Phillips, O.L., Baker, T.R., Lloyd, J., Affum-Baffoe, K., Arets, E.J.M.M., Berry, N.J., Bradford, M., Brienen, R.J.W., Davies, S., Drescher, M., Higuchi, N., Hilbert, D.W., Hladik, A., Iida, Y., Salim, K.A., Kassim, A.R., King, D.A., Lopez-Gonzalez, G., Metcalfe, D., Nilus, R., Peh, K.S.-H., Reitsma, J.M., Sonké, B., Taedoumg, H., Tan, S., White, L., Wöll, H., Lewis, S.L., 2012. What controls tropical forest architecture? Testing environmental, structural and floristic drivers. Glob. Ecol. Biogeogr. 21, 1179–1190. doi:10.1111/j.1466-8238.2012.00778.x

Barbier, N., Couteron, P., 2015. Attenuating the bidirectional texture variation of satellite images of tropical forest canopies. Remote Sens. Environ. 171, 245–260. doi:10.1016/j.rse.2015.10.007

Barbier, N., Proisy, C., Véga, C., Sabatier, D., Couteron, P., 2011. Bidirectional texture function of high resolution optical images of tropical forest: An approach using LiDAR hillshade simulations. Remote Sens. Environ. 115, 167–179.

Bastin, J.-F., Barbier, N., Couteron, P., Adams, B., Shapiro, A., Bogaert, J., De Cannière, C., 2014. Aboveground biomass mapping of African forest mosaics using canopy texture analysis: toward a regional approach. Ecol. Appl. 24, 1984–2001.

Bastin, J.-F., Barbier, N., Réjou-Méchain, M., Fayolle, A., Gourlet-Fleury, S., Maniatis, D., de Haulleville, T., Baya, F., Beeckman, H., Beina, D., 2015. Seeing Central African forests through their largest trees. Sci. Rep. 5.

Bénédet, F., Vincke, D., Fayolle, A., Doucet, F., Gourlet-Fleury, S., 2014. Cofortraits, African plant traits information database. version 1.0 [WWW Document]. URL http://coforchan ge.cirad.fr/ african_plant_trait (accessed 1.1.16).

Blanchard, E., Birnbaum, P., Ibanez, T., Boutreux, T., Antin, C., Ploton, P., Vincent, G., Pouteau, R., Vandrot, H., Hequet, V., 2016. Contrasted allometries between stem diameter, crown area, and tree height in five tropical biogeographic areas. Trees 1–16.

Bohlman, S., O'Brien, S., 2006. Allometry, adult stature and regeneration requirement of 65 tree species on Barro Colorado Island, Panama. J. Trop. Ecol. 22, 123–136.

Bouvier, M., Durrieu, S., Fournier, R.A., Renaud, J.-P., 2015. Generalizing predictive models of forest inventory attributes using an area-based approach with airborne LiDAR data. Remote Sens. Environ. 156, 322–334. doi:10.1016/j.rse.2014.10.004

Calders, K., Newnham, G., Burt, A., Murphy, S., Raumonen, P., Herold, M., Culvenor, D., Avitabile, V., Disney, M., Armston, J., Kaasalainen, M., 2015. Nondestructive estimates of above-ground biomass using terrestrial laser scanning. Methods Ecol. Evol. 6, 198–208. doi:10.1111/2041-210X.12301

Chave, J., Andalo, C., Brown, S., Cairns, M.A., Chambers, J.Q., Eamus, D., Fölster, H., Fromard, F., Higuchi, N., Kira, T., Lescure, J.-P., Nelson, B.W., Ogawa, H., Puig, H., Riéra, B., Yamakura, T., 2005. Tree allometry and improved estimation of carbon stocks and balance in tropical forests. Oecologia 145, 87–99. doi:10.1007/s00442-005-0100-x

Chave, J., Réjou-Méchain, M., Búrquez, A., Chidumayo, E., Colgan, M.S., Delitti, W.B.C., Duque, A., Eid, T., Fearnside, P.M., Goodman, R.C., Henry, M., Martínez-Yrízar, A., Mugasha, W.A., Muller-Landau, H.C., Mencuccini, M., Nelson, B.W., Ngomanda, A., Nogueira, E.M., Ortiz-Malavassi, E., Pélissier, R., Ploton, P., Ryan, C.M., Saldarriaga, J.G., Vieilledent, G., 2014. Improved

allometric models to estimate the aboveground biomass of tropical trees. Glob. Change Biol. 20, 3177–3190. doi:10.1111/gcb.12629
Couteron, P., Pelissier, R., Nicolini, E.A., Paget, D., 2005. Predicting tropical forest stand structure parameters from Fourier transform of very high-resolution remotely sensed canopy images. J. Appl. Ecol. 42, 1121–1128.
Cusset, G., 1980. Sur des paramétres intervenant dans la croissance des arbres. La relation hauteur/diametre de l'axe primaire aerien. Candollea.
Enquist, B.J., Allen, A.P., Brown, J.H., Gillooly, J.F., Kerkhoff, A.J., Niklas, K.J., Price, C.A., West, G.B., 2007. Biological scaling: Does the exception prove the rule? Nature 445, E9–E10. doi:10.1038/nature05548
Feldpausch, T.R., Lloyd, J., Lewis, S.L., Brienen, R.J., Gloor, M., Monteagudo Mendoza, A., Lopez-Gonzalez, G., Banin, L., Abu Salim, K., Affum-Baffoe, K., 2012. Tree height integrated into pantropical forest biomass estimates. Biogeosciences 3381–3403.
Frazer, G.W., Wulder, M.A., Niemann, K.O., 2005. Simulation and quantification of the fine-scale spatial pattern and heterogeneity of forest canopy structure: A lacunarity-based method designed for analysis of continuous canopy heights. For. Ecol. Manag. 214, 65–90.
Guitet, S., Hérault, B., Molto, Q., Brunaux, O., Couteron, P., 2015. Spatial structure of above-ground biomass limits accuracy of carbon mapping in rainforest but large scale forest inventories can help to overcome. PloS One 10, e0138456.
Gül, A.U., Misir, M., Misir, N., Yavuz, H., 2005. Calculation of uneven-aged stand structures with the negative exponential diameter distribution and Sterba's modified competition density rule. For. Ecol. Manag. 214, 212–220. doi:10.1016/j.foreco.2005.04.012
Hackenberg, J., Morhart, C., Sheppard, J., Spiecker, H., Disney, M., 2014. Highly accurate tree models derived from terrestrial laser scan data: A method description. Forests 5, 1069–1105.
Hallé, F., Oldeman, R.A.A., Tomlinson, P.B., 1978. Tropical trees and forests: an architectural analysis. Springer Verl. Berl. Heidelb. doi:10.1007/978-3-642-81190-6
Hemp, A., Zimmermann, R., Remmele, S., Pommer, U., Berauer, B., Hemp, C., Fischer, M., 2016. Africa's highest mountain harbours Africa's tallest trees. Biodivers. Conserv. doi:10.1007/s10531-016-1226-3
Horn, H.S., 2000. Twigs, trees, and the dynamics of carbon in the landscape. Scaling Biol. 199–220.
Horn, H.S., 1971. The adaptive geometry of trees. Princeton University Press.
Kattge, J., Diaz, S., Lavorel, S., Prentice, I.C., Leadley, P., Bönisch, G., Garnier, E., Westoby, M., Reich, P.B., Wright, I.J., 2011. TRY–a global database of plant traits. Glob. Change Biol. 17, 2905–2935.
King, D.A., 1996. Allometry and life history of tropical trees. J. Trop. Ecol. 12, 25–44.
Loehle, C., 2016. Biomechanical constraints on tree architecture. Trees. doi:10.1007/s00468-016-1433-2
Malhi, Y., Román-Cuesta, R.M., 2008. Analysis of lacunarity and scales of spatial homogeneity in IKONOS images of Amazonian tropical forest canopies. Remote Sens. Environ. 112, 2074–2087.
Marvin, D.C., Koh, L.P., Lynam, A.J., Wich, S., Davies, A.B., Krishnamurthy, R., Stokes, E., Starkey, R., Asner, G.P., 2016. Integrating technologies for scalable ecology and conservation. Glob. Ecol. Conserv. 7, 262–275. doi:10.1016/j.gecco.2016.07.002
Molto, Q., Hérault, B., Boreux, J.-J., Daullet, M., Rousteau, A., Rossi, V., 2014. Predicting tree heights for biomass estimates in tropical forests – a test from French Guiana. Biogeosciences 11, 3121–3130. doi:10.5194/bg-11-3121-2014
Niklas, K.J., Spatz, H.-C., 2004. Growth and hydraulic (not mechanical) constraints govern the scaling of tree height and mass. Proc. Natl. Acad. Sci. U. S. A. 101, 15661–15663.
Oldeman, R., 1974. L'architecture de la forêt guyanaise, Mémoires ORSTOM. ORSTOM, Paris.
Ouédraogo, D.-Y., Fayolle, A., Gourlet-Fleury, S., Mortier, F., Freycon, V., Fauvet, N., Rabaud, S., Cornu, G., Bénédet, F., Gillet, J.-F., Oslisly, R., Doucet, J.-L., Lejeune, P., Favier, C., 2016. The determinants of tropical forest deciduousness: disentangling the effects of rainfall and geology in central Africa. J. Ecol. doi:10.1111/1365-2745.12589

Ploton, P., Pélissier, R., Proisy, C., Flavenot, T., Barbier, N., Rai, S.N., Couteron, P., 2012. Assessing aboveground tropical forest biomass using Google Earth canopy images. Ecol. Appl. 22, 993–1003. doi:10.1890/11-1606.1

Poorter, L., Bongers, F., Sterck, F.J., Wöll, H., 2003. Architecture of 53 rain forest tree species differing in adult stature and shade tolerance. Ecology 84, 602–608. doi:10.1890/0012-9658(2003)084[0602:AORFTS]2.0.CO;2

Poorter, L., Bongers, L., Bongers, F., 2006. Architecture of 54 moist-forest tree species: traits, trade-offs, and functional groups. Ecology 87, 1289–1301. doi:10.1890/0012-9658(2006)87[1289:AOMTST]2.0.CO;2

Proisy, C., Couteron, P., Fromard, F., 2007. Predicting and mapping mangrove biomass from canopy grain analysis using Fourier-based textural ordination of IKONOS images. Remote Sens. Environ. 109, 379–392.

Proisy, C., Féret, J.-B., Lauret, N., Gastellu-Etchegorry, J.-P., 2016. Mangrove forest dynamics using very high spatial resolution optical remote sensing., in: Remote Sensing of Land Surfaces: Urban and Coastal Area. N.N. Baghdadi & M. Zribi, Paris, pp. 274–300.

Raumonen, P., Kaasalainen, M., Åkerblom, M., Kaasalainen, S., Kaartinen, H., Vastaranta, M., Holopainen, M., Disney, M., Lewis, P., 2013. Fast Automatic Precision Tree Models from Terrestrial Laser Scanner Data. Remote Sens. 5, 491–520. doi:10.3390/rs5020491

Reineke, L.H., 1933. Perfecting a stand-density index for even-aged forests.

Réjou-Méchain, M., Muller-Landau, H.C., Detto, M., Thomas, S.C., Le Toan, T., Saatchi, S.S., Barreto-Silva, J.S., Bourg, N.A., Bunyavejchewin, S., Butt, N., Brockelman, W.Y., Cao, M., Cárdenas, D., Chiang, J.-M., Chuyong, G.B., Clay, K., Condit, R., Dattaraja, H.S., Davies, S.J., Duque, A., Esufali, S., Ewango, C., Fernando, R.H.S., Fletcher, C.D., Gunatilleke, I.A.U.N., Hao, Z., Harms, K.E., Hart, T.B., Hérault, B., Howe, R.W., Hubbell, S.P., Johnson, D.J., Kenfack, D., Larson, A.J., Lin, L., Lin, Y., Lutz, J.A., Makana, J.-R., Malhi, Y., Marthews, T.R., McEwan, R.W., McMahon, S.M., McShea, W.J., Muscarella, R., Nathalang, A., Noor, N.S.M., Nytch, C.J., Oliveira, A.A., Phillips, R.P., Pongpattananurak, N., Punchi-Manage, R., Salim, R., Schurman, J., Sukumar, R., Suresh, H.S., Suwanvecho, U., Thomas, D.W., Thompson, J., Uríarte, M., Valencia, R., Vicentini, A., Wolf, A.T., Yap, S., Yuan, Z., Zartman, C.E., Zimmerman, J.K., Chave, J., 2014. Local spatial structure of forest biomass and its consequences for remote sensing of carbon stocks. Biogeosciences 11, 6827–6840. doi:10.5194/bg-11-6827-2014

Réjou-Méchain, M., Tymen, B., Blanc, L., Fauset, S., Feldpausch, T.R., Monteagudo, A., Phillips, O.L., Richard, H., Chave, J., 2015. Using repeated small-footprint LiDAR acquisitions to infer spatial and temporal variations of a high-biomass Neotropical forest. Remote Sens. Environ. 169, 93–101.

Schneider, F.D., Leiterer, R., Morsdorf, F., Gastellu-Etchegorry, J.-P., Lauret, N., Pfeifer, N., Schaepman, M.E., 2014. Simulating imaging spectrometer data: 3D forest modeling based on LiDAR and in situ data. Remote Sens. Environ. 152, 235–250. doi:10.1016/j.rse.2014.06.015

Singh, M., Evans, D., Friess, D.A., Tan, B.S., Nin, C.S., 2015. Mapping Above-Ground Biomass in a Tropical Forest in Cambodia Using Canopy Textures Derived from Google Earth. Remote Sens. 7, 5057–5076. doi:10.3390/rs70505057

Singh, M., Malhi, Y., Bhagwat, S., 2014. Biomass estimation of mixed forest landscape using a Fourier transform texture-based approach on very-high-resolution optical satellite imagery. Int. J. Remote Sens. 35, 3331–3349. doi:10.1080/01431161.2014.903441

Slik, J.W., Paoli, G., McGuire, K., Amaral, I., Barroso, J., Bastian, M., Blanc, L., Bongers, F., Boundja, P., Clark, C., 2013. Large trees drive forest aboveground biomass variation in moist lowland forests across the tropics. Glob. Ecol. Biogeogr. 22, 1261–1271.

Smith, D.D., Sperry, J.S., Enquist, B.J., Savage, V.M., McCulloh, K.A., Bentley, L.P., 2014. Deviation from symmetrically self-similar branching in trees predicts altered hydraulics, mechanics, light interception and metabolic scaling. New Phytol. 201, 217–229. doi:10.1111/nph.12487

Stephenson, N.L., Das, A.J., Condit, R., Russo, S.E., Baker, P.J., Beckman, N.G., Coomes, D.A., Lines, E.R., Morris, W.K., Rüger, N., Álvarez, E., Blundo, C., Bunyavejchewin, S., Chuyong, G., Davies, S.J.,

Duque, Á., Ewango, C.N., Flores, O., Franklin, J.F., Grau, H.R., Hao, Z., Harmon, M.E., Hubbell, S.P., Kenfack, D., Lin, Y., Makana, J.-R., Malizia, A., Malizia, L.R., Pabst, R.J., Pongpattananurak, N., Su, S.-H., Sun, I.-F., Tan, S., Thomas, D., van Mantgem, P.J., Wang, X., Wiser, S.K., Zavala, M.A., 2014. Rate of tree carbon accumulation increases continuously with tree size. Nature 507, 90–93. doi:10.1038/nature12914

Sterba, H., Monserud, R.A., 1993. The maximum density concept applied to uneven-aged mixed-species stands. For. Sci. 39, 432–452.

Sterck, F.J., Bongers, F., 2001. Crown development in tropical rain forest trees: patterns with tree height and light availability. J. Ecol. 89, 1–13. doi:10.1046/j.1365-2745.2001.00525.x

Véga, C., Vepakomma, U., Morel, J., Bader, J.-L., Rajashekar, G., Jha, C.S., Ferêt, J., Proisy, C., Pélissier, R., Dadhwal, V.K., 2015. Aboveground-Biomass Estimation of a Complex Tropical Forest in India Using Lidar. Remote Sens. 7, 10607–10625.

Yang, X.-D., Yan, E.-R., Chang, S.X., Da, L.-J., Wang, X.-H., 2015. Tree architecture varies with forest succession in evergreen broad-leaved forests in Eastern China. Trees 29, 43–57. doi:10.1007/s00468-014-1054-6

Yang, Y., Saatchi, S., Xu, L., Yu, Y., Lefsky, M., White, L., Knyazikhin, Y., Myneni, R., 2016. Abiotic Controls on Macroscale Variations of Humid Tropical Forest Height. Remote Sens. 8, 494. doi:10.3390/rs8060494

Zanne, A.E., Lopez-Gonzalez, G., Coomes, D.A., Ilic, J., Jansen, S., Lewis, S.L., Miller, R.B., Swenson, N.G., Wiemann, M.C., Chave, J., 2009. Global wood density database.

Résumé étendu (Extended summary in French)

Amélioration des estimations de biomasse des forêts tropicales : apport de la structure et de l'organisation spatiale des arbres de canopée

Pierre Ploton

IRD-UMR AMAP/ AgroParisTech, Montpellier (France)
Technische Universitat Dresden (Allemagne)

Mots clés : carbone forestier, REDD, modèle de biomasse pantropical, structure de canopée, texture de canopée, imagerie optique passive, transformée de Fourier, lacunarité

Introduction

L'inquiétude grandissante autour des effets du changement climatique global a mené à l'émergence de politiques internationales visant à suivre et à gérer durablement les stocks de carbone séquestrés par la végétation terrestre, et en particulier par les forêts tropicales (REDD+). La déforestation et la dégradation de ces forêts associées au développement économique des pays sont en effet considérées comme étant la deuxième source la plus importante d'émission de dioxyde de carbone d'origine anthropique de ces dernières décennies. L'initiative REDD+ repose en partie sur notre capacité à quantifier avec exactitude et précision les stocks de carbone forestier à diverses échelles spatiales (ex. province, pays, bassin forestier), et ce de façon répétée (suivi temporel), ce qui constitue un chalenge scientifique et technique majeur. Une approche classique consiste à cartographier le carbone forestier, ou la biomasse forestière épigée (AGB, un proxy fréquemment utilisé), en extrapolant des estimations d'AGB locales (i.e. réalisées au sein de parcelles d'inventaire, étape 1) au moyen de données de télédétection (étape 2). Ces deux étapes impliquent l'utilisation de modèles biophysiques plus ou moins performants dont les erreurs, qui ne sont pas totalement connues et maitrisées, se propagent jusqu'aux estimations finales. L'amélioration des ces modèles soulève un certain nombre de questions à l'interface entre la biomécanique, l'architecture et l'écologie des espèces d'arbre, l'organisation des peuplements forestiers et le traitement du signal, notamment. Dans cette thèse, nous nous sommes intéressés aux deux étapes de la chaine de traitement en focalisant notre attention sur les grands arbres de canopée. Cette attention particulière nous est apparue pertinente à la fois parce que les grands arbres représentent la majeure partie de la biomasse d'un peuplement forestier mais également parce que ces arbres sont visibles sur les images satellitaires optiques utilisées dans ce travail.

Deux objectifs principaux ont guidé notre étude. Le premier était de mieux comprendre la contribution des grands arbres à l'erreur d'un modèle pantropical de biomasse populaire au sein de la communauté scientifique internationale et de mieux intégrer leurs particularités structurelles dans un nouveau modèle. Le deuxième objectif visait à améliorer une méthode d'extrapolation de la biomasse basée sur les

propriétés de texture d'images satellites optiques à très haute résolution spatiale par une meilleure prise en compte des variations de l'organisation des grands arbres de canopée entre types de forêt.

L'une des originalités de ce travail tient sans aucun doute au travail de terrain qui a été réalisé. Couper et peser des arbres pour développer des modèles de biomasse est un travail notoirement difficile, a fortiori quand les arbres sont de grande taille. Dans le cadre de cette thèse, 77 grands arbres de canopée ont été pesés, parmi lesquels 17 des 30 plus grands arbres de la base de données pantropicale. J'ai également participé à l'établissement de près de 80 parcelles d'inventaire de 1-ha en Afrique centrale au cours des années précédent ma thèse et durant ma thèse (Figure 1). Ce travail d'échantillonnage important m'a permis d'asseoir mes analyses sur tout un panel de peuplements aux structures et organisations spatiales contrastées, que ce soit pour étudier la propagation de l'erreur des modèles allométriques à l'échelle des parcelles, ou le potentiel des indices de texture de canopée pour caractériser la biomasse des peuplements.

Une seconde originalité de ce travail vient probablement aussi de l'ancrage des analyses et réflexions dans des approches théoriques. Au-delà de l'établissement de modèles de biomasse empiriques, les données destructives ont par exemple été utilisées pour tester des hypothèses fondamentales de la Théorie Métabolique de l'Ecologie. Le modèle de télédétection visant à inverser la biomasse des peuplements à partir des propriétés de texture des canopées a, quant à lui, été développé via une approche de représentation simplifiée des arbres et des peuplements, de façon à conduire les analyses dans un cadre maitrisé et donner aux résultats une portée assez générale.

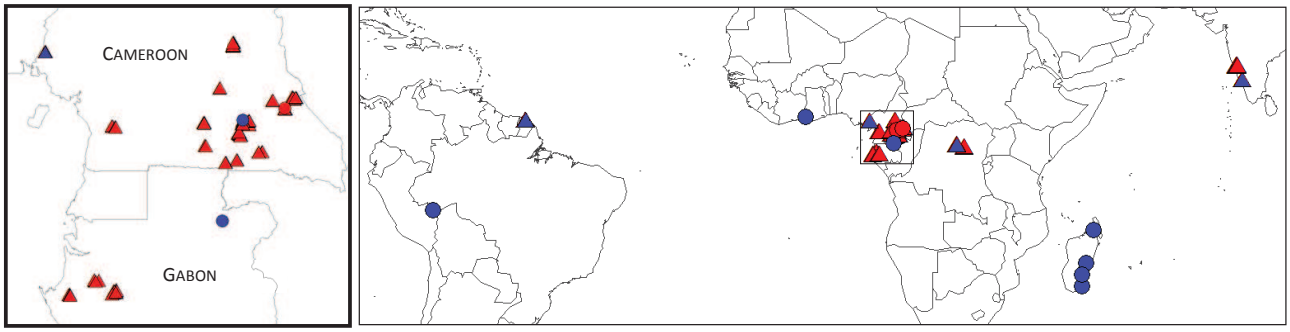

Figure 1. Distribution spatiale des jeux de données utilisés. Les points et les triangles représentent les sites où des arbres ont été coupés/pesés et les sites où des parcelles d'inventaire ont été établies, respectivement. La couleur rouge indique que les données ont été collectées par l'IRD. La couleur bleue indique que les données proviennent de la littérature, d'institutions ou de chercheurs partenaires.

Le manuscrit de thèse est structuré en 6 chapitres incluant :

1. Une introduction décrivant le contexte général et les enjeux scientifiques. Les objectifs de recherche y sont détaillés, ainsi que les jeux de données utilisés et l'organisation du manuscrit.
2. Une étude de l'influence de la forme des grands arbres, en particulier des dimensions des couronnes, sur l'erreur du modèle de biomasse pantropical. Nous quantifions également la propagation de l'erreur de ce modèle à l'échelle des parcelles forestières, et proposons un modèle alternatif prenant mieux en compte les variations physionomiques des arbres. Ce travail a été publié dans le journal Biogeosciences.

3. Une étude exploratoire sur les propriétés de structure des couronnes des grands arbres pouvant expliquer l'écart entre la biomasse de ces arbres et les prédictions du modèle pantropicale évoqué en 2. Une évaluation empirique d'hypothèses de la Théorie Métabolique de l'Ecologie sur la structure des couronnes est fournie.
4. Une synthèse sur les fondements de la méthode FOTO i.e. une méthode visant à décrire les gradients de structure et de biomasse des peuplements forestiers sur base des propriétés de texture d'images optiques à très haute résolution spatiale. Une synthèse des résultats de cas d'étude sur différents types de forêts est donnée et met en exergue le potentiel de l'approche mais également ses limites pour la caractérisation de la biomasse à large échelle. Ce chapitre a été publié dans le livre *Treetops at Risk* (Springer).
5. Une étude présentant un modèle d'inversion de biomasse à large échelle basée sur les propriétés de texture des canopées. Une approche par simulation, incluant la production de maquettes forestières tridimensionnelles et l'utilisation d'un modèle de transfert radiatif, est utilisée pour investiguer le potentiel de métriques de texture complémentaires à celles de FOTO pour palier aux limites identifiées en 4. Un modèle de biomasse « généralisé » est proposé. Cette étude est en cours de révision dans le journal *Remote Sensing of Environment*.

Voici un résumé étendu des 5 derniers chapitres.

Chapitre 2. Modèle allométrique pantropical de biomasse: vers une prise en compte des variations de masse dans les couronnes

Dans la mesure où les estimations de biomasses faites dans les parcelles d'inventaires sont à la base des chaines de modélisation/cartographie du carbone forestier, il est particulièrement important de bien connaitre les erreurs associées à ces estimations et, autant que possible, de les réduire. La biomasse d'une parcelle forestière est obtenue en sommant la biomasse des arbres qui la compose. A l'échelle de l'arbre, les modèles de biomasses les plus performants combinent le diamètre du tronc, la hauteur de l'arbre et la densité du bois. Un modèle de biomasse pantropical, qui combine ces trois prédicteurs, a les faveurs des scientifiques et gestionnaires des forêts tropicales depuis plus d'une dizaine d'années, et restera sans doute une référence pour les années à venir. Néanmoins, ce modèle présente une sous-estimation systématique de la biomasse des grands arbres. Etant donné l'importance des grands arbres dans la biomasse d'un peuplement, et leur rôle prépondérant dans les variations spatiales de la biomasse, il est crucial de mieux comprendre l'origine et les conséquences du biais du modèle pantropical.

Dans cette étude, nous avons assemblé des données sur les dimensions et masses de plus de 650 arbres provenant de 5 pays tropicaux. Ce jeu de données contient plus de 100 arbres de diamètre à hauteur de poitrine supérieur à 100 cm, ce qui est remarquable. Ce jeu de données dit « destructif » a été utilisé pour étudier le mécanisme sous-jacent au biais du modèle pantropical, en mettant l'accent sur les variations de dimensions et de masses des couronnes le long du gradient de taille d'arbre, ce que le modèle pantropical ne prend pas en compte. Nous avons également utilisé 130 parcelles d'inventaires de 1-ha distribuées dans des types de forêts contrastées en Afrique centrale pour quantifier l'erreur associée au

biais du modèle un fois propagée à l'échelle de la parcelle, ainsi que l'influence de la structure de la forêt sur cette erreur.

Notre analyse montre tout d'abord que la contribution de la couronne à la masse totale de l'arbre varie considérablement, de 3 à 88%, chez les arbres étudiés. Cette contribution est constante en moyenne pour les arbres de moins de 10 Mg (c. 34% de la masse de l'arbre), mais au-delà de ce seuil, elle augmente fortement avec la masse de l'arbre pour atteindre plus de 50% en moyenne chez les arbres ≥ 45 Mg (Figure 2, haut-gauche).

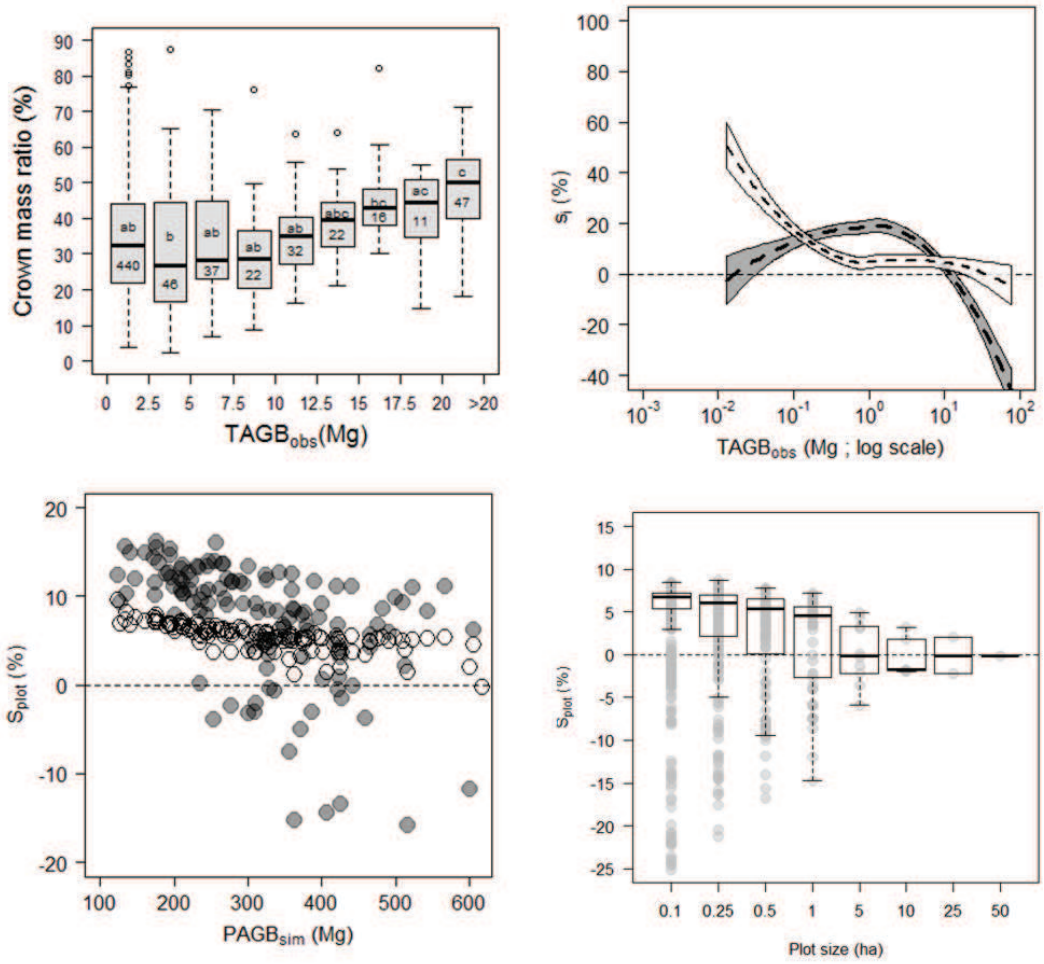

Figure 2. (**Haut-gauche**) Variation du ratio de masse de couronne avec la biomasse totale de l'arbre ($TAGB_{obs}$). (**Haut-droit**) Erreur relative moyenne sur l'estimation de la biomasse de l'arbre (s, en %) du modèle pantropical de référence (gris) et du modèle alternatif développé dans la présente étude (blanc). (**Bas-gauche**) Erreur relative moyenne sur l'estimation de la biomasse de parcelles de 1-ha (S_{plot}, en %) du modèle pantropical de référence (points gris) et du modèle alternatif développé dans la présente étude (points blancs). (**Bas-droit**) Evolution de l'erreur relative à l'échelle de la parcelle (S_{plot}, en %) avec la taille de la parcelle.

Cette augmentation progressive de la proportion de masse de couronne après 10 Mg coïncide avec la déviation progressive entre la masse de l'arbre et la prédiction de cette masse par le modèle pantropical de référence (Figure 1, haut-droit). Forts de cette observation, nous avons développé un ensemble de proxy de masse de couronne sur la base de paramètres dendrométriques disponibles (diamètre du tronc, hauteur de l'arbre, densité du bois) ou facilement mesurables sur le terrain (hauteur du tronc). L'inclusion du proxy de masse de couronne le plus performant dans un modèle de biomasse décomposant l'arbre en deux parties (tronc et couronne) a permis d'obtenir des estimations de masse non-biaisées pour les arbres > 1 Mg (Figure 1, haut-droit).

Nous avons également développé une méthode de propagation d'erreur de l'arbre à la parcelle prenant explicitement en compte le biais des modèles de biomasse. Nous montrons que la dépendance entre le biais du modèle de référence et la masse des arbres crée une interaction entre la structure du peuplement dans la parcelle et l'erreur associée à l'estimation de biomasse de la parcelle. En essence, la biomasse des parcelles tend à être sur- ou sous-estimée quand celles-ci sont dominées pars des petits (≤ 10 mg) ou gros (> 10 Mg) arbres, respectivement. Nous montrons que la forme du modèle de référence génère un biais sur les estimations de biomasse à l'échelle de parcelles de 1-ha variant de -23 à +16% (figure 1, bas-gauche). Ce biais est largement réduit (0 à 10%) avec le modèle alternatif que nous proposons. L'amplitude du biais est également dépendante de la taille de la parcelle, avec des erreurs moyennes plus importantes observées dans les parcelles de petites tailles (Figure 1, bas-droit) où un biais d'estimation sur quelques gros arbres a relativement plus d'importance sur la biomasse de la parcelle.

Cette étude met en évidence une source d'erreur systématique sur la biomasse des parcelles qui est loin d'être négligeable, et qui n'est généralement pas prise en compte dans la littérature. L'utilisation d'un modèle incluant des dimensions de couronne, au moins pour les plus gros arbres au sein des parcelles, permet de réduire fortement cette erreur et suggère qu'une amélioration substantielle des estimations de biomasse peut être obtenue à coût minimal.

Chapitre 3. Evaluation de la loi de conservation des aires sur de grands arbres tropicaux et pistes de regroupement d'espèce pour l'estimation de la biomasse

Les allométries observables entre les dimensions des arbres reflètent des contraintes biologiques et physiques respectées par tout arbre afin d'éviter la mort (ex. par cavitation, par effondrement) au cours de sa croissance. La compréhension des principes généraux qui régissent les formes et fonctions des arbres est une thématique de recherche fascinante qui a traditionnellement été abordée par l'hydrodynamique et la biomécanique. Il y a une vingtaine d'années, la Théorie Métabolique de l'Ecologie (MTE) unifiait ces différentes perspectives et postulait que les allométries émergent d'une optimisation évolutive des propriétés de structure et d'hydrodynamique du réseau vasculaire de distribution des ressources des organismes biologiques. Cette théorie, comme certaines de ces prédécesseurs (la théorie 'Pipe model', notamment), repose sur un ensemble d'hypothèses décrivant la structure de l'arbre de façon simplifiée. Si les fondements et prédictions de la MTE ont été et sont toujours activement débattus, relativement peu d'études ont testé les hypothèses faites dans la MTE sur la structure du réseau de branches que constitue un arbre. Dans ce chapitre, nous avons testé un ensemble d'hypothèses de la

MTE, focalisant notre attention sur la loi de conservation des aires. Cette loi, qui dérive d'observations faites par Leonardo Da Vinci il y a plus de 500 ans, postule que la somme des surfaces des sections des branches « filles » à un nœud donné est égale à la surface de la section de la branche « mère ». Toutes choses égales par ailleurs, cette loi a des conséquences directes sur l'allométrie de biomasse des arbres, ce qui justifie en partie notre attention.

Mettant à profit le jeu de données destructif regroupant 77 grands arbres de canopée au Cameroun, nous avons testé la loi de conservation des aires sur des espèces aux architectures contrastées (notamment en termes de symétrie du houppier, Figure 3). L'influence de la structure des branches au niveau du nœud (nombre et symétrie des branches filles, notamment) a été étudiée.

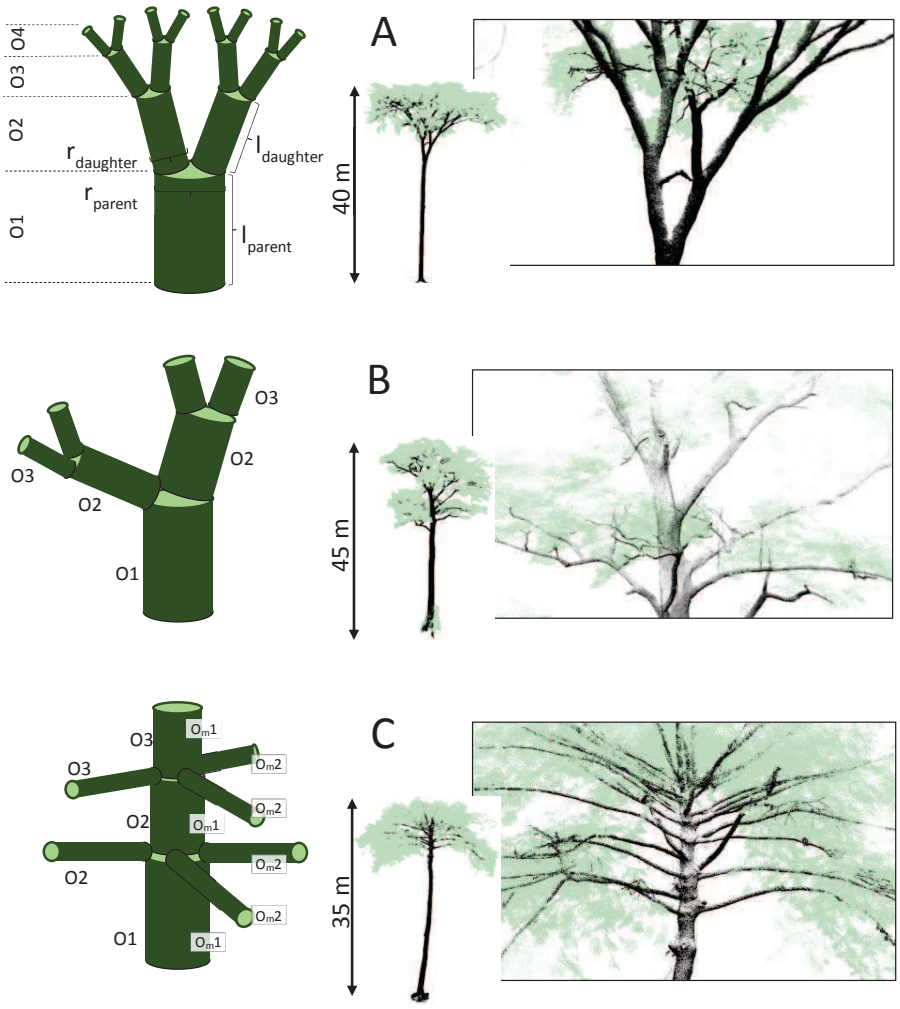

Figure 3. Représentation schématique de différents niveaux d'asymétrie du houppier (colonne de gauche), de l'arbre optimal de la MTE (A) à une asymétrie modérée (B) et importante (C). Ces niveaux d'asymétrie sont illustrés par des espèces abondantes en Afrique centrale (colonne de droite), de haut en bas : l'Okan, l'Ayous et l'Ilomba.

Notre analyse montre que contrairement à la prédiction de la loi de conservation des aires, le ratio des surfaces des sections des branches filles sur celui de la mère (noté *R*) est supérieur à 1 en moyenne chez les grands arbres tropicaux (c. 1.17). Nous avons mis en évidence l'influence systématique de certains paramètres de structure des couronnes sur *R*, notamment le nombre de branches filles à un nœud donné (Figure 4, haut-gauche) et leur symétrie (Figure 4, haut-gauche).

Ces paramètres de structure étant caractéristiques de l'organisation générale des couronnes de certaines espèces, nous mettons en évidence des variations systématiques de *R* entre espèces (Figure 4, bas).

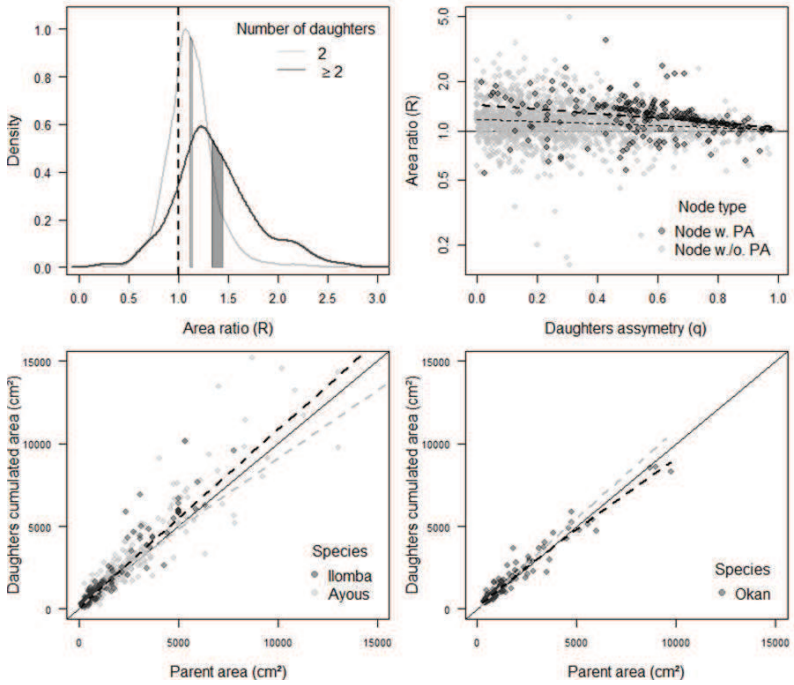

Figure 4. (Haut-gauche) Distribution de fréquence des ratios des surfaces des sections des branches filles sur celles des mères (*R*) pour des nœuds à 2 filles (gris clair) et pour ceux à plus de 2 filles (gris foncé). (Haut-droite) Effet de l'asymétrie des filles (noté *q*) sur *R*. Les nœuds portant une fille dominante, verticale, centrale au houppier (notée *PA*) sont distingués des autres. (Bas-gauche) Somme cumulée des surfaces des sections des branches filles en fonction de celle de la mère pour l'Ayous et l'Ilomba. La droite d'ajustement du modèle est représentée en gris foncé. (Bas-droit) Somme cumulée des surfaces des sections des branches filles en fonction de celle de la mère pour l'Okan. La droite d'ajustement du modèle est représentée en gris foncé.

L'organisation générale des couronnes reflétant, dans une certaine mesure, la stratégie de vie des essences (ex. pionnière à croissance rapide *vs* tolérante à l'ombre à croissance lente), les résultats donnent lieu à une discussion sur les possibilités de regroupement des espèces dans les modèles de biomasse.

Chapitre 4. Analyse des propriétés de texture des canopées sur images à très haute résolution spatiale pour la cartographie de la biomasse forestière

L'organisation structurelle de la canopée d'une forêt est un descripteur important de la dynamique du peuplement et peut fournir des informations pour la cartographie des végétations et la gestion des forêts. Dans ce chapitre, je présente une approche relativement nouvelle d'analyse de texture de canopées sur images optiques très haute résolution spatiale (THRS). Basée sur une ordination multivariée des spectres de Fourier, la méthode FOTO permet de classer les imagettes de canopée (extraites de photographies aériennes ou d'image satellitaires à THRS) selon la taille du grain de canopée i.e., une combinaison de la taille moyenne et de la densité des couronnes apparentes sur les imagettes. Durant la dernière décennie, la méthode a été appliquée à plusieurs types d'écosystèmes forestiers (des mangroves aux forêts denses humides de terre ferme), avec plusieurs types d'images (THRS commerciales des satellites IKONOS, GeoEye ou Quickbird, images fausses couleurs extraites de la plateforme Google Earth, photographies aériennes). Les indices de texture FOTO ont montré un potentiel intéressant pour caractériser certains paramètres de structure des peuplements, notamment la biomasse épigée et ce sans saturation évidente jusqu'à des niveaux de biomasse élevés (c. 500 $Mg.ha^{-1}$). La revue des cas d'études laisse également apparaitre les limites de l'approche pour son application à large échelle (au-delà de quelques centaines de km^2), notamment la sensibilité des indices de texture aux conditions d'acquisition des images (ex. angle du soleil), aux variations de topographie, ou encore le manque de stabilité des relations entre paramètres de structure du peuplement et indices de texture entre types de forêts. Les perspectives de développement méthodologique, dont certaines ont donné lieu à plusieurs publications au cours des dernières années, sont présentées. L'une d'entre elle est abordée dans le chapitre suivant.

Chapitre 5. Combinaisons d'indices de texture de canopées forestières: vers un modèle d'inversion robuste

Afin d'exploiter le plein potentiel des images THSR pour la cartographie à large échelle du carbone des forêts tropicales, un enjeu crucial est de stabiliser la relation entre la biomasse des peuplements et les métriques extraites des images. Si les indices de texture FOTO ont montré un bon potentiel à échelle locale (quelques dizaines à quelques centaines de km^2) pour caractériser les variations spatiales de la biomasse épigée, les relations AGB – texture diffèrent entre types forestiers. L'analyse conduite dans ce chapitre vise à développer un modèle d'inversion générique de l'AGB des forêts tropicales i.e., qui puisse être appliqué simultanément à plusieurs types forestiers. Cet enjeu est particulièrement important pour pouvoir utiliser la texture de canopée pour décrire les variations de biomasse des forêts d'Afrique centrale, en particulier celles des forêts semi-décidues de l'Est Cameroun où le paysage forestier s'apparente souvent à une mosaïques de types de forêts aux structures contrastées, enchevêtrées à petite échelle spatiale (Figure 5).

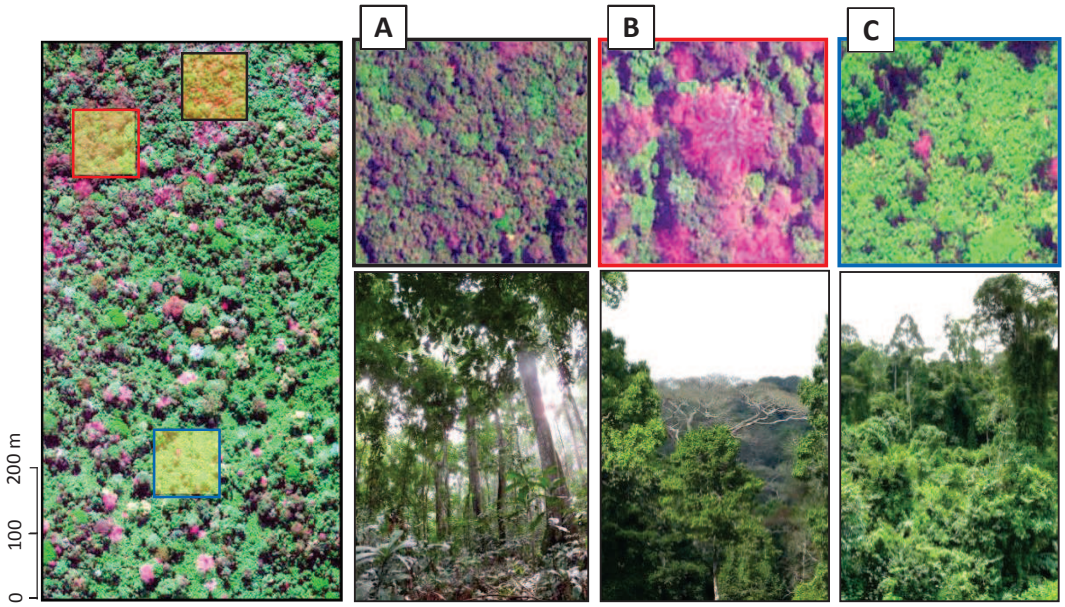

Figure 5. Image THRS (Geoeye) d'une mosaïque forestière typique des forêts semi-décidues de l'Est Cameroun. Sur quelques km², des peuplements monodominants de *Gilbertiodendron dewevrei* (A) se mêlent à des forêts mixtes aux canopées fermées (B) et à des forêts ouvertes à *Marantaceae* (C).

L'analyse a reposé sur deux hypothèses principales : (1) les indices de texture FOTO ne permettant pas de discriminer les trouées (agrégats de pixel sombres) des couronnes (agrégats de pixel claires), les différences d'abondances et de dynamiques de trouées entre sites et types forestiers contribuent à l'instabilité de la relation AGB – indices de texture ; (2) l'importance de la hauteur de la forêt comme prédicteur de la biomasse épigée est bien connue. L'information contenue dans les images optiques 2D ne permettant pas de caractériser les variations de hauteur à moyenne et large échelle (entre sites forestiers), l'inclusion d'un proxy pour prendre en compte ses variations dans un modèle générique / régionale devrait permettre de réduire les biais de prédiction entre sites.

Pour investiguer ces hypothèses, nous avons assemblé une base de données de 279 parcelles d'inventaires de 1-ha réparties sur trois continents, généré des maquettes tridimensionnelles des parcelles en utilisant une représentation simplifiée des arbres (modèle Allostand) et simulé une image optique THRS de chaque maquette à l'aide d'un modèle de transfert radiatif (Discrete Anisotropic Radiative Transfer model, DART). Cette approche

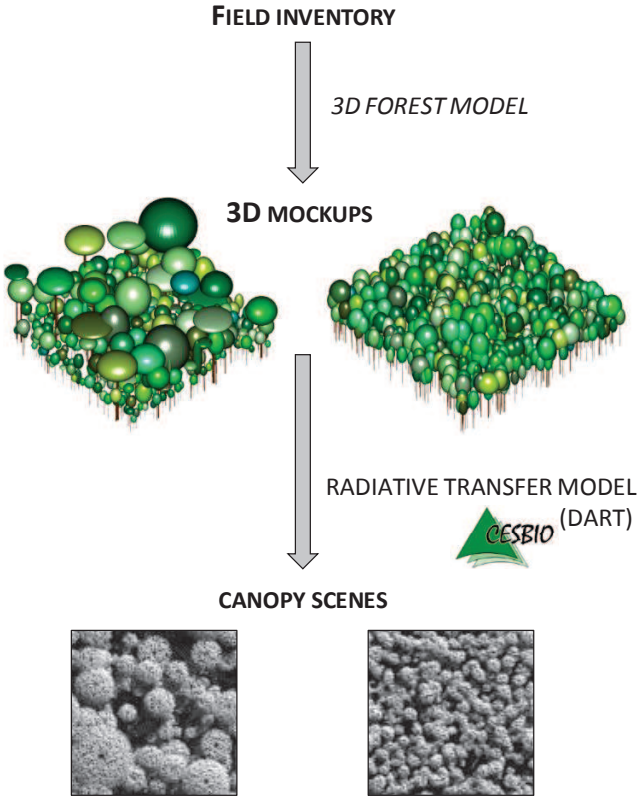

Figure 6. Chaine de simulation des imagettes scènes THSR simulée à partir des données d'inventaire.

par simulation (illustrée en Figure 6) nous a permis de contrôler l'influence des paramètres d'acquisition des images sur la texture de canopée, et ainsi de se focaliser sur l'effet des variations de structure des peuplements sur la relation AGB – indices de texture.

Nos résultats montrent qu'un modèle global (i.e. inter-site) d'inversion de la biomasse basé sur les seuls indices de texture FOTO (noté « F-model » en Figure 7) explique modérément les variations de biomasse entre scènes simulées (R^2=0.46, erreur relative de c. 30%). Un second modèle basé sur des indices de lacunarité (noté « L-model »), une autre forme d'analyse de texture ayant montré une bonne sensibilité aux trouées et à l'hétérogénéité verticale de la canopée, explique faiblement les variations de biomasse entre scènes (R^2=0.31, erreur relative de c. 38%). Néanmoins, la combinaison des deux types d'indices (« FL-model ») permet d'améliorer substantiellement l'ajustement du modèle (R^2=0.76, erreur relative de c. 20%). Ce résultat, en ligne avec la première hypothèse de cette étude, indique que des gradients de structure distincts et complémentaires pour la description de la biomasse des forêts peuvent être extraits des images THSR en combinant différents types d'analyses de texture.

Une seconde partie des résultats s'articule autour de l'inclusion d'une variable publiée, notée *E*, dans le modèle FL (menant au modèle « FLE »). Cette variable, construite pour capturer l'effet de diverses paramètres bioclimatiques sur l'allométrie hauteur-diamètre des arbres, permet de réaliser un gain supplémentaire dans l'ajustement du modèle de texture (R^2= 0.88, erreur relative de c. 14%) en diminuant, notamment, l'erreur moyenne des prédictions entre sites (Figure 7).

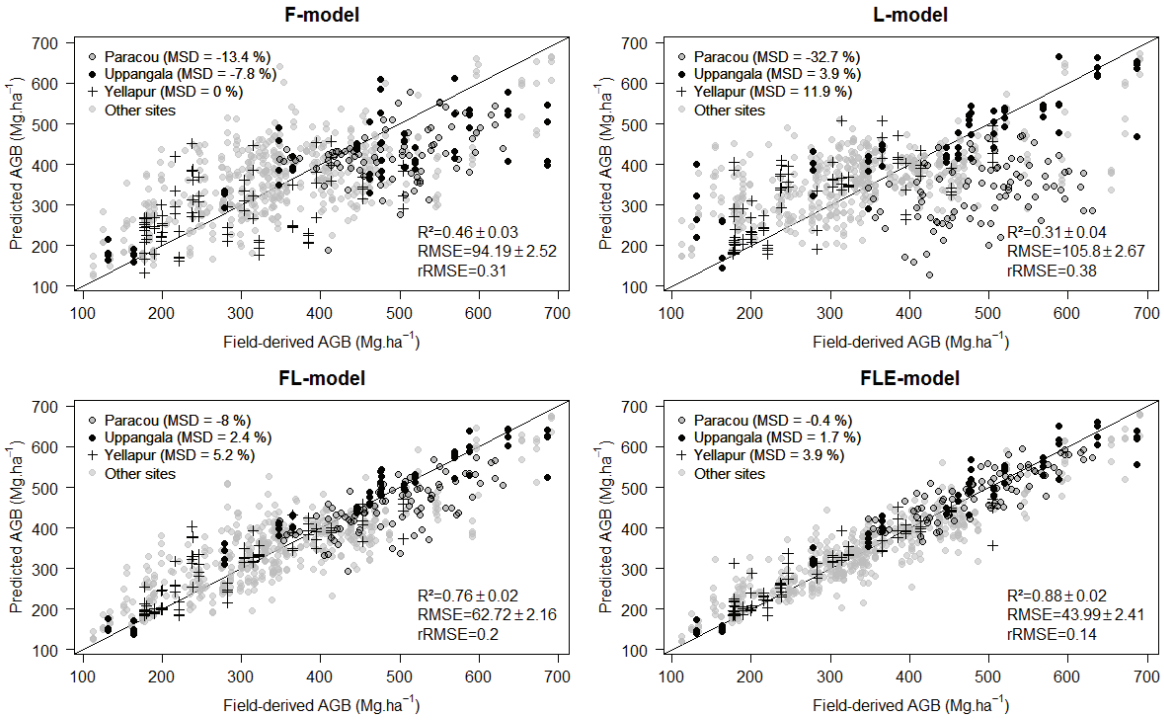

Figure 7. Résultats des modèles d'inversion de biomasse basés sur les indices de texture FOTO (haut-gauche), les indices de lacunarité (haut-droit), la combinaison des deux types d'indices (bas-droit) auxquels nous avons aussi ajouté un proxy de hauteur de canopée *E* (bas-droit).

Enfin, le modèle final (FLE) a été testé sur des données « réelles » : 49 parcelles de 1-ha distribuées sur trois images Pléiades couvrant une mosaïque forestière dans l'Est Cameroun. Le modèle a mené à un niveau d'erreur (RMSE = 62 $Mg.ha^{-1}$, erreur relative de c. 21%, Figure 8) seulement légèrement supérieur à ceux reportés dans la littérature sur la base de données LiDAR aériennes, en particulier sur les forêts à fortes biomasses telles que rencontrées dans la zone d'étude (jusqu'à 600 $Mg.ha^{-1}$).

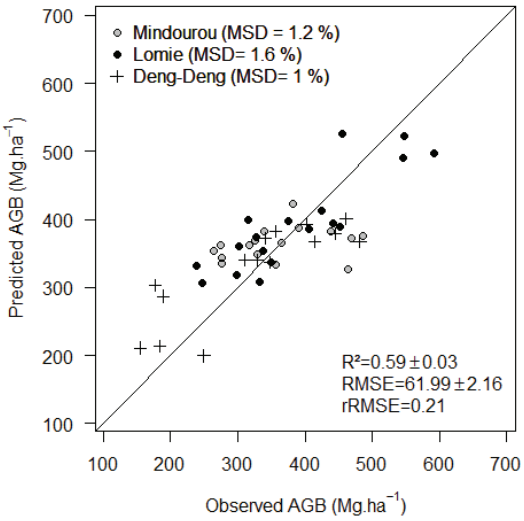

Figure 8. Résultats du modèle d'inversion de biomasse (FLE) basé sur 49 parcelles de 1-ha dans l'Est Cameroun.

La disponibilité grandissante des images optiques THSR (e.g. issues de constellation de microsatellites) suggèrent que des couvertures complètes et fréquentes des forêts tropicales pourraient être disponibles dans un futur proche. Cette étude montre que les analyses de texture des canopées pourraient devenir un outil essentiel des efforts internationaux pour suivre les émissions de carbone liées à la déforestation et à la dégradation des forêts.

6 Synthèse générale

Cette thèse a donné lieu aux études publiées, soumises ou en cours de soumission suivantes :

Estimation de la biomasse des parcelles forestières

- **Ploton, P.**, Barbier, N., Takoudjou Momo, S., Réjou-Méchain, M., Boyemba Bosela, F., Chuyong, G., Dauby, G., Droissart, V., Fayolle, A., Goodman, R.C., Henry, M., Kamdem, N.G., Mukirania, J.K., Kenfack, D., Libalah, M., Ngomanda, A., Rossi, V., Sonké, B., Texier, N., Thomas, D., Zebaze, D., Couteron, P., Berger, U., Pélissier, R., 2016. Closing a gap in tropical forest biomass estimation: taking crown mass variation into account in pantropical allometries. Biogeosciences 13, 1571–1585. doi:10.5194/bg-13-1571-2016

- **Ploton, P.**, Barbier, N., Couteron, P., Momo, S.T., Griffon, S., Bonaventure, S., Uta, B., Pélissie,r R. Assessing Leonardo's rule on large tropical trees of contrasted architectures. **<u>En preparation</u>** pour *Trees – Structure and Function.*
- Picard, N., Rutishauser, E., **Ploton, P.**, Ngomanda, A., Henry, M., 2015. Should tree biomass allometry be restricted to power models? For. Ecol. Manag. 353, 156–163. doi:10.1016/j.foreco.2015.05.035
- Chave, J., Réjou-Méchain, M., Búrquez, A., Chidumayo, E., Colgan, M.S., Delitti, W.B.C., Duque, A., Eid, T., Fearnside, P.M., Goodman, R.C., Henry, M., Martínez-Yrízar, A., Mugasha, W.A., Muller-Landau, H.C., Mencuccini, M., Nelson, B.W., Ngomanda, A., Nogueira, E.M., Ortiz-Malavassi, E., Pélissier, R., **Ploton, P.**, Ryan, C.M., Saldarriaga, J.G., Vieilledent, G., 2014. Improved allometric models to estimate the aboveground biomass of tropical trees. Glob. Change Biol. 20, 3177–3190. doi:10.1111/gcb.12629

Lien entre arbres de canopée visibles sur images THRS et biomasse de la forêt

- Bastin, J.-F., Barbier, N., Réjou-Méchain, M., Fayolle, A., Gourlet-Fleury, S., Maniatis, D., de Haulleville, T., Baya, F., Beeckman, H., Beina, D., Couteron, P., Chuyong, G., Dauby, G., Doucet, J.-L., Droissart, V., Dufrêne, M., Ewango, C., Gillet, J.F., Gonmadje, C.H., Hart, T., Kavali, T., Kenfack, D., Libalah, M., Malhi, Y., Makana, J.-R., Pélissier, R., **Ploton, P.**, Serckx, A., Sonké, B., Stevart, T., Thomas, D.W., De Cannière, C., Bogaert, J., 2015c. Seeing Central African forests through their largest trees. Sci. Rep. 5, 13156. doi:10.1038/srep13156
- Blanchard, E., Birnbaum, P., Ibanez, T., Boutreux, T., Antin, C., **Ploton, P.**, Vincent, G., Pouteau, R., Vandrot, H., Hequet, V., 2016. Contrasted allometries between stem diameter, crown area, and tree height in five tropical biogeographic areas. Trees 1–16.
- Jucker, T., Caspersen, J., Chave, J., Antin, C., Barbier, N., Bongers, F., Dalponte, M., van Ewijk, K.Y., Forrester, D.I., Haeni, M., Higgins, S.I., Holdaway, R.J., Iida, Y., Lorimer, C., Marshall, P.L., Momo, S., Moncrieff, G.R., **Ploton, P.**, Poorter, L., Rahman, K.A., Schlund, M., Sonké, B., Sterck, F.J., Trugman, A.T., Usoltsev, V.A., Vanderwel, M.C., Waldner, P., Wedeux, B.M.M., Wirth, C., Wöll, H., Woods, M., Xiang, W., Zimmermann, N.E., Coomes, D.A., 2016. Allometric equations for integrating remote sensing imagery into forest monitoring programmes. Glob. Change Biol. doi:10.1111/gcb.13388

Estimation de la biomasse sur base des propriétés de texture des canopées

- **Ploton, P.**, Pélissier, R., Barbier, N., Proisy, C., Ramesh, B.R., Couteron, P., 2013. Canopy texture analysis for large-scale assessments of tropical forest stand structure and biomass, in: Treetops at Risk. Springer, pp. 237–245.
- **Ploton, P.**, Barbier, N., Couteron, P., Ayyappan, N., Antin, C.M., Bastin, J.-F., Chuyong, G., Dauby, G., Droissart, V., Gastellu-Etchegorry, J.-P., Kamdem, N.G., Kenfack, D., Libalah, M., Momo, S., Pargal, S., Proisy, C., Sonké, B., Texier, N., Thomas, D., Zebaze, D., Verley, P., Vincent, G., Berger, U., Pélissier, R. Combining canopy texture metrics from optical data to retrieve tropical forest aboveground biomass in complex forest mosaics. **<u>En révision</u>** dans *Remote Sensing of Environment.*
- **Ploton, P.**, Pélissier, R., Proisy, C., Flavenot, T., Barbier, N., Rai, S.N., Couteron, P., 2012. Assessing aboveground tropical forest biomass using Google Earth canopy images. Ecol. Appl. 22, 993–1003. doi:10.1890/11-1606.1
- Couteron, P., Barbier, N., Deblauwe, V., Pélissier, R., Ploton, P., 2015. Texture Analysis of Very High Spatial Resolution Optical Images as a Way to Monitor Vegetation and Forest Biomass in the Tropics. Multi-Scale For. Biomass Assess. Monit. Hindu Kush Himal. Reg. Geospatial Perspect. 157.

Title : Improving tropical forest aboveground biomass estimations : insights from canopy trees structure and spatial organization

Keywords : forest carbon, REDD, pantropical biomass allometric model, canopy structure, canopy texture, passive optical imagery, Fourier transform, lacunarity

Abstract : Tropical forests store more than half of the world's forest carbon and are particularly threatened by deforestation and degradation processes, which together represent the second largest source of anthropogenic CO_2 emissions. Consequently, tropical forests are the focus of international climate policies (i.e. Reducing emissions from deforestation and forest degradation, REDD) aiming at reducing forest-related CO_2 emissions. The REDD initiative lies on our ability to map forest carbon stocks (i.e. spatial dynamics) and to detect deforestation and degradations (i.e. temporal dynamics) at large spatial scales (e.g. national, forested basin), with accuracy and precision. Remote-sensing is as a key tool for this purpose, but numerous sources of error along the carbon mapping chain makes meeting REDD criteria an outstanding challenge. In the present thesis, we assessed carbon (quantified through aboveground biomass, AGB) estimation error at the tree- and plot-level using a widely used pantropical AGB model, and at the landscape-level using a remote sensing method based on canopy texture features from very high resolution (VHR) optical data. Our objective was to better understand and reduce AGB estimation error at each level using information on large canopy tree structure, distribution and spatial organization.

Although large trees disproportionally contributed to forest carbon stock, they are under-represented in destructive datasets and subject to an under-estimation bias with the pantropical AGB model. We destructively sampled 77 very large tropical trees and assembled a large (pantropical) dataset to study how variation in tree form (through crown sizes and crown mass ratio) contributed to this error pattern. We showed that the source of bias in the pantropical model was a systematic increase in the proportion of tree mass allocated to the crown in canopy trees. An alternative AGB model accounting for this phenomenon was proposed. We also propagated the AGB model bias at the plot-level and showed that the interaction between forest structure and model bias, although often overlooked, might in fact be substantial. We further analyzed the structural properties of crown branching networks in light of the assumptions and predictions of the Metabolic Theory of Ecology, which supports the power-form of the pantropical AGB model. Important deviations were observed, notably from Leonardo's rule (i.e. the principle of area conservation), which, all else being equal, could support the higher proportion of mass in large tree crowns.

A second part of the thesis dealt with the extrapolation of field-plot AGB via canopy texture features of VHR optical data. A major barrier for the development of a broad-scale forest carbon monitoring method based on canopy texture is that relationships between canopy texture and stand structure parameters (including AGB) vary among forest types and regions of the world. We investigated this discrepancy using a simulation approach: virtual canopy scenes were generated for 279 1-ha plots distributed on contrasted forest types across the tropics. We showed that complementing FOTO texture with additional descriptors of forest structure, notably on canopy openness (from a lacunarity analysis) and tree slenderness (from a bioclimatic proxy) allows developing a stable inversion frame for forest AGB at large scale. Although the approach we proposed requires further empirical validation, a first case study on a forests mosaic in the Congo basin gave promising results.

Overall, this work increased our understanding of mechanisms behind AGB estimation errors at the tree-, plot- and landscape-level. It stresses the need to better account for variation patterns in tree structure (e.g. ontogenetic pattern of carbon allocation) and forest structural organization (across forest types, under different environmental conditions) to improve general AGB models, and *in fine* our ability to accurately map forest AGB at large scale.

Titre : Amélioration des estimations de biomasse en forêt tropicale : apport de la structure et de l'organisation spatiale des arbres de canopée

Mots clés : carbone forestier, REDD, modèle de biomasse pantropical, structure de canopée, texture de canopée, imagerie optique passive, transformée de Fourier, lacunarité

Résumé : Les forêts tropicales séquestrent plus de la moitié du carbone forestier mondial et sont particulièrement menacées par les processus de déforestation et de dégradation, qui représentent la deuxième source d'émissions anthropogéniques de CO_2. De fait, les forêts tropicales sont au centre de politiques climatiques internationales (i.e. Reducing emissions from deforestation and forest degradation, REDD) visant à réduire ces émissions. L'initiative REDD repose sur notre capacité à cartographier les stocks de carbone forestier (dynamique spatiale) et à détecter la déforestation et la dégradation (dynamique temporelle) à large échelle spatiale (e.g. nationale, bassin forestier), avec exactitude et précision. Dans ce cadre, la télédétection apparait comme un outil crucial, mais les nombreuses sources d'erreur dans la chaîne de cartographie du carbone font des objectifs du REDD un challenge ambitieux. Dans cette thèse, nous avons évalué les erreurs associées aux estimations de carbone forestier (quantifié au travers de la biomasse épigée, AGB) (1) aux échelles de l'arbre et du peuplement en utilisant un modèle pantropical largement employé et (2) à l'échelle du paysage en utilisant une méthode de télédétection basée sur les caractéristiques texturales d'images optiques à très haute résolution spatiale. Notre objectif général était de mieux comprendre et de réduire l'erreur d'estimation de l'AGB à chaque échelle par une meilleure prise en compte de la structure, de la distribution et de l'organisation spatiale des arbres de canopée.

Malgré l'importance des grands arbres dans la dynamique du carbone forestier, ils sont sous-représentés dans les jeux de données destructifs et soumis à un biais de sous-estimation dans le modèle d'AGB pantropical. Nous avons assemblé une base de données pantropicale et étudié l'influence de la forme de l'arbre sur le patron d'erreur du modèle. Nos résultats montrent que la source de biais du modèle est une augmentation de la masse de l'arbre dans la couronne chez les arbres de canopée. Un modèle d'AGB prenant ce phénomène en compte a été proposé. Nous avons aussi propagé le biais du modèle à l'échelle du peuplement et montré que l'interaction entre la structure du peuplement et l'erreur du modèle, qui est souvent négligée, peut en fait être substantielle. Une analyse des propriétés structurelles des couronnes a également été menée au regard des hypothèses de la Théorie Métabolique de l'Ecologie Des déviations ont été observées, notamment à la loi de Léonardo (i.e. principe de conservation des aires), qui, toutes choses égales par ailleurs, pourraient justifier la grande proportion de masse trouvée dans les couronnes des arbres de canopée.

Une seconde partie de la thèse porte sur l'extrapolation des estimations d'AGB des parcelles de terrain via les caractéristiques de texture des canopées extraites par transformée de Fourier (i.e. méthode FOTO). Un obstacle majeur au développement d'une méthode d'estimation de l'AGB à large échelle basée sur la texture tient au fait que la relation texture – paramètres de structure du peuplement varie entre types de forêt et régions du monde. Nous avons investigué cette question en simulant des scènes de canopées virtuelles pour 279 parcelles de 1 ha établies dans des types de forêts tropicales contrastés. Nous montrons qu'en complémentant les indices de texture FOTO avec d'autres descripteurs structuraux, notamment sur l'ouverture de la canopée (via une analyse de lacunarité) et l'élancement des arbres (via un proxy bioclimatique), il devrait être possible de développer un cadre d'inversion stable de l'AGB à large échelle. Un premier cas d'étude empirique dans une mosaïque forestière du bassin du Congo a donné des résultats prometteurs.

Globalement, ce travail met en évidence le besoin de mieux prendre en compte les patrons de variation de structure de l'arbre (e.g. ontogénétique) et de la forêt afin d'améliorer les modèles génériques d'AGB.